ROLE OF PHYSIOCHEMICAL PARAMETERS IN THE OSTEOGENIC POTENTIAL OF CALCIUM PHOSPHATE BIOMATERIALS

Charlie Campion

Submitted in partial fulfilment of the requirements of the Degree of Doctor of Philosophy

June 2015

School of Engineering and Material Sciences
Queen Mary University London

I Statement of originality

I, Charlie Campion, confirm that the research included within this thesis is my own work or that where it has been carried out in collaboration with, or supported by others, that this is duly acknowledged below and my contribution indicated. Previously published material is also acknowledged below.

I attest that I have exercised reasonable care to ensure that the work is original, and does not to the best of my knowledge break any UK law, infringe any third party's copyright or other Intellectual Property Right, or contain any confidential material.

I accept that the College has the right to use plagiarism detection software to check the electronic version of the thesis.

I confirm that this thesis has not been previously submitted for the award of a degree by this or any other university.

Signature:

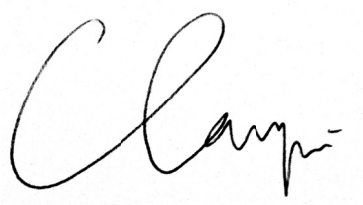

Date: 14th June 2015

II Acknowledgements

I would first and foremost like to thank Dr K. A. Hing from Queen Mary, University of London, UK, as my academic supervisor, confidant and mentor for her commitment, guidance and persistence during the development of this thesis. This research would not have been possible without her unwavering support and most of all, her patience. I would also like to thank Dr T. Buckland, formerly of ApaTech Limited, UK, as my manager at the inception of this research for sponsoring my studies and for gaining financial support from my industrial sponsor. Dr K. A. Hing and Dr T. Buckland provided scientific contributions to Chapters 3, 4, 5, 6 and 7.

My thanks also go to Prof I. R. Gibson of the University of Aberdeen, UK, who provided expert guidance and laboratory resources for the Fourier transform infrared spectroscopy described in Chapter 3. Likewise, I would like to recognise the laboratory time contributed by Miss S. L. Ball and Mr D. L. Clarke, both formerly of ApaTech Limited, UK, to the scanning electron microscopy described in Chapters 3, 4 and 5, and their scientific contribution to the associated publication "*Microstructure and chemistry affects apatite nucleation on calcium phosphate bone graft substitutes*". The laboratory team at Lucideon Limted, UK, operated the X-ray fluorescence spectroscopy and inductively coupled plasma optical emission spectroscopy equipment described in Chapter 3.

I owe a debt of gratitude to Dr A. M. New of Apogee Limited with whom I collaborated on shear box testing and finite element analysis. Dr A. M. New provided laboratory equipment and scientific expertise towards Chapter 4. The laboratory team at Intertek Group Plc, UK, operated the energy dispersive x-ray analysis, scanning electron microscopy and inductively coupled plasma optical emission spectroscopy equipment described in Chapter 5.

Prof G. W. Blunn, Dr M. J. Coathup, Dr A. Nesbitt, Dr C. Y. Ho, Dr O. Chan, Dr Y. S. Fang, Dr S. Samizadeh from the Institute for Musculoskeletal Science at University College London, UK, provided scientific expertise and contributed laboratory support to the experiments described in Chapter 6, including all of the animal care and surgeries, and much of the sample preparation and histological analysis. In particular, I would like to thank Gordon and Melanie for their expert guidance, for access to their equipment and facilities, and for challenging me to complete this research in spite of my industry-related workload.

I would like to recognise the team at Namsa Inc, France, who performed the *in vivo* experiments described in Chapter 7. I am further indebted to Dr C. Chander, formerly of ApaTech Limited, UK, for editorial guidance in developing Chapter 7 and to Dr T. Hardman of Niche Science & Technology Limited, UK, for editorial support in submitting the associated publication "*Increasing strut porosity in silicate-substituted calcium-phosphate bone graft substitutes enhances osteogenesis*".

For the duration of this research Dr K. Guth and Mr D. Johnson were my inspiration, friends and co-collaborators. Without Kat, Dan and Karin I might have doubted it was possible. Last but not least, I would like to dedicate this research to my family. Thank you Debbie, Joe and Stefano for encouraging me to complete this work at every opportunity. Thank you Rachel for supporting me through thick and thin. Thank you Robin for giving me a reason to achieve something in my life, may you rest in peace.

This research was funded by ApaTech Limited, a wholly owned subsidiary of Baxter Healthcare Inc.

III Publications

Campion, C. R., S. L. Ball, D. L. Clarke and K. A. Hing (2013). "Microstructure and chemistry affects apatite nucleation on calcium phosphate bone graft substitutes." J Mater Sci Mater Med **24**(3): 597-610.

Campion, C. R., C. Chander, T. Buckland and K. Hing (2011). "Increasing strut porosity in silicate-substituted calcium-phosphate bone graft substitutes enhances osteogenesis." J Biomed Mater Res B Appl Biomater **97**(2): 245-254.

Chan, O., M. J. Coathup, A. Nesbitt, C. Y. Ho, K. A. Hing, T. Buckland, C. Campion and G. W. Blunn "The effects of microporosity on osteoinduction of calcium phosphate bone graft substitute biomaterials." Acta Biomater.

Coathup, M. J., K. A. Hing, S. Samizadeh, O. Chan, Y. S. Fang, C. Campion, T. Buckland and G. W. Blunn "Effect of increased strut porosity of calcium phosphate bone graft substitute biomaterials on osteoinduction." J Biomed Mater Res A **100**(6): 1550-1555.

IVAbstract

The number of clinical procedures performed in the USA using bone graft substitutes was estimated at 1.1 million in 2010 and is projected to reach 1.3 million in 2015. This increasing demand for bone graft substitutes is a result of an ever-ageing population coupled with recent reports in the clinical literature of concerns regarding the safety of allograft and recombinant bone morphogenetic proteins such as rh-BMP-2 and the supply of autograft, which has led to an increased clinical interest in synthetic alternatives to allograft; autograft; and recombinant growth factors.

One such synthetic material is silicate-substituted hydroxyapatite (SiCaP). Mechanical testing revealed SiCaP to have similar mechanical behaviour to morcellised cancellous bone. In computated spinal and hip models the simulated stresses in SiCaP were determined to be low when *in situ*, indicating a stress-shielding effect from the implanted metalwork and surrounding bone. We also found an inverse relationship between porosity and Young's Modulus. Our results indicated that the strut-porosity of a material substrate should be increased to maximise the potential for formation of a precursor to bone-like apatite after implantation in osseous defects and further confirmed previous reports that beta-tricalcium phosphate is less bioactive than hydroxyapatite. We demonstrated a direct link between the amount of strut-porosity and the osteoinductivity of SiCaP. We learned that adding a resorbable carrier phase did not impair the osteoinductive potential of SiCaP, suggesting that osteoinductivity is not necessarily determined in the first 24-48 hours post implantation. Most notably from our studies we determined that the osteoinductivity of SiCaP correlated with its performance in orthotopic defects.

Our research confirmed our hypothesis that modifying the micron-scale physical structure of a hierarchical porous SiCaP based biomaterial influences its functional performance *in vitro* and such modifications can be applied to improve its performance outcomes in ectopic and orthotopic treatment sites *in vivo*.

V Contents

VI Table of Figures

VII Table of Tables

VIII Glossary

- **Biomaterial:** Any non-drug material that can be used to treat, enhance, or replace any tissue, organ, or function in an organism. Also refers to biologically derived material that is used for its structural rather than its biological properties, for example, using collagen, the protein found in bone and connective tissues, as a cosmetic ingredient. Carbohydrates modified with biotechnological processes have been used as lubricants for biomedical applications or as bulking agents in food manufacture (Dark 1997).
- **Bone Morphogenetic Protein (BMP):** The osteogenetic chemical components of the matrix of bone, dentin, and other hard tissues that are deinsulated by demineralization and associated intimately with collagen fibrils, are termed the bone morphogenetic proteins (Urist 1965).
- **Bone Morphogenetic Substratum:** The structure of the demineralized matrix is a substratum for differentiation of mesenchymal cells, not only into bone as a tissue, but also bone as an organ consisting of a shell of lamellar bone with a marrow cavity filled with hematopoietic bone marrow (Urist 1965).
- **Callus:** Mass of new bony trabeculae and cartilaginous tissue formed by osteoblasts early in the healing of a bone fracture (Dark 1997).
- **Cell Contact:** The contact between inducing and responding cells is mediated by intercellular substances and is dynamic rather than static in nature (Urist 1965).
- **Demineralised Bone Matrix:** Bone divested of inorganic salts, with minimal leaching or denaturation of the organic components of the matrix is demineralized bone matrix. Demineralization is carried out in the cold at 2 degrees Celsius, avoiding protein-polysaccharide extractants such as Ethylenediaminetetraacetic acid (EDTA). Acids such as hydrochloric acid, phosphoric acid, or citric acid, over a period of not more than three to five days, at concentrations of not more than 0.6 N, are preferable. Higher temperatures, higher concentration, and most organic acids extract variable quantities of the organic components of bone matrix and destroy bone morphogenetic proteins. The highly cross-linked matrix of dentin, although highly permeable, protects the BMP against the deleterious actions of organic acids, high temperatures, and long periods of exposure (Urist 1965).
- **Filopodial Extensions of the Cell:** Tubular extensions of the plasma membranes of mesenchymal cells, containing micro filaments, free of other

cell organelles, averaging about 1 μm in length and 0.3 μm in diameter, are termed filopodial extensions. Comparable to filopods of migratory ameboid cells, filopods of mesenchymal cells are contractile organs that probe the microcanalicular system, vascular channels, and other interstices of an implant of bone matrix (Urist 1965).

- **Hydroxyapatite:** A calcium phosphate ceramic with a calcium to phosphorous ratio of 1.67 and nominal composition ($Ca_{10}(PO_4)_6(OH)_2$). HA is similar to the mineral constituent of bone (Park and Bronzino 2003).
- **Induction:** The process of tissue differentiation initiated by close contact and mutual interaction of cell populations of diverse origins is called induction (Urist 1965).
- **Inductive Matrix:** The organic framework produced by demineralization of bones, teeth, and other calcified tissues serves as an inductive matrix for differentiation of mesenchymal cell populations with determination or competence to develop into cartilage, bone, and bone marrow (Urist 1965).
- **Lacunae:** any small cavity, such as those containing bone or cartilage cells (Thain and Hickman 1994).
- **Lacunocanalicular porosity:** complex structure of pores and cannels (Burger and Klein-Nulend 1999a).
- **Mechanotransduction:** is the process in which mechanical energy in converted into electrical and or biochemical signals (Burger and Klein-Nulend 1999a).
- **Osteoconductive:** Osteoconduction is a phenomenon in which there is an ingrowth of sprouting capillaries, perivascular mesenchymal tissues, and osteoprogenitor cells from the recipient host bed into the three-dimensional structure of an implant or graft (Einhorn 2003).
- **Osteoinductive:** Osteoinduction is a phenomenon in which there is a mitogenesis of undifferentiated perivascular mesenchymal cells leading to the formation of osteoprogenitor cells with the capacity to form new bone (Einhorn 2003).
- **Osteointegration:** procedure by which mature bone is deposited directly onto implant materials without intervening soft and/or fibrous tissue (Ahmad, McCarthy et al. 1999).

Chapter One: Introduction

1.1 Background

The number of clinical procedures performed in the USA in which bone graft was implanted was estimated at 1,109,000 in 2010 and is projected to reach 1,295,260 in 2015 (BioMedGPS 2012). This increasing demand for bone graft substitutes as a result of an ever-ageing population coupled with recent reports in the clinical literature of concerns regarding the safety of recombinant bone morphogenetic proteins such as rh-BMP-2 (Carragee, Ghanayem et al. 2011, Carragee, Hurwitz et al. 2011a, Carragee, Hurwitz et al. 2011b, Carragee, Mitsunaga et al. 2011) has led to an increased clinical interest in synthetic alternatives (such as porous calcium phosphate ceramics) to allograft; autograft; and recombinant growth factors.

Whilst the preclinical and clinical efficacy of calcium phosphates is relatively well described in the scientific and clinical literature there is still a need to better understand the mechanisms behind their therapeutic action so that the next generation of synthetic bone graft substitutes can be developed with improved safety and efficacy. The impact of characteristics such as phase purity, metal oxide composition, surface area, total porosity, pore size, and pore interconnectivity on the occurrence and extent of bone growth in bony (orthotopic) and non-bony (ectopic) sites treated with calcium phosphate based biomaterials has been reported in the literature across a number of preclinical studies (Hing, Best et al. 1998b, Hing, Gibson et al. 1998, Hing, Merry et al. 1999, Hing, Gibson et al. 2001, Hing 2004b, Hing 2004a, Hing, Saeed et al. 2004, Hing, Best et al. 2004, Hing 2005, Hing, Annaz et al. 2005, Hing, Revell et al. 2006, Hing, Wilson et al. 2007, Campion, Chander et al. 2011). However, a gap in understanding currently exists between knowing how to manipulate the properties of such devices to elicit the desired biological response *in situ* and knowing by which mechanisms this manipulation takes effect.

This author wishes to fill that gap in scientific knowledge by elucidating the mechanisms behind calcium phosphate biomaterial-derived osteoinductivity and its impact on performance in clinically relevant treatment sites. This will be achieved by evaluating test articles of well-defined physiochemical properties using a combination of *in vitro* characterisation, *in vivo* ectopic performance testing, and *in vivo* orthotopic performance studies. This knowledge could be used to commercialise a calcium phosphate based biomaterial with improved bone healing properties, ultimately leading to improved patient outcomes.

1.2 Hypothesis

Modifying the micron-scale physical structure of a hierarchical porous calcium phosphate based biomaterial influences its functional performance *in vitro*, which can be applied to improve its performance outcomes in ectopic and orthotopic treatment sites *in vivo*.

1.3 Objectives

In order to test this hypothesis this research is intended to:

- characterise a calcium phosphate biomaterial of varying microporosity using all chemical and physical analytical techniques described for osteoinductive calcium phosphates in the scientific literature;

- determine the effect of microporosity on the mechanical properties of calcium phosphate biomaterials using a combination of physical testing and a computational model;

- determine the effect of structure and chemistry on propensity of a calcium phosphate to form an apatite-like layer once submerged in simulated body fluid

- determine the effect of calcium and phosphorus dissolution on the osteoinductivity of calcium phosphate biomaterials;

- determine the effect of microporosity on performance of calcium phosphate biomaterials in an orthotopic bone defect study

Chapter Two: Literature Review

2.1 Introduction

In addition to its role in mineral homeostasis, bone performs a mechanical function by bearing loads during anatomical movement and by providing support to soft tissues all over the human body. It is the combination of the porous, brittle bone apatite mineral with a biological matrix of collagen, proteins, cells and polysaccharides to form a strong, non-brittle composite material that allows bone to fulfil this function. Attempts to develop synthetic hydroxyapatite bone substitute materials have centred on providing a porous mineral scaffold through which the surrounding bone can vascularise, then infiltrate and, therefore, regain the mechanical integrity of the lost bone (Ripamonti 1996, Gauthier, Bouler et al. 1998, Yuan, Yang et al. 2001, Hing 2005). It is also not only intended that the bone matrix infiltrates the porous structure of a bone substitute but also that new mineral bone itself forms within the implant and ultimately replaces the substitute material with new bone by the process of chemical resorption or more favourably cellular remodelling. Bone undergoes continuous remodelling in response to mechanical loading according to Wolff's law. However, the underlying mechanism by which bone cells respond to their changing environment, that is strain in the load-bearing matrix or fluid flow through the porous canicular network, has not been fully resolved or understood.

Novel synthetic calcium phosphate bone graft substitute materials with improved biological performance mediated through chemical and structural enhancements are being developed in relatively large numbers (Hing 2005). However, whilst a significant amount of work has been undertaken to investigate the relationship between substrate chemistry and bioactivity (Hing, Merry et al. 1999, Hing, Gibson et al. 2001, Balas, Perez-Pariente et al. 2003, Hing 2004a) and between pore structure, material permeability and bioactivity (Annaz 2003, Bignon, Chouteau et al. 2003, Annaz, Hing et al. 2004a, Annaz, Hing et al. 2004b, Hing 2004b, Hing, Best et al. 2004, Hing, Annaz et al. 2005) in hydroxyapatite materials, there have been no significant advances in characterising the role of substrate structure in determining the mechanical environment and the subsequent effects of the mechanical environment on the biological responses to synthetic bone graft substitutes and in particular synthetic hydroxyapatite bone graft substitutes.

The trade-off for ceramic bone graft materials by incorporating a large volume fraction of porosity to aid bone in-growth is that they lack structural integrity until a sufficient volume of new bone has filled the pores. Any steps taken to up-regulate the rate of bone growth within the substitute through the characterisation and optimisation of its mechanical properties could reduce the period of time for which the defect experiences mechanical instability and, therefore, increase the likelihood of successful graft incorporation.

In the following sections this author examines through literature review the structure and chemistry of physiological bone. As the subject of this thesis is to understand how both structure and chemistry affect bone repair at the cellular and macroscopic level, further attention is paid to *in vitro* studies of mechanobiology, specifically how substrate structure and physical properties relate to bone cell response. Next we will examine the various types of bone graft currently used in the clinical field of bone repair to understand the need for research in this area of biomaterials. Last of all, in order to consider the possible mechanisms for osteogenic potential in biomaterials and to inform the design of our own preclinical models we will research through the literature *in vitro* and in *vivo studies* of osteoinductivity.

2.2 Bone Physiology

Bone is a fine example of a natural material which humans can only dream of having invented. It has evolved to cope with the extremes of the mechanical environment forced upon it from early development right through to the end of its exceptionally dynamic life. Day to day it actively adapts its composition, structure and its interactions with its surroundings to cope with the chemical and physical demands placed upon it. It is bone's multiphase composition that allows it to behave as one of the most multifunctional organs of the human body. The composite structure of bone can be divided into the organic (collagen fibres, lipids, peptides, proteins, glycoproteins, polysaccharides and citrates) and the inorganic (calcium-phosphates, carbonates, sodium, magnesium and fluoride salts) (Hing 2004c). The make-up of bone depends on its location, age, and role in the body. Therefore, its composition varies considerably across the skeletal system and, in addition, between individuals depending on their diet, age and health (Boyne 1970, Heiple, Goldberg et al. 1987, Buckwalter, Einhorn et al. 1996, Betz 2003). The roles of bone can be categorized as support, storage of minerals and lipids, blood cell production, protection and leverage (Martini 1998). But, as previously mentioned, bone's role in the body is

dynamic as it reacts to both hormonal and mechanical stimuli which result in a constant cycle of resorption and remodeling.

2.2.1.A **Classification**

Bone exists in compact and spongy forms depending on the location and function of the osseous tissue. Compact bone, or cortical bone as it is otherwise known, is always located on the surface of a bone, where it forms a sturdy protective layer (Martini 1998). Compact bone is distinguished from spongy bone by the spatial orientation of its mineral and organic elements and by its characteristic locations in the skeleton (Yaszemski, Payne et al. 1996).

2.2.2 Structure

The basic functional unit of mature compact bone is the osteon or *Haversian system*. The Haversian system consists of canals (*Haversian canals*) surrounded by concentric rings of mineralised lamellar bone in which bone cells are sandwiched between layers of calcified matrix (*lamellae*) in small semi-isolated spaces called lacunae. Canaliculi penetrate the lamellae, radiating through the matrix and connecting lacunae with one another and with nutrient sources. Perforating canals, the *canals of Volkmann,* extend perpendicular to the osteons and supply blood to osteons deeper in the bone and to tissues of the marrow cavity (Martini 1998).

Spongy bone, or cancellous bone as it is also referred to, does not contain osteons. The matrix forms struts and plates called trabeculae which branch into an open structure with an interconnected network of pores. The trabeculae have an approximate thickness of 100-300 μm with spacing's of 300-1500 μm between adjacent trabeculae. In all, the porosity accounts for approximately 75-95% of the total volume of cancellous bone (Athanasiou, Zhu et al. 2000). Nutrient transfer to the osteocytes occurs via diffusion along canaliculi which open onto the surfaces of the trabeculae.

2.2.3 Mechanical Properties

2.2.3.A **Cancellous Bone**

Although changes in mineralization of the trabeculae have little effect (Hodgskinson and Currey 1990), apparent density and trabecular architecture strongly influence the mechanical properties of cancellous-bone tissue (Carter and Hayes 1976, Gibson

1985, Hodgskinson and Currey 1990, Linde, Norgaard et al. 1991). The structural or apparent density of cancellous bone is the mass per unit bulk volume of the tissue, whereas the matrix material density is the mass per unit volume of the bone trabeculae. For comparison, compact bone has a structural density of approximately 1.80 g/cm3, whereas cancellous bone has a density of 0.20 g/cm3 with a porosity of more than 75%. The strength and moduli of cancellous bone are related to its apparent density by a power law function (Keller 1994). The strength of cancellous bone varies widely over the range of observed densities - unlike the density of cortical bone the density of cancellous bone can vary by an order of magnitude so this is quite a significant variation potential; it is related to the square of the apparent density. Its modulus varies as either the square or cube of the apparent density. Both strength and modulus are sensitive to the rate of loading as well as the loading direction, although the effect of loading rate is less sensitive than the effect of density (Ouyang, Yang et al. 1997). Mid-range values for the strength and modulus of cancellous bone are 2.00–5.00 MPa and 90.0–400 MPa, respectively (Rohl, Larsen et al. 1991). As would be expected, the mechanical strength of cancellous bone is also highly dependent upon on the age of the individual due to age related variation in mineral content dependant on changes in diet, health and lifestyle (McCalden, McGeough et al. 1997).

2.2.3.B **Compact Bone**

Wolff's hypothesis that cortical bone is simply dense cancellous bone was shown to be misleading by Rho et al (Rho, Ashman et al. 1993). However, like cancellous bone, compact bone is anisotropic and to a great extent the direction of the osteons determines its mechanical properties. In a review by Yaszemski et al, (Yaszemski, Payne et al. 1996), the strength of compact bone in the longitudinal orientation (parallel to the long axis of bone and osteons) was reported as between 78.8 and 151 MPa in tension, and 131 and 224 MPa in compression. Compact bone was reported to be weaker in the transverse direction (perpendicular to the bone long axis and osteons direction), showing strengths of 51.0–56.0 MPa in tension, and 106–133 MPa in compression. The shear strength of compact bone, when tested in torsion, is between 53.1 and 70.0 MPa. In addition, the elastic moduli of compact bone are 17.0–20.0 GPa in the longitudinal direction (both in tension and compression), and 6–13 GPa in the transverse direction. The reported shear modulus is 3.30 GPa.

2.2.4 Composition

Histologically, bone can be divided into three components; the matrix, the cells of bone and the bone marrow. The matrix provides a supporting framework for the other components of bone and offers protection against the compressive, tensile, torsional and flexural stresses applied across the tissue during every-day events. The matrix also contains the *bank* of minerals which are reserved in bone. The various cell types found in bone are responsible for the up-keep of the supporting framework and release of minerals from the bank; ensuring that it responds to the changing demands placed upon it. Finally, the marrow contains the stem cells and vasculature required to supply the bone with an adequate supply of oxygen and nutrients and to maintain communication to the nervous system.

2.2.4.A **Matrix**

The matrix consists of two intimate phases; the inorganic or *mineral* and the organic (collagen and non-collagenous proteins) resulting in a well-engineered composite structure which gives bone its mechanical strength in all dimensions.

2.2.4.A.a *Inorganic*

Calcium phosphate $Ca_3(PO)_4$ mineral accounts for almost two-thirds of the weight of bone (Martini 1998). In a review of calcium phosphate biomaterials, Le Geros reported the now widely accepted view that the mineral component of bone is actually a carbonate-substituted hydroxyapatite with the approximate formula $(Ca,Mg,Na)_{10}(PO_4HPO_4CO_3)_6(OH)_2$ (LeGeros 2002). As a result of the substitution of trace elements at the calcium site and carbonate ions, predominately at the phosphate site (type B) (Elliott 1994), into bone apatite the calcium to phosphorus of bone mineral is reported as between 1.37-1.87 (Hing 2004c) compared to 1.67 for stoichiometric hydroxyapatite (Aoki 1991). Bone mineral consists of irregularly shaped platelets (of variable lengths with widths 30 to 45 nm and thickness of approximately 5 nm) that are oriented with their c axis parallel to one another and lie intimately along the collagen fibrils (Landis, Hodgens et al. 1996).

2.2.4.A.b *Organic*

The organic phase of the matrix is comprised of the collagenous and non-collagenous proteins which have varying involvement in determining the structure and regulation of bone:

2.2.4.A.b.i ***Collagen***

Collagen constitutes a high volume fraction within bone, typically in the region of 80-90%. This is in contrast to other connective tissues of the body where it constitutes closer to a volume fraction of 10% (Young 2003). Collagen is formed from a triple helix structure comprising two forms of collagen polypeptide chain. Several variants of collagen exist in physiological tissues (38 to be precise), but by far the most abundant variant in bone is type I collagen in which the triple helix structure is formed from two a1 chains, also expressed in the literature as COL1A1 or α1-I, and one a2 chain, also referred to as COL2A1 or a2-I.

Whilst within the cell the collagen chains comprise a precursor to collagen known as procollagen. This precursor contains proteins on each end called amino and carboxy procollagen extension propeptides. The presence of these extensions makes procollagen approximately one thousand times more soluble than collagen in its final form. Once procollagen chains have been assembled into fibrils they pass through the cell membrane. Outside of the cell, the collagen chains begin to form a tertiary structure through the crosslinking of adjacent chains. This ability for collagen to form complex hierarchical structures is what is thought to give bone its toughness. The strength and toughness of bone have been linked to the amount of cross-linking present in the collagen component (Knott and Bailey 1998).

2.2.4.A.c *Non-collagenous proteins*

The four most significant non-collagenous proteins found in bone are: Osteocalcin (OC), Osteonectin (ON), Osteopontin (OP) and bone sialoprotein (BSP). These proteins are of special interest since they have been demonstrated to regulate bone remodeling and mineralisation (Roach 1994).

Osteocalcin: this non-collagenous protein may play a role in bone resorption. Osteocalcin has an affinity for calcium and can be applied *in vitro* to inhibit mineralisation. Osteocalcin is thought to play a role in regulating osteoclasts by facilitating their differentiation (Roach 1994). At circa. 20%, it comprises the largest fraction of the non-collagenous proteins (Rammelt, Neumann et al. 2005).

Osteonectin: this protein has a close affinity to hydroxyapatite and calcium so is proposed as a nucleator for mineralisation of collagen. This non-collagenous protein is found at sites of remodeling. Previous studies have shown that osteonectin can

promote the formation of hydroxyapatite *in vitro* (Cowles, DeRome et al. 1998, Knabe, Berger et al. 2004).

Bone sialoprotein: this non-collagenous protein is proposed to act as a crystal nucleator (Roach 1994). BSP, as it is often referred to, has other proposed mechanisms of action; specifically that it mediates osteoblastic cell adhesion and stimulates the differentiation of osteoblasts. BSP has been suggested to be critical in de novo bone formation, whereas it is less important in bone growth (Cowles, DeRome et al. 1998, Knabe, Berger et al. 2004).

Osteopontin: sialoproteins are those that are conjugated with sialic acid. Osteopontin is one such sialic protein and is implicated in cell attachment within bone matrix. According to Roach et al., the role of osteopontin is less certain than for bone sialoprotein, but might be related to ensuring that only the right type of crystal is formed (Roach 1994). It was also proposed by Uemura et al., that osteopontin may be involved in signalling between osteoblasts and osteoclasts, via autocrine and paracrine interactions (Cowles, DeRome et al. 1998, Puleo and Nanci 1999, Uemura, Nemoto et al. 2001).

Alkaline phosphatase: ALP is a non-collagenous protein that is secreted from osteoblasts and is commonly used by researchers as a means to test for osteoblastic differentiation *in vitro* and *in vivo*. It is thought to promote crystal formation in matrix vesicles by removing nucleation inhibitors (Cowles, DeRome et al. 1998).

Fibronectin: this protein is expressed during intramembranous bone formation. Fibronectin has the ability to stimulate osteoblast progenitor proliferation, which makes this protein critical in early bone formation (Cowles, Brailey et al. 2000). As FN has also been shown to readily be adsorbed onto hydroxyapatite and cause the proliferation of osteoblasts, this protein is interesting to the researchers with an interest in osteoblast upregulation on biomaterials (Veiga, Elias et al. 1997, Garcia, Ducheyne et al. 1998, Degasne, Basle et al. 1999).

Vitronectin: this non-collagenous protein is necessary for cell attachment (Kim, Arakawa et al. 2003) and for cell migration (McKeown-Longo and Panetti 1996). Fibronectin and vitronectin are incorporated into extracellular matrices, including soft tissue organs, as well as being abundant in the human serum (Kilpadi, Sawyer et al. 2004) at a concentration varying between 200 and 400µg/ml (McKeown-Longo and Panetti 1996).

2.2.4.A.d *Soluble Factors*

Prostaglandins: these fatty acids promote the proliferation and differentiation of osteoclasts over extended periods. In contrast, they play an inhibitory role early on in the process of remodeling (Buckwalter, Glimcher et al. 1996b, Buckwalter, Glimcher et al. 1996a).

Fibroblast growth factors (FGF): this family of growth factors stimulate the proliferation of mesenchymal stem cells, pre-osteoblasts, osteoblasts and chondrocytes.

Insulin-like growth factors (IGF): this family of growth factors stimulate the proliferation of osteoblasts and chondrocytes and upregulates extracellular matrix secretion from both cell phenotypes (Buckwalter, Glimcher et al. 1996b, Buckwalter, Glimcher et al. 1996a).

Platelet-derived growth factor (PDGF): this growth factor upregulates the proliferation of chondrocytes and osteoblasts. At certain concentrations it has been found to have a down-regulating effect and has been linked to resorption (Buckwalter, Glimcher et al. 1996b, Buckwalter, Glimcher et al. 1996a).

Transforming growth factor (TGF): this growth factor upregulates differentiation of mesenchymal stem cells into chondrocytes, and may also induce osteoblast proliferation. Similarly to PDGF, TGF has been shown to increase bone resorption so it is thought to be responsible for coupling bone formation and resorption mechanisms (Buckwalter, Glimcher et al. 1996b, Buckwalter, Glimcher et al. 1996a).

Bone morphogenic proteins (BMP): this cellular messaging molecule is a cytokine and member of the TGF family of factors that stimulates proliferation and differentiation of both chondrocytes and osteoblasts (Buckwalter, Glimcher et al. 1996b, Buckwalter, Glimcher et al. 1996a).

Parathyroid hormone (PTH): this polypeptide causes the release of calcium from bone as well as upregulating osteoclast differentiation from osteoprecursor cells. It is thought to inhibit osteoblast function (Buckwalter, Glimcher et al. 1996b, Buckwalter, Glimcher et al. 1996a).

Oestrogen: this hormone has a complex effect on bone metabolism with the predominant outcome being down-regulated osteoclasts and decreased bone resorption (Buckwalter, Glimcher et al. 1996b, Buckwalter, Glimcher et al. 1996a).

Dexamethasone: this corticosteroid regulates events early in the differentiation of chondrocytes and induces fully differentiated chondrocytes to secrete alkaline phosphatase, suggesting it may be important in endochondral bone formation (Buckwalter, Glimcher et al. 1996b, Buckwalter, Glimcher et al. 1996a).

Thyroxin: this thyroid hormone stimulates osteoclastic bone resorption (Buckwalter, Glimcher et al. 1996b, Buckwalter, Glimcher et al. 1996a).

Calcitonin: this polypeptide lowers levels of blood calcium by inhibiting osteoclast function (Buckwalter, Glimcher et al. 1996b, Buckwalter, Glimcher et al. 1996a).

Interleukin-1 (IL-1): this protein stimulates proliferation of osteoclast precursor cells, thus increasing bone resorption (Buckwalter, Glimcher et al. 1996b, Buckwalter, Glimcher et al. 1996a).

Vitamin D: is implicated in osteoclast proliferation through the production of molecules such as osteopontin and osteonectin. It has been linked to bone resorption and matrix mineralization (Buckwalter, Glimcher et al. 1996b, Buckwalter, Glimcher et al. 1996a).

2.2.4.B **Bone cells**

Osteoblasts, osteocytes and osteoclasts are the three key bone cell phenotypes which coexist in bone and are responsible for the formation of bone, the maintenance of bone and remodeling of bone, respectively. Although other cells are necessary for the regular upkeep of bone, the endothelial cells of bone-vascularising tissues for example, the ‘bone cells’ are critical to the development of a micro- and macro-structure which is capable of responding to its mechanical and to some extent chemical environment.

2.2.4.B.a *Osteoblasts*

These cells are specialised cells of mesenchymal stem cell origin. They are

differentiated from pre-osteoblasts known as osteoprogenitor cells that originate from pluripotent mesenchymal stems cells of the bone marrow. When active, osteoblasts adopt a cuboidal morphology and are found on the surface of new bone, where there is active bone formation. The principal function of osteoblasts is to lay down new bone through the process of lamellar bone formation. They achieve this by secreting extracellular matrix that is subsequently mineralised to form woven bone. Type I collagen is produced in vast amounts by osteoblasts during the process of bone formation. Osteoblasts also release extracellular organelles, known as matrix vesicles which contain alkaline phosphatase amongst other regulating molecules (Mohamed 2008).

2.2.4.B.b *Osteocytes and bone lining cells*

Osteocytes are cells that have become trapped in mineralising matrix as the process of lamellar bone proceeds. They are effectively osteoblasts that have been submerged within the mineralised extracellular matrix that they themselves have produced. Osteocytes are post-proliferative and constitute the final cell phenotype in the osteoblastic lineage. The osteocytes reside in lacunae, which are the regularly distributed pores and channels of approximately 25 microns in size that are found in the microstructure of mature physiological bone. The morphology of osteocytes becomes gradually more and more dendritic and they become less populated by organelles as they age. The dendritic extensions of osteocytes allow them to communicate between each other and osteoblasts in the mineralising front (Mohamed 2008).

2.2.4.B.c *Osteoclasts*

Osteoclasts are multinucleated phagocytic cells derived from the macrophage monocyte lineage. These cells migrate from bone marrow and can fuse together to from *de novo* multinucleated cells. Osteoclasts are involved in bone remodelling through resorption of mineralised bone matrix. During resorption osteoclasts exhibit characteristic ruffled borders, a sealing zone, the basal membrane, and a functional membrane zone. Within the ruffled zone, organic acids and proteolytic enzymes, such as collagenase, are secreted onto the surface of bone. The sealing zone localises these organic acids and proteinases on the surface of the substrate. The dissolved inorganic components and digested organic molecules are enveloped by the osteoclasts and removed from the resorptive zone (Mohamed 2008).

2.2.4.C **Bone Repair**

In highly vascularised tissues, such as mature cancellous bone, an acute traumatic injury results in a series of physiological responses including inflammation, repair and remodelling. These physiological responses lead to a sequence of cellular, hormonal and vascular events, beginning with the release of inflammatory mediators such as cytokines and ending when the remodelling of the damaged tissue (Alberts, Bray et al. 1994, Buckwalter, Einhorn et al. 1996).

2.2.4.D **Inflammation**

A haematoma forms in bone immediately post-injury and is formed from cells of the periphery vascular system and intramedullary canal (McKibbin 1978, Marsell and Einhorn 2011). An inflammatory response is required for healing to take place as the haematoma forms the scaffold in which a callous is developed in the later phases of bone healing. An acute inflammatory phase begins within 24 hours immediately post-trauma and typically continues for a further 7 days (McKibbin 1978, Marsell and Einhorn 2011). Tumour necrosis factor-α (TNF-α), interleukin-1 (IL-1), IL-6, IL-11 and IL-18 are secreted as part of the proinflammatory response. The factors are known to be responsible for the recruitment of inflammatory cells and to promote angiogenesis. During the first 3 days of the inflammatory response TNF-α is secreted by macrophages. This molecule is responsible for inducing secondary inflammatory signalling molecules and for chemotaxis inflammatory cells. TNF-α has been shown to upregulate mesenchymal stem cell differentiation *in vitro*. IL-1 and IL-6 are thought to be the most important in bone healing. Like TNF-α, IL-1 is produced by macrophages in the acute phase of inflammation and upregulates production of IL-6 by osteoblasts. IL-1 also promotes the formation of a callus and angiogenesis in the site of injury. IL-6 upregulates the production of vascular endothelial growth factor (VEGF) and the differentiation of osteoblasts and osteoclasts (McKibbin 1978, Marsell and Einhorn 2011).

2.2.4.E **Mesenchymal stem cell recruitment**

In order for repair of the injury to occur MSCs must be recruited to the site and then differentiate into chondrocytes and osteoblasts (Marsell and Einhorn 2011). The source of these MSCs is not currently fully understood. Undoubtedly some of these MSCs originate from the surrounding tissues to the injury site, but data also supports the theory that circulating systemic MSCs are important to bone repair. Bone morphogenetic proteins (BMP2 and BMP-7) are reported to be responsible for

recruitment of stem cells, as are the cytokine SDF-1; nitric oxide; and growth factors, such as VEGF and G-CSF (Rennert, Sorkin et al. 2012).

2.2.4.F **Callus formation**

During direct fracture healing, also termed contact healing (for reductions of <0.01mm) or gap healing (for reductions >0.01mm <1mm) is often the primary goal after open reduction and internal fixation orthopaedic surgery (Marsell and Einhorn 2011). Contact healing does not result in the formation of a callus as the damaged end plates of bone are restored only through osteoclastic and osteoblastic resorption and bone formation in alignment with the existing micro- and macro-structure of the pre-existing bone. For gap healing a callus is formed from woven bone that is produced through lamellar bone formation. Endochondral bone formation is not characteristic of direct fracture healing (Marsell and Einhorn 2011).

For indirect fracture healing, which is the predominant process for bone repair when there is poor anatomical or biomechanical alignment between the damaged ends of bone, a callus is formed via a cartilaginous phase. Indirect bone healing most closely resembles the embryonic process of bone formation. Following the formation of a haematoma, a granulation tissue that is rich in fibrin is formed. Endochondral bone is formed in between the fracture surfaces. This soft, collagenous tissue is less mechanically stable than intramembranous bone, but provides a stable scaffold for the fracture site to heal. A hard callus is formed as intramembranous bone is laid down on the fracture end plates. This mineralised callus forms a bridge across the fracture site which provides mechanical stability. The process of callus formation is dependent upon MSC recruitment, since without these cells the bone formation cascade cannot commence (Marsell and Einhorn 2011, Rennert, Sorkin et al. 2012). The peak of callus formation is usually reached by day 14 in preclinical models as determined with hard tissue histology and also with histochemistry for extracellular markers such as type I collagen, osteocalcin, alkaline phosphatase, and osteonectin (Marsell and Einhorn 2011).

2.2.4.A **Mineralisation and resorption of the cartilaginous callus**

For indirect fracture healing, the primary soft cartilaginous callus is removed from the defect site in order for a hard tissue callus to replace it. This process is akin to embryonic bone formation during which proliferation and differentiation is followed by cell volume expansion and matrix deposition (Marsell and Einhorn 2011).

2.2.4.A **Neovascularisation**

The presence of an adequate blood supply is critical to the provision of oxygen and essential nutrients to the cells recruited to the site of injury. During endochondral bone formation the vascular system is required to remove apoptised chondrocytes and extracellular matrix (Marsell and Einhorn 2011). Revascularisation of injured bone is regulated via two pathways, an angiogenic pathway and a vascular endothelial growth factor-dependent pathway (Marsell and Einhorn 2011, Stegen, van Gastel et al. 2015). Angioproteins, which are responsible for angiogenesis, are vascular morphogenetic proteins and their expression occurs early in the bone formation cascade, suggesting that they are responsible for the initial phases of neovascularisation (Stegen, van Gastel et al. 2015). VEGF is thought to be the predominant regulator of revascularisation since osteoblasts and chondrocytes both express high levels of VEGF during bone repair (Stegen, van Gastel et al. 2015).

2.2.4.B **Remodelling**

For both pathways of bone healing the resultant callus (whether formed from woven bone or mineralised cartilaginous tissue) has the primary function of providing mechanical stability within the repair site as soon as possible after injury. However, in the longer term the desired outcome is for the tissue to be returned to its mature physiological state, which in the case of cancellous bone is of a trabecular structure. The final step in the healing of a fracture site is a secondary resorptive phase that is responsible for developing an open and interconnected macroporous and microporous lamellar bone morphology. This phase is regulated by IL-1 and TNF-α, whilst BMP-2 also plays a significant role in this stage of bone repair (Marsell and Einhorn 2011).Osteoclasts are responsible for remodeling bone into a trabecular structure. Osteoclasts and osteoblasts act in consort to lie down and resorb lamellar bone in response to the mechanical stresses which are applied to the injury site. Osteoclasts are active within site of injury within 3-4 weeks in humans (Marsell and Einhorn 2011) but even earlier in some animal models (Campion, Chander et al. 2011).

2.3 *In Vivo* and *in vitro* Studies of Mechanobiology

One significant barrier to a greater understanding of bone physiology at the cellular level is the lack of methodology to study bone cells in their native environment. In

addition, no harmonised method for the study of bone biology *in vitro* has emerged from the myriad of experimental work which has been undertaken in the field over the last thirty years. A vast amount of work has focussed on the empirical responses of individual and occasionally co-cultured cells to mechanical and chemical stimuli (Klein-Nulend, Semeins et al. 1995, Klein-Nulend, van der Plas et al. 1995, Roelofsen, Klein-Nulend et al. 1995, Klein-Nulend, Roelofsen et al. 1997, Klein-Nulend, Helfrich et al. 1998, Pavalko, Chen et al. 1998, Sterck, Klein-Nulend et al. 1998, Ajubi, Klein-Nulend et al. 1999, Joldersma, Burger et al. 2000, Westbroek, Ajubi et al. 2000, Bakker, Soejima et al. 2001, Bakker, Joldersma et al. 2003, Bacabac, Smit et al. 2004, McGarry and Prendergast 2004, Bacabac, Smit et al. 2005, McGarry, Klein-Nulend et al. 2005), but few studies have taken investigations a step further by determining material-specific responses driven by the micro-cellular mechanobiological environment (Di Palma, Douet et al. 2003, Sikavitsas, Bancroft et al. 2003, Wang, Uemura et al. 2003, Mauney, Sjostorm et al. 2004, Di Palma, Guignandon et al. 2005, Ignatius, Blessing et al. 2005, Sikavitsas, Bancroft et al. 2005, Tanaka, Sun et al. 2005). Those studies that have looked at the substrates' influence on mechano-stimulation of bone cell cultures have generally focussed on one attribute of the material such as substrate roughness (Di Palma, Guignandon et al. 2005), substrate chemistry (Di Palma, Douet et al. 2003, Sikavitsas, Bancroft et al. 2005), or pore size (Tanaka, Sun et al. 2005). No one study has used an integrated approach to differentiate between the influences that surface topography; material permeability; pore geometry; or bulk modulus might have on the Mechanobiology of *in vitro* bone cell cultures. This, surely, is the next step to bridging the gap between our understanding of 2D in vitro cell behaviour and the Mechanobiology of bone *in vivo*.

It is also reasonable to suggest that when a cell is removed from its native environment and reintroduced into an extracorporeal setting, it is expected that the cell will have to adapt to its new environment; the cell must recondition itself to respond to different cues. Sorkin suggests that this 'culture shock' can be better mitigated by better emulating physiological conditions *in vitro* (Sorkin, Dee et al. 2004).

2.3.1 Osteocytes as mechanosensory cells

Mechanical adaptation is a cellular process and needs a biological system that senses the applied mechanical loading. The loading information must then be communicated to effector cells that can be make new bone or destroy old bone.

Osteoblasts produce new bone by calcifying collagen; and osteoclasts are the cells that can degrade bone matrix by demineralisation and collagen degradation. However, the great majority of cells residing in bone (95%) are osteocytes which are embedded within the calcified matrix and bone-lining cells on the surfaces of bone. Unlike osteoblasts and osteoclasts, osteocytes are buried in bone matrix and are connected to neighbouring osteocytes via long slender cell processes which are joined by gap-junctions. The matrix directly surrounding the osteocytes is not calcified and allows the formation of a three-dimensional network of connected cells. As new osteoblasts are recruited to the new bone-forming surface to replace the old osteoblasts that have become isolated in mineralised matrix, they also become trapped in matrix and differentiate into osteocytes. As recruitment fades, osteoblasts at the surface flatten out to form bone-lining cells. The formation of an interconnected three-dimensional network is a very attractive structure for providing a mechano-sensing function (Burger and Klein-Nulend 1999b). The lacunar-canalicular is an interconnected porous scaffold that allows for the transfer of fluid and small molecules from the surface to the centre of bone. This lacunar-canalicular porosity allows for the recruitment of new osteoblasts with anabolic paracrine factors excreted in the extracellular matrix by osteocytes, the mechanosensing cells of bone (Sikavitsas, Bancroft et al. 2003).

Although the concept that osteocytes are the primary cells involved in the mechanosensory role in bone, they are relatively unstudied *in vitro*. This is attributed to the fact that osteocytes are post-mitotic and therefore do not differentiate. They are also relatively inactive with respect to protein synthesis.

2.3.1.A **Fluid flow as a mechanical stimulus for osteocytes**

A number of researchers hypothesise that flow of interstitial fluid flow is the most probable way of informing bone cells about mechanical loading (Pavalko, Chen et al. 1998, Ajubi, Klein-Nulend et al. 1999, Joldersma, Burger et al. 2000, Westbroek, Ajubi et al. 2000, Bakker, Soejima et al. 2001, Wang, Uemura et al. 2003, Sikavitsas, Bancroft et al. 2005). Flow of interstitial fluid occurs because the application of mechanical strain causes the volume of some pores to decrease slightly, creating differences in bone fluid pressure, which results in fluid flow (Sikavitsas, Temenoff et al. 2001). Although it is important in the lacunar-canalicular porosity, it is negligible in the Haversian lumens and Volkmann canals (vascular porosity) because these are 1000 times larger and their pressure is more uniform since it must be equal to the blood pressure (Cowin and Weinbaum 1998). Since

osteocytes are the only cells which inhabit the lacunar-canalicular porosity previous studies have postulated that they must be considerably involved in mechanotransduction.

2.3.1.B *In vivo* studies of the mechanosensory role of osteocytes

In vivo studies of osteocytes are relatively sparse since osteocytes are trapped within hard mineralised matrix. However, one *in vivo* study showed that osteocytes express mRNA for ß-actin, Osteocalcin, connexion-43, insulin-like growth factor I (IGF-I), cc-fos and c-jun but not tumour necrosis factor α (TNF-α) or tartate-resistant acid phosphatase (TRAP) (Mason, Hillam et al. 1996).

2.3.1.C Effect of fluid flow on osteocytes *in vitro*

Osteocytes isolated from chicken calvariae responded to between five and sixty minutes of pulsating fluid flow (PFF) by producing higher basal and PFF-stimulated levels of NO than mixed bone cells; whilst Fibroblasts did not respond to flow at all (Klein-Nulend, Semeins et al. 1995). The pulsatile frequency used in the study was 5Hz with a fluid shear stress of 0.5±0.02Pa and the peak shear stress rate 0.4 Pa/sec. The characteristic osteocytic morphology was restored *in vitro* following PFF treatment. PFF also increased PGE2 production. PGE2 production was delayed but continued throughout the hour whilst NO production was transient and only occurred for the first 5-10 minutes. Prostaglandins are found to be essential in the transduction of mechanical stimuli into bone formation.

Klein Nulend, Van der Plas et al., had shown previously that osteocytes respond to a lesser extent to intermittent hydrostatic compression (IHC) (Klein-Nulend, van der Plas et al. 1995). For IHC, osteocytes responded by an increase in PGE2 after 6/24 hours and an increased PGI2 after 24hours. Osteoblasts only showed a significant increase after 6hours and periosteal fibroblasts didn't respond at all. PFF stimulated release of Prostaglandin E_2 (PGE_2) from osteocytes but not from Osteoblasts or from fibroblasts. No effect was found for Prostaglandin I_2 (PGI_2) in any cell group after PFF treatment. Osteocytes response was sustained 1hour after flow whereas Osteoblasts/fibroblasts did not respond after five minutes following treatment.

Osteocytes exhibit inducible prostaglandin G/H synthase-2 (PGHS-2) activity, therefore, observations made regarding effects of PFF are linked to mechanosensitivity of osteocytes and not ability to express PGHS-2 (Westbroek,

Ajubi et al. 2000). Osteocytes are more sensitive to fluid shear stress than osteoblasts, as measured by PHGS-2 expression. Westbroek postulated that Klein-Nulend may have observed PGE_2 expression in osteoblasts in previous studies due to presence of osteocytes in the culture of the state of differentiation in the relatively mature neonatal murine cell cultures.

In osteocytes modulation of NO production occurs by cytoskeleton disruption (McGarry, Klein-Nulend et al. 2005). The inhibition of PFF-induced PGE2 response in osteocytes with cytoskeleton disruption indicates a high dependence of osteocytes on actin-rich cytoskeleton. Cellular deformation as a result of fluid flow induced stresses leads to actin-dependent opening of calcium (Ca^{2+}) - permeable, gadolinium sensitive ion channels in the osteocyte cell membrane (Ajubi, Klein-Nulend et al. 1999). Ajubi suggested that the Ca^{2+} influx near surface membrane stimulates phospholipase C (PLC), which generates secondary Ca2+ responses from internal stores. Diaclyglyderol (DAG-a by-product of PLC) and Ca2+ activate protein kinase C (PKC) which enhances PLA sensitivity to Ca2+, leading eventually to increased arachidonic acid (AA) release. This together with NO production mediated cyclooxygenase (COX-2) activation leads to PG synthesis.

2.3.2 The role of osteoblasts in Mechanotransduction

Although osteocytes appear to be involved in bone mechanotransduction, osteoblasts seem to be affected by mechanical signals too. A number of studies have investigated the effect of mechanical stimuli on osteoblasts (Table 01). Osteoblasts are pre-mitotic and therefore differentiate. They are also relatively active with respect to protein synthesis compared to osteocytes. These two factors, in combination with the availability of a number of different osteoblastic cell lines, have made them a popular choice in the investigative field of mechanotransduction.

2.3.2.A **Effect of fluid flow on osteoblasts *in vitro***

Apart from the direct effect of mechanical strain on osteoblasts, fluid shear stresses may act as mechanical stimuli on osteoblasts. Application of fluid shear induces development of actin stress fibres and the formation of focal adhesions containing B-integrins and A-actinin (Pavalko, Chen et al. 1998). Osteoblasts upregulate Cox-2 and c-fos expression in response to fluid shear through a mechanism that involves the reorganisation of the actin cytoskeleton. Inhibition of actin stress fibre development by treatment of osteoblastic cells with cytochalasin D, by expression of

a dominant negative form of the small GTPase Rho, or by microinjection into the cells of a proteolytic fragment of α-actinin that inhibits α-actinin-mediated anchoring of actin filaments to integrins at the plasma membrane each blocked fluid-shear-induced gene expression in osteoblasts. Rho-mediated stress fibre formation and the α-actinin-dependent anchorage of stress fibres to integrins in focal adhesions may promote fluid-shear-induced metabolic changes in osteoblasts.

Osteoblastic bone cells respond to flow in a dose-dependent manner (Bakker, Soejima et al. 2001). Increasing viscosity also increases responses. Increasing the viscosity will simultaneously heighten the mean shear stress and the amplitude of the pulsatile shear stress, but the exact mode of Upregulation has not determined. In a second study of the effects of viscosity dextran was added to the media to increase the viscosity which increased mineralised matrix deposition (Sikavitsas, Bancroft et al. 2003). Alkaline phosphatise (AP) was significantly higher for fluid sheared cells. Upregulation from a change in fluid shear stress modulated by viscosity and not flow rate indicates that the rate of chemotransport is not a factor in the upregulation of osteoblastic cells in response to increased fluid shear.

Bone cell response to fluid shear stress is rate-dependent (Bacabac, Smit et al. 2004). Increasing amplitude or frequency without changing average stress enhances NO production. NO production is linearly dependent on the rate of fluid shear stress. Later it was shown that although osteoblastic cell response to fluid stress is rate dependent, an initial stress kick is required for the cells to respond (Bacabac, Smit et al. 2005). Cytoskeletal arrangement during a pre-treatment phase may explain the lack of response without a stress kick. Cellular sensitivity to stress occurs in under 1 min. However, cells were not affected by a short stress kick (10s; 0.7Pa) so the effect of stress on NO production occurs between 10s - 1min. In addition, treatment with parathyroid hormone (PTH) without shear stress stimulated PGE_2 production but not NO production (Bakker, Joldersma et al. 2003). When PTH was added <1min before shear stress treatment it blocked NO production. It is suggested, therefore, that PTH inhibits NOS (ecNOS) in bone cell production of NO.

PGE_2 and PGI_2 have been upregulated in mature human osteoblasts following PFF treatment, whereas PGF_2 was upregulated for 1 hour only (Joldersma, Burger et al. 2000). Treatment with PFF increased COX-2 but not COX-1 expression. The levels of prostaglandin production varied significantly between cell-donors and were related to the variation in residual osteocyte population numbers. Interestingly, a correlation analysis showed there was no relationship between donor age and bone

cell sensitivity.

2.3.3 Comparison of bone cell responses to fluid flow and strain-induced stresses

Various mechanical stimuli have been studied in the field of mechanotransduction, including: Intermittent hydrostatic compression (Klein-Nulend, van der Plas et al. 1995, Roelofsen, Klein-Nulend et al. 1995, Klein-Nulend, Roelofsen et al. 1997, Nagatomi, Arulanandam et al. 2003); continuous fluid flow (Pavalko, Chen et al. 1998, Sikavitsas, Bancroft et al. 2003, Wang, Uemura et al. 2003, Sikavitsas, Bancroft et al. 2005); pulsating fluid flow (Klein-Nulend, Semeins et al. 1995, Klein-Nulend, Helfrich et al. 1998, Sterck, Klein-Nulend et al. 1998, Ajubi, Klein-Nulend et al. 1999, Joldersma, Burger et al. 2000, Westbroek, Ajubi et al. 2000, Bakker, Soejima et al. 2001, Bakker, Klein-Nulend et al. 2003, Nagatomi, Arulanandam et al. 2003, Bacabac, Smit et al. 2004, McGarry, Klein-Nulend et al. 2005); piezoelectric induced strain (Di Palma, Douet et al. 2003, Di Palma, Guignandon et al. 2005, Tanaka, Sun et al. 2005); four-point bending induced strain (Mauney, Sjostorm et al. 2004, McGarry and Prendergast 2004); and tensile-induced strain (Ignatius, Blessing et al. 2005).

To further clarify the nature of the actual sensing mechanism of mechanotransduction on osteoblasts, mechanosensing in osteoblasts by shear stress has been compared with mechanosensing by direct mechanical strain. In one comparative study the investigators found that both fluid flow and mechanical strain increased NO production, whilst only fluid flow increased prostaglandin production (Mullender, El Haj et al. 2004). Furthermore, substrate strains enhanced the bone matrix protein collagen I two-fold, whereas fluid shear caused a 50% reduction in collagen type I.

FEA modelling has revealed that fluid flow effected all cell model components whereas strain only effected the cell attachments (McGarry and Prendergast 2004). Fluid flow (not strain) increases PGE_2 due to upregulation of Cox2 and re-organization of actin. Mechanically-induced NO production results from activation of ecNOS in the plasma membrane and is affected most by fluid-shear. Collagen production was upregulated by strain and not fluid shear and the applied strain induced cell behaviour associated with the osteoblastic phenotype. Whereas, fluid-shear did not elicit responses of the osteoblast phenotype. Instead increased cell signalling molecules (NO/PGE_2) are reported. Both of which are thought to be

involved in osteocyte mediation.

2.3.4 Osteoclasts and mechanotransduction

Osteoclasts are not thought to be mechanosensory cells although one proposed theory explains their involvement as a secondary effector in the mechanotransductory response (Burger, Klein-Nulend et al. 2003): the alignment of secondary osteons as well as the constancy of their diameter is a product of osteoclast attraction and rejection by osteocytes under opposite local strains, leading to reduced and enhanced canalicular flow, respectively. NO is likely a key molecule in this process, as its absence would lead to osteoclast attraction by causing osteocyte apoptosis, while its production by well-strained osteocytes leads to osteoclast withdrawal.

2.4 Bone Grafting

Bone grafts are required for a wide range of situations in which the bone cannot naturally regenerate. They are typically used to fill small voids (such as small bone tumours, following bone fracture reduction or in osteotomies and plastic surgery). Bone grafts are also applied clinically to enhance and stabilize instrumentation over time. With a variety of sources of bone graft, both natural and synthetic, comes a wide range of inherent properties. An entire nomenclature exists for these properties that can be used to differentiate between these grafts in terms of their clinical utility. Here follows definitions for each of the most commonly used terms:

Osteoconductive: Biocompatible materials which provide a physical structure into and along which bone may grow (Miyazaki, Tsumura et al. 2009).

Osteoinductive: Capable of inducing bone formation in a non-bony site by recruiting and inducing (pluripotent) stem cells to become osteoblasts (Miyazaki, Tsumura et al. 2009).

Osteogenic: Containing the cells required to produce bone (Miyazaki, Tsumura et al. 2009).

Osteostimulative: The ability to signal or activate cells to enhance bone growth (Miyazaki, Tsumura et al. 2009).

Bioactive: Has the propensity to form a bone-like mineral layer on its surface following submersion in simulated body fluid (Kokubo, Ito et al. 1990, Kokubo, Kushitani et al. 1990).

2.4.1 Autografts

Autologous bone, otherwise known as autograft, is bone harvested from the patient's own body (Giannoudis, Dinopoulos et al. 2005, Dinopoulos, Dimitriou et al. 2012). Autologous bone is most frequently harvested from the iliac crest as it provides access to relatively good quality and quantity cancellous bone. Autologous graft can also be collected during surgery and applied in a defect local to the harvest site. As such this autograft is known as 'local bone'. Local autologous bone can typically be collected during surgeries such as posterolateral and interbody lumbar fusions in the spine, during which the spinous processes; facets; and lamina may be expended for the reasons of procedural access or in order to provide local graft, or both.

Autograft, whether from the iliac crest or from local sources, has been the standard of care for bone grafting for many years and is thus considered the 'gold standard' by clinicians (Giannoudis, Dinopoulos et al. 2005, Dinopoulos, Dimitriou et al. 2012). The advantage of autografting is that there are no direct acquisition costs relating to sourcing the graft, which is in contrast to other sources, as we will discuss next. As autograft is harvested and implanted in the same patient there is no chance for disease transmission and a very low risk of immunogenic response (Giannoudis, Dinopoulos et al. 2005, Dinopoulos, Dimitriou et al. 2012). According to the definitions provided above, autograft can be considered osteoconductive, osteogenic, and osteoinductive.

Despite the wide use of autografting, there are several known clinical and logistical limitations with using this approach. The most commonly understood include: a wide range of complication rates (9-49%), donor site pain, scarring, increased risk of infection, poor quality donor bone, elongated surgery time, additional need for post-operative analgesia, and limited supply (Giannoudis, Dinopoulos et al. 2005, Kim, Rhim et al. 2009, Dinopoulos, Dimitriou et al. 2012). Furthermore, additional adverse clinical effects include: haematoma formation, increased blood loss, nerve damage, hernia formation, arterial injury, ureteral injury, pelvic instability, cosmetic defects, and tumour transplantation (Giannoudis, Dinopoulos et al. 2005, Dinopoulos, Dimitriou et al. 2012).

The disadvantages of autograft are only too well understood by this author. With the permission of the reader this author would like to briefly deviate from this objective review of the literature to provide a subjective testimonial. Despite being only 26 years old in 1985 my mother required a bone graft after having major surgery on her hip due to developing osteoarthritis of the joint. My mother was not offered a choice over which bone graft she would receive, because at the time only autologous bone was a viable option. A wedge resection of her iliac crest was performed to collect the necessary bone. Unfortunately my mother suffered a suspected infection that prevented spontaneous healing of the wedge defect. I was only 5 years old at the time, but I remember her being very immobile and needing a crutch to walk for nearly a year after the operation. Despite it being thirty years since her procedure she still complains of pain and weakness in her pelvis in the region of the harvest site. Not every patient who undergoes an autografting procedure experiences this degree of complications, but despite autograft being considered the gold standard, it is certainly not without its faults.

2.4.2 Allografts

An alternative option available to clinicians is the use of allograft human bone which is bone donated either from a live patient, for example a femoral head as a result of a hip procedure, or from the deceased (Giannoudis, Dinopoulos et al. 2005, Miyazaki, Tsumura et al. 2009, Dinopoulos, Dimitriou et al. 2012). The advantage of using an allograft compared to autograft is that there is no need for a second procedure to harvest the graft material. On top of the reduced surgery time this eliminates the problems of donor site morbidity and pain. Allografts are claimed to retain their osteoinductive potential, since the non-collagenous proteins remain in the graft prior to implantation. However, *in vitro* studies have demonstrated variability with regards the osteoinductivity of allografts as a result of the means to process them ready for clinical use (Giannoudis, Dinopoulos et al. 2005, Miyazaki, Tsumura et al. 2009, Dinopoulos, Dimitriou et al. 2012). Other disadvantages to allografting include: variability quality of the donor bone, risk of disease transmission, infection, low therapeutic dose of osteoinductive factors, and donor consent (Giannoudis, Dinopoulos et al. 2005, Miyazaki, Tsumura et al. 2009, Dinopoulos, Dimitriou et al. 2012).

2.4.3 Demineralised bone matrix (DBM)

Often considered, the modern allograft, DBM's were developed to provide clinicians with an alternative to traditional strut allograft. The process of manufacture of such grafts typically involves submerging and rinsing the donated bone in acid solutions in order to remove the mineral content of bone. This process leaves behind all the collagen and non-collagenous proteins in the source bone. The resultant material is typically admixed to natural or synthetic biomaterials that provide cohesivity, mouldability, and adhesiveness to the graft. This provides surgical utility to the graft during a grafting procedure. The advantages of DBMs are that they have been demonstrated as osteoinductive through in vitro and in vivo tests, they provide some degree of osteoconductive scaffold through the provision of collagen particles and fibres, and they have advantageous handling properties (Giannoudis, Dinopoulos et al. 2005, Lee, Roper et al. 2005, Miyazaki, Tsumura et al. 2009, Bae, Zhao et al. 2010, Dinopoulos, Dimitriou et al. 2012).

The disadvantages of DBM include: no mineral scaffold for osteoconduction, the potential for migration due to compression or irrigation, the variable quality due to the donor, the cost, and the risk of infection (Giannoudis, Dinopoulos et al. 2005, Lee, Roper et al. 2005, Miyazaki, Tsumura et al. 2009, Bae, Zhao et al. 2010, Dinopoulos, Dimitriou et al. 2012).

2.4.4 Synthetic bone grafts

Synthetic bone grafts such as hydroxyapatite, tricalcium phosphate, calcium sulphate, and bioglass have been used in clinical practice for several decades. In the previous sections of this chapter, the clinical need for synthetic replacements of autograft and allograft has been outlined. Carbonate-substituted hydroxyapatite with the approximate formula $(Ca,Mg,Na)_{10}(PO_4HPO_4CO_3)_6(OH)_2$ exists as approximately 5% of the human body mass (Ravaglioli 1992), so the development of pure synthetic hydroxyapatite forms which are readily available and compatible with sterilisation led to a considerable interest in the material as a biomaterial for the treatment, augmentation and replacement of osseous tissue in the twentieth century. The term "Apatite's" was derived from the Greek word "apato", meaning deceit, by a mineralogist named Werner in the 1970's. Apatite's can undergo numerous ionic substitutions into their crystalline structure and can assume many identities which was Werner's' basis for naming apatite's in such a way. Biologically this phenomenon is observed in the numerous substitutions, such as Fe^{2+}, Mg^{2+}, Zn^{2+}, F-, Cl- and citrate ionic substitutions, that occur in tissues such as bone, dentine and

enamel (Aoki 1994). Importantly, the ability of bone mineral to perform ionic substitutions to such an extent allows it to act as a calcium and mineral reservoir which necessitates a significant role in mineral homeostasis. Synthetic hydroxyapatite, however, is generally manufactured in the pure form but is an attractive biomaterial since it closely resembles bone mineral chemically and has been proven to be compatible with bone tissues in vitro and in vivo (Jarcho 1981, Winter 1981).

The perceived clinical disadvantage to phase pure hydroxyapatite is its slow rate of resorption *in vivo* due to its high crystallinity and stability (Suchanek, Yashima et al. 1996, Greenspan 1999, Laurencin 2003). The fact that the hydroxyapatite remains *in situ* might not offer any significant biological disadvantages, but clinicians anecdotally expressed a desire to see such bone grafts resorb so that clinical x-rays could be used to identify the rate and progress of remodelling of new bone. Hydroxyapatite is radiopaque and hence masks, to a certain extent, the presence of new bone on x-ray. The technical solution to this is to select a more resorbable phase of calcium phosphate (Barrere, van der Valk et al. 2003) which will dissolve *in situ* and thus be less radiopaque. Tricalcium phosphate (TCP), with the chemical formula $Ca_3(PO_4)_6$ and a calcium to phosphorus ratio of 1.5, is one such example which has been investigated in preclinical studies and used in clinical practice (Blitterswijk, Bakker et al. 1991, Hunter, Archer et al. 1995, Boyan, Hummert et al. 1996, Cao and Hench 1996, Healy, Thomas et al. 1996, Ozawa and Kasugai 1996, Anselme 2000, Park and Bronzino 2003). Another such example is calcium sulphate (CaS), otherwise known as plaster of Paris. The challenge with highly resorbable phases such as TCP and CaS is that due to their relative instability compared to hydroxyapatite they can dissolve too quickly for complete osteointegration into a treated bone defect (Hing, Wilson et al. 2007).

2.4.5 Bone morphogenetic proteins (BMPs)

In recent years recombinant human bone morphogenetic proteins have found a place within the bone grafting treatment paradigm since these cytokines can direct mesenchymal stem cells to differentiate into an osteogenic bone line. The advantages of rhBMPs in clinical application are that they are osteoinductive, effective at promoting bone growth and they are supported with a substantial amount of clinical data. The adverse event profile of these therapies are becoming better understood in recent years. The reported disadvantages of rhBMPs include ectopic bone growth, swelling and excessive resorption, amongst many others (Vaidya, Weir et al. 2007,

Wong, Kumar et al. 2008).

2.5 Osteoinductivity

Osteoinduction is a well-known phenomenon; in fact as of January 2015 a search of the U.S. National Library of Medicine at the National Institutes of Health will elicit 657 related articles using only the term 'osteoinduction'. The challenge for any reviewer doesn't stop at the number of articles to review but also the breadth of associations with this phenomenon.

2.5.1 A history of osteoinduction

Osteoinduction is a scientific reference to a biological process; the induction of bone formation (osteogenesis), but this process is also referred to by clinicians as either ectopic bone formation (the pathological condition) or heterotrophic ossification (the process behind the pathological condition). Clinical manifestations of osteoinduction are well known. *Myositis ossificans traumatica* (ossification occurring after recalled trauma, such as blunt injury, surgery, or burns); *Shooter's bones* (localized ossification in the deltoid muscle of shooters); and *Rider's bones* (localized ossification of the inner aspect of the lower end of the tendon of the adductor muscle of the thigh; sometimes seen in horseback riders) are three of the most common examples. Expanding the literature search to include all of the above terms leads to 3992 hits when searching the same library.

The term osteoinduction is also used to describe a number of different observations within the scientific literature. It was over eighty years ago that Charles Huggins (Huggins 1931) reported that he could stimulate the formation of bone in the abdominal fibrous tissue of a dog using transplants of the urinary bladder epithelium, which he referred to as heterotrophic ossification. In 1965 Marshall Urist then discovered that he could induce the process of osteogenesis in the muscle pouches of rats, rabbits, pigs, calves, and even humans using decalcified bone tissue (Urist 1965). Urist subsequently linked this effect with bone morphogenetic proteins (BMPs) which remained in the devitalised tissue after decalcification. Since Urist's work was published the term osteoinduction has been closely associated BMPs even though at the time he referred to the process as osteogenesis by autoinduction. The enormous volume of scientific research on BMPs since (18883 journal publications in January 2015) and the use of the term osteoinduction in this context have further

consolidated this association.

From the 1970's until the present day a number of researchers have also demonstrated osteoinduction by biomaterials. Winter was the first in 1970 (Winter 1970). Each researcher has since used whichever term was appropriate to their own perspective at the time. Some researchers have even described the same process in as many as six different ways over a period of only ten years: "Material-induced bone formation (osteoinduction)" (Yuan, van Blitterswijk et al. 2006b); "Induced osteogenesis" (Yuan, De Bruijn et al. 2001a); "Bone formation in extraskeletal sites" (Yuan, Zou et al. 1998); "Bone formation induced in non-osseous sites" (Yuan, Li et al. 2000); "Induced bone formation in extraskeletal sites without additional osteogenic cells or bone morphogenetic proteins" (Yuan, Kurashina et al. 1999); "Induced bone morphogenesis in extraskeletal tissues" (Yang, Yuan et al. 1997).

The use of so many different terms to describe what is seemingly the same biological process and outcome has only led to repetitions in the claims of scientific discovery and progress. For the purpose of clarity during this review the author wishes to use a modified version of Gunzburg's definition: **"Process by which primitive, undifferentiated and pluripotent cells are stimulated to develop into the bone-forming cell lineage, leading to the formation of mature mineralised bone (osteogenesis)"** (Gunzburg, Szpalski et al. 2001). This definition applies to osteoinduction no matter how it is caused, where it occurs, when it is observed, or how it is measured.

2.5.2 Preclinical studies for Osteoinductivity

2.5.2.A **Commercial models for assessing Osteoinductivity**

The largest market for osteoinductive bone graft products is the USA where demineralised bone matrix (DBM) alone is classified in the category of human cells, tissues, and cellular and tissue-based product (HCT/P) (section 361 of the Public Health Service Act) and is regulated by the Consumer Affairs Branch (CBER) of the Food and Drug Administration (FDA). As well as being the largest single market for commercialised osteoinductive products, the USA is also the largest single exporter of these products, which are sold and clinically applied throughout Europe and most of the western world. As tissue-bank materials, solely DBM materials can be used for broad clinical indications. In 2001, the FDA issued new HCT/P criteria in 2001 which prohibited the combination of a HCT/P with a drug or a device (with the

exception of a sterilizing, preserving, or storage agent). Consequently, DBM products that are combined with carriers (e.g. calcium phosphate, glycerol, sodium hyaluronate) are classified as a medical device and are regulated under the Centre for Devices and Radiological Health (CDRH).

Since this ruling, most DBM products combined with carriers received FDA approval via the 510k regulatory process as bone void fillers with specific indications. Many of these products claim to be osteoinductive, but test each batch for this attribute in order to be deemed suitable for clinical use. These osteoinductive batch validation tests either consist of in-vivo athymic rodent models or in-vitro tests that have been validated to correlate with athymic rodent models. Approximately half of the *in vivo* validation assays specify athymic mice, while the other half specifies athymic rats. It can thus be concluded that the FDA accepts both athymic mice and rat models to verify osteoinductivity.

While the specific in-vivo osteoinductivity test protocols are not provided in the 510k summaries, some details have been published in peer-reviewed articles, white papers, or product brochures (Bacterin , Etex , Synthes , Zhang, Powers et al. 1997b, Zhang, Powers et al. 1997a, Edwards, Diegmann et al. 1998, Coulson and Lalor 2000, Takikawa, Bauer et al. 2003, Kay 2004, Honsawek, Powers et al. 2005, Boyan, Ranly et al. 2006a). Eight of these studies utilised athymic mice while three utilised athymic rats. Within the athymic mouse studies; two studies performed subcutaneous implantation (Etex , Zhang, Powers et al. 1997b) while the remaining performed muscle implantation in the longissimus dorsi (Zhang, Powers et al. 1997a, Zhang, Powers et al. 1997b, Honsawek, Powers et al. 2005), hamstrings (Synthes), quadriceps (Kay 2004), gastrocnemius (Boyan, Ranly et al. 2006a), and biceps femoris (Bacterin). Within the athymic rat studies; two performed subcutaneous implantation (Edwards, Diegmann et al. 1998, Coulson and Lalor 2000) while the rest conducted muscle implantation in the pectoralis muscle (Takikawa, Bauer et al. 2003) and in the upper hind limb (at the interface of semimembranous and adductor brevis muscles) (Edwards, Diegmann et al. 1998, Takikawa, Bauer et al. 2003).

On average, ~20 mg (ranging from 11-40 mg) of DBM was placed in the implantation site. Eight of the studies had a time point of 28 days, one study had a time point of 21 days (Coulson and Lalor 2000), and another study had a time point of 56 days (Boyan, Ranly et al. 2006a). Most of the studies performed decalcified paraffin-embedded histology to assess ectopic bone formation. Three studies performed non-decalcified resin-embedded histology (Edwards, Diegmann et al.

1998, Coulson and Lalor 2000, Takikawa, Bauer et al. 2003), two studies performed non-decalcified resin-embedded histomorphometry (Edwards, Diegmann et al. 1998, Coulson and Lalor 2000), two studies performed decalcified paraffin-embedded histomorphometry (Honsawek, Powers et al. 2005, Boyan, Ranly et al. 2006a), two studies evaluated explant calcium content (Zhang, Powers et al. 1997b, Zhang, Powers et al. 1997a), and two studies assessed explant alkaline phosphatase content (Coulson and Lalor 2000, Kay 2004).

Bone morphogenetic proteins (BMP) comprise two commercially available products as INFUSE® (BMP-2: Medtronic) and OP-1™ (BMP-7: Olympus Biotech Corporation). INFUSE® and OP-1™ do not have to perform batch to batch osteoinductivity validation testing. However, Barr et al. published an in-vivo mouse thigh muscle pouch study comparing the osteoinductivity of the two products (Barr, McNamara et al. 2010). After 28 days of implantation, ectopic bone formation was assessed with micro CT measurement of bone volume and decalcified paraffin embedded histology with haematoxylin and eosin staining. The in-vivo mouse muscle pouch study showed that OP-1™ induced greater bone volume than INFUSE®. Barr et al. also assessed INFUSE® and OP-1™ in an in-vitro C2C12 cell assay in the same publication and found that INFUSE® stimulated greater alkaline phosphatase activity compared to OP-1™ (Barr, McNamara et al. 2010).

A literature search of more recently published articles also confirmed that the athymic mouse model has been used to assess biologic devices consisting of carriers combined with live cells, carriers combined with growth factors (including bone morphogenetic proteins but not specifically INFUSE® or OP-1™), as well as carriers combined with live cells and growth factors (Ranly, McMillan et al. 2005, Boyan, Ranly et al. 2006b, Lin, Wang et al. 2007, Liu, Zhao et al. 2007, Na, Kim et al. 2007, Ranly, Lohmann et al. 2007, Han, Sun et al. 2008, Tampieri, Sandri et al. 2008, Oliveira, Mijares et al. 2009, Schaeren, Jaquiery et al. 2010, Wang, Ma et al. 2011, Wang, Huang et al. 2011, Zhang, Mao et al. 2011).

Boyan et al. conducted gastrocnemius muscle implantation with 10 mg of material per implantation site (Ranly, McMillan et al. 2005, Boyan, Ranly et al. 2006b, Ranly, Lohmann et al. 2007). The remaining studies used dorsal subcutaneous implantation and indicated the material quantities volumetrically (250 µl)(Na, Kim et al. 2007), or as blocks (5 mm x 5 mm x 1.5 mm (Lin, Wang et al. 2007), 3 mm x 3 mm x 3 mm (Lin, Wang et al. 2007), 4 mm x 4 mm x 1 mm (Oliveira, Mijares et al. 2009), or as cylinders (6 mm D x 4 mm (Schaeren, Jaquiery et al. 2010), 8 mm D x 6

mm (Tampieri, Sandri et al. 2008), 5.2 mm D x 1.5 mm (Wang, Ma et al. 2011), 4 mm D x 2 mm (Wang, Huang et al. 2011), 8 mm D x 2 mm (Zhang, Mao et al. 2011)).

Most of the studies had an 8 week time point with the exception of three studies which had a 4 week time point (Wang, Huang et al. 2011), a 12 week time point (Liu, Zhao et al. 2007), and a 5 month time point (Lin, Wang et al. 2007). Boyan et al. conducted decalcified paraffin-embedded histology, histomorphometry, and utilised a semiquantitative osteoinduction scoring system based on the presence of bone and number of ossicles (Ranly, McMillan et al. 2005, Boyan, Ranly et al. 2006b, Ranly, Lohmann et al. 2007). Most of the other studies also performed decalcified paraffin-embedded histology (Lin, Wang et al. 2007, Liu, Zhao et al. 2007, Han, Sun et al. 2008, Tampieri, Sandri et al. 2008, Schaeren, Jaquiery et al. 2010, Wang, Ma et al. 2011, Wang, Huang et al. 2011, Zhang, Mao et al. 2011), and a few others performed decalcified paraffin-embedded histomorphometry (Schaeren, Jaquiery et al. 2010, Wang, Huang et al. 2011, Zhang, Mao et al. 2011). Two studies performed non-decalcified resin-embedded histology (Lin, Wang et al. 2007, Na, Kim et al. 2007). One study immunohistochemically assessed osteopontin and osteocalcin (Lin, Wang et al. 2007) while another immunohistochemically measured dentin sialoprotein (Wang, Ma et al. 2011). Na et al. measured explant alkaline phosphatase content and also conducted RT-PCR analysis of type I collagen, type II collagen, and osteocalcin on explant extracts (Na, Kim et al. 2007, Standring 2008). Oliveira et al. utilized micro CT to quantify bone volume and also assessed the explants with BSE-SEM and FTIR (Oliveira, Mijares et al. 2009).

2.5.2.A **Osteoinductivity as a function on genetic disposition**

Urist, in his seminal 1965 study on osteoinductivity, investigated the effect of decalcified homogenous diaphyseal bone from rabbits on bone formation in the soft tissues of rabbits, rats, mice and guineapigs (Urist 1965). Urist discovered that when the donor and host were matched there was a high chance (>90%) of achieving ectopic bone formation but there was variation between species in that success was 90% for rats and 98% for rabbits with mice and guineapigs falling between. This is the first reported species-related dependency of osteoinductivity. Urist also demonstrated that when donor and host were un-matched the chance of success was considerably less, as low as 50% for guineapig DBM when implanted in rats, for example.

Since Urist's 1965 study, osteoinductivity has been investigated in many different species of animal, including but not limited to: mice (Yuan, van Blitterswijk et al. 2006b), Fischer rats (Okumura, Ohgushi et al. 1991), Sprague-Dawley rats (Urist and Strates 1971), hamsters (Heughebaert, LeGeros et al. 1988), cats (Daculsi 2004), beagle dogs (Piecuch 1982), milk goats (Barrere, van der Valk et al. 2003), Saanen goats (Bodde, Cammaert et al. 2007), Dutch goats (Li, Habibovic et al. 2007), sheep (Gosain, Song et al. 2002), pigs (Urist 1965), baboons (Ripamonti 1991). A more complete list of the species studied can be found in Appendix II of this thesis. The outcomes of these studies were variable, however confounding factors such as the test material; implantation site, length of implantation, and histological method may contribute significantly towards this variation. Despite this, a common theme was apparent: osteoinductivity of biomaterials was more frequently observed in larger animals, such as rabbits; dogs; and goats, than in smaller animals, such as rodents.

In 1996 Ripamonti investigated osteoinduction in porous hydroxyapatite following implantation in heterotopic sites of different animal models (Ripamonti 1996). This was the first study of its kind, since Urists 1965 work, in which most research parameters were kept constant whilst investigating the effect of genetic deposition to biomaterial-derived osteoinductivity. Study materials comprised replicas of porous hydroxyapatite that had been obtained after hydrothermal conversion of the calcium carbonate exoskeleton of coral (genus Goniopora). A total of 40 hydroxyapatite rods were implanted bilaterally in intramuscular pouches created by sharp and blunt dissection in the rectus abdominis of four clinically healthy outbred Chacma baboons (Papio ursinus) with normal haematological and biochemical profiles; two adult inbred beagles; and four adult rabbits which were of the New Zealand white strain. Ripamonti found that implants harvested from rabbits and dogs were less vascularised than those from Baboons at the macroscopic level. Bone area in Rabbits was 0.5±0.3%; in Dogs was 0.79±0.49%; and in Baboons was 11.3±3.02%. The amount of bone did vary considerably between specimens. Ripamonti speculated that osteoinductivity is not inherent but that bone morphogenetic proteins (BMP's) bind preferentially to the surface of the materials tested in the study. Bone differentiation occurred after sixty days post-implantation. However, no bone formation occurred after thirty days implantation so Ripamonti postulated that this indicates that a critical level of endogenous BMP is required to be adsorbed to the surface to start the bone formation cascade.

In 2006 Yuan and van Blitterswijk embarked on a cross-species comparison of ectopic bone formation in biphasic calcium phosphate (BCP) and hydroxyapatite

(HA) scaffolds (Yuan, van Blitterswijk et al. 2006b). The test materials included two ceramics with macropores between 100 and 1000 μm in size and micropores 0.1–10 μm on their macropore surface. The HA samples contained a macroporosity of 52 % while BCP contained a macroporosity of 40%. A trace of TCP was present in the HA, whilst the BCP contained 38%weight TCP. Eight dogs, four rabbits, eight rats, and sixteen mice were included in the study. Materials were implanted in the gluteal muscles of dogs, thigh muscles of rabbits & rats, and dorsal subcutaneous pouches in the mice. All implants were left in situ for 90 days. Yuan et al. found that bone incidence was as follows: dogs (8/8), rabbits (4/4), rats (0/8), and mice (3/16). For materials retrieved from dogs, bone volume was 14±5% in HA implants and 30±6% in the BCP implants. Bone volume was only seen in BCP implants in rabbits but at <5%. No bone was seen in any materials implanted in rats and only 3/16 materials implanted in mice. Bone found in the materials implanted in dogs was mature with trapped osteocytes, an osteoblast line, mineralised osteoid and osteoclast-like cells. The authors concluded that the reason for the differences in material-induced bone formation for each animal species remained unclear but in addition to Ripamonti's hypothesis on variation in extracellular BMP between species another hypothesis could well be that the number of stem cells not only varies per animal species but also per implantation sites.

Perhaps the most compelling evidence for the genetic predisposition to osteoinductivity is provided by a study conducted by Barradas et al., (Barradas, Yuan et al. 2012). In their recent study the investigators screened mice from 11 different inbred mouse strains for their responsiveness to subcutaneous implantation of osteoinductive tricalcium phosphate (TCP). In only two strains (FVB and 129S2) the ceramic induced bone formation, and in particularly, in FVB mice, bone was found in all the tested mice.

2.5.2.B **Osteoinductivity as a function of implantation site**

While Dr. Urist utilised muscle implantation for osteoinductivity assessment, the surveyed osteoinductive athymic rodent models utilised both subcutaneous and muscle implantation. Zhang et al. found that more bone formed in muscle pouches compared to subcutaneous pouches implanted with DBM in athymic mice (Zhang, Powers et al. 1997b). Likewise, Edwards et al. found that more bone formed in muscle pouches implanted with DBM compared to subcutaneous pouches in athymic rats (Edwards, Diegmann et al. 1998). Similar phenomena have been observed with bone morphogenetic protein-2 (BMP-2). Okubo et al. implanted BMP-2 on a

collagen carrier into Wistar rats in intramuscular, intermuscular, subcutaneous, and intrafatty sites. New bone formation was highest in the intramuscular site and lowest in the intrafatty site (Okubo, Bessho et al. 2000). To standardize DBM osteoinductivity testing, some investigators have recommended muscle implantation in the gluteus maximum claiming that implantation in the biceps femoris and gastrocnemius muscles places the implant too close to native bone which may promote orthotopic as opposed to ectopic bone formation (Linthurst 2008).

2.5.2.C **Osteoinductivity as a function of implantation period**

The period over which bone was observed in calcium phosphate materials implanted in non-bony sites across the animal studies reported in the literature might perhaps give some indication as to what the mechanism responsible for osteoinduction is for this type of material. For instance, there was very little or no bone observed in test article treated defects within 21 days (Eid, Zelicof et al. 2001) or 8 weeks (Piecuch 1982, Ohgushi and Okumura 1990, Ripamonti 1996) of implantation. However, bone was generally observed in other studies at later time points: 60-90 days (Yang, Yuan et al. 1996); 3 months (Ripamonti 1991, Yuan, Kurashina et al. 1999); 4 months (Pollick, Shors et al. 1995); 5 months (Yuan, De Bruijn et al. 2001a); 1 year (Gosain, Song et al. 2002, Fujibayashi, Neo et al. 2004); and 2.5 years (Yuan, Yang et al. 2001). There exist some contradictions to these trends in that some investigators have reported observing bone as early as 45 days after treatment (Yuan, De Bruijn et al. 2001a), and some at 60 days post-implantation (Yuan, Zou et al. 1998, Yuan, Li et al. 2000), although bone was observed only in a small number of pores (Yuan, Li et al. 2000, Yuan, De Bruijn et al. 2001a) or the study was performed in a pig rather the more typical sheep or goat model (Yuan, Zou et al. 1998). The apparent 8 week minimum time period required for the osteoinductive potential of calcium phosphate biomaterials to take effect would support theories 1, 2, 5, and 6 proposed by Barrere et al. (Barrere, van der Valk et al. 2003) in that one might expect a delay would be observed for adsorption of the necessary concentration of BMP's to stimulate osteogenesis; for the development of a low oxygen tension, local to the defect site; for the precipitation of an apatite-like layer; or for the dissolution of a sufficient amount of calcium and phosphorus ions to precipitate the apatite-like layer.

2.5.3 Osteoinductivity of Biomaterial Scaffolds

A summary of proposed mechanisms of action for biomaterial induced bone formation is provided by Barrere et al. and Barradas et al. (Barrere, van der Valk et

al. 2003, Barradas, Yuan et al. 2011). This group suggested that osteoinduction by porous Ca-P ceramics can be attributed to either (1) the incorporation and concentration of bone morphogenetic proteins (BMPs) by Ca-P crystals; (2) a low oxygen tension in the central region of the implant that triggered the pericytes of microvessels to differentiate into osteoblasts; (3) a rough surface produced by the 3D microstructure, which caused the asymmetrical division of mesenchymal cells that produce osteoblasts; (4) the surface charge of the substrate, which triggered cell differentiation; (5) the bone-like apatite layer formed in vivo that recognized mesenchymal cells; and/or (6) the local high level of free Ca^{2+} provided by the Ca-P material, which triggered cell differentiation and bone formation (Figure 2-1).

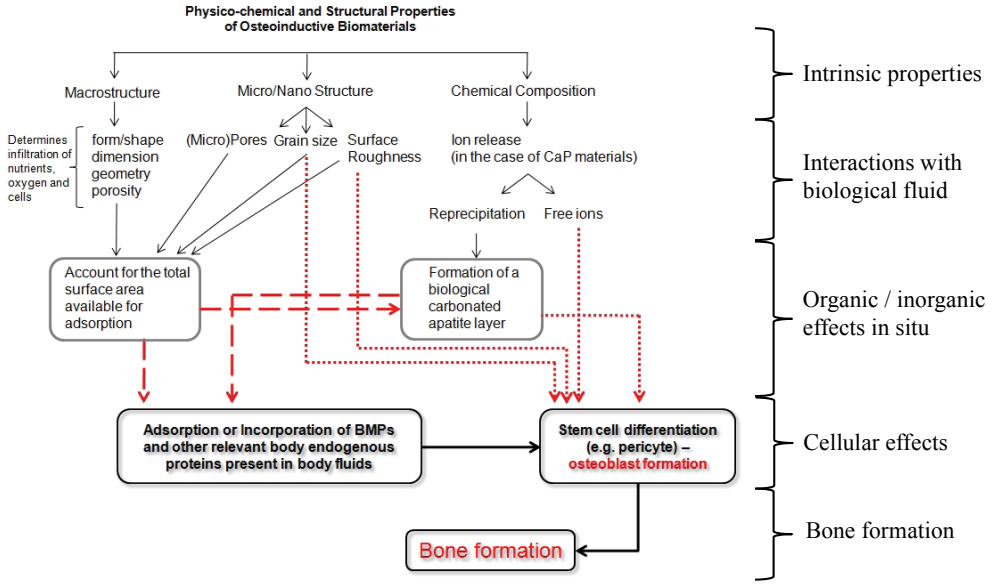

Figure 2-1: Important physiochemical and structural properties of Osteoinductive biomaterials

Modified from Barradas, Yuan et al. (2011). This mechanism for calcium phosphate derived osteoinductivity, proposed by Barradas et al., includes both physical and chemical cues for bone formation in non-bony sites. The authors propose that physico-chemical and/or structural properties of osteoinductive biomaterials may trigger the process of heterotopic bone formation directly or indirectly. Micro and nano structural properties can favour the interaction with BMPs and other essential endogenous proteins that in turn trigger stem cell differentiation into osteoblasts and hence bone formation. But surface topography and inorganic ion release (in the case of calcium phosphate based ceramics), may also be a direct trigger of the process of osteogenic differentiation and bone formation.

2.5.3.A **Osteoinductivity as a function of calcium and phosphorus ion release**

The absence of bone observed in defects in which a large volume of calcium and phosphorus has dissolved over a long time period (as for TCP and OCP implants) in contrast to the observation of bone in HA (sparingly soluble calcium phosphate) materials at long time points (Yuan, Yang et al. 2001, Gosain, Song et al. 2002) highlights the potential importance of the dose dependent effect of calcium and phosphorus ions in the progression of biomaterial-derived osteoinductivity (Figure 2-2).

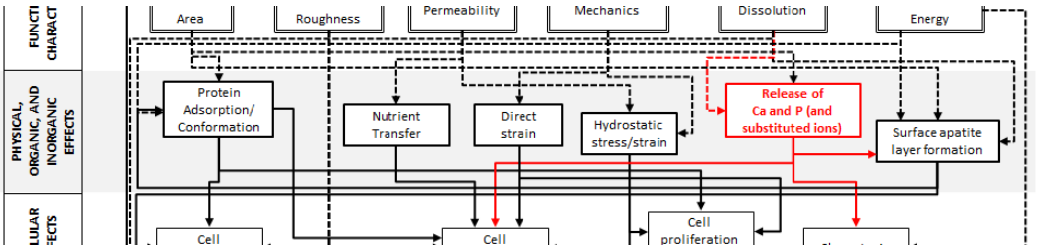

Figure 2-2 Osteoinductivity and Ca / P ion release

The release of calcium and phosphorus ions may have direct effects on bone mineralisation by recruiting pre-osteoblast cells through chemotaxis, upregulating osteoblast differentiation through ion channel activation, or in-direct effects on bone mineralisation through the precipitation of an apatite-like layer.

2.5.3.B **Osteoinductivity as a function of scaffold dissolution**

Also of interest is the variation with which bone was observed in implanted materials at relatively longer timepoints. Bone and graft material were absent at only 150 – 168 days post-implantation for TCP (Yuan, De Bruijn et al. 2001a) and OCP (Barrere, van der Valk et al. 2003). Whereas bone and graft were present after 1 - 2.5 years for HA (Yuan, Yang et al. 2001, Gosain, Song et al. 2002) and Titanium materials (Fujibayashi, Neo et al. 2004). This indicates that graft stability and the sustained presence of a scaffold may be important in the long-term osteoinductive effect of biomaterials.

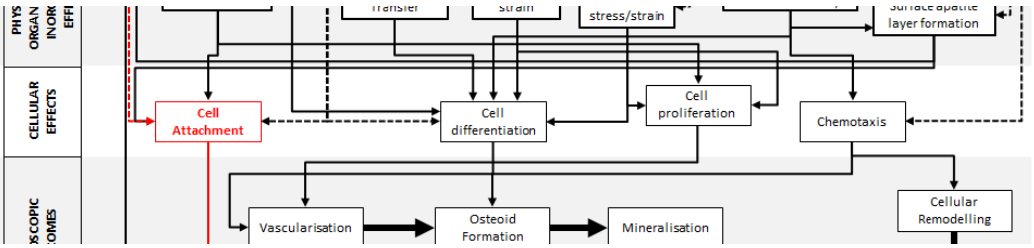

Figure 2-3 Osteoinductivity and scaffold stability

The stability of any calcium phosphate biomaterial *in situ* is likely to impact the extent to which pre-osteoblast cells are able to attach and subsequently differentiate into osteoblasts.

2.5.3.C **Osteoinductivity as a function of neovascularisation**

Some authors have suggested that osteoinduction is heavily dependent upon early vascularisation of implanted biomaterials (Ripamonti 1991, van Gaalen 2009). Vascularisation is thought likely to be responsible for the provision of BMP's and other osteogenic factors to the site of implantation (Figure 2-4). Also hypothesised is the potential for local osteogenic factors leading to the differentiation of pericytes into osteoblasts. However, recent studies in which TCP was implanted subcutaneously in FVB strain mice with and without local treatment of VEGF demonstrated there to be very little direct effect of the application of VEGF on the incidence of bone formation or the amount observed in the graft (Barradas, Yuan et al. 2012).

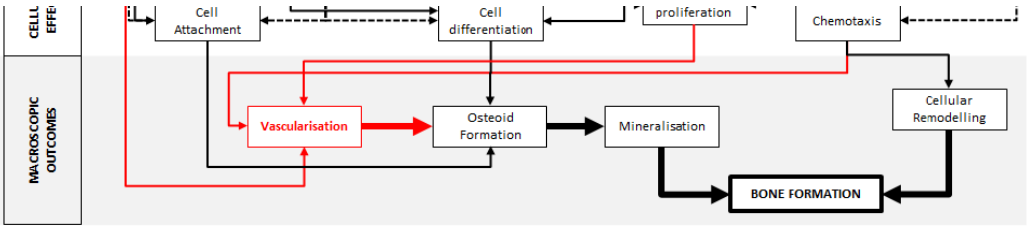

Figure 2-4 Osteoinductivity and neovascularisation

Vascularisation of biomaterial scaffolds is seen as a pre-requisite to bone healing in orthotopic defect sites, so logic follows that the same is likely to apply in ectopic defects. The extent and speed of vascularisation is dependent upon the intrinsic structural properties of the implanted material.

2.5.3.D **Osteoinductivity as a function of adsorption of osteogenic factors**

Locally adsorbed osteogenic protein factors are a proposed mechanism for biomaterial-derived osteoinductivity (Figure 2-5). In one study performed by Yuan et al., bone morphogenetic protein and ceramic-induced osteogenesis in intra-muscular implantation sites was investigated (Yuan, Zou et al. 1998). The test materials included in the study were biphasic calcium phosphate comprising TCP/HA (30TCP/70HA, porosity, 50-70%, average pore size 400 µm) rods (diameter 5 mm x6 mm). Four rods were implanted into the dorsal muscle of one pig. Fifteen days later another four rods implanted on the other side of the dorsal muscle of the same animal. All implants retrieved after 45 days from start of study.

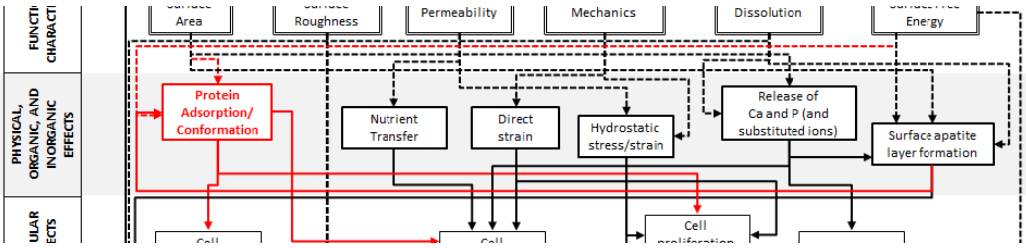

Figure 2-5 Osteoinductivity and adsorptive factors

The hypothesis that biomaterial-derived osteoinductivity is directed by adsorbed factors such as bone morphogenetic proteins is a long-standing one. Such as mechanism would be dependent upon factors such material parameters as surface area and surface free energy.

Bone formation could be detected inside the ceramics implanted in the dorsal muscle of the domestic pig at 45 days post-implantation, while no bone formation could be observed at the earlier endpoint of 30 days. At 30 days post-implantation, however, the organic matrix and polymorphic cells on the pore surface of the implants and some cells in the pores stained positively by bBMP-McAb compared to a negative control. This data seems to corroborate Ripamonti's earlier hypothesis that BMP adsorption is a key driver in biomaterial-derived osteoinduction (Ripamonti 1996).

2.5.3.A **Osteoinductivity as a function of silicon ion composition**

Silicon has been known to be fundamental for normal bone healing for over forty years. Carlisle discovered that silicon-deficient diets led to abnormal bone and

cartilage formation in chicks and later demonstrated that chicks fed a silicon supplemented diet had enhanced bone growth, increased amounts of cartilage, increased bone water content and biochemical changes in the mineral, hexosamine and collagen content of bone (Carlisle 1970, Carlisle 1972, Carlisle 1974, Carlisle 1975, Carlisle 1976, Carlisle 1980a, Carlisle 1980b, Carlisle 1981, Carlisle 1982, Carlisle 1986, Carlisle 1988). Schwarz also corroborated the importance of dietary silicon intake on normal bone physiology (Schwarz 1973).

Preclinical studies demonstrate that the speed, extent and quality of *de novo* bone formation is dependent upon the amount of silicon substituted into hydroxyapatite biomaterials when tested in orthotopic defect sites *in vivo* (Hing 2004a, Hing, Saeed et al. 2004, Hing, Revell et al. 2006, Hing, Wilson et al. 2007). A more recent study demonstrated that the amount of silicon substituted into hydroxyapatite can also affect the amount of bone formation observed in ectopic defect sites *in vivo* (Coathup, Samizadeh et al. 2011). In Coathup's study implants with a macroporosity of 80% and a strut porosity of 30% were inserted into sites located in the left and right paraspinal muscles of six female sheep. After twelve weeks *in vivo*, a longitudinal thin section was prepared through the centre of each implant. Bone formation within the implant, bone formation in contact with the implant surface, and implant resorption were quantified from histology with use of a line intersection method. The specimens were also analysed with the use of backscattered scanning electron microscopy and energy-dispersive x-ray analysis. Silicate substitution had a significant effect on the formation of bone both within the hydroxyapatite implants and on the implant surface during the twelve-week period. Bone area within the implant was greater in the silicate-substituted hydroxyapatite group (mean, 7.65% +/- 3.2%) than in the stoichiometric hydroxyapatite group (0.99% +/- 0.9%, $p = 0.01$). The amount of bone formed at the surface of the implant was also significantly greater in the silicate-substituted hydroxyapatite group (mean, 26.00% +/- 7.8%) than in the stoichiometric hydroxyapatite group (2.2% +/- 2.0%, $p = 0.01$). Scanning electron microscopy demonstrated bone formation within pores that were <5 mum in size, and energy-dispersive x-ray analysis confirmed the presence of silicon within the new bone in the silicate-substituted hydroxyapatite group. New bone formation occurred through an intramembranous process within the implant structure. The precise mechanism for these observations of a silicon-dependent upregulation of bone formation in orthotopic and ectopic preclinical studies has so far not been elucidated. It is unknown whether the silicon is imparting a direct influence on cell metabolism and on protein synthesis or an in-direct effect on cell recruitment, attachment, differentiation and proliferation. However, several studies have

investigated the effects of silicon on bone healing, some of which are discussed in the following text.

Silicon-containing calcium phosphates such as silicon-substituted hydroxyapatite have been shown to dissolve *in vivo*, eliciting free silicon in the form of orthosilicic acid into the surrounding tissues. Studies by Porter et al., examining the *in vivo* dissolution processes in phase-pure hydroxyapatite and silicon-substituted hydroxyapatite found that an increased number of triple junctions in silicon-substituted hydroxyapatite compared to hydroxyapatite may have a significant role in increasing the solubility of the material and the subsequent rate at which bone apposes these ceramics (Porter, Patel et al. 2003, Porter, Best et al. 2004, Porter, Botelho et al. 2004, Porter, Patel et al. 2004). In one of these studies, high-resolution transmission electron microscopy was used to observe dissolution from hydroxyapatite (HA), 0.8 wt% silicon-substituted hydroxyapatite (0.8wt% Si-HA) and 1.5 wt% silicon-substituted hydroxyapatite (1.5wt% Si-HA) implants after 6 and 12 weeks *in vivo* (Porter, Patel et al. 2003). Observations confirmed that defects, in particular those involving grain boundaries, were the starting point of dissolution *in vivo*. Dissolution was observed to follow the order 1.5 wt% Si-HA>0.8 wt% Si-HA>pure HA and it was found to be particularly prevalent at grain boundaries and triple-junctions. These observations may help to explain the mechanism by which silicate ions increase the *in vivo* bioactivity of hydroxyapatite.

Much of the earlier work investigating the role of free silicon on bone formation focused on its role in collagen synthesis. Schwarz demonstrated that silicon is essential to the normal development of the glycosaminoglycan network in the extracellular matrix, helping to stabilise complex polysaccharide structures and forming crosslinks via silanolate (R–O–Si–O–R and R–O–Si–O–Si–O–R) bonds that regulate the structure and function of these molecules (Schwarz 1973). Carlisle's analysis of chick bone development revealed that silicon was concentrated in the growth areas of bone. In the developing chicks, silicon supplementation led to a 100% increase in bone collagen content over silicon-deficient bones after twelve days in culture (Carlisle 1974). Later studies demonstrated that *in vitro*, collagen type I expression is upregulated in human osteoblasts which were supplemented with orthosilicic acid (Reffitt, Ogston et al. 2003). Silicon, in the form of orthosilicic acid, has also been implicated in the binding of aluminium to form aluminosilicates which prevent aluminium competing from metal ion binding sites (Birchall 1993). For example, complexes of silicon and aluminium prevent aluminium ions competing with iron for binding sites in molecules involved in collagen synthesis, such as prolyl

hydroxlase.

More recent research has focused on the role of free silicon on the upregulation of osteoblast cells *in vitro*. Gao et al. studied the impact of varying silicon content of two bioglass compositions in 2001 (Gao, Aro et al. 2001). Saos-2 osteoblastic cells with proven osteogenic phenotype were cultured for 4, 7 and 14 days on two bioactive glasses with different silicon contents. Gao et al., observed a significant increase in Col-I, ALP and BMP-2 mRNA levels in cells grown on the two bioactive glasses when compared with those grown on controls containing no silicon at 4 and 7 days. The BMP-2 mRNA level was greatest for the test material containing the largest amount of silicon at 4, 7 and 14 days, although this did not reach statistical significance. The effect of the ionic products of Bioglass 45S5 dissolution on the gene-expression profile of human osteoblasts was investigated with cDNA microarray analysis by Xynos et al. (Xynos, Edgar et al. 2001). The increase in silicon concentration in the supernatant was substantially higher than the other ionic products (Ca, P, Na). Xynos et al., observed the induction of genes with known roles in processes relevant to osteoblast metabolism and bone homeostasis. These included genes that encode products that can induce osteoblast proliferation (e.g. RCL), participate in the dynamic processes of extracellular matrix remodelling (e.g. metalloproteinases), perform differentiated functions (e.g. CD44), and promote cell-cell and cell matrix attachment (e.g., integrin β1). Studies of other silicon-containing biomaterials, such as silicate-substituted hydroxyapatite, have also demonstrated that osteoblast cells are upregulated by silicon. Osteoblasts cultured on silicate-substituted hydroxyapatite were upregulated compared to stoichiometric hydroxyapatite (Gibson, Huang et al. 1999, Cameron, Travers et al. 2013, Cameron, Travers et al. In Press) and bioglass (De Godoy, Hutchens et al. 2015).

The role of silicon in bone development in biomaterials may be indirect instead of or as well as the direct mechanisms described above. Upregulated bone development can be explained in part by other *in vitro* studies in which substitution of silicate into hydroxyapatite has been demonstrated to influence the surface charge, hydrophilicity, protein adsorption, and cell attachment of silicate-substituted hydroxyapatite biomaterials *in vitro* (Rashid 2008, Guth, Campion et al. 2010a, Guth, Campion et al. 2010b). In this instance the role of silicon is to modify the inherent properties of the material surface (such as surface charge and surface free energy) such that an optimal layer of protein is adsorbed to the biomaterial surface after implantation. This layer of protein, comprising predominantly fibronectin and vitronectin, two proteins with a well-established role in bone cell attachment, leads

to the preferential attachment and subsequent differentiation of preosteoblasts. Other researchers have discovered alternative mechanisms for the indirect role of silicon in bone formation. Li and Chang found that silicon ions upregulated endothelial growth factor (VEGF) expression in fibroblasts and endothelial cells, and since VEGF upregulates bone morphogenetic protein expression, silicon might play an indirect role in bone formation via this molecular pathway (Li and Chang 2013). The effect of bioglass ionic dissolution products on the metabolism of osteoclasts was studied by Mladenovic et al., (Mladenovic, Johansson et al. 2014). Mladenovic et al., concluded that silicon causes significant inhibition of osteoclast phenotypic gene expressions, osteoclast formation and bone resorption *in vitro*.

2.6 Conclusion

Bone is an incredibly complex and dynamic organ of the human body and as such there exists disparity in the efficacy of current treatments to augment or replace bone in the clinical setting. *In vitro* experiments have come a long way to understand the mechanobiology of material substrates and their impact on bone cell upregulation either in response to fluid shear or direct substrate strain. However, a lot is still unknown with respect to the precise mechanisms for biomaterial-derived osteogenic potential of synthetic bone grafts. Studies for osteoinductivity have highlighted the importance of bone graft stability, propensity for apatite-like layer formation, osteogenic factor upregulation, bone cell attachment, bone cell differentiation, and bone cell proliferation but the precise relationship between these factors is not clear. The many intrinsic properties (e.g. pore size, pore connectivity, pore volume etc.) and associated functional characteristics (e.g. permeability & dissolution) of a biomaterial can affect multiple components of the bone formation process (e.g. cell attachment, differentiation, proliferation etc.), meaning that in reality the mechanism for biomaterial-derived osteoinductivity is far more complex (Figure 2-6) than that proposed by Barradas et al. (Barradas, Yuan et al. 2011). Silicon has been demonstrated to have a significant impact on bone formation both in orthotopic and also in ectopic defects *in vivo*, but despite much research in this area, whether this occurs via direct or indirect bone cell upregulation is not understood. In all likelihood it is a combination of some or all of these mechanisms. Additional research is required to uncover the role of physiochemical parameters in the osteogenic potential of phosphate biomaterials.

Figure 2-6: Role of Physiochemical Parameters in the osteoinductivity of calcium phosphate biomaterials - as proposed by this author.

The many intrinsic properties (e.g. pore size, pore connectivity, pore volume etc.) and associated functional characteristics (e.g. permeability & dissolution) of a biomaterial can affect multiple components of the bone formation process (e.g. cell attachment, differentiation, proliferation etc.), meaning that in reality the mechanism for biomaterial-derived osteoinductivity is far more complex than that proposed by Barradas et al. (2011).

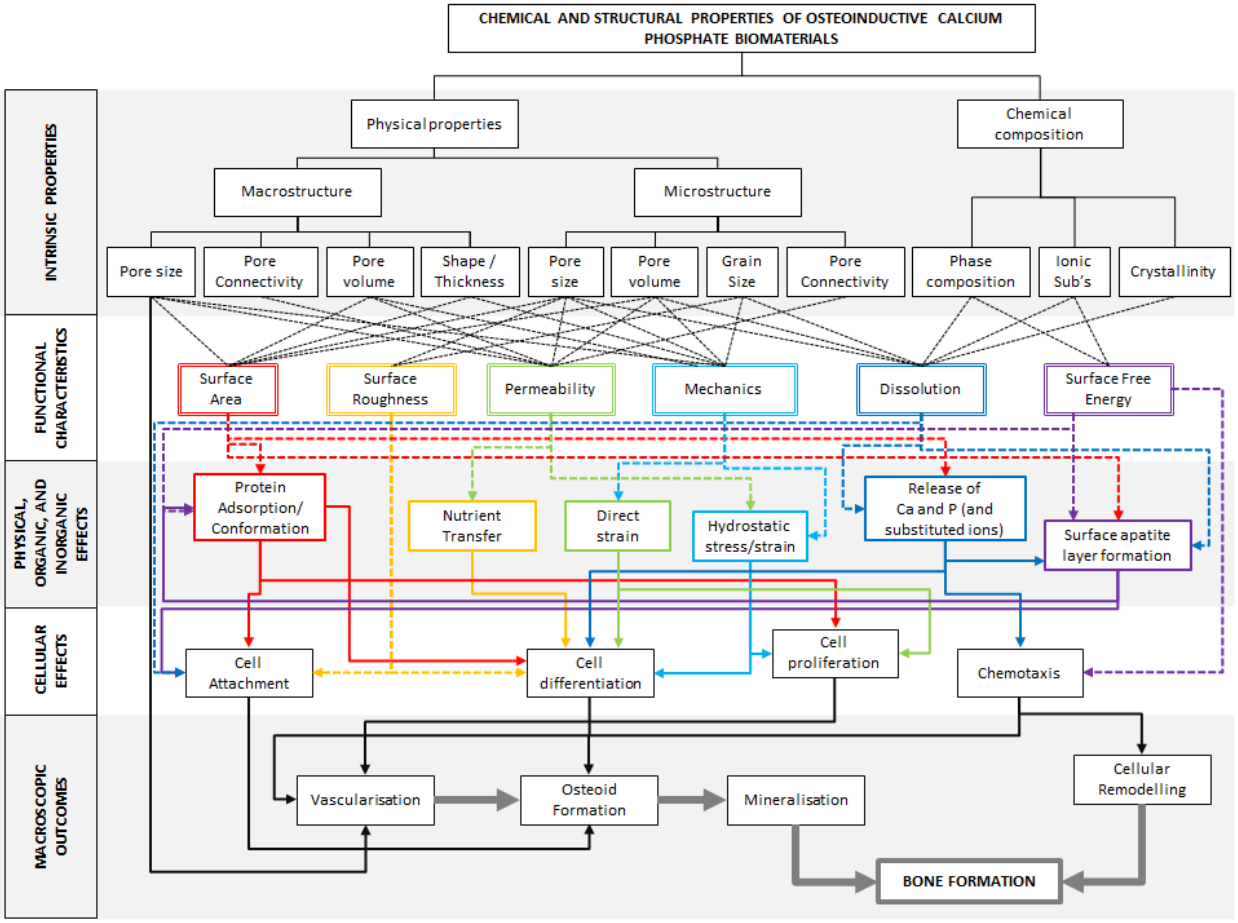

Chapter Three: Physiochemical Characterisation

3.1 Introduction

Porous hydroxyapatite (HA) has been used as a biomaterial to repair, augment, and replace bone since the early 1970's when it was first used in bulk for dental restorative surgery (Monroe, Votava et al. 1971). Since hydroxyapatite's first medical application in surgery the importance of structure and chemistry in the biological performance of all phases of synthetic calcium phosphate-based biomaterials has been extensively researched. Consequently there are now many recognised analytical methods with which these materials can be characterised and a large body of data against which new data can be compared. This chapter provides an analysis of the fundamental chemical and physical features of commercially available silicate-substituted phosphate (SiCaP) and tricalcium phosphate (TCP).

3.2 Materials

The test materials investigated in subsequent chapters were provided by ApaTech Limited, UK and Orthovita, USA. In the following sections the physical and chemical techniques used to characterise the test materials are described. Seven test groups of varying strut-porosity and formulation were provided for testing (Table 3-1).

3.2.1 Method of Manufacture

In the following sections an overview of the methods for manufacture of the SiCaP groups is described. The method of manufacture of the commercially available tricalcium phosphate test group (Vitoss, Orthovita, USA) is not disclosed in the literature or by the manufacturer and is therefore not provided.

3.2.1.A **SiCaP Intermediate Powder Preparation**

The basis for the synthesis of the silicon-substituted apatite is the preparation of a stoichiometric HA using an aqueous acid-base neutralization precipitation reaction between calcium hydroxide, $Ca(OH)_2$, and orthophosphoric acid, H_3PO_4. The appropriate quantities of reactants to prepare the silicon-substituted apatite were calculated from quantities required to prepare a stoichiometric HA, with stoichiometric HA defined as a synthetic HA with a Ca/P molar ratio that of 1.67 and

which, after sintering/calcining at temperatures between 800° and 1300°C, does not decompose to form secondary phases such as TCP or calcium oxide (CaO). The quantities of reactants were calculated by assuming that silicon (or silicate) would substitute for phosphorus (or phosphate). Therefore, the number of moles of H_3PO_4 in stoichiometric HA was the same as the number of moles of (H_3PO_4 + SiAcetate) in the silicon-substituted apatite; the number of moles of $Ca(OH)_2$ was kept constant. The precipitation reaction was carried out at room temperature and the pH was maintained at 10.5 by the addition of ammonium hydroxide solution. After complete mixing of the reactants, the suspension was aged overnight. The aged precipitate was filtered in air, dried at elevated temperature, and then milled to form a powder. The resulting precipitate was filtered, dried at 80°C overnight, and then ground, milled, and sieved.

3.2.1.B **Preparation of Porous Sintered SiCaP**

Porous ceramic foams were manufactured from the milled precipitate using a method equivalent to that described in Example 1 of International patent WO/2000/020353 'FOAMED CERAMICS'. Briefly, polyvinyl alcohol was dissolved in double distilled water at 40°C, under conditions of continuous stirring. This binder solution was then combined with hydroxyapatite powder with a particle d.50 of 3.3 μm and a surface area of 13.4 m^2g^{-1}. The resulting slip was then placed in a mill pot with milling media (18 mm diameter balls) and milled at a speed of 120 rpm for 3 hours. The thus foamed slip was then cast into a mould. Castings were dried in air at a temperature of 40-50°C for up to 48 hours. The dried green castings underwent a stepped heat treatment in a ventilated furnace for binder burn-out and densification by sintering. Castings were heated at a rate of 2.5°$Cmin^{-1}$ to 500°C, and held at this temperature for 4 hours. Upon burn-out the castings were then heated at a rate of 2.5°$Cmin^{-1}$ to temperatures of 1200-1300°C, with no air flow and held for 2 hours.

Table 3-1 Test material summary

Test Group	Description	Nominal Total Porosity (%)	Nominal Strut-porosity (%)
SiCaP-23G	SiCaP material (Actifuse® Microgranules, ApaTech, Herts, UK) consisted of porous (80-82.5% total porosity), irregularly shaped microgranules (1–2 mm) of phase pure SiCaP (0.8 wt% Si) with a strut porosity of 23%	80	23
SiCaP-23P	SiCaP-23G granules in an aqueous carrier containing 33% by weight Poloxamer 407	80	23
SiCaP-32G	SiCaP material (ApaTech, Herts, UK) consisted of porous (80-82.5% total porosity), irregularly shaped microgranules (1–2 mm) of phase pure SiCaP (0.8 wt% Si) with a strut porosity of 32%	80	32
SiCaP-32P	SiCaP-32G granules in an aqueous carrier containing 33% by weight Poloxamer 407	80	32
SiCaP-46G	SiCaP material (ApaTech, Herts, UK) consisted of porous (80-82.5% total porosity), irregularly shaped microgranules (1–2 mm) of phase pure SiCaP (0.8 wt% Si) with a strut porosity of 46%	80	46
SiCaP-46P	SiCaP-46G granules in an aqueous carrier containing 33% by weight Poloxamer 407	80	46
β-TCP	Vitoss® Scaffold Morsels, (Orthovita, USA) consisting of porous (90 % total porosity) irregularly shaped granules (1–4 mm) of beta-tricalcium phosphate (β-TCP, $Ca_3(PO_4)_2$) with a strut-porosity of 48%	90	48

3.3 Methods of Characterisation

The materials were first characterised for phase purity, ionic composition, and crystallinity in order to confirm the claims of the manufacturers from whom the commercially available products were supplied (Table 3-1). The same characteristics were also used to assess the impact of suspending the SiCaP granules in an aqueous based carrier. To determine the effects of structure on the osteogenic potential and mechanical properties of calcium phosphates in later chapters, the silicate-substituted calcium phosphate materials were fully characterised in this chapter for strut-porosity; device density; total porosity; and surface area. The elements of microstructure and chemistry of the silicate-substituted calcium phosphate and tricalcium phosphate materials hypothesised to have an impact the bioactivity of

biomaterials were also compared, including: phase purity; crystallinity; strut-porosity; and surface area. Lastly, the effects of the strut-porosity on the resultant dissolution profile and bulk handling properties of silicate-substituted calcium phosphates were assessed with dissolution and mechanical testing. These are important to the clinical application of these materials.

3.3.1 Chemical Characterisation

Characterisation of phase purity by X-ray diffraction spectroscopy (XRD) and Fourier Transform Infrared spectroscopy (FTIR) as well as calcium, phosphorus, and silicon contents by X-ray fluorescence spectroscopy (XRF) was performed as described previously (Gibson, Best et al. 1999, Guth, Campion et al. 2010b, Guth, Campion et al. 2010a).

3.3.1.A **X-ray Diffraction Spectroscopy**

XRD was used to qualitatively determine crystallinity and identify the phases present in the as supplied materials. Powdered specimens were prepared in a pestle and mortar prior to analysis. Diffraction patterns were obtained using a Siemens D5000 X-Ray Diffractometer in flat plate geometry between 2θ values of 20 and 40°, using a step size of 0.02° and a step time of 2.5 seconds. The ICDD standards for HA, β-TCP and CaO (ICCD: 9-432, 9-348, 37-1497 respectively) were used for identification of any crystalline phases.

3.3.1.B **X-ray fluorescence (XRF) spectroscopy**

The calcium, phosphorus, and silicon contents of the samples were determined by quantification of a range of metal oxides using X-ray fluorescence (XRF) spectroscopy on a Philips PW1606 spectrometer at a UKAS (United Kingdom Accreditation Service) accredited laboratory (Ceram Research, UK). Analyses were performed in accordance with the international standard ISO EN 12677:2003 – Chemical analysis of refractory products by XRF – Fused casting method. The ionic molar Ca/(P+Si) Ratio was calculated to the 2nd decimal place from the measured percentage weight (wt%) of calcium oxide (CaO) and phosphorus pentoxide (P_2O_5). The wt% silicon substitution in the samples was calculated from the measured silicon dioxide (SiO_2) content.

The Ca:P Ratio was calculated using Equation 1.

$$Ca{:}P = \left(\frac{\text{wt\% of CaO}}{\text{wt \% of } P_2O_5}\right) \times \left[\left(\frac{A_r\ P_2O_5}{2(A_r\ P)}\right) \left(\frac{A_r\ CaO}{A_r\ Ca}\right)\right] \times \left(\frac{A_r\ P}{A_r\ Ca}\right) \qquad \textbf{Equation 1}$$

Where Ar = Relative Atomic Mass. Specimens were also analysed for Titanium Dioxide; Aluminium Oxide; Iron (III) Oxide; Magnesium Oxide; Potassium Oxide; Sodium Oxide; Chromium (III) Oxide; Manganese (II, III) Oxide; Zirconium Oxide; Hafnium Oxide; Lead Oxide; Zinc Oxide; Barium Oxide; Strontium (II) Oxide; and Tin (IV) Oxide.

3.3.1.C **Fourier transform infrared spectroscopy (FTIR)**

Fourier transform infrared spectroscopy (FTIR) was used to determine the absence of impurity groups or moieties within ceramics that exhibit vibrational frequencies in the 4,000 to 650 wavenumber range. Typically, this technique can determine such chemical moieties at levels down to 0.5% m/m.

The test materials are formed from highly crystalline hydroxyapatite and as such exhibits vibrational frequencies corresponding to the hydroxyapatite material. FTIR spectra were obtained on a Thermo Nicolet Nexus spectrometer, using an MTech Photoacoustic 3000 cell (University of Aberdeen, UK). A background spectrum was collected at the beginning of the analysis and this was applied to all of the subsequent spectra. Samples were purged for 30 minutes in argon to (as far as possible) remove water and carbon dioxide. Spectra were collected at 4 cm-1 resolution, and 100 scans collected.

3.3.2 Physical Characterisation

The materials were characterised as having two populations of porosity. Pores visible to the naked eye without magnification, the macropores, are circular, well-interconnected pores framed by the struts which make up the scaffold-like structure of the bulk material.

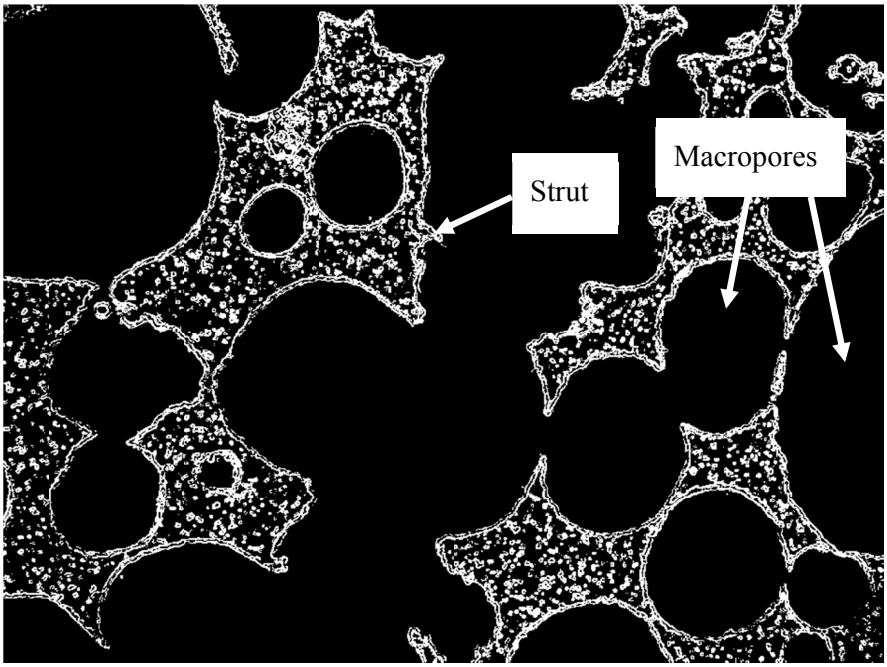

Figure 3-1 OM Micrograph of Macroporosity (with binary layer)
Overlaid image showing struts and macropores as viewed at x40 magnification with optical microscopy and image analysis. The macropores are large spherical voids that are well interconnected with one another. The strut-pores are smaller interstices which form a network of porosity within the walls of the macropores. Using image analysis an improved depth of contrast can be developed which improves the accuracy with which the volume of macro/strut-porosity is measured.

Under low magnification (x40) it is possible to observe a second population of porosity within the struts themselves, the strut-porosity (Figure 3-1). In common research terms, microporosity and strut porosity are used interchangeably. Strut pores are formed from the interconnected spaces existing between particles of calcium phosphate which have been sintered together to form the struts in the silicate-substituted hydroxyapatite scaffold. The term "strut-porosity" is used to describe the pore volume fraction of each strut. The typical size of an interconnection linking the strut pores together is between 0.2 – 5.0 microns, as measured by Mercury Intrusion Porosimetry, while the typical diameter of a strut pore is approximately 5 – 10 microns, as measured by Optical Microscopy and Image Analysis. The volume fraction strut-porosity can be measured by Optical Microscopy with image analysis, Scanning Electron Microscopy with Image Analysis, or Mercury Porosimetry in combination with Helium Pyconometry.

3.3.2.A **Sample Preparation for Characterisation with Image Analysis**

Specimens were vacuum embedded in Epofix resin (Struers, Glasgow) using an Epovac air ejector device (Struers, Glasgow) and left to cure at room temperature in a fume hood overnight. Cured samples were removed from embedding moulds and fixed in a Tegra-Force sample holder to be ground and polished on a TegraPol-21 polishing wheel (Struers, Glasgow). Embedded samples were first ground on a range of Epoxy bonded diamond pads at 150 rotations per min (rpm) and at 15N using water as a lubricant in the following order: 2 min with MD Piano 120 (Struers, Glasgow, UK), then for 4 min using MD Piano 220 (Struers, Glasgow, UK), 8 min using MD Piano 600 (Struers, Glasgow, UK) and finally 12 min on MD Piano 1200 (Struers, Glasgow, UK). Between each grinding step the samples were thoroughly washed with water to remove any diamond or ceramic debris from the specimens. For final polishing, 6μm and 1μm Diaduo lubricant/diamond suspensions (Struers, Glasgow, UK) were used on a MD-Dac cloth (Struers, Glasgow, UK) for 10 minutes and a MD-Napcloth for 12 minutes respectively. The polishing force was 30N.

3.3.2.B **Strut-porosity by Optical Microscopy and Image Analysis (OM)**

Quantification of strut-porosity was performed using serial sections and an optical ML7000 metallurgical microscope (Meiji, Japan) linked to a DS-1 digital camera (Nikon, UK). Areas of strut large enough to fill a measurement frame were found at x40 magnification using a x4 objective lens (Nikon, UK) (Figure 3-2).

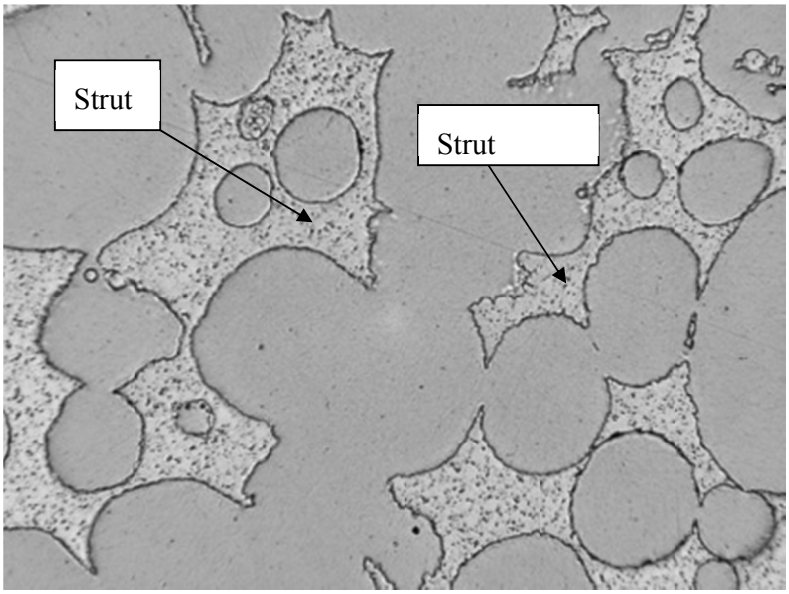

Figure 3-2 OM Micrograph of Macroporosity (without binary layer) Same photo, showing struts and strut porosity as viewed at x40 magnification with optical microscopy and image analysis. A number of binary treatments are required to process this raw image file into the binary layer shown above in Figure 3-1.

Areas of strut were captured using a x40 objective lens (Nikon, UK), which coupled with the power of the column of the microscope, gave an overall magnification of x400. Sample sections were analysed in NIS Elements Basic Research (Version 2.3) image analysis software (Nikon, UK). Briefly, sample images were first captured before being converted to grey scale for image processing. In order to improve contrast and sharpness at the pore-ceramic interface images were then processed using automatic contrast adjustment, a median transform adjustment, and lastly and an automatic sharpen adjustment. A binary layer was applied to the image so that it covered all areas of porosity but not ceramic. This was achieved using a standard treatment of opening, closing, filling, and eroding the binary layer. Finally, the binary was manually adjusted using an editing suite to ensure that the binary layer matched the underlying pore phase in the test material (Figure 3-3). Analysis was performed on three images of struts taken from each embedded specimen.

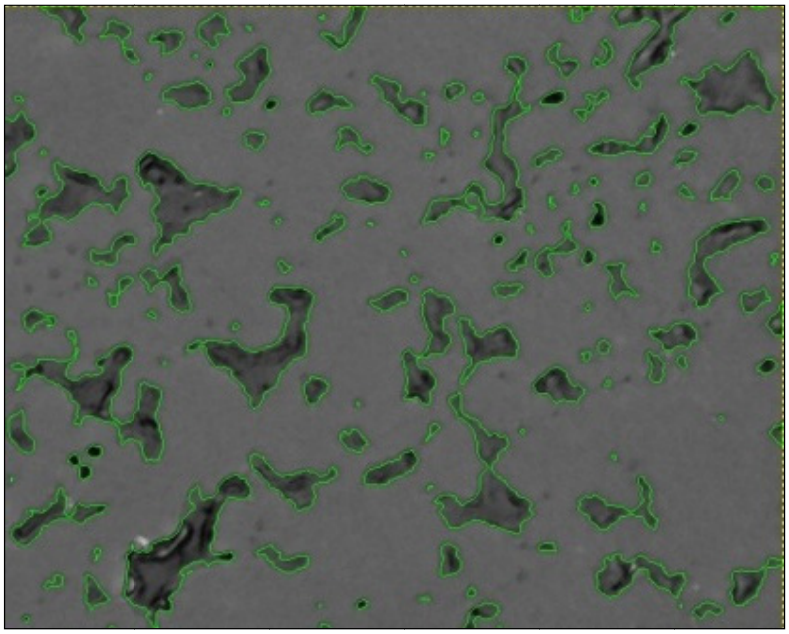

Figure 3-3 OM Micrograph of Strut-porosity
Strut-porosity (dark areas outlined in green) as viewed at x400 magnification with optical microscopy and image analysis. The image analysis software is able to detect the edges of strut-porosity and by manually picking up a grayscale range for the porosity from the grayscale histogram the analyst is able to determine the area fraction of porosity within the field of measurement.

The area ratio of strut-porosity (Figure 3-3) to total strut area within the analysis measurement frame is equivalent to the volume fraction of strut which is occupied by the strut-porosity (Equation 2).

$$\%\ Strut\ Porosity = \frac{Area_{STRUT\ POROSITY}}{Area_{MEASUREMENT\ FRAME}} \times 100\% \qquad \textbf{Equation 2}$$

3.3.2.C Strut-Porosity by Scanning Electron Microscopy and Image Analysis (SEM)

Quantification of strut-porosity was also performed using serial sections and a Scanning Electron Microscope linked to the same Nikon image analysing system described above for Optical Microscopy. Image analysis was performed on 3 images of sections taken from an embedded specimen. The specimens were vacuum embedded in Epofix resin (Struers, Glasgow) and left to cure at room temperature overnight. Once cured the specimens are polished on a Struers automatic polishing

machine to determine the area fraction of porosity in the measurement frame at x500 magnification (Figure 3-4).

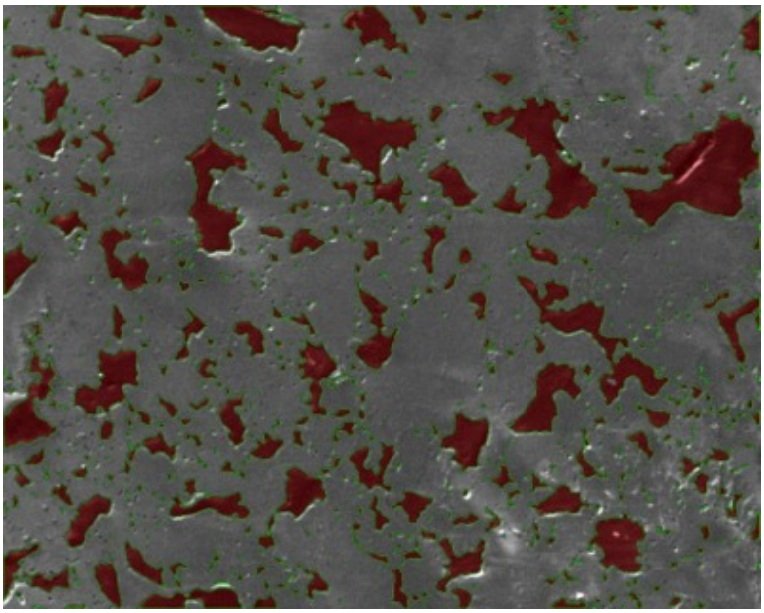

Figure 3-4 SEM Micrograph of Strut-porosity
Strut-porosity (red areas outlined in green) as viewed at x500 magnification with scanning electron microscopy and image analysis. The scanning electron microscopy technique elicits images with a much higher depth of contrast which improves the accuracy with which the edges of porosity can be detected and subsequently analysed.

The area ratio of strut-porosity to total strut area within the analysis measurement frame is equivalent to the volume fraction of strut which is occupied by the strut-porosity (Equation 2).

3.3.2.D **Helium Pyconometry**

Helium pyconometry was used to determine the bulk density of the test materials. That is the density inclusive of pores which are closed to intrusion by helium under pressure but exclusive of open porosity. Helium pyconometry calculates by subtraction the volume of a sample using a sample cell of known volume (to a high precision) and a known volume of Helium gas. The measurement assumes a theoretical density of phase pure hydroxyapatite of 1.356g/cm^3 (Hing, Best et al. 1999). The following conditions were used for the Pyconometry measurement: a purge pressure of 19 Psi; measurements were carried out at ambient temperature and pressure (20-25˚C and 1 atmosphere).

3.3.2.E **Mercury Intrusion Porosimetry (MIP)**

The strut-porosity was measured by Mercury Intrusion Porosimetry using a PoreMasterGT60 (Quantachrome, UK). If dV is the volume element of all pores with radii between r and r+ dr, then (Equation 3):

$$dV = D_v(r)\,dr \qquad \textbf{Equation 3}$$

where $D_v(r)$ is the volume pore size distribution function defined as the pore volume per unit interval of radius. Differentiation of the Washburn equation (described in a later section - Equation 14), assuming constancy of γ and θ, gives (Equation 4):

$$Pdr + rdP = 0 \qquad \textbf{Equation 4}$$

Combining Equation 3 & Equation 4 gives (Equation 5):

$$-dV = D_v(r)\frac{r}{P}dP \qquad \textbf{Equation 5}$$

Equation 5 represents a convenient means of reducing the cumulative curve (Figure 3-6) to the distribution curve (Figure 3-7) which gives the pore volume per unit radius interval. Briefly, a series of $\frac{\Delta V}{\Delta P}$ values are taken from the raw data. Each value of $\frac{\Delta V}{\Delta P}$ is multiplied by the pressure at the upper end of the interval and divided by the corresponding radius. The resulting value is then plotted versus the pore interconnection radius. The distribution curve is convenient for identifying the lower and upper bounds of the interconnection sizes of strut-porosity which is typically in the region of 0.2 - 5.0 microns. With the interconnection size range determined from the distribution curve for each sample the volume intruded per unit volume of the device can be extracted from the data table and used to determine the volume strut-porosity per unit volume of device.

The following conditions were used for the Porosimetry measurement: an advancing contact angle of 140 degrees, a liquid-vapour interfacial free energy for mercury of 0.480 mJ/m^2, and a mercury density of 13.5335 g/ml.

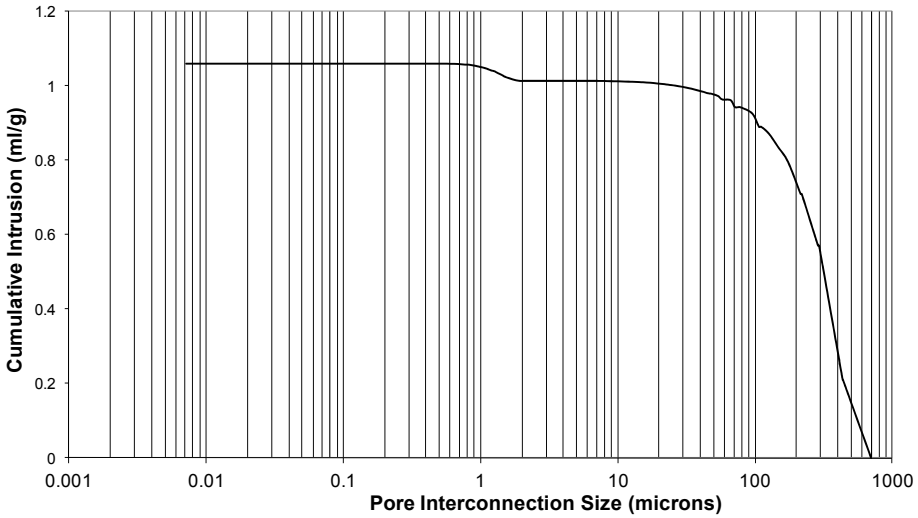

Figure 3-5 Typical MIP Intrusion Curve
Sample shown is SiCaP-32G. This intrusion curve demonstrates a step change in intrusion at approximately 1 ml/g. This indicates the break through pressure at which mercury intrudes the strut-porosity.

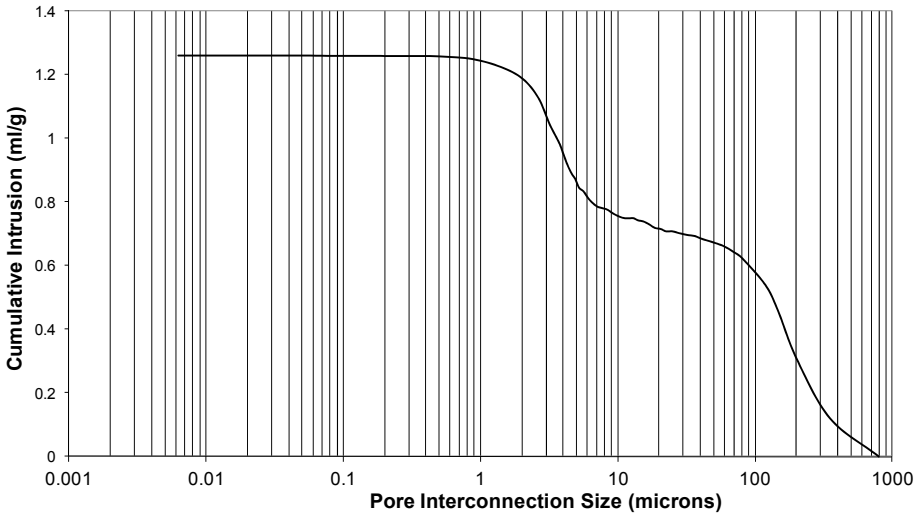

Figure 3-6 Typical MIP Intrusion Curve
Sample shown is β-TCP. The difference in intrusion curve between this material (β-TCP) and that shown above in Figure 3-5 demonstrates that the two test materials have substantially different microstructures.

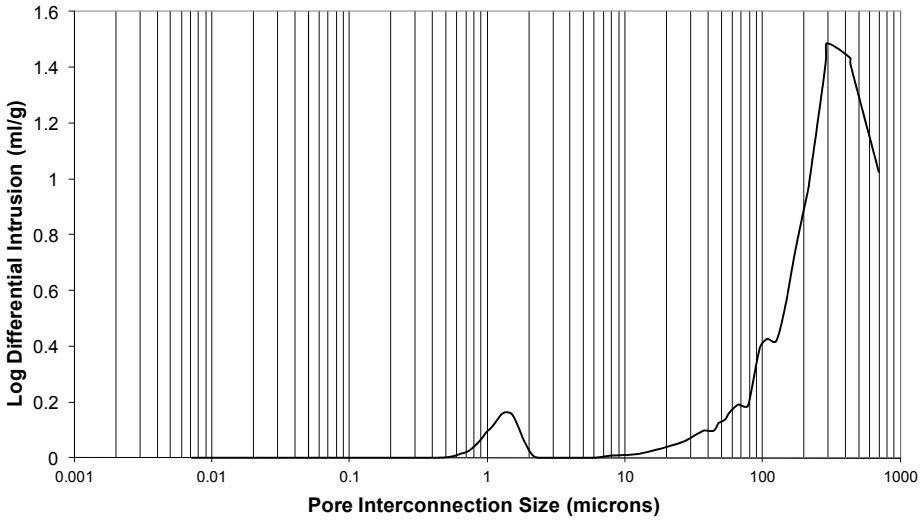

Figure 3-7 Typical Pore Interconnection Size Distribution by MIP
The log differential intrusion plot clearly demonstrates the existence of two populations of porosity in the silicate-substituted calcium phosphate test material over the pore interconnection sizes of 0.1-5 microns and 10-1000 microns. Sample shown is SiCaP-23G.

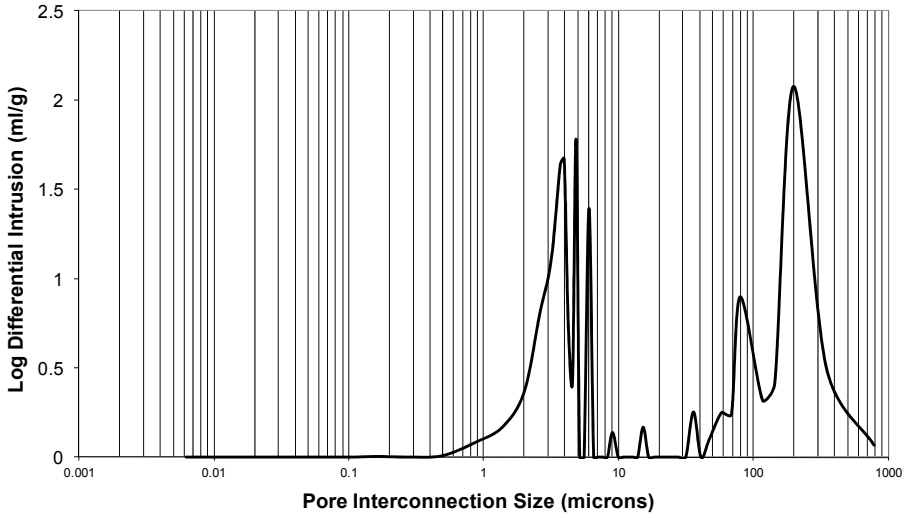

Figure 3-8 Typical Pore Interconnection Size Distribution by MIP.
A similar bi-modal pore size distribution was evident in the β-TCP test material. There appeared to be a greater volume of porosity overall in the β-TCP test material and a greater proportion in the strut-porosity population compared to the macroporosity population when compared to the silicate-substituted calcium phosphate.

The volume of closed strut pores, determined by the Pyconometry, is added to the volume of open strut pores, determined by Porosimetry, to give the total pore volume fraction of strut-porosity which is expressed as a percentage of the strut volume (Equation 6).

$$\%\ Strut\ Porosity = \frac{Volume_{OPEN\ STRUT\ POROSITY} + Volume_{CLOSED\ STRUT\ POROSITY}}{Volume_{STRUT}} \times 100\% \qquad \textbf{Equation 6}$$

3.3.2.F **Conversion between stereological (Image analysis) and absolute (Mercury Intrusion Porosimetry) techniques**

Planar characterisation of structural features of sectioned materials has historically been the preferred method for measurement of strut-porosity. However, with volumetric techniques for structural characterisation, such as mercury intrusion porosimetry, being used more frequently as a research tool there is a need to compare techniques. From this authors study of the literature the comparison between planar techniques and mercury intrusion porosimetry has not previously been reported or indeed investigated.

In stereology Delesse's principle states that the percentage area attributed to a feature in a planar section is equivalent to the volume fraction occupied by the same feature in three dimensions. Historically, Delesse's principle has been used to determine the volume fraction strut-porosity from planar sections of the test materials. Like any stereological technique this method makes assumptions about the structure of the material, principally that it is entirely homogeneous. In practice this means that there is a difference found between the volume fraction strut-porosity determined by optical microscopy or scanning electron microscopy and the volume fraction determined by mercury intrusion porosimetry. However, this difference is repeatable and predictable, and has been experimentally characterized. In the following sections the methods for comparison of the techniques are described.

3.3.2.F.a *Method comparison*

The data acquired is intended to provide objective evidence at every stage of testing that the porosimetry system performs similarly or better than the microscopy system, according to the challenges described in Table 3-2 & Table 3-3.

Table 3-2 Method comparison acceptance criteria

Challenge	Pass Criteria	Fail Criteria
Linearity	$r^2 \geq 0.9$	$r^2 < 0.9$
Range	Min & max within 95% confidence level of linear regression	Min & max outside 95% confidence level of linear regression
Repeatability	$Variance_{MIP} < Variance_{Microscopy}$	$Variance_{MIP} > Variance_{Microscopy}$
Accuracy	Measurements of standard reference material within 95% reproducibility limits	Measurements of standard reference material outside 95% reproducibility limits

Table 3-3 Reference Material Parameters and Acceptance Criteria for Accuracy

		Acceptance Criteria
Material	Coarse silica powder (SiO_2)	N/A
Catalogue No.	3002	N/A
Lot No.	107	N/A
Total Intruded volume	0.2847 cc/g ± 0.0464	0.2383 – 0.3311 (95% CL)
Median Pore Diameter	42.40 μm ± 7.48	34.92 – 49.88 (95% CL)

For each set of sample results, an F-test for sample variance was performed to determine whether the variances of the sample can be assumed to be the same. Where this was the case (F < F-critical) a two-tailed t-test was carried out with p=0.05, assuming equal variances. Where the variances are dissimilar (F > F-critical) the t-test was performed assuming unequal variances. In both cases, the null hypothesis was that the sample means are similar. The alternative hypothesis was that the sample means are different. The null hypothesis was accepted where t-stat < t-critical. An ANOVA was used to determine the variance in the results, and this will be compared to that of optical microscopy. A linear regression with a 95% confidence level will be plotted using means of the measurements from each batch.

3.3.2.F.b *Linearity*

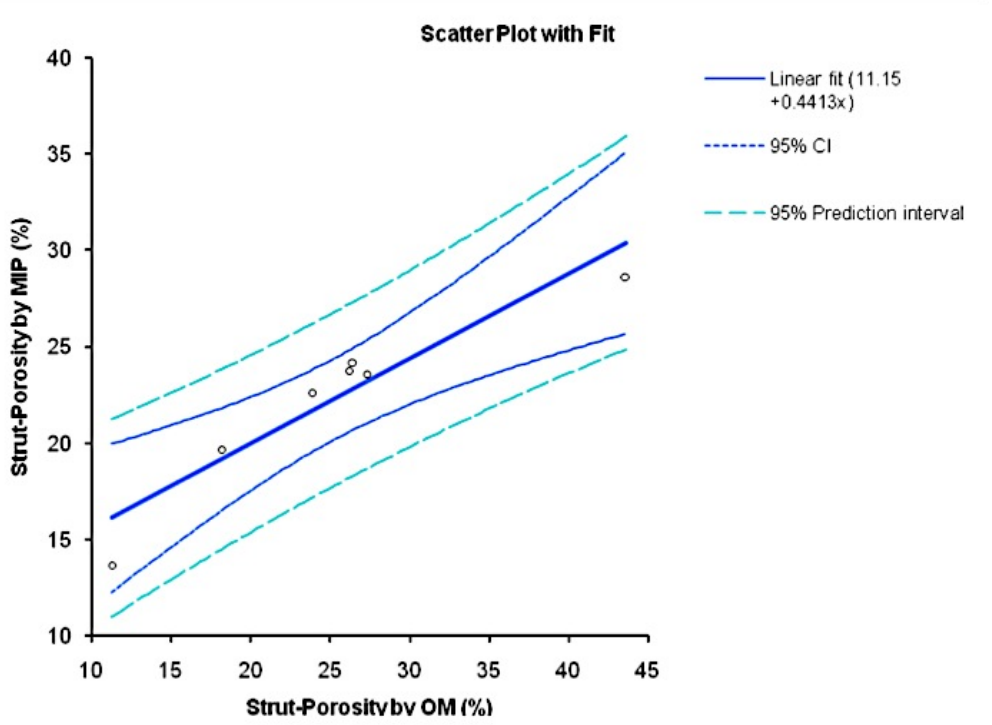

Figure 3-9 Linear regression for Strut-porosity OMvMIP

A linear regression for strut-porosity measured by Mercury intrusion porosimetry and Optical Microscopy provided a reasonable correlation between the two techniques (R^2=0.895).

A residual is defined as the difference between the observed and fitted values of the dependent variable in the regression analysis ($y = y_x - y_y$); basically, it is the distance between the data point and the regression line (Twomey and Kroll 2008). The y-axis is freely scalable and the x-axis consists of the comparative method and bisects the y-axis at zero. The residual plot is useful for the judgement of linearity – if there is an even spread of points around y = 0 throughout the x-axis this implies that there is linearity between the two methods.

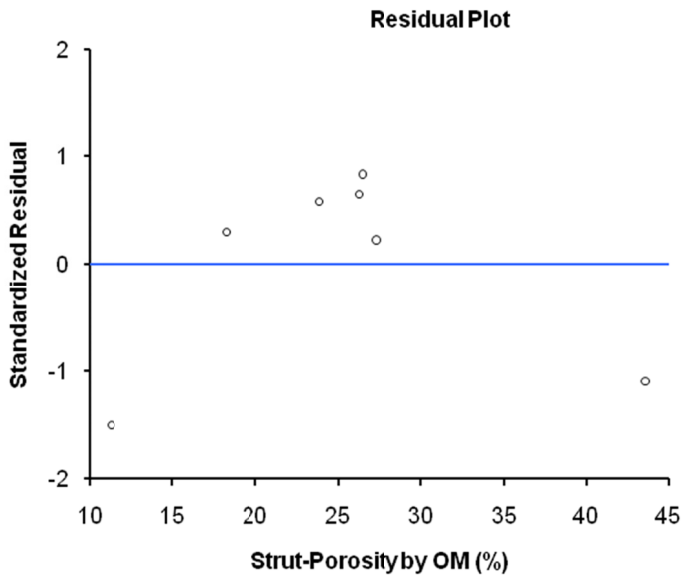

Figure 3-10 Residuals plot for Strut-porosity OMvMIP

A residuals plot for strut-porosity measured by Mercury intrusion porosimetry and Optical Microscopy was used to examine linearity. This plot demonstrated a lack of linearity between the two techniques since the residuals were not evenly spaced about the standard line.

The residual plot for linear regression described above (Figure 3-9 & Figure 3-10) indicates that a non-linear relationship exists between optical microscopy and mercury intrusion porosimetry as measurement techniques for strut-porosity. A non-linear relationship is identifiable from the un-even spread of residuals along the x-axis, particularly at the extents of the measured range.

The log fit and transformation graphs in Figure 3-11 and Figure 3-12 demonstrate the better prediction interval obtained after transformation compared with before transformation (Figure 3-9).

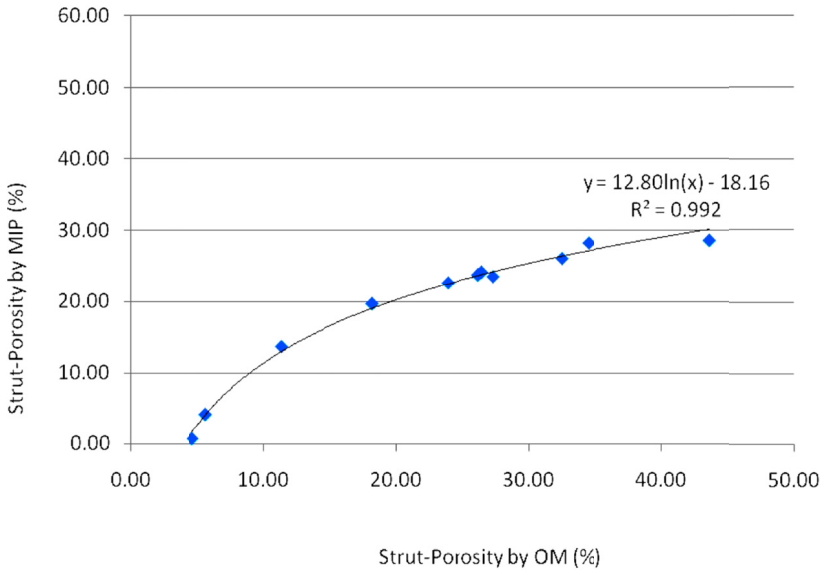

Figure 3-11 Log fit for Strut-porosity OMvMIP

Using a log fit for the relationship between strut-porosity measured by Mercury intrusion porosimetry and Optical Microscopy elicited a much stronger correlation (R^2=0.992) between the two datasets.

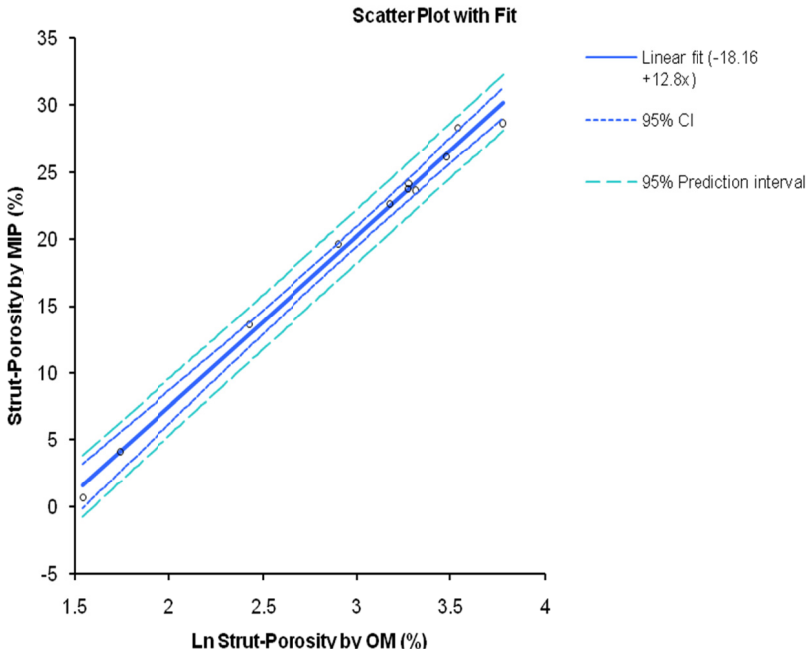

Figure 3-12 Transformed Log fit for Strut-porosity OMvMIP

The log transformation for the log fit described in Figure 3-11, with a much improved confidence interval and prediction interval.

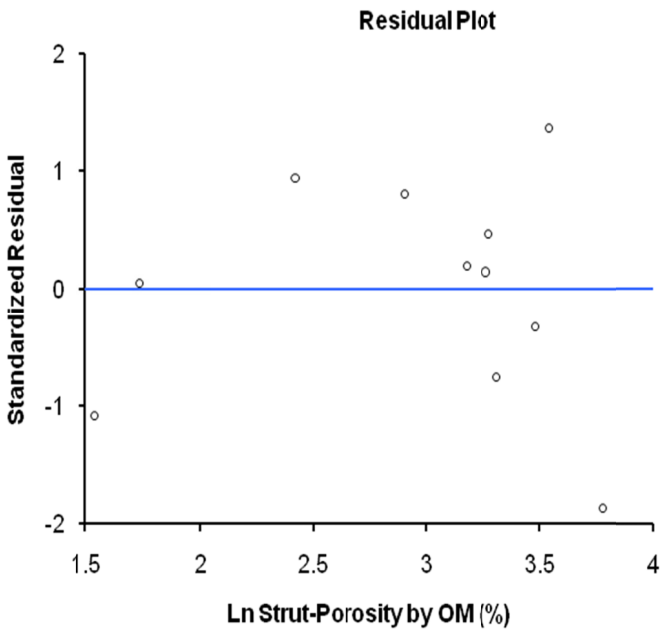

Figure 3-13 Residuals plot for transformed Log fit for Strut-porosity OMvMIP
The residuals plot for the transformed data indicates a linear relationship between the transformed data sets since the residuals are more evenly distributed above and below the standard line.

The residual plot for the transformation (Figure 3-13) demonstrates that the distribution of residuals through the measured range is more even than for the un-transformed data.

Deming's linear regression analysis

Deming's linear regression minimises the distances of the data points orthogonal (at right angles) to the regression line as opposed to least squares regression which does so only in the y direction. This is relevant to this particular method validation because variation is known to occur in both the x-axis (optical microscopy) and y-axis (mercury intrusion porosimetry), and so a Deming's regression will take this into account better than least square's regression.

One further advantage to running the Deming's regression analysis in Analyse-it® Method Evaluation edition (Method validation software For IVDs, clinical laboratories and researchers to help establish, verify and demonstrate method performance during development, compliance, implementation, QA, proficiency testing & support) is that the Sy|x statistic is reported.

Sy|x is the standard deviation of the residuals and is calculated by parametric regression methods (in this case Deming's linear fit – which minimises the squared residuals in the x and y direction). Sy|x represents the degree of total random error [including sample-related effects, total analytical precision ($S_{a,\,tot}$), drift or shift, and non-linearity] between two methods. Sy|x is independent of the data range and is more likely to have a greater degree of change with increasing random error. Sy|x should always be compared to $S_{a,\,tot}$ to assess sample-related effects.

Usually, both methods contribute to Sy|x and so an F-test must be applied to determine which test variance contributes most, or least, to the Sy|x. If Sy|x is representative across the whole range (as determined by equal variance) then 95% of values will be within ±2 Sy|x, applied in the same way SD's are applied to data.

An F-test for variance demonstrated there was difference between the test methods.

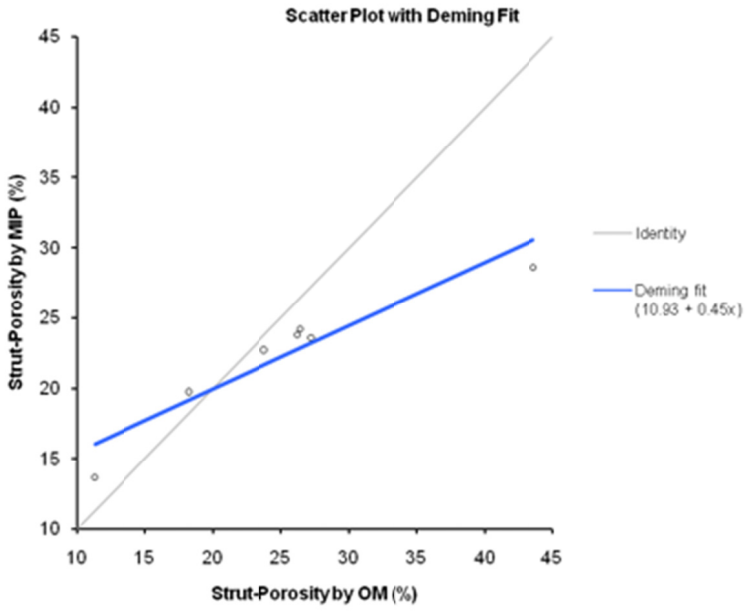

Figure 3-14 Deming's regression of Strut-porosity OMvMIP

Deming's linear regression for un-transformed data (Sy|x [vertical] = 1.640).

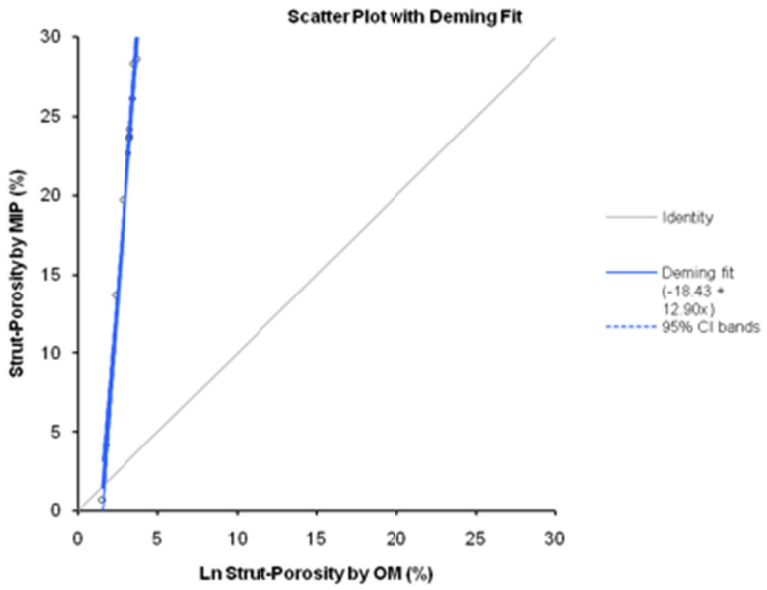

Figure 3-15 Deming's regression of transformed Strut-porosity OMvMIP

Deming's linear regression for log-transformed data (Sy|x [vertical] = 0.846)

The Sy|x in the vertical axis for transformed data (Figure 3-15) is approximately half the value for un-transformed data (Figure 3-14).

3.3.2.F.c *Repeatability*

Analysis of the relative variance of each technique is the simplest method of comparing the repeatability of the measurement method. The variance of each method was determined over the intended range of measurement, from low to high strut-porosity (Table 3-4). There was no apparent trend of variance with the position within the range, although the greatest variance was observed in the upper half of the range for both techniques. This is consistent with variance being a function of the number of artefacts which could be incorporated in the measurement, particularly for optical microscopy coupled with image analysis for which artefact-related errors have more impact due to the sample size relative to MIP.

Table 3-4 Repeatability data

Batch	Density (g/cc)	MIP			Optical Microscopy		
		Mean Strut Porosity (%)	Variance	S.D.	Mean Strut Porosity (%)	Variance	S.D.
1	3.0723	23.56	2.75	1.66	27.31	4.42	2.10
2	3.0288	23.78	2.35	1.53	26.22	10.48	3.24
3	3.1373	24.18	8.88	2.98	26.46	3.58	1.89
4	3.0437	22.64	4.20	2.05	23.87	4.15	2.04
5	3.0826	13.69	2.63	1.62	11.30	0.45	0.67
6	3.1489	28.61	5.31	2.30	43.60	14.78	3.85
7	3.1882	19.69	3.32	1.82	18.22	6.11	2.47
		Average:	4.21	2.00	Average:	6.28	2.32

3.3.2.F.d *Accuracy*

Standard reference materials (Quantachrome, UK) were tested in order to determine whether the technique accuracy was within the tolerances specified by the equipment supplier.

Table 3-5 Accuracy data

Sample	Total Intruded Volume (cc/g)		Median Pore Diameter (micron)	
	Measured	Limits	Measured	Limits
1	0.2662	0.2383 - 0.3311	45.18	34.92 - 49.88
2	0.2711	0.2383 - 0.3311	42.17	34.92 - 49.88

3.3.2.F.e *Range*

The model generated with the use of experimental data in this validation can be used reliably to predict the equivalent strut-porosity by optical microscopy when the measured values by mercury porosimetry coupled with helium pyconometry are between 5.00-33.00 %. This range of data from mercury porosimetry coupled with helium pyconometry is equivalent to 5.00-47.00 % by optical microscopy.

3.3.2.F.f *Method Comparison Results summary*

The data presented in the preceding sections indicates that a predictive model can

successfully be used to compare between Mercury Intrusion Porosimetry and stereological techniques. The relationship is not directly linear but a Log transform results in a fit with a r^2 predictive value of 0.992 which is considered acceptable for method comparison. The likely cause for the non-linear relationship is that the comparison is made between an absolute, volumetric measurement (MIP) with a planar method which assumes that the measured area of a feature is equivalent to the same proportion of the feature in three dimensions (Optical Microscopy). Further root causes could include measurement error, sample size, or contamination related effects. This method comparison could prove useful to the scientific community if MIP becomes a routine measurement tool.

Table 3-6 MIP Method validation data

Challenge	Pass Criteria	Fail Criteria	Results
Linearity	$r^2 \geq 0.9$	$r^2 < 0.9$	$r^2 = 0.90$ (Linear)
	$r^2 \geq 0.9$	$r^2 < 0.9$	$r^2 = 0.992$ (Log)
Range	Min & max within 95% confidence level of linear regression	Min & max outside 95% confidence level of linear regression	Min & max within 95% confidence level of linear regression
Repeatability	$Variance_{MIP} < Variance_{Microscopy}$	$Variance_{MIP} > Variance_{Microscopy}$	$Variance_{MIP}$ (4.21) < $Variance_{Microscopy}$(6.28)
Accuracy	Measurements of standard reference material within 95% reproducibility limits	Measurements of standard reference material outside 95% reproducibility limits	Total intruded volumes 0.2662 cc/g and 0.2711 cc/g

3.3.2.G **Total Porosity and Device Density**

Specimen density and porosity was calculated according to a water immersion densitometry method (Hing, Best et al. 1999). The density of specimens was determined using the Archimedes principle, which is described as: The buoyant force is equal to the weight of the displaced fluid (also called the law of buoyancy). The real and apparent densities of specimens were thus calculated according to Equation 7 and Equation 8. The apparent density measurements include both open and closed porosity in the material, whereas the real density excludes open porosity and only

considers closed pores. The density of water was read from Table 3-7 provided with a density determination kit (Sartorius, UK) and an LE225D 5-point analytical balance (Sartorius, UK).

Table 3-7 Density table of deionised water (dH_2O)
(Table adapted from Ohaus)

Temperature (^oC)	Density (g/ml)	Temperature (^oC)	Density (g/ml)
17.5	0.9987	21.5	0.9979
18	0.9986	22	0.9978
18.5	0.9985	22.5	0.9976
19	0.9984	23	0.9975
19.5	0.9983	23.5	0.9974
20	0.9982	24	0.9973
20.5	0.9981	24.5	0.9972
21	0.9980	25	0.9971

For the analysis of specimens, samples were weighed dry (W_{dry}). Following this, the same specimens were placed in boiling deionised water for 1 hour to ensure all possible pores are filled with water. Specimens were then weight again (W_{sat}) and submerged (W_{sub}) in deionised water. This was performed using the Density AP solids Kit (Ohaus, Leicester, UK). The balance used was an Analytical Plus electronic balance AP250D (Ohaus, Leicester, UK). The commercially available β-TCP group was not analysed for total porosity as the granule sizes available from the manufacturer (1-4mm) were not compatible with the water immersion densitometry method. The total porosity provided by the manufacturer (Orthovita, USA) was used for reference.

The results obtained were used to determine closed strut porosity and total porosity using Equation 9 and Equation 10. HA was assumed to have a density of 3.156g/cm^3 (Hing, Best et al. 1999).

$$D_{apparent} = \left(\frac{W_{dry}}{W_{sat} - W_{sub}} \right) \rho H_2O \quad \textbf{Equation 7}$$

$$D_{real} = \left(\frac{W_{dry}}{W_{dry} - W_{sub}} \right) \rho H_2O \quad \textbf{Equation 8}$$

$$CS\mu = \left(1 - \frac{D_{real}}{\rho HA} \right) \times 100 \quad \textbf{Equation 9}$$

$$TP = \left(1 - \frac{D_{apparent}}{\rho HA} \right) \times 100 \quad \textbf{Equation 10}$$

D = Density
W = Weight
ρH_2O = density of deionised water at given temperature $CS\mu$ = Closed Strut porosity
ρHA = density of HA (3.156g/cm^3)
ρH_2O = density of deionised water at given temperature

3.3.2.H **Surface Area per Unit Mass**

The surface of the biomaterial was measured by Mercury Intrusion Porosimetry (MIP). The surface area of a liquid is defined as the work required to produce one square centimetre of surface. When forced under pressure into a pore of radius r and length L, the area of a volume of mercury external to the pore decreases by (Equation 11):

$$A = 2\pi r l \quad \textbf{Equation 11}$$

assuming cylindrical pores. The work required to create the additional area is (Equation 12):

$$W_1 = -2\pi r l \cos\theta \quad \textbf{Equation 12}$$

The term cosθ is introduced because the force preventing the mercury from getting into the pore acts through the contact angle θ. The work required to force the mercury into the cylindrical pore is given by the applied pressure times the pore area times the pore length or (Equation 13):

$$W_2 = P\pi r^2 l \quad \textbf{Equation 13}$$

Since W_1 must equal W_2, Equation 12 & Equation 13 can be combined to give (Equation 14):

$$\mathrm{Pr} = -2\gamma\cos\theta \qquad \textbf{Equation 14}$$

Equation 14, the Washburn equation, dictates that as the pressure is increased, the mercury will intrude into progressively narrower pores assuming that θ and γ remain constant.

Figure 3-6 is a cumulative pore volume curve which shows the summation of volume intruded into the pores and inter-particle voids plotted versus the applied pressure. The surface area of all pores and voids filled up to pressure P is calculated using Equation 12 & Equation 13 as follows (Equation 15):

$$-2\pi r l\gamma\left|\cos\theta\right| = P\Delta V \qquad \textbf{Equation 15}$$

Assuming cylindrical pores open at each end and recognising that 2πrl is the pore area S, gives (Equation 16):

$$S\gamma\left|\cos\theta\right| = P\Delta V \qquad \textbf{Equation 16}$$

Then, pores in the radius range dr which take up volume dv will exhibit a surface area, dS, given by (Equation 17):

$$dS = \frac{PdV}{\gamma\left|\cos\theta\right|} \qquad \textbf{Equation 17}$$

The following conditions are used for the Porosimetry measurement: an advancing contact angle of 140 degrees, a liquid-vapour interfacial free energy for mercury of 0.480 mJ/m^2, and a mercury density of 13.5335 g/ml. From strut-porosity and macro-porosity, strut-porosity is expected to contribute the greatest surface area to total surface area of the device. In addition, the range of detection of the Mercury Intrusion Porosimeter (0.0064 – 950 microns) does not cover the full range of porosity found in the materials described in this study so the surface area data was measured only in the range of strut-porosity.

3.3.3 Functional Characterisation

3.3.3.A **Static Dissolution Testing**

Testing of dissolution was performed in accordance with ISO 10993-14. Biological evaluation of medical devices – Part 14: Identification and quantification of

degradation products from ceramics. Samples (nominally 5g) were stored in Tris buffer (simulated conditions), at pH = 7.4, in 500ml polypropylene bottles. Samples were placed in an oven (Genlab Oven set to 37±1^{o}C) for 120 hours. The weight loss of three samples of each material was measured after storage in simulated conditions and the mean and standard deviation for each material calculated.

3.3.3.B **Bulk Strength Testing**

An 85 mL volume of each sample was measured out in a measuring cylinder of 30mm nominal inside diameter. This volume of granules was weighed and the divided into ten equal specimens by weight to give nominal specimen volume of 8.5 mL each. Each specimen was loosely loaded into a steel cylinder of 30mm inside diameter. And a loose fitting steel piston was gently placed on the surface of the granules. The cylinder was placed between the compression platens of an Instron model 4464 mechanical testing machine, fitted with a 2kN load cell.

The testing machine crosshead was lowered at a rate of 3.33 x 10^{-5} m/s until a preload of 10N was reached. The crosshead speed was then changed to 8.33 x 10^{-6} m/s. Crosshead displacement and load were recorded until the compressive load reached a threshold of 1kN, at which point the test terminated.

3.4 Results

3.4.1 Chemical Characterisation

3.4.1.A **X-ray Diffraction Spectroscopy**

Analysis of the crystalline composition all SiCaP groups with X-Ray diffractometry demonstrated that all SiCaP materials were phase pure. All spectral peaks could be accounted for by the Hydroxyapatite powder diffraction file (9-432). The diffraction spectra showed narrow, high-resolution peaks and were consistent with highly crystalline material (Figure 3-16).

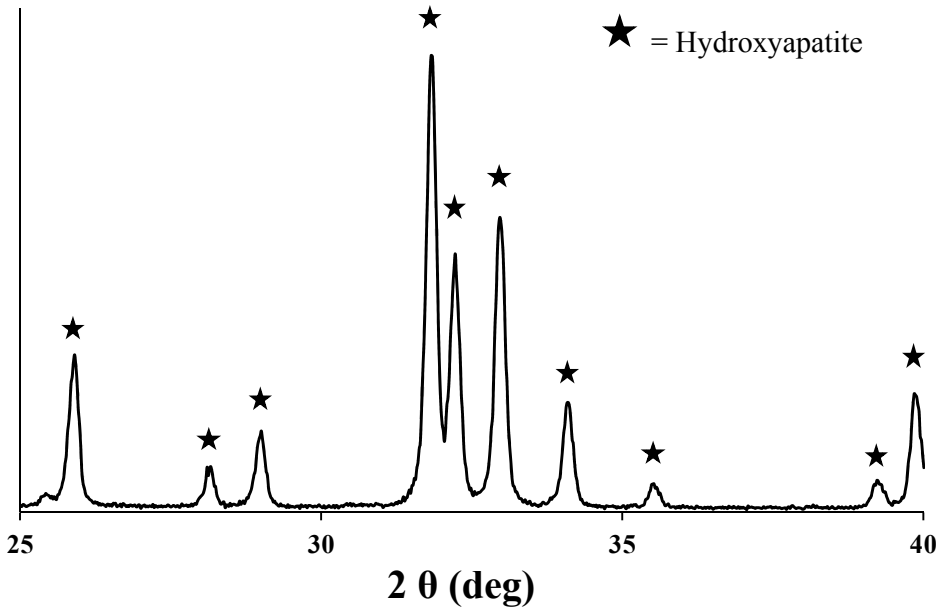

Figure 3-16 Typical XRD Spectra

X-ray diffraction spectra for the silicate-substituted hydroxyapatite test group showed narrow peaks, indicating a high degree of crystallinity, which corresponded with the library file for phase pure hydroxyapatite. There was no evidence of phase impurities such as calcium oxide or tricalcium phosphate. Spectra shown is for SiCaP-32P

Analysis of the crystalline composition the β-TCP group with X-Ray diffractometry demonstrated that the β-TCP material was phase pure. All spectral peaks could be accounted for by the beta-tricalcium phosphate powder diffraction file (9-348). The diffraction spectra showed narrow, high-resolution peaks and were consistent with highly crystalline material (Figure 3-17).

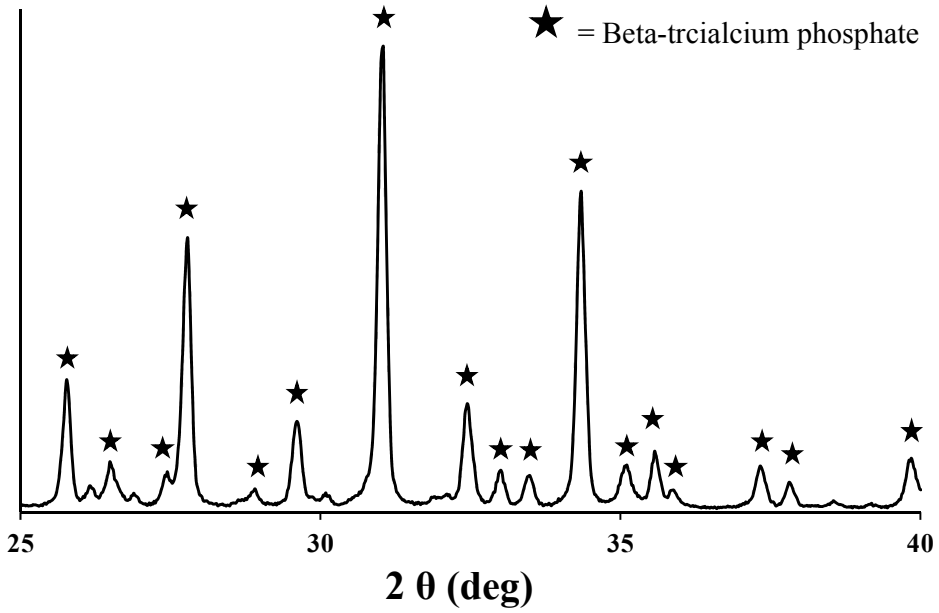

Figure 3-17 Typical XRD Spectra

X-ray diffraction spectra for the β-TCP group was indicative of a crystalline material. The spectra closely matched the library pattern for β-TCP.

3.4.1.B **X-ray fluorescence (XRF) spectroscopy**

X-Ray fluorescence spectroscopy showed all SiCaP groups to have Ca/(P+Si) ratios in the expected range for phase pure Hydroxyapatite (Table 3-8). There was no significant difference ($p \geq 0.05$) in Ca/(P+Si) ratio between the groups. XRF also demonstrated that all SiCaP samples were substituted with 0.80 ± 0.1 % silicon by weight. X-Ray fluorescence spectroscopy showed the β-TCP group to have a Ca/(P+Si) ratio in the expected range for phase pure beta-tricalcium phosphate (Table 3-8).

Table 3-8 Typical XRF Results

	Metal Oxide Content (%)	
	SiCaP (Sample data for SiCaP-23P)	β-TCP
Silicon Dioxide	1.71	<0.02
Titanium Dioxide	<0.01	<0.01
Aluminium Oxide	<0.02	<0.02
Iron (III) Oxide	<0.01	<0.02
Calcium Oxide	56.50	52.45
Magnesium Oxide	<0.02	<0.02
Potassium Oxide	<0.01	<0.01
Sodium Oxide	<0.03	0.47
Phosphorus Pentoxide	40.69	46.58
Chromium (III) Oxide	<0.01	<0.01
Manganese (II, III) Oxide	<0.01	<0.01
Zirconium Oxide	<0.02	<0.02
Hafnium Oxide	<0.01	<0.01
Lead Oxide	<0.02	<0.02
Zinc Oxide	<0.01	<0.01
Barium Oxide	<0.01	<0.01
Strontium (II) Oxide	<0.01	<0.01
Tin (IV) Oxide	<0.01	<0.01

Table 3-9Calculated Ca/P Ratio and %Wt Silicon

	Expected		Measured			
	Ca/(P+Si) Ratio	Silicon by Weight (%)	Ca/P Ratio	Silicon Dioxide by Weight (%)	Ca/(P+Si) Ratio	Silicon by Weight (%)
SiCaP	1.67	0.80	1.76	1.71	1.67	0.80
β-TCP	1.50	0.00	1.84	0.00	1.43	0.00

3.4.1.C **Fourier transform infrared spectroscopy (FTIR)**

All materials demonstrated the presence of the expected vibrational frequencies corresponding to hydroxyl (-OH) stretching and bending frequencies and the

corresponding phosphate group (P=O) stretching frequencies (Figure 3-18).

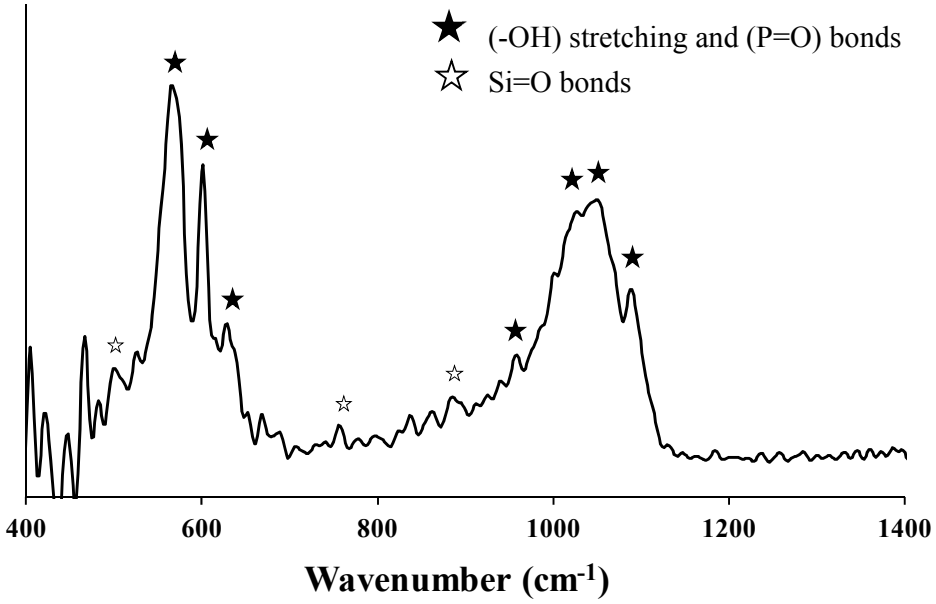

Figure 3-18 Typical FTIR Spectra

The Fourier Transform Infrared spectroscopy revealed the silicate-substituted hydroxyapatite test material to have an expected composition, comprising (OH) stretching bonds, P=O bonds, and Si=O bonds. Spectra shown is for SiCaP-32G

The spectra for all samples contained the characteristic peaks of a hydroxyapatite structure ($Ca_{10}(PO_4)_6(OH)_2$) at 573, 602, 631, 961, 1029, 1048 and 1088 cm^{-1} (Black-filled stars). Additional weak peaks at 892, 758 (very weak) and 503 cm^{-1} are indicative of the presence of SiO_4 groups in the structure and were observed in all samples (White-filled stars).

3.4.2 Physical Characterisation

3.4.2.A **Strut-porosity by Scanning Electron Microscopy**

Table 3-10 Strut-porosity as measured by Scanning Electron Microscopy

Test Material	Nominal Strut-porosity (%)	Measured Strut-porosity (%)
SiCaP-23G	23	22.83 ± 3.762
SiCaP-32G	32	29.67 ± 2.958
SiCaP-46G	46	45.33 ± 3.939

The mean strut-porosity as measured with Scanning Electron Microscopy for each treatment group was tested using a student t-test assuming equal variances. There was statistical difference between the mean strut-porosity for SiCaP-23G versus SiCaP-32G ($p=0.0002$); SiCaP-23G versus SiCaP-46G ($p<0.0001$); or SiCaP-32G versus SiCaP-46G ($p<0.0001$).

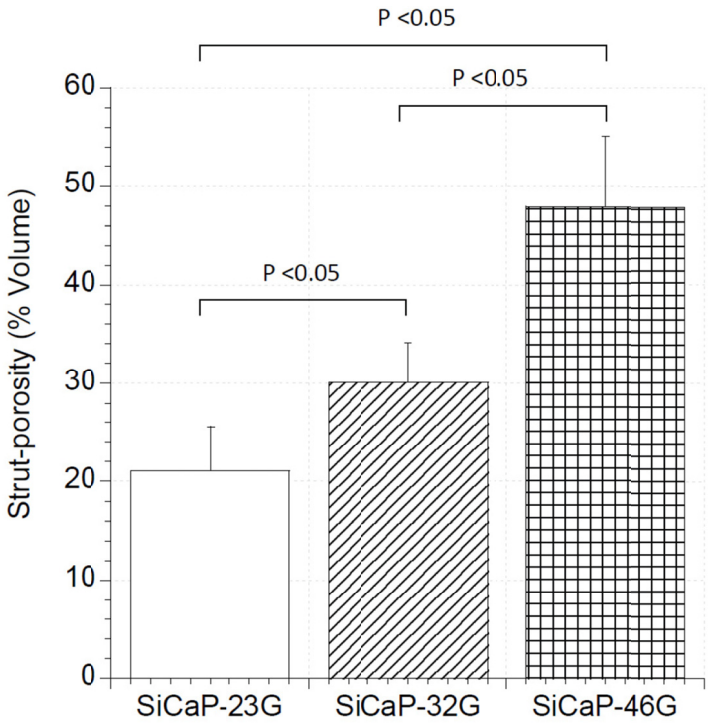

Figure 3-19 Mean Strut-porosity of test materials.

Mean strut-porosity for silicate-substituted calcium phosphate microgranules when measured with Scanning Electron Microscopy (Column=mean; whiskers=1sd). A student t-test revealed significant differences ($p<0.05$) between all test groups.

3.4.2.B **Strut-porosity by Mercury Intrusion Porosimetry**

The mean strut-porosity as measured with Scanning Electron Microscopy for each treatment group was tested using a student t-test assuming equal variances. There was statistical difference between the mean strut-porosity for SiCaP-23G versus SiCaP-32G ($p=0.0041$); SiCaP-23G versus SiCaP-46G ($p<0.0001$); or SiCaP-32G versus SiCaP-46G ($p=0.0003$).

Table 3-11 Strut-porosity as measured by Mercury Intrusion Porosimetry

Test Material	Nominal Strut-porosity (%)	Measured Strut-porosity (%)
SiCaP-23G	23	21.11 ± 4.481
SiCaP-32G	32	30.12 ± 3.941
SiCaP-46G	46	48.89 ± 7.199
β-TCP	48	48.04 ± 3.043

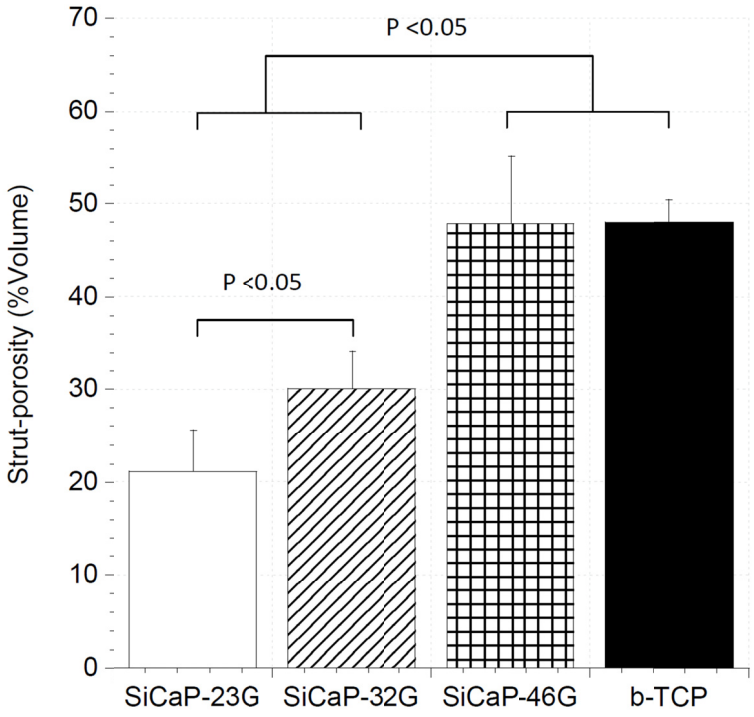

Figure 3-20 Mean Strut-porosity of test materials.

Mean strut-porosity for silicate-substituted calcium phosphate microgranules when measured with Mercury Intrusion Porosimetry. (Column=mean; whiskers=1sd). A student t-test revealed that the difference between groups was statistically significant ($p<0.05$) for all comparisons, excluding a comparison between SiCaP-32G and SiCaP-46G.

3.4.2.C **Total Porosity**

Table 3-12 Total Porosity

Test Material	Nominal Strut-porosity (%)	Total Porosity (%)
SiCaP-23G	23	79.75 ± 1.893
SiCaP-32G	32	79.27 ± 1.893
SiCaP-46G	46	82.02 ± 2.000

The mean total porosity for each treatment group was tested using a student t-test assuming equal variances. There was no statistical difference between the mean total porosity for SiCaP-23G versus SiCaP-32G (p=0.7216); SiCaP-23G versus SiCaP-46G (p=0.1534); or SiCaP-32G versus SiCaP-46G (p=0.0923).

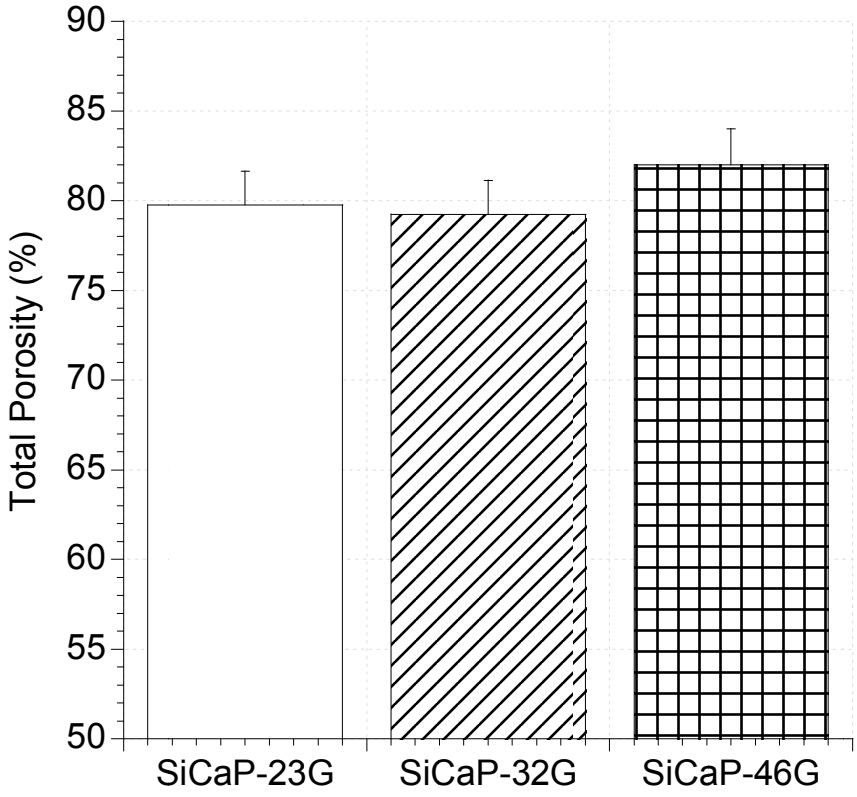

Figure 3-21 Mean total porosity of test materials

Mean total porosity for silicate-substituted calcium phosphate microgranules with varying strut-porosity (Column=mean; whiskers=1sd). There was no significant difference between the test groups (student t-test, p>0.05).

3.4.2.D **Surface Area per Unit Mass**

The mean surface areas for each device were tested using a student t-test assuming equal variances. There was no statistical difference between the mean surface areas for SiCaP-32G versus SiCaP-46G (p=0.1595). However, the mean surface area for SiCaP-23G is statistically lower than for the three other groups (p<0.05).

Table 3-13 Surface Area per Unit Mass

Test Material	Nominal Strut-porosity (%)	Average Surface Area per Unit Mass (m^2/g)
SiCaP-23G	23	0.410 ± 0.085
SiCaP-32G	32	0.600 ± 0.021
SiCaP-46G	46	0.561 ± 0.033
β-TCP	48	0.568 ± 0.071

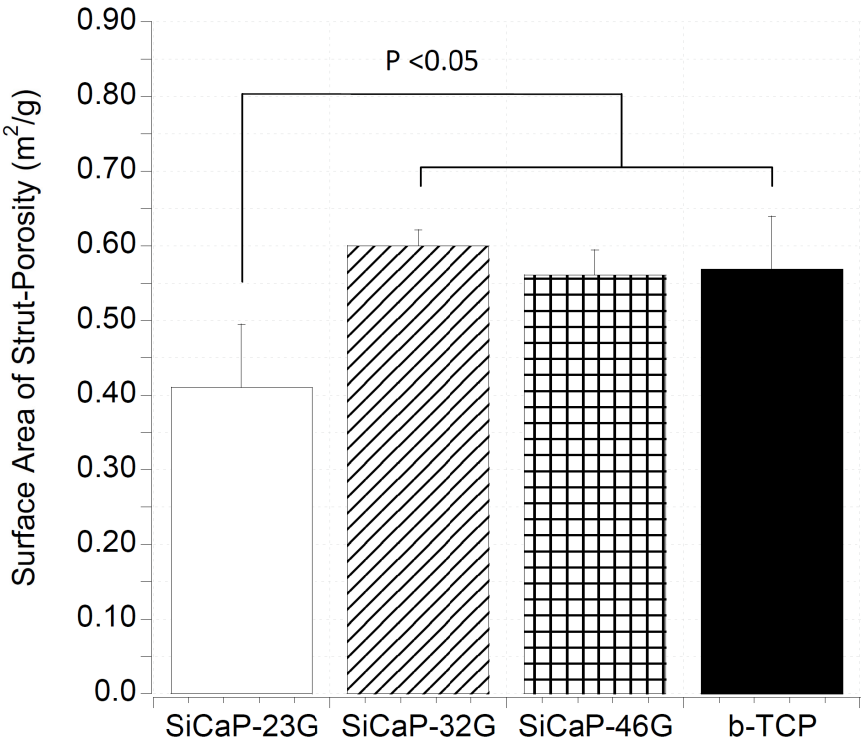

Figure 3-22 Mean surface area of test materials

Mean surface area for silicate-substituted calcium phosphate microgranules with varying strut-porosity (Column=mean; whiskers=1sd). According to a student t-test, there was no significant difference between SiCaP-32G; SiCaP-46G; and β-TCP. SiCaP-23G had a lower surface area than all other test groups (p<0.05).

3.4.3 Functional Characterisation

3.4.3.A **Static Dissolution Testing**

Table 3-14 Sample Weight Loss

Test Group	Sample 1 (%)	Sample 2 (%)	Sample 3 (%)	Average (%)
SiCaP-23G	0.356	0.421	0.264	0.347 ± 0.079
SiCaP-32G	0.448	0.343	0.442	0.411 ± 0.059

The weight losses measured for all test samples was small. A student t-test (two-tail) was performed on the weight loss data, which indicated there was no significant difference ($p>0.05$) in weight loss between the materials.

The levels of calcium (Ca), phosphorus (P), and silicon (Si) in the TRIS buffer soaking solution were measured with ICP-OES prior to the dissolution period (Table 3-15) and following the 120 hour dissolution period. Three solutions for each material were measured and the mean and standard deviations for each ion calculated (Table 3-16).

Table 3-15 Calcium, Phosphorus, and Silicon in the soaking solution by ICP-OES

Test Group	Ca (mg/L)	P (mg/L)	Si (mg/L)
TRIS BUFFER	<0.05	<0.05	<0.1

Table 3-16 Calcium, Phosphorus, and Silicon in the soaking solution after dissolution of the materials by ICP-OES

Test Group	Ca (mg/L)	P (mg/L)	Si (mg/L)
SiCaP-23G	34.3 ± 2.5	1.2 ± 0.1	0.8 ± 0.1
SiCaP-32G	20.3 ± 3.8	2.2 ± 0.5	1.7 ± 0.3

A significant difference in dissolution of calcium ions ($p<0.05$) and silicon ions ($p<0.05$), but no significant difference in dissolution of phosphorus ions ($p=0.526$) between the test groups. The difference in Ca, P, and Si ion release between the test materials may be attributed to the small variations in granule size or surface area of the device as a result of batch-batch variability in the test groups (See section 3.3.2.H). Under static conditions there was very little impact of porosity on weight

loss or ionic dissolution from the test materials. This is likely due to the fact that both test materials comprise a highly crystalline phase of hydroxyapatite. A significant difference in dissolution may be observed if the same materials were tested in dynamic conditions.

3.4.3.B **Bulk Strength Testing**

There was no substantial difference in the displacement at 1kN load/displacement curve between the test materials despite there being a considerable difference in the volume of macroporosity and microporosity in the struts of the scaffold (Section 3.3.2.B). All test groups demonstrated a plastic region of deformation as the space between the granules was compacted and the macropores collapsed under load. This was followed by a region demonstrating a sharp increase in load relative to the displacement characteristic of a microporous material resisting deformation (Figure 3-23).

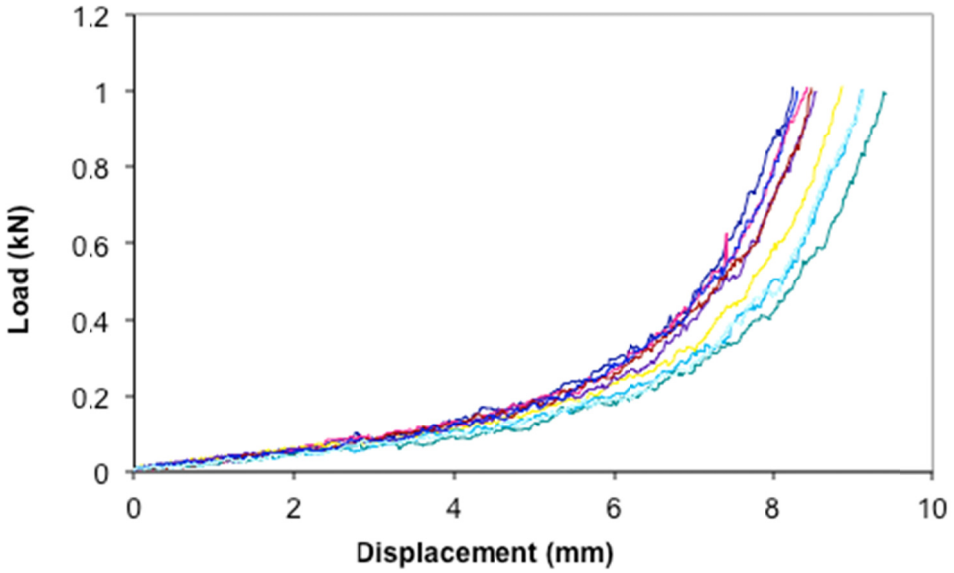

Figure 3-23 Load / displacement graph for SiCaP-23G

The load / displacement graphs demonstrated two regions of plastic deformation in all test materials. The first being attributed to the packing down of granules and the failure of the macropore struts, the second being attributed to the compression of the bulk material to remove the microporous spaces. The failure load was not reached before the test was stopped at 1kN.

There was a significant difference ($p<0.05$) in the final displacement reached for SiCaP-32G and SiCaP-46G compared to SiCaP-23G (Table 3-17 & Figure 3-24). There was no significant difference ($p>0.05$) between the final displacement reached

for SiCaP-32G and SiCaP-46G.

Table 3-17 Displacement under 1kN load

Test Material	Nominal Strut-porosity (%)	Displacement at 1kN load (mm)
SiCaP-23G	23	7.04 ± 0.44
SiCaP-32G	32	7.66 ± 0.26
SiCaP-46G	46	7.93 ± 0.23

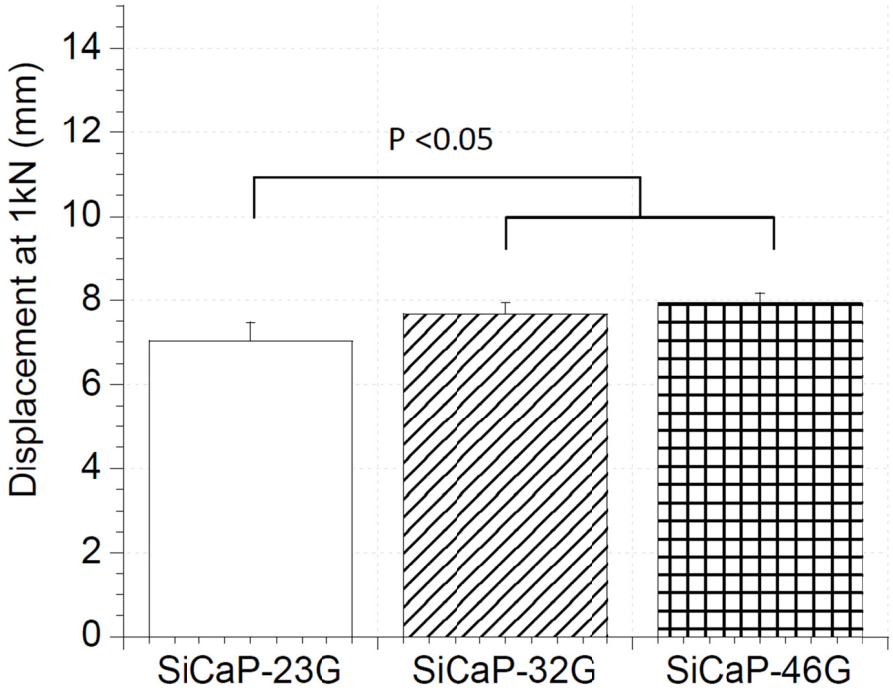

Figure 3-24 Maximum displacement for microgranules of varying strut-porosity (Column=mean; whiskers=1sd). There was no significant difference (p>0.05) in the displacement under load when comparing SiCaP-32G and SiCaP-46G. However, SiCaP-23G was significantly less resistant to load (p<0.05).

3.5 Discussion

3.5.1 Chemical Characterisation

The materials were first characterised for phase purity, ionic composition, and

crystallinity in order to confirm the claims of the manufacturers from whom the commercially available products were supplied (Table 3-1). Chemical characterisation of the SiCaP materials provided by ApaTech revealed the samples to be phase-pure, highly crystalline, silicate-substituted hydroxyapatite with a Ca/P+Si ratio of 1.67 and 0.80% silicon by weight substituted into the crystal lattice. This is consistent with all previous research for materials manufactured by the same novel aqueous precipitation and foaming route. The presence of hydroxyapatite as a highly crystalline phase is consistent with other bone graft substitutes characterised by the same techniques (Tadic and Epple 2004).

X-ray Fluorescence spectroscopy (XRF) confirmed the absence of any metal contaminants in the form of metal oxides, including: titanium dioxide; aluminium oxide; iron (III) oxide; magnesium oxide; potassium oxide; sodium oxide; chromium (III) oxide; manganese (II, III) oxide; zirconium oxide; hafnium oxide; lead oxide; zinc oxide; barium oxide; strontium (II) oxide; and tin (IV) oxide. There was no noticeable change in chemistry with increasing porosity. Nor was there an appreciable difference in phase purity, crystallinity, or ionic composition between those SiCaP groups incorporating an aqueous poloxamer carrier and those not.

Fourier transform infrared spectroscopy (FTIR) of the silicated calcium phosphate confirmed all SiCaP materials to be free of impurity moieties which is consistent with that reported by previous researchers (Figure 3-25).

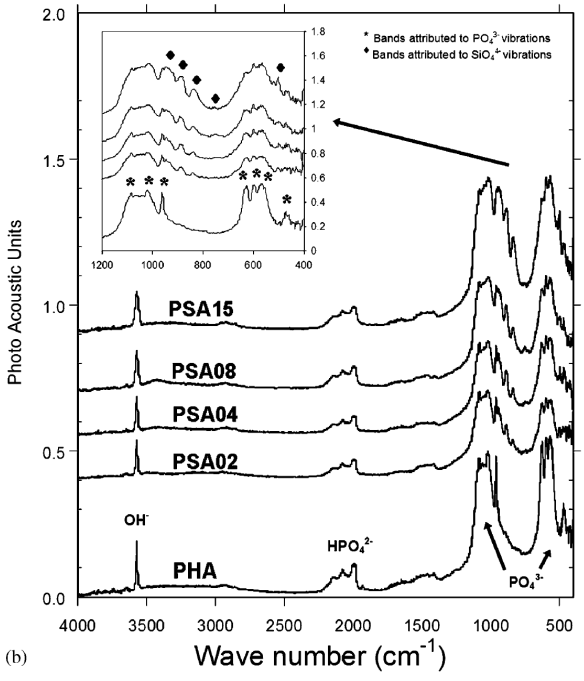

Figure 3-25 FTIR Analysis of SiCaP-32G

FTIR trace for SiHA as reported in the literature – reproduced with permission from (Hing, Revell et al. 2006);

The FTIR trace for the silicate-substituted calcium phosphate test group (Figure 3-18) shared similar peak patterns over the range of 500-1500 cm^{-1} as those reported previously in the literature.

X-ray diffraction spectroscopy confirmed that the commercially available β-TCP manufactured by Orthovita (USA) was phase-pure and did not contain any traces of phase impurities such as hydroxyapatite or calcium oxide. This analysis also confirmed the β-TCP to be of relatively high crystallinity, as demonstrated by the narrow peak breadth in the TCP pattern. Both these observations were consistent with previous studies of the same commercially available β-TCP (Tadic and Epple 2004). Similar to the SiCaP materials there was no evidence of substantial metal oxide contamination following XRF analysis, although a trace level of sodium oxide (0.47%) was detected.

3.5.2 Physical Characterisation

To determine the effects of structure on the osteogenic potential and mechanical properties of calcium phosphates in later chapters, the silicate-substituted calcium phosphate materials were fully characterised in this chapter for strut-porosity; device density; total porosity; and surface area.

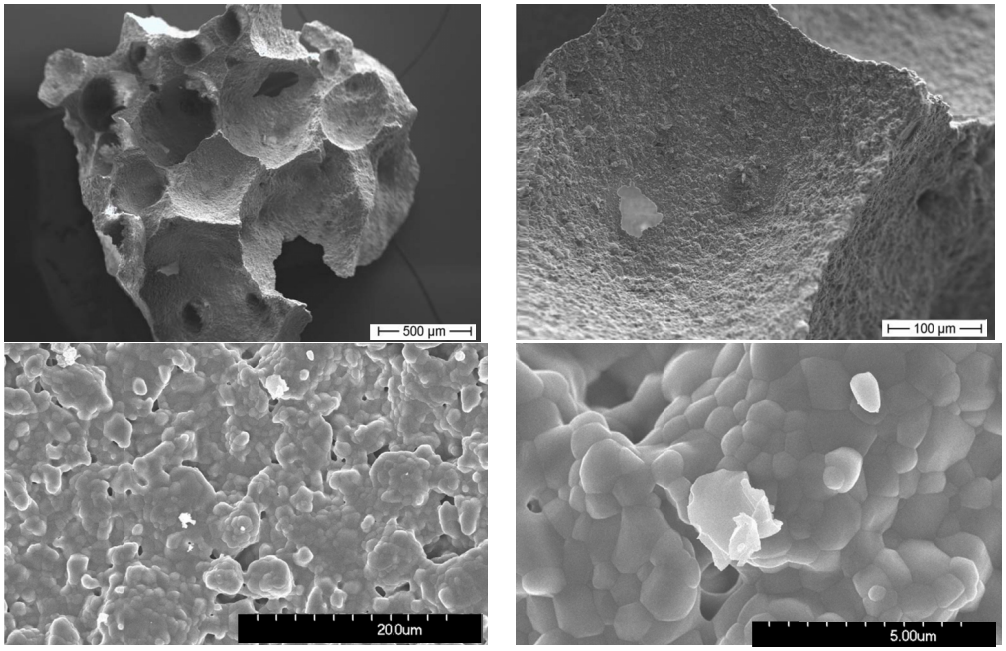

Figure 3-26 SEM images of SiCaP-23G

Scanning electron microscopy revealed the silicate-substituted test group to comprise of two populations of porosity. Large interconnected macropores framed by struts, containing a network of smaller pores (strut-porosity). Top: Low (left) and high (right) SEM of SiCaP-23G using secondary electron detector; Bottom: Low (left) and high (right) SEM of SiCaP-23G using back-scattered detector

All test groups consisted of porous materials with two distinct populations of porosity: those pores visible to the naked eye being approximately 50-1000 microns in size with interconnections of approximately 150 microns; and those pores present between the ceramic particulates making up the struts of the macropores being approximately 0.2-5.0 microns in diameter and having interconnections of approximately 1.0 microns (Figure 3-26 & Figure 3-27).

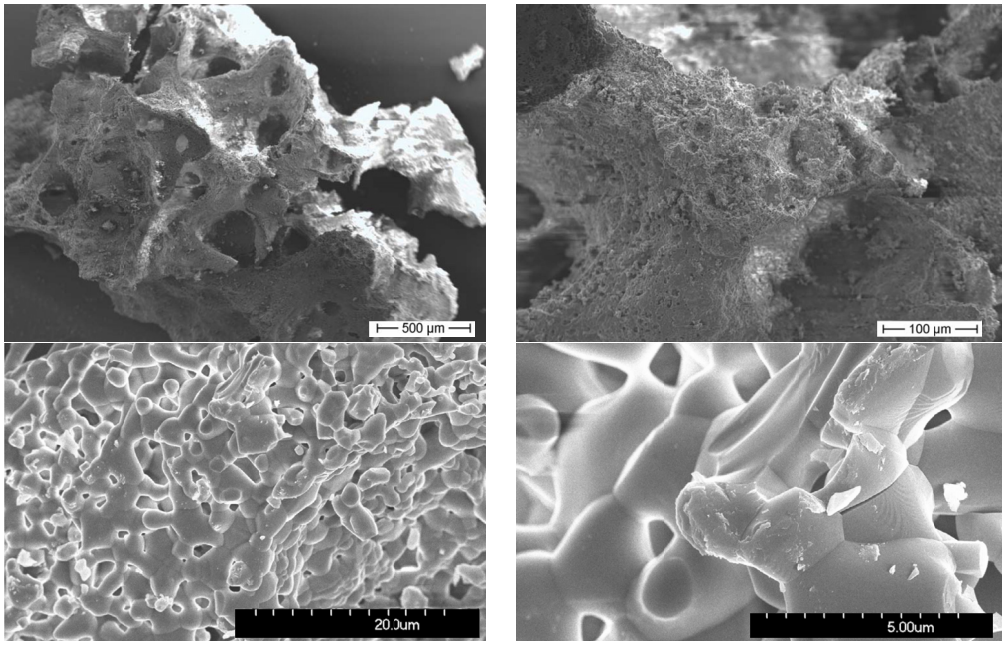

Figure 3-27 SEM images of β-TCP

Scanning electron microscopy revealed the β-TCP test group to comprise of two populations of porosity. Large interconnected macropores framed by struts, containing a network of smaller pores (strut-porosity). Top: Low (left) and high (right) SEM of β-TCP using secondary electron detector; Bottom: Low (left) and high (right) SEM of β-TCP using back-scattered detector

The volume of strut-porosity varied with test group from 23% for SiCaP-23G up to 46% for SiCaP-46G and 48% for β-TCP. The presence of macro-porosity and micro-porosity as two distinct populations of porosity is reported for other bone graft substitutes characterised by scanning electron microscopy (Tadic and Epple 2004) and mercury intrusion porosimetry (Figure 3-7). Bi-modal distributions of porosity in the region of 1-10 microns (micro-porosity) and 50-1000 microns (macroporosity) are reported for other novel osteoinductive calcium phosphate materials (Yang, Yuan et al. 1996, Yang, Yuan et al. 1997, Yuan, Yang et al. 1998, Yuan, Kurashina et al.

1999, Yuan, De Bruijn et al. 2001a, Yuan, van Blitterswijk et al. 2006b).

As might be expected the effect of increasing the volume of strut-porosity increased the surface area of the material. In our studies the selection of mercury intrusion porosimetry over more traditional techniques such as gas adsorption (helium or nitrogen) was one largely driven by availability of equipment at the time of the analysis. This could be a limitation in our study design since gas adsorption would have elicited a more accurate absolute measurement of surface area, as the gas would be more likely than mercury to infiltrate the smallest of pores. Indeed, the surface area measured by mercury porosimetry in our experiments was considerably lower (up to 12 times lower) than that reported for other microporous grafts with microporosity in the same range when measured by gas adsorption. Nevertheless our analysis was useful in providing a comparison between our test groups. No previous studies have reported surface area measured by mercury intrusion porosimetry for equivalent materials so our results do provide a benchmark against which future studies of alternative materials could be measured.

3.5.3 Functional Characterisation

The effects of the strut-porosity on the resultant dissolution profile and bulk handling properties of silicate-substituted calcium phosphates were assessed with dissolution and mechanical testing. These are important to the clinical application of these materials. The increase in strut-porosity translated to both a difference in dissolution and mechanical properties between the test groups.

There was no relationship between strut-porosity and bulk weight loss after soaking in TRIS buffer at 37^{o}C for 120 hours. However, increasing the strut-porosity corresponded with an increase in silicon and phosphorus ion concentration in the soaking solution, but a decrease in the amount of calcium dissolved. The measured ion release concentrations of all materials tested were consistent with resorbable calcium-phosphate bone grafts that have limited solubility at pH 7, and are lower than those detected previously for porous hydroxyapatite (HA) coatings. For comparison, Fazan et al (Fazan and Marquis 2000) reported values of approximately 40-50 mg/L for Ca and 10-15 mg/L for P released into Tris buffer after soaking of plasma-sprayed HA coating. This may be of the mode of dissolution taking place and the location of dissolution occurs with respect to the sintered grain structure.

The bulk handling strength test was included to indicate whether the differences in

strut-porosity would impact the clinical utility of the materials, specifically the handling strength of the material and its suitability for use in further preclinical studies and eventually as a bone graft substitute in humans. All porous SiCaP groups were found to fail in a manner typical of an elastic-brittle foam, exhibiting a linear elastic region during which brittle failure of the macropores dominated, followed by a second elastic region characteristic of brittle fracture of the struts. This is consistent with previous finding for coralline hydroxyapatite materials (Hing, Best et al. 1999). The mechanical properties were modified by increasing strut-porosity, as might be expected. Increasing the strut-porosity led to a significant increase in the displacement measured at maximum load. However, interestingly, whilst there was a significant difference in the maximum displacement for SiCaP-23G versus SiCaP-32G and SiCaP-46G, there was no significant difference between SiCaP-32G and SiCaP-46G. This is likely to be attributed to variations in structural parameters other than strut-porosity volume taking precedence in determining the nature of brittle failure, such as variations in pore shape, pore interconnection size, and macropore size distribution. Despite there being a detectable change in mechanical properties with increasing strut-porosity, all groups retained a sufficient degree of structural integrity for use as a bone void filler. The significance of the impact of intrinsic mechanical properties on the biological performance of the materials is explored further in Chapter 4.

Chapter Four: Effect of Strut-Porosity on the Mechanical Properties of Calcium Phosphate Biomaterials

4.1 Introduction

Several studies have investigated the influence of substrate properties on mechano-stimulation of bone cell cultures but the majority of these studies have focussed on one attribute of the material alone, such as substrate roughness (Di Palma, Guignandon et al. 2005), substrate chemistry (Di Palma, Douet et al. 2003, Sikavitsas, Bancroft et al. 2005), or pore size (Tanaka, Sun et al. 2005). The greater body of work has focussed on the empirical responses of individual, and occasionally co-cultured cells, to experimental mechanical and chemical stimuli (Klein-Nulend, Semeins et al. 1995, Klein-Nulend, van der Plas et al. 1995, Roelofsen, Klein-Nulend et al. 1995, Klein-Nulend, Roelofsen et al. 1997, Klein-Nulend, Helfrich et al. 1998, Pavalko, Chen et al. 1998, Sterck, Klein-Nulend et al. 1998, Ajubi, Klein-Nulend et al. 1999, Joldersma, Burger et al. 2000, Westbroek, Ajubi et al. 2000, Bakker, Soejima et al. 2001, Bakker, Joldersma et al. 2003, Bacabac, Smit et al. 2004, McGarry and Prendergast 2004, Bacabac, Smit et al. 2005, McGarry, Klein-Nulend et al. 2005). Research in this area has centred on the effects of either fluid shear stress or direct strain (or both) on cell regulation. The design of these *in vitro* models has predominantly been based on empirical calculations for the expected fluid stress or direct strain in physiological bone but few, if any at all, have calculated the expected physical properties of biomaterial substrates when applied in the clinical setting and related this data to *in vitro* or *in vivo* data for the same biomaterial.

In this chapter we determine the mechanical environment of porous calcium phosphate biomaterials in clinical application and explore the use of computational tools to allow better understanding of structure-property relationships for experimental and hypothetical biomaterials.

The specific objectives are:

- To use 3D finite element models to ascertain the mechanical environment of

calcium phosphate biomaterials in clinical applications;

- To develop a procedure for generating microstructural-level finite element models of calcium phosphate biomaterials from electron micrographs and to use the models to estimate the effective Young's modulus and the microstructural level stress and strain distribution under loading representative of the clinical mechanical environment

As these are two distinct research objectives the methods, results, and discussion for each will be captured in two separate sections in this chapter.

4.2 Typical Mechanical Loading in Clinical Application

To evaluate the mechanical environment of calcium phosphate biomaterials in typical clinical applications, 3D finite element models of a proximal femur containing a void in the greater trochanter (representative of a fluid filled cyst or other defect) and of a section of the lumbar spine undergoing a simulated instrumented (supposedly non-load-bearing) intervertebral fusion were generated.

4.2.1 Jenike shear test

Mechanical testing to provide the necessary materials parameters for continuum-level modelling of the calcium phosphate biomaterials was also carried out.

4.2.1.A **Methods**

4.2.1.A.a *Methods and Materials*

The continuum-level material model chosen to be most appropriate for the finite element modelling of the calcium phosphate biomaterials (a granular material in clinical application) was the Drucker-Prager plasticity model. Drucker-Prager plasticity is commonly used for modelling materials such as soils and aggregates, and has been used by other authors for modelling the mechanical behaviour of morcellised cancellous bone graft (Phillips, Pankaj et al. 2006). The Drucker-Prager model is an approximation of the empirical Mohr-Coulomb failure law. Details can be found in standard soil mechanics texts (Das 2009) but briefly, the Mohr-Coulomb failure law (Equation 18) states that the shear strength, τ, of a granular aggregate depends on the angle of internal friction, Φ, expressed as the angle at which the

aggregate will slide, the interlocking or cohesion of the particles, c, expressed as a stress and the normal (compressive) stress, σ, produced by the load supported by the aggregate.

$$\tau = c + \sigma \tan \Phi \qquad \textbf{Equation 18}$$

The inter-particle cohesion and the angle of internal friction were measured for SiCaP-23G and SiCaP-46G materials using a modification of the "Jenike" or Cam shear test (Bolland, Partridge et al. 2006).

The test apparatus is shown schematically in Figure 4-1 and photographs of the actual test set-up are shown in Figure 4-2. The principal components of the apparatus are an upper and lower stainless steel ring which together forms a cylindrical chamber in which the material under test is placed. A plunger, which passes through a fixed vertical linear bearing, allows the application of normal stress to the sample via dead-weights. The lower ring is mounted in horizontal linear bearings, and application of horizontal force to the lower ring causes the sample to be subjected to shear stress, with failure in the ideal situation occurring at the shear plane at the junction of the upper and lower rings. Small holes in the lower ring beneath sample allow the escape of excess fluid from the sample during test and eliminate any hydraulic stiffening effects. By conducting tests at each of several fixed normal forces and measuring the change in load as the lower ring is displaced horizontally under controlled conditions, the shear strength at a range of normal stresses and hence the Mohr-Coulomb failure law for the material under test can be determined.

Forty gram (40g) samples of each material were each mixed with 40 ml of 25% bovine serum in water (with sodium azide preservative). Three tests at three different normal stress levels were performed for each material, giving a total of 18 tests. Dead-weights of 50, 150 and 250 N were chosen to give normal stresses of 102, 306 and 509 kPa respectively. The rate of displacement of the lower ring in all tests was 0.02 mm/sec (1.2 mm/min).

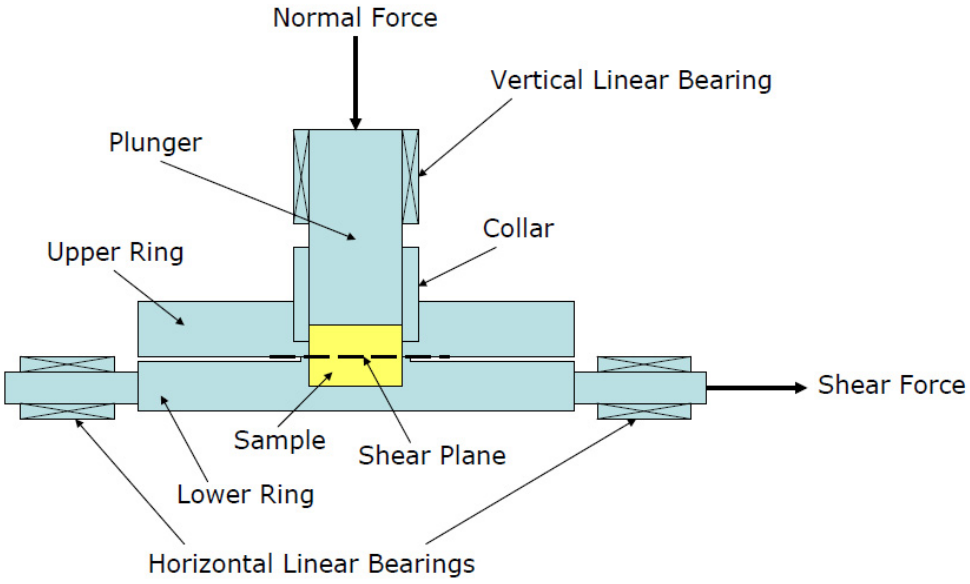

Figure 4-1 Schematic of the Jenike shear test apparatus

The principal components of the apparatus are an upper and lower stainless steel ring which together forms a cylindrical chamber in which the material under test is placed. A plunger, which passes through a fixed vertical linear bearing, allows the application of normal stress to the sample via dead-weights. The lower ring is mounted in horizontal linear bearings, and application of horizontal force to the lower ring causes the sample to be subjected to shear stress, with failure in the ideal situation occurring at the shear plane at the junction of the upper and lower rings.

Figure 4-2 Jenike shear test set-up

Photo demonstrates pre-test layout and sample loaded into the test chamber prior to shear testing.

4.2.1.B **Results**

4.2.1.B.a *Shear Stress vs. Shear Strain*

Plots of the shear stress vs. shear strain as a function of normal load for all 18 samples are shown in Figure 4-4. The shear modulus of the two materials was determined by fitting straight lines to the initial linear portions of the shear stress vs. shear strain curves (Figure 4-3). The Mohr-Coulomb failure parameters were determined by measuring the shear stress at a shear strain of 0.1 (10%) for each sample, then plotting this value against the normal stress (Figure 4-5). There was no statistical difference ($p>0.05$) between the test groups at each load.

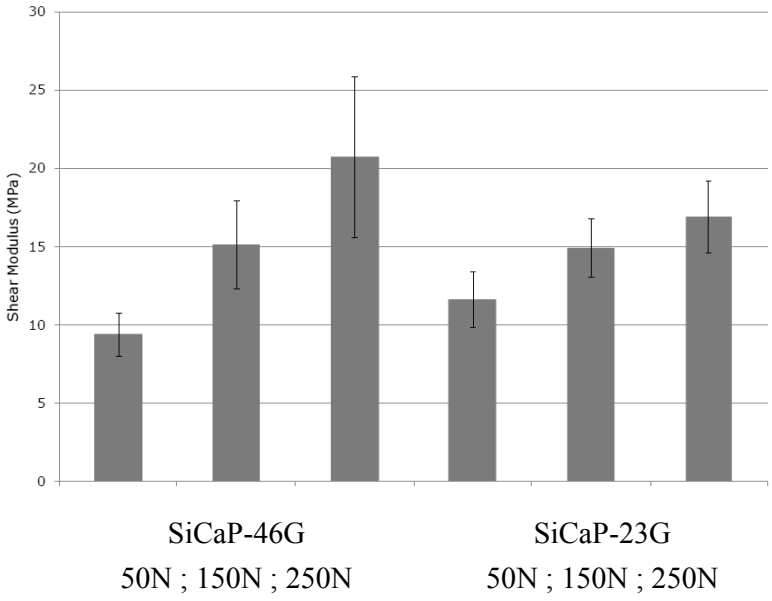

Figure 4-3 Shear modulus for the two materials as a function of normal load
The shear modulus of the two materials was determined by fitting straight lines to the initial linear portions of the shear stress vs. shear strain curves. Error bars represent plus/minus one standard deviation.

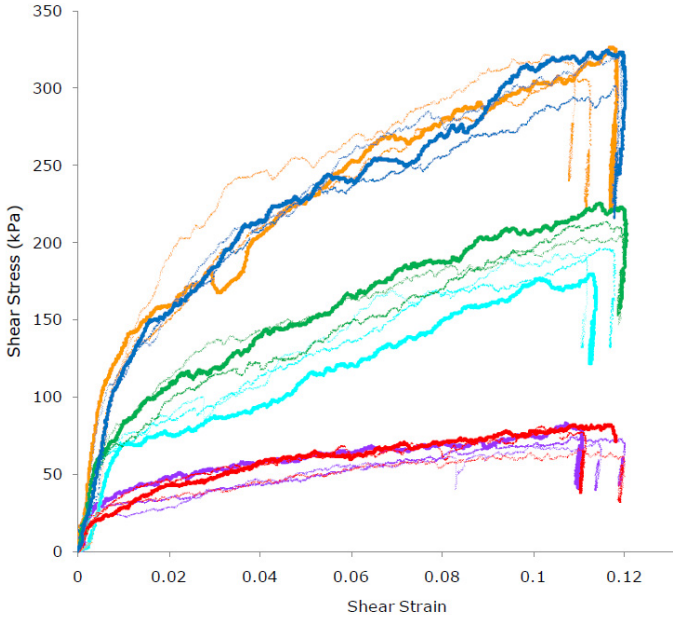

Figure 4-4 Plots of the shear stress vs. shear strain as a function of normal load (Bottom group – 50N; Middle group – 150N; Top group – 250N)

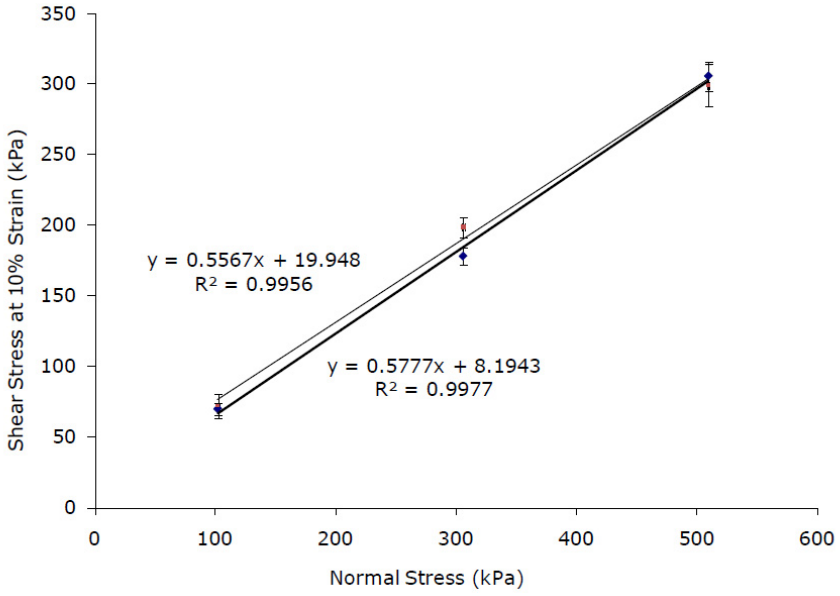

Figure 4-5 Plot of shear stress at 10% shear strain as a function of normal stress

The Mohr-Coulomb failure parameters were determined by measuring the shear stress at a shear strain of 0.1 (10%) for each sample, then plotting this value against the normal stress. Error bars represent plus/minus one standard deviation; Top trendline = SiCaP-23G; Bottom trendline = SiCaP-46G.

From best fit straight lines to the plots of shear stress at 10% shear strain vs. normal stress, the cohesion (the intercept of the shear stress at 10% shear strain vs. Normal stress plot) and the angle of internal friction (the arctangent of the slope of the shear stress at 10% shear strain vs. normal stress plot) were determined and are shown in Table 4-1.

Table 4-1 Cohesions and angles of internal friction

Material	Cohesion (kPa)	Angle of Internal Friction (^{o})
SiCaP-23G	8.19	30.0
SiCaP-46G	19.95	29.1

4.2.2 Femur Finite Element Model

4.2.2.A **Model Geometry**

In order to determine the stresses that would act upon silicate-substituted calcium phosphate used to fill a hypothetical defect (representing, for example, a bone cyst) in the proximal femur, a geometric (CAD) model of a proximal femur was developed from a computed tomography scan of a patient. A portion of the pelvis was also included, and the femur and pelvis were separated by layers of cartilage as in a real hip joint. CT image segmentation and conversion to a surface model (in STL format) was performed using the open source "3DSlicer" software. Further geometry operations (including surface clean-up and positioning of the defect) were performed using Rhinoceros CAD software. Final conversion of the geometry to a finite element model was performed using Gmsh software.

Lateral and anterior-posterior views of the defect position are shown in Figure 4-6. The defect was assumed to be an oblate spheroid with major diameter (aligned approximately with the frontal plane) of 20 mm and minor diameter (aligned approximately with the sagittal plane) of 10 mm, giving a defect volume of approximately 2.1 cm^{3}.

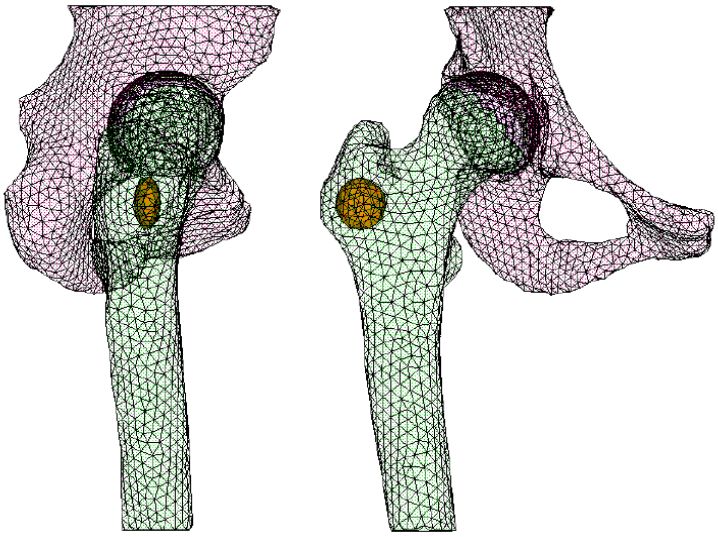

Figure 4-6 Lateral and anterior-posterior views of the position of the defect (orange region) in the greater trochanter. The green mesh represents the proximal aspect of the femur, in which the defect was simulated. The pink region represents the pelvis, specifically the acetabulum into which the head of the femur articulates.

Immediately after implantation, the silicate-substituted calcium phosphate occupying the defect is not bonded to the surrounding bone, although presumably in the ideal situation fibrous tissue (in the form of haematoma) forms rapidly around the silicate-substituted calcium phosphate and then differentiates down the fibro-cartilaginous and ossification pathway in the same manner as a healing fracture. For this reason, the silicate-substituted calcium phosphate was assumed not to be bonded to the surrounding bone. Transfer of load into the silicate-substituted calcium phosphate s was achieved by overlaying the surface of the silicate-substituted calcium phosphate with contact elements, and correspondingly overlaying the internal surface of the defect with target elements, the frictionless contact pair so formed transferring compressive but not shear stresses between the two materials. Similarly, load transfer between the bearing surfaces in the hip joint was achieved using a frictionless contact pair.

4.2.2.B **Materials Properties**

Element-by-element materials properties for bone were derived from the CT scans using a modified version of the Bonemat software described by Taddei et al (Taddei, Pancanti et al. 2004) Plots of the Young's modulus distribution in the bone are shown in Figure 4-7.

A Drucker-Prager material model as described above was used to model the silicate-substituted calcium phosphates. The parameters for material SiCaP-46G (Table 4-1) were used. In many particulate materials dilation accompanies shearing as particles ride-up over each other. However, the simple Drucker-Prager plasticity model tends to predict excessive dilation, so following Phillips et al, a modification to the standard Drucker Prager model using a non-associated flow rule, which introduces a further materials parameter, the dilatancy angle, was used. The dilatancy angle was set at half the internal friction angle (if the dilatancy angle is equal to the friction angle, the flow rule is associative).

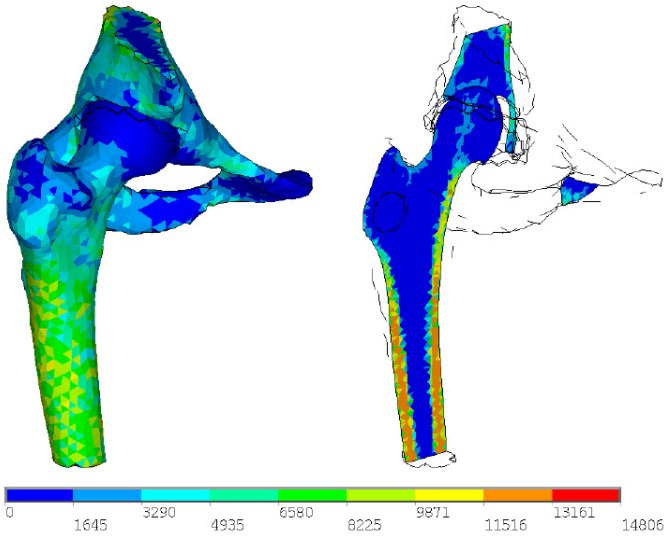

Figure 4-7 Plots of the distribution of Young's modulus (MPa) in the bone
Element-by-element materials properties for bone were derived from the CT scans using a modified version of the Bonemat software described by Taddei et al (Taddei, Pancanti et al. 2004). The distribution of modulus in the loaded simulation indicates that bone tissue is stiffest in the cortical regions. The defect was in a region of cancellous bone with a modulus lower than the surrounding cortical bone.

Other materials properties used in the finite element model are shown in Table 4-2. The value of Young's modulus for the silicate-substituted calcium phosphate was determined from the minimum value of the shear modulus from the mechanical tests (6 MPa for SiCaP-46G-50N, Figure 4-3) and the standard equation relating Young's modulus E, shear modulus G, and Poisson's ratio υ, (Equation 19). A Poisson's ratio of 0.4 was assumed, based on the value relevant to medium to loose sands (Anon 2010). Note the stress-dependence of the shear and Young's modulus (Figure 4-3**)**

has been neglected due to software limitations, even though for aggregates and similar materials it may have a significant effect (Brown, Bray et al. 1989, Phillips, Pankaj et al. 2006).

$$E = 2G(1+\upsilon) \qquad \textbf{Equation 19}$$

Table 4-2 Materials properties for the femur finite element model

Material	Young's Modulus (MPa)	Poisson's Ratio
Bone	Various (Figure 4-7)	0.3
Cartilage	12.00	0.45
SiCaP-23G	26.32	0.4

4.2.2.C **Loads and Boundary Conditions**

To prevent rigid body motions of the femur, all nodes on the distal margin of the femur were constrained to have zero displacements in all three coordinate directions. Nodes on the proximal margin of the pelvis were constrained to have zero displacements in the x and y directions, and nodes at the pubic symphysis were constrained to have zero displacements in the x direction. A load of 785 N (corresponding to 1 x body weight for a body mass of 80 kg) acting in the z direction was applied to the proximal margin of the pelvis to represent body weight, and loads of 455 N (0.580 x body weight) in the negative-x direction, 34 N (0.043 x body weight) in the negative-y direction and 679 N (0.865 x body weight) in the negative-z direction distributed over several nodes on superior aspect of the greater trochanter to represent the action of the abductor muscles. This force system approximates the forces acting around the hip at the instant of the gait cycle at which the hip joint reaction force is greatest (Bergmann 2009).

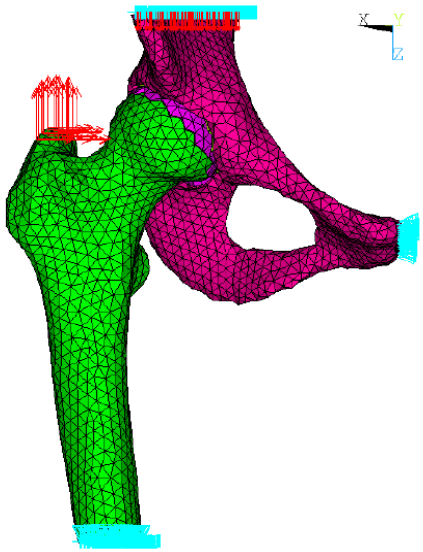

Figure 4-8 Loads and boundary conditions applied to the femur model
Nodes on the proximal margin of the pelvis were constrained to have zero displacements in the x and y directions, and nodes at the pubic symphysis were constrained to have zero displacements in the x direction. X and Y planes are indicated in this graphic, red arrows indicate displacements that were constrained to zero.

4.2.2.D **Results**

Plots of the 1st and 3rd principal stress in the femoral defect model are shown in Figure 4-9 and Figure 4-10 respectively. Plots of various parameters characterising the mechanical environment of the silicate-substituted calcium phosphate in the femoral defect are shown in Figure 4-11 and Figure 4-12. The principal stress plots revealed the typical bending and torsional stress distributions expected from loading with hip joint reaction and abductor muscle forces, high first principal stresses (indicative of predominantly tensile stresses) on the lateral aspect of the femur and high third principal stresses (indicative of predominantly compressive stresses) on the medial aspect of the femur.

Peak contact pressures at the interface between the bone and the silicate-substituted calcium phosphate at the boundary of the defect were around 27 kPa, which is an order of magnitude lower than that observed in this model for the surrounding bone. Peak von Mises stress and peak von Mises strain in the silicate-substituted calcium phosphate (12 kPa and 0.05% respectively) were correspondingly low.

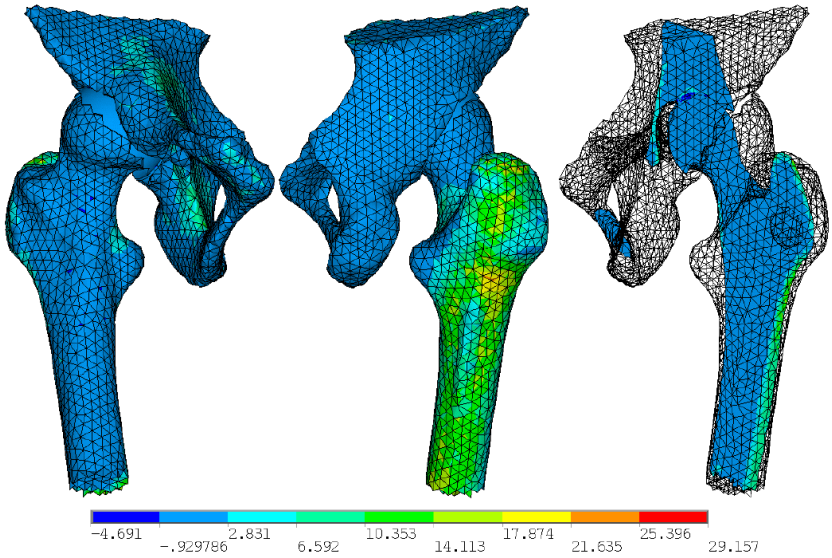

Figure 4-9 Plot of 1st principal stress (MPa) in the femoral defect model

The analysis revealed high first principal stresses (indicative of predominantly tensile stresses) on the lateral aspect of the femur (green regions)

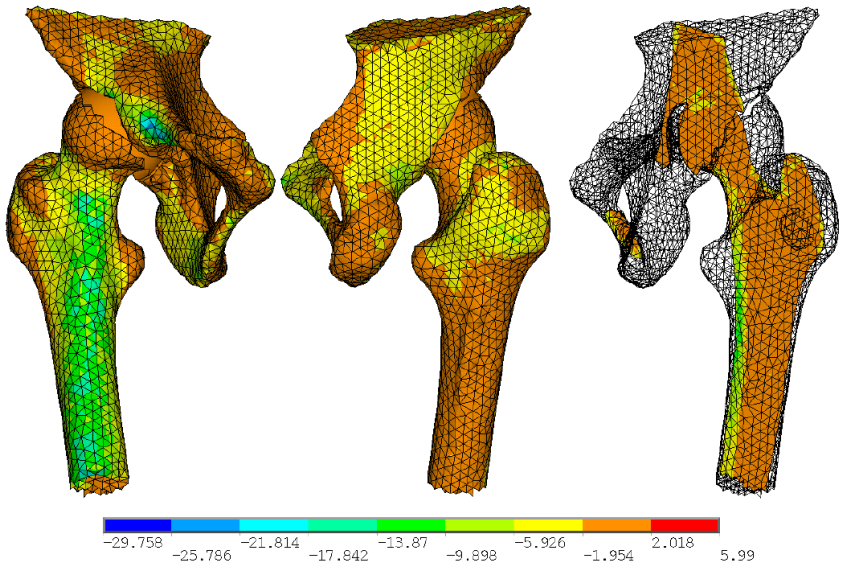

Figure 4-10 Plot of 3rd principal stress (MPa) in the femoral defect model

The analysis revealed high third principal stresses (indicative of predominantly compressive stresses) on the medial aspect of the femur (green regions)

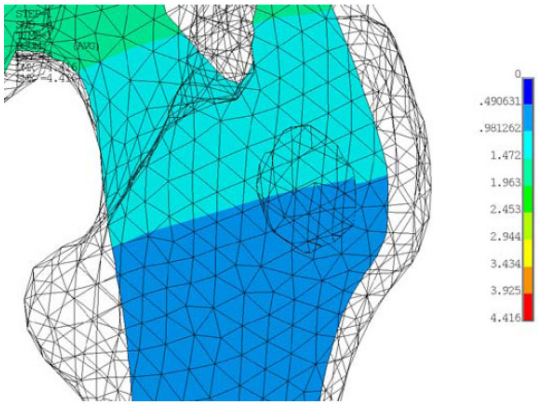

Displacements (mm) in the region of the defect showing discontinuity of displacement around the defect.

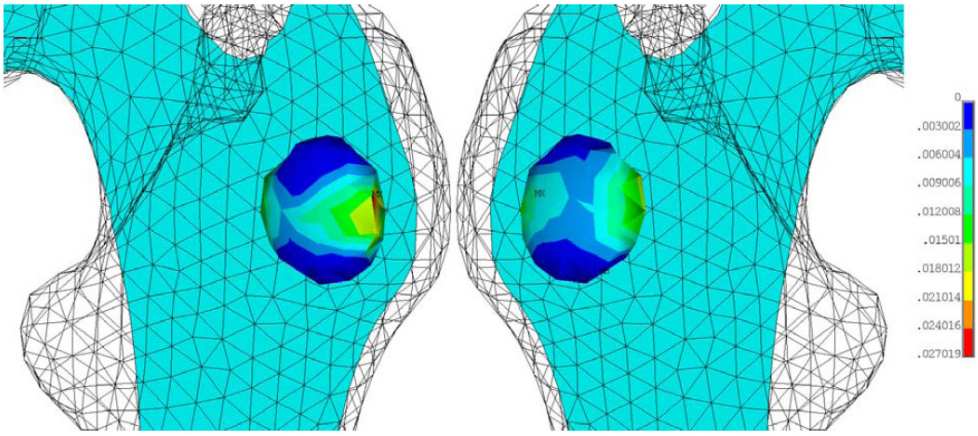

Contact pressures (MPa) imposed upon the Actifuse by the surrounding bone.

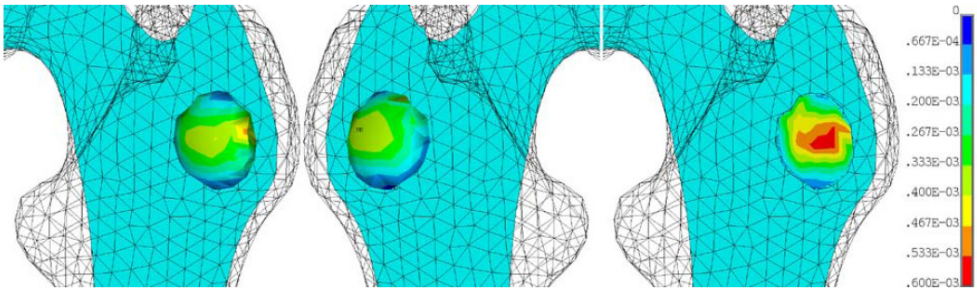

Von Mises equivalent strain in the Actifuse material.

Figure 4-11 Plots of various parameters charactering the mechanical environment of the silicate-substituted calcium phosphate in the femoral defect model

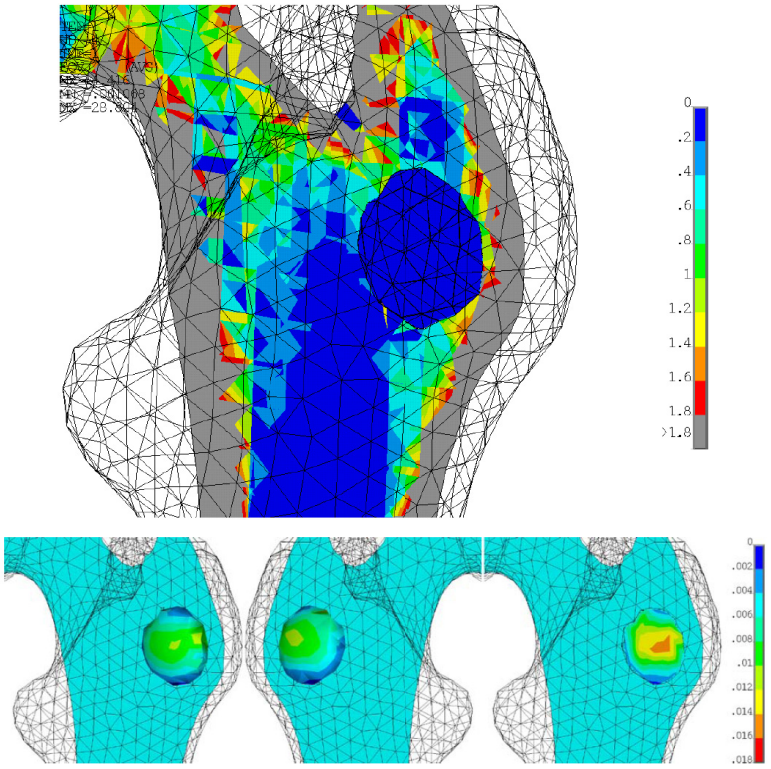

Von Mises equivalent stress (MPa) in the Actifuse material (below) and in context of the surrounding bone (note different scales.)

Figure 4-12 Plots of various parameters charactering the mechanical environment of the silicate-substituted calcium phosphate in the femoral defect model

4.2.3 Vertebral Finite Element Model

4.2.3.A **Model Geometry**

In order to determine the stresses that would act upon silicate-substituted calcium phosphate used as a fusion-promoter in a lumbar spinal fusion procedure, a finite element model of a section of the lumbar spine with additional stabilisation hardware and silicate-substituted calcium phosphate was generated based on the model of Smit and co-workers. Full details of the model are given in the Smit paper; briefly the model consists of representations of three lumbar vertebrae and the corresponding intervertebral discs, facet joints and major ligaments. The model was modified to enable the simulation of a lumbar spinal fusion and included representations of silicate-substituted calcium phosphate (modelled as being suspended within the soft tissues between the transverse processes extending outwards from the vertebral bodies) and of typical stabilisation hardware. The intervertebral discs remained intact. The model was also reduced to a half-symmetry model in order to reduce

compute time. The bone, facet joint cartilage, hardware, disc nucleus and the annulus ground substance were modelled using 10 node tetrahedral solid elements and the ligaments and the fibres of the annulus modelled using link elements. Contact at the facet joints and between the silicate-substituted calcium phosphate and the spinous processes was modelled using frictionless contact. Since the material model used to represent the silicate-substituted calcium phosphate could result in the silicate-substituted calcium phosphate becoming geometrically (and hence numerically) unstable, the silicate-substituted calcium phosphate was surrounded by a layer of membrane elements of low stiffness to simulate the supporting effects of the surrounding soft tissues. Note that the soft tissues (or their confining effects) were not explicitly included in the model, although the application of external pressure to the membrane elements to simulate the soft tissue confinement could be explored in further work. Four views of the complete model are shown in Figure 4-13.

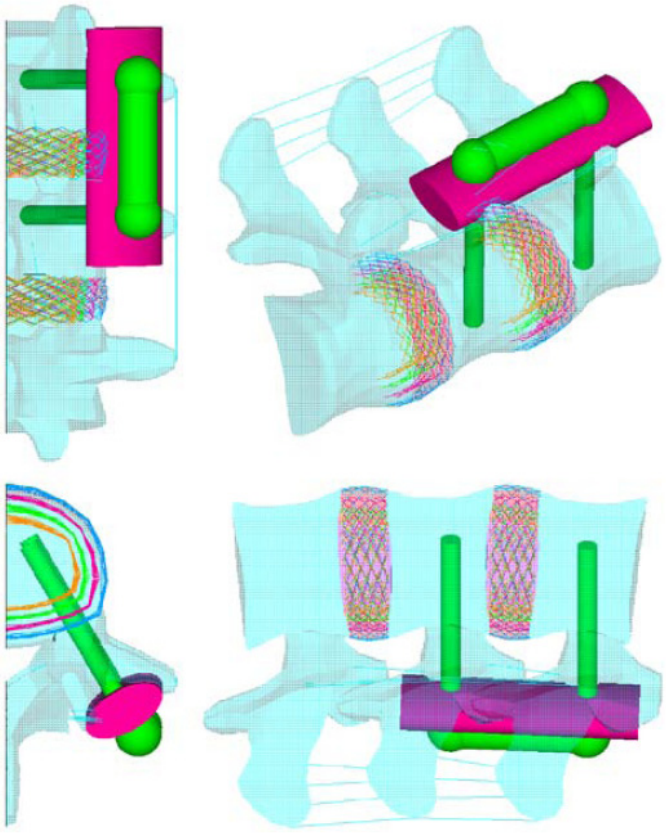

Figure 4-13 Finite element model of the lumbar spine undergoing fusion
Light blue regions are bone, green regions are implanted metalwork, pink regions are the implanted graft material.

4.2.3.B **Materials Properties**

All materials with the exception of the silicate-substituted calcium phosphate and the ligaments were assumed to behave as linear elastic, isotropic solids. Materials properties for all except the silicate-substituted calcium phosphate and ligament materials are shown in Table 4-3.

Table 4-3 Materials properties for the lumbar spine finite element model

Material	Young's Modulus (MPa)	Poisson's Ratio	Cross-sectional area (mm²)
Bone	3000	0.3	-
Facet joint cartilage	50	0.4	-
Hardware (typical implant-grade titanium alloy)	110000	0.31	-
Nucleus	1	0.49	-
Annulus ground substance	4.2	0.45	-
Membrane	0.1	0.3	-
Annulus fibres layer 1	550	-	0.50
Annulus fibres layer 2	485	-	0.39
Annulus fibres layer 3	420	-	0.29
Annulus fibres layer 4	360	-	0.21

A tri-linear stiffness model was used for the ligaments. The model is shown schematically in Figure 4-14, and the model parameters for the various ligaments shown in Table 4-4. The length of each link element representing the ligament was used in conjunction with the parameters of Table 4-4 to determine the stiffness of the links on an element by element basis.

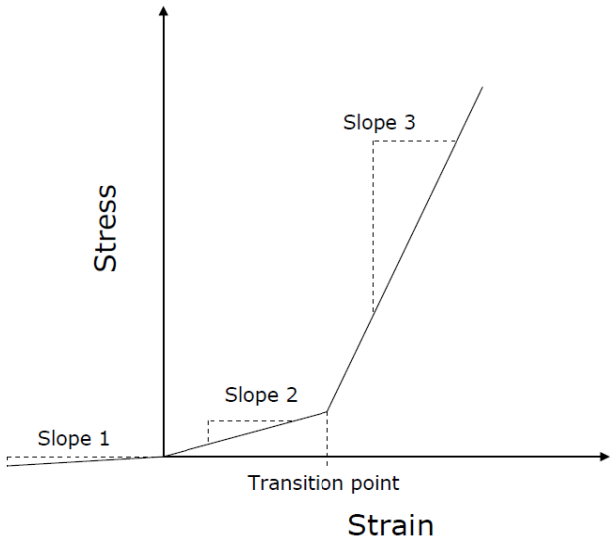

Figure 4-14 Schematic of ligament stress-strain behavior

Table 4-4 Parameters for the ligament stiffness models

Ligament	Slope 1 (MPa)	Slope 2 (MPa)	Slope 3 (MPa)	Transition point (strain)	Cross-sectional area (mm^2)
Anterior longitudinal ligament	0.078	7.8	41	0.12	64
Posterior longitudinal ligament	0.1	10	80	0.11	20
Ligamentum flavelum	0.15	15	115	0.06	40
Transverse ligament	0.1	10	350	0.18	1.8
Capsular ligament	0.075	7.5	80	0.25	30
Interspinous ligament	0.1	10	110	0.14	40
Supraspinous ligament	0.08	8	110	0.20	30

4.2.3.C **Loads and Boundary Conditions**

Loads and boundary conditions applied to the model are shown graphically in Figure 4-15. To prevent rigid body motions, all nodes on the distal end-plate of the distal vertebral body were constrained to have zero displacements in the z (axial) direction. All nodes lying in the sagittal (yz) plane were constrained to have zero displacement in the x direction to enforce the symmetry condition. To eliminate the last remaining unrestrained rigid body mode, a single node on the most anterior point of the distal vertebra was constrained to have zero displacement in the y direction. Following Smit et al., axial spinal loading was simulated by applying a distributed load to the proximal end plate of the proximal vertebra. The distributed load was applied as a pressure which when integrated over the area of load application was equivalent to an axial load of 400 N (equivalent to a spinal axial load of 800 N, approximately 1 x body weight, over the end plate of a full model).

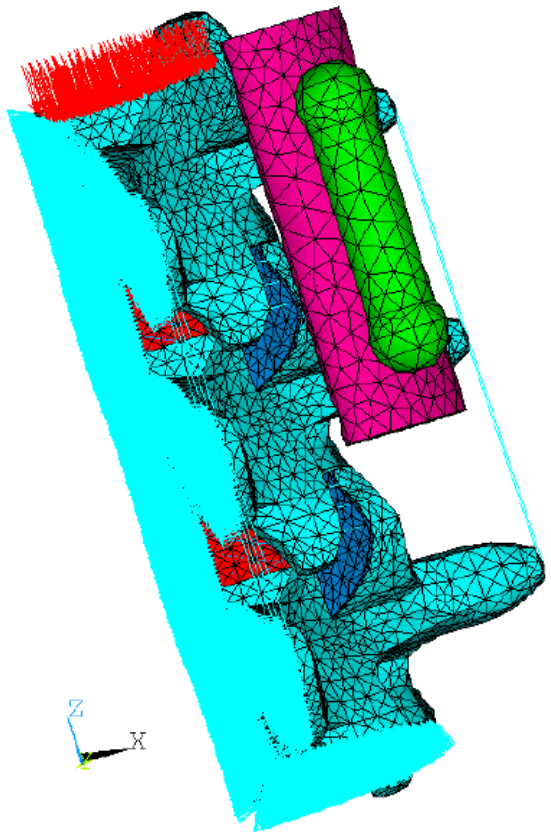

Figure 4-15 Loads and boundary conditions applied to the spine model

Direction of X and Y planes is indicated in this figure, red arrows indicate where displacement was constrained to zero. Blue regions represent the soft tissues and bone, green regions represent the implanted metalwork and pink regions represent the implanted graft. To prevent rigid body motions, all nodes on the distal end-plate of the distal vertebral body were constrained to have zero displacements in the z (axial) direction. All nodes lying in the sagittal (yz) plane were constrained to have zero displacement in the x direction to enforce the symmetry condition. To eliminate the last remaining unrestrained rigid body mode, a single node on the most anterior point of the distal vertebra was constrained to have zero displacement in the y direction.

4.2.3.D **Results**

A plot of the overall displacement in the spinal model under load is shown in Figure 4-16. Figure 4-17 shows overall von Mises strain in the model. Plots of the von Mises stress and von Mises strain in the silicate-substituted calcium phosphate are shown in Figure 4-18 & Figure 4-19. Peak stresses in the silicate-substituted calcium

phosphate occurred in the vicinity of the contact of the silicate-substituted calcium phosphate with the processes of the middle vertebra. Peak stress was approximately 22 kPa.

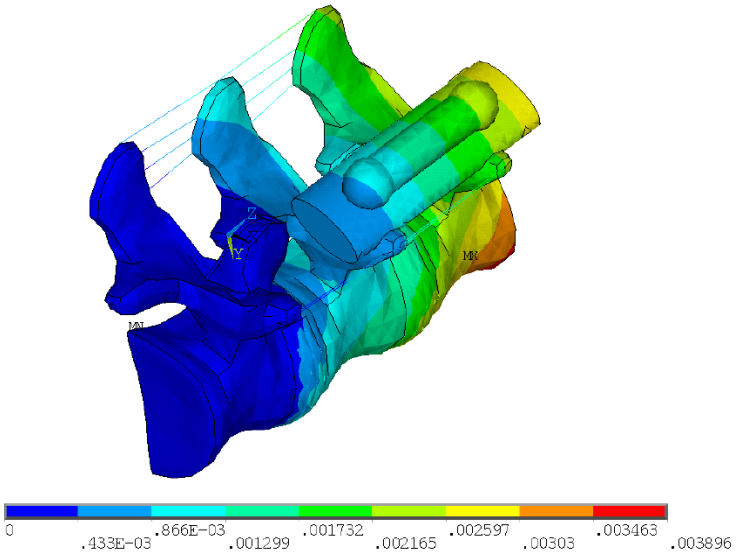

Figure 4-16 Plot of overall displacements (m) in the spinal model under load

Red, yellow and green regions indicate peak displacement under load.

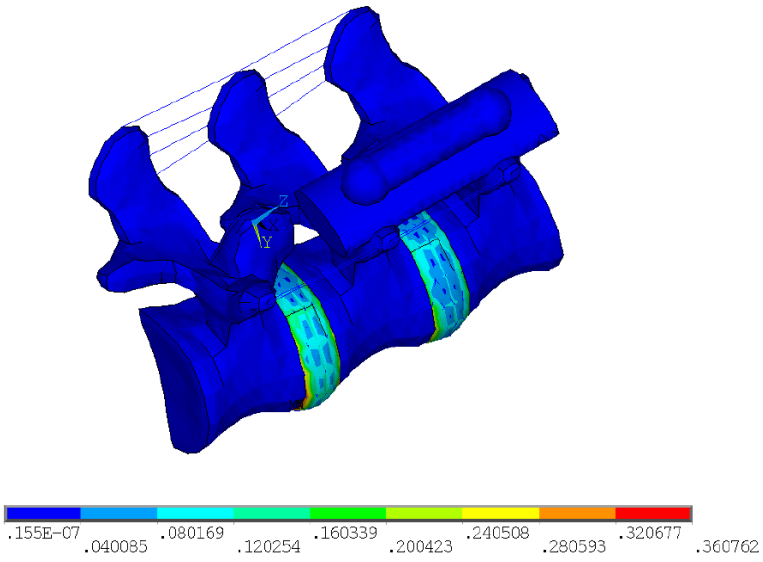

Figure 4-17 Plot of overall von Mises strain in the spinal model under load

Peak regions of strain are indicated in light blue, green and yellow. These corresponded with the soft tissues of the intervertebral disc.

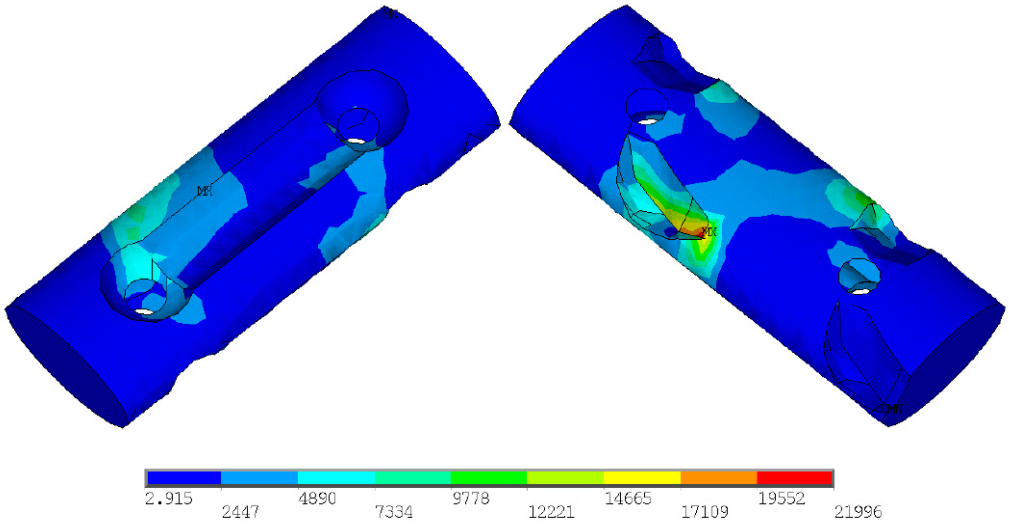

Figure 4-18 Plot of von Mises stress (Pa) in the silicate-substituted calcium phosphate component of the spinal model under load.

The distribution of stress in the silicate-substituted calcium phosphate material was non-uniform (light blue, green and yellow regions).

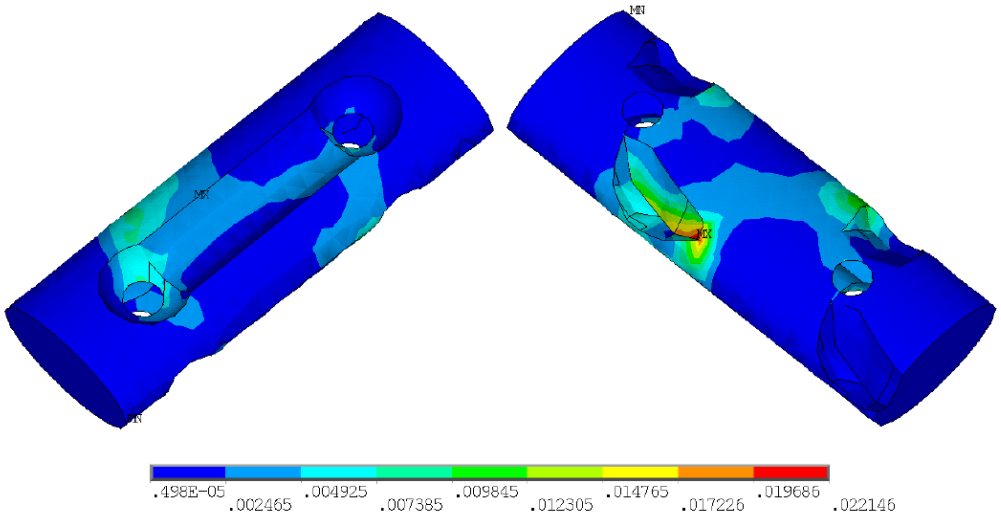

Figure 4-19 Plot of von Mises strain in the silicate-substituted calcium phosphate component of the spinal model under load

The distribution of strain in the silicate-substituted calcium phosphate material was non-uniform (light blue, green and yellow regions).

4.2.4 Discussion

Mechanical testing revealed silicate-substituted calcium phosphate to have similar mechanical behaviour to morcellised cancellous bone under similar test conditions. Data for morcellised femoral head cancellous bone is provided in Figure 4-20 for reference. Comparison of Figure 4-4 and Figure 4-20 reveals silicate-substituted calcium phosphate to have slightly lower resistance to shear than morcellised cancellous bone, although the cancellous bone particles used in the tests reported in Figure 4-20 were somewhat bigger (3-5 mm in diameter) than the silicate-substituted calcium phosphate particles used in the present work, which could explain the apparent difference in properties. The cohesion reported for cancellous bone (approximately 40 kPa) is somewhat higher than the 8 - 20 kPa found for silicate-substituted calcium phosphate, but the angle of internal friction is essentially identical (Bolland, Tilley et al. 2007).

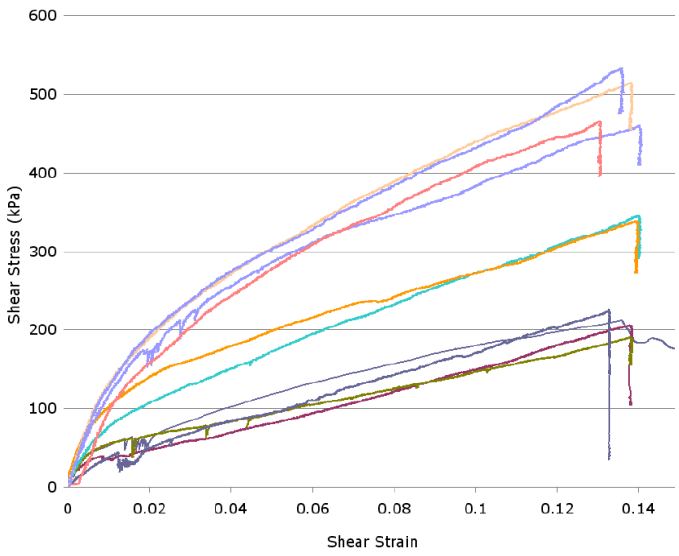

Figure 4-20 Plots of shear stress vs. shear strain as a function of normal load for morcellised femoral head cancellous bone

In the femur model, stresses in the silicate-substituted calcium phosphate were an order of magnitude lower than those in the surrounding bone, owing to the considerably greater stiffness (Young's modulus) of the surrounding bone (Figure 4-21). The bone is considerably stiffer than the silicate-substituted calcium phosphate since this model assumes that the material has only recently been implanted and has thus not been infiltrated by surrounding soft tissues nor been integrated into the bone. The porous granules of silicate-substituted calcium

phosphate are, in effect, "stress-shielded" by the surrounding bone in much the same way as bone may itself be "stress-shielded" in the presence of stiffer materials such as joint replacement components. In such circumstances the impact of stress-shielding is the resorption of bone leading in some cases to the failure of the joint replacement. The impact of stress-shielding on the progress of bone repair in our simulated defect is also likely to be negative to a certain extent. The *in vitro* studies of mechanobiology reviewed in section 2.3 teach us that osteocytes and osteoblasts are upregulated in the presence of direct substrate strain and in response to fluid shear stress. In regions of low stress, such as those observed in our simulated defect, one might expect the osteocytes and osteoblasts to be upregulated to a lesser extent than those in the surrounding bone where the stresses are more typical of physiological loading.

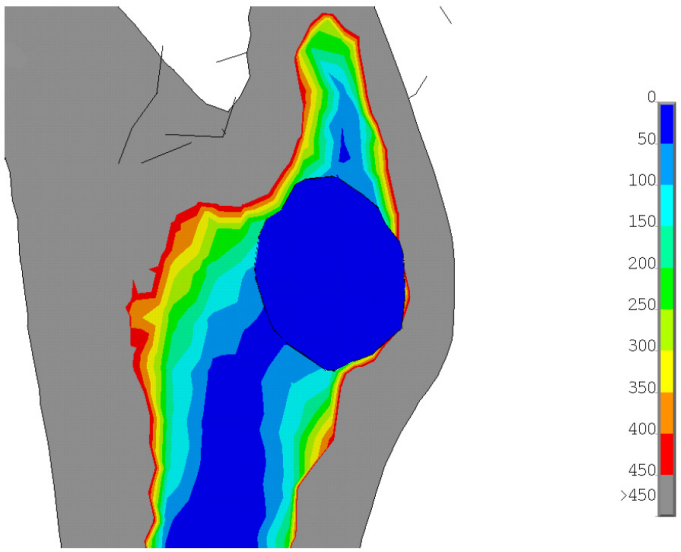

Figure 4-21 Distribution of Young's modulus (MPa) in the region of the defect
The silicate-substituted calcium phosphate appears to be "stress-shielded" by the surrounding bone in much the same way as bone may itself be "stress-shielded" in the presence of stiffer materials such as joint replacement components, owing to the considerably greater stiffness (Young's modulus) of the surrounding bone. Red, yellow and green regions indicate peak stiffness.

One possible source of error is that the present model does not take into account the stress-dependence of the Young's modulus of the silicate-substituted calcium phosphate. While the effect of stress on the Young's modulus of silicate-substituted calcium phosphate is currently unknown, other comparable materials are known to

have stress-dependent Young's modulus. For example, Phillips et al. used a linear relationship to describe the variation of Young's modulus of morcellised bone graft as a function of stress (pressure),

$$E = c_1 + c_2 \sigma$$ **Equation 20**

where c_1 and c_2 are constants set to 5 N/mm² and 35, when and are expressed in units of N/mm².

Assuming a similar relationship holds for silicate-substituted calcium phosphate (Figure 4-3 suggests that it does), the increase in Young's modulus induced by the imposed stresses (approximately 0.016 MPa maximum) would be less than 5%, a negligibly small amount.

In the spinal model, stresses in the silicate-substituted calcium phosphate were also rather low, reaching peak values of around 22 kPa. This again reflects the low Young's modulus of the silicate-substituted calcium phosphate in particulate form and its limited load-carrying capacity. In clinical use in this application it is likely that tensile stresses applied to the region occupied by the silicate-substituted calcium phosphate would be carried by fibrous tissue derived from the haematoma and subsequent tissue differentiation within the region rather than the silicate-substituted calcium phosphate itself, at least until cellular activity began to generate hard tissue bridges between the silicate-substituted calcium phosphate particles.

4.3 Effect of Porosity on Elastic Modulus

To estimate the Young's modulus of the biomaterials in this study, 2D plane stress finite element models were generated from electron micrographs. Segmentation of the images into pore and non-pore regions followed by finite element meshing of the non-pore regions has been carried out in order to explicitly model the microstructure of the biomaterial. The non-pore regions were assumed to have the same mechanical properties as bulk "pore-free" biomaterial. Young's modulus was determined from the induced continuum level displacements and strains. Local stresses and strains in the biomaterials were derived for loadings equivalent to those described in Section 4.2.

Samples from a single batch of porous silicate-substituted calcium phosphate in cylinders measuring approximately 5mm in diameter and 10mm in length were

donated by ApaTech Limited, UK. These samples were confirmed as phase pure hydroxyapatite containing 0.8% weight silicate, according to the methods described in Chapter 3. The strut-porosity of the material was confirmed as 46.59% using the Scanning Electron Microscopy method described in Chapter 3. The test specimens did not contain macroporosity. Samples were tested using compression testing according to the methods described in the following section. The results from static compression testing were compared to those derived from the finite element analysis.

4.3.1 Methods and Materials

4.3.1.A **Image Processing and Segmentation**

Scanning electron micrographs were processed and segmented using ImageTool software. The sequence of image processing steps is shown in Figure 4-22; Figure 4-23; and Figure 4-24. The images were converted from 24-bit RGB to 8-bit grey scale images, then Gaussian filtered before being manually thresholded to separate "pore" from "non-pore" material. The images were then further smoothed using a "close" filter, in which a sequence of dilation operations was followed by an equal number of erosion operations. The effect of the close filter is to close holes in objects while minimally altering the overall shape and size of the objects, and was performed to reduce the number of small features which would cause the subsequently generated finite element meshes to have very large numbers of elements. Finally, the object detection and classification functions were invoked, and the resulting object properties and boundary points saved as text files for further processing.

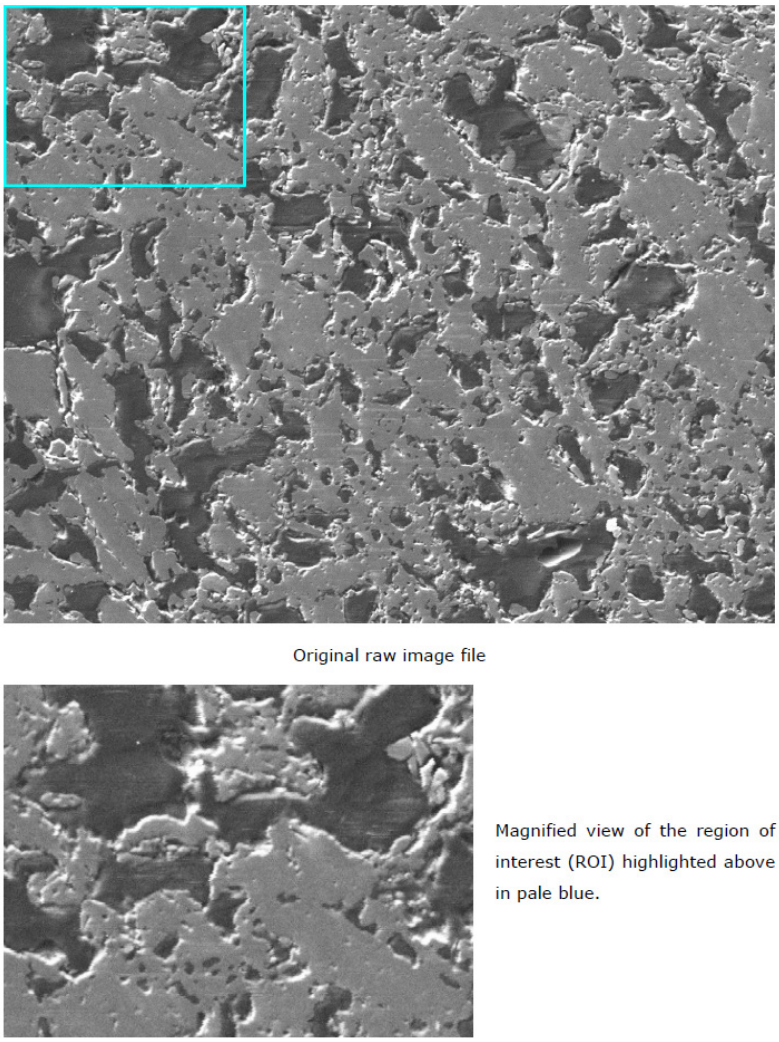

Figure 4-22 Image processing and segmentation sequence

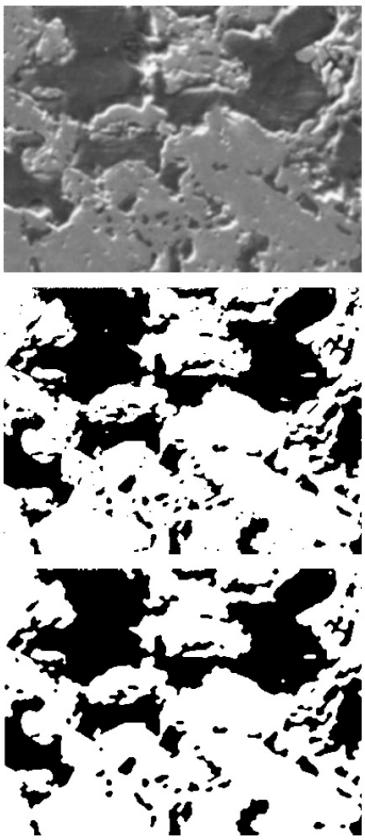

ROI following application of 5x5 matrix Gaussian filter.

1	1	2	1	1
1	2	4	2	1
2	4	8	4	2
1	2	4	2	1
1	1	2	1	1

ROI following manual thresholding to separate "pore" and "non-pore".

ROI following "close" filtering (neighbourhood size 5, open-close iterations 8)

Figure 4-23 Image processing and segmentation sequence

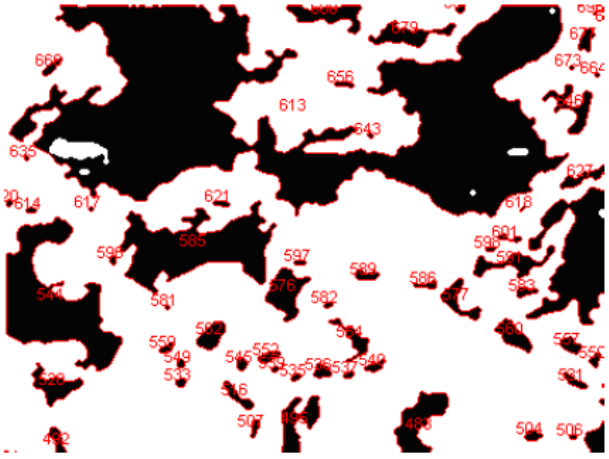

ROI following object detection and classification functions.

Figure 4-24 Image processing and segmentation sequence

4.3.1.B **Generation of Finite Element Models**

Subsequent to the image processing steps the resulting boundary points were converted into finite element meshes using the procedure summarised in Figure 4-25. This sequence was developed in order to overcome various limitations and file format incompatibilities between the constituent software packages. First, using a custom-written Visual Basic application, the boundary points were converted into an Ansys input script for generating CAD lines and areas in the Ansys pre-processor. The CAD entities were then exported from Ansys as IGES files and imported into the Rhino3D[f] CAD package where they were further processed and converted into facetted "STL" files, the facets of which formed the finite elements of the finite element mesh. Further file conversions using the free GMSH application and a second custom-written Visual Basic application were performed in order to generate node co-ordinate and element connectivity tables for input back into Ansys for analysis. Within the Ansys environment, mid-side nodes were then added. Plane-stress behaviour was assumed. For some models, a small number of elements were deleted at this stage since their shapes were not adequate for analysis purposes (Table 4-4). The number of elements that required deletion was always small with respect to the total number of elements in the model and in most cases was zero. Element deletion enabled the models to solve without failures due to numerical problems related to the poorly-shaped ("pathological") elements; the effects of element deletion on the results are believed to be insignificant.

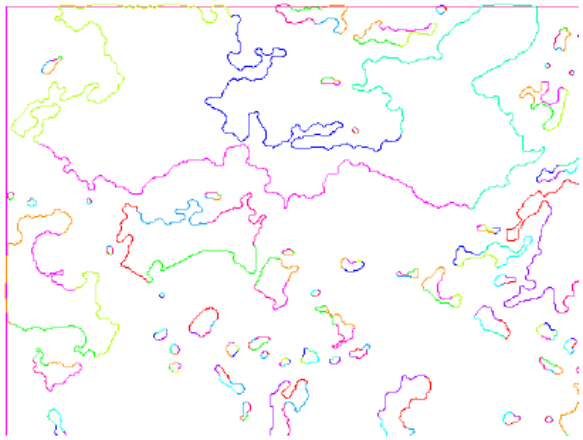

Boundary points from image processing steps (ROI as in Figure 19) converted to CAD entities using custom-written software and Ansys pre-processor.

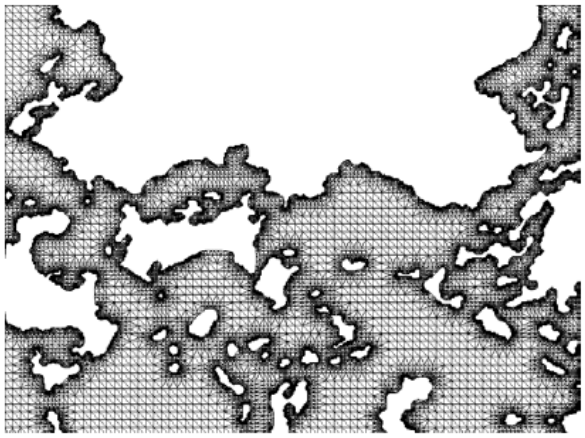

Finite element mesh following processing with Rhino3D, GMSH and second piece of custom-written software. Note the removal of a large "island" at the top of the model.

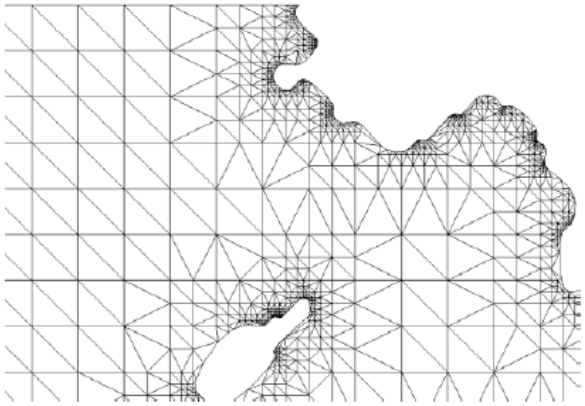

Close up of the mesh showing element refinement around small features.

Figure 4-25 Operations for converting image objects into finite element models

In the final mesh preparation step, any elements that were not connected to other elements in the mesh ("islands") were also deleted. Since these elements lacked continuity with the rest of the mesh, loads could not be transmitted to them and they thus had no structural function, so deletion had no effect on the overall behaviour of the models.

4.3.1.C **Materials Properties**

The Young's modulus of the silicate-substituted calcium phosphate constituent material was assumed to be 0.051 Newtons/micron² (equivalent to 51 GPa), based on ~0.8 wt.% silicon-substitution and a sintering temperature of ~1300°C (Patel 2003). Poisson's ratio was assumed to be 0.24 (Fritsch, Dormieux et al. 2009).

4.3.1.D **Loads and Boundary Conditions**

Loads and boundary conditions typical for all the models are shown graphically in Figure 4-26. All nodes on the left-hand boundary of the model were constrained to have zero displacements in the x-direction. The node closest to the origin on this boundary was additionally constrained to have zero displacement in the y-direction. Fixed displacements of 1 μm in the negative x-direction were applied to all nodes on the right-hand boundary of the mesh in order to simulate the action of, for example, the loading platen of a materials testing machine during a compression test.

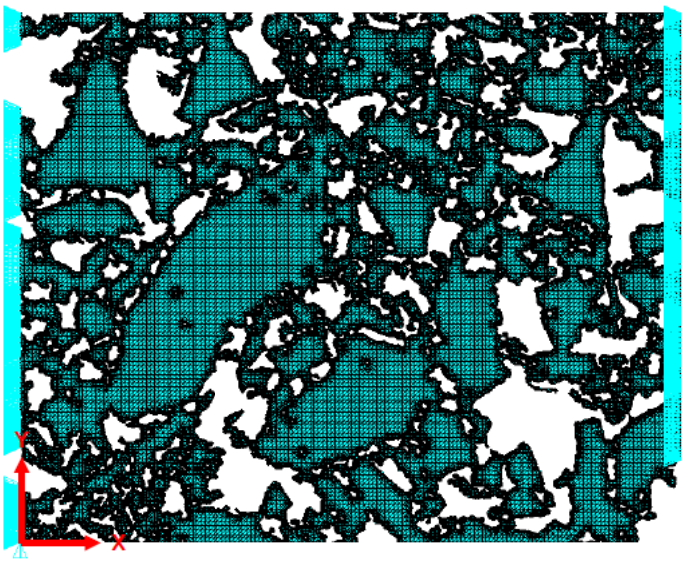

Figure 4-26 Loads and boundary conditions

All nodes on the left-hand boundary of the model were constrained to have zero displacements in the x-direction. The node closest to the origin on this boundary was additionally constrained to have zero displacement in the y-direction.

4.3.1.E **Analysis Details**

To verify the finite element models, a mesh convergence study was performed for

one example, whereby the solution outputs of interest, namely the predicted effective Young's modulus of the material and the material level stresses, were determined as a function of the number of elements in the model. Reductions in the number of elements were achieved by increasing the minimum and maximum allowable element edge lengths. All other mesh control settings remained constant for all models.

4.3.1.F **Compression testing**

Ten cylindrical samples of nominal diameter of 5mm and of nominal length 10mm were provided by ApaTech Limited, UK, as described above. The diameter and length of each specimen was measured using calibrated digital verniers (RS Components, UK). The samples were placed, in turn, on to the articulated plates of an Intron Universal testing machine (Instron, UK) and tested in compression under a 10kN load cell (Series 2580, Instron, UK). The samples were pre-loaded with a nominal 7N load to stabilize the set up. The samples were then tested for compressive stress at a crosshead speed of 20mm/min (0.03 s^{-1}) with a data-sampling rate of 100Hz until failure. The data was cleaned so that true strain and stress could be calculated and used as per the following section to calculate the effective Young's Modulus.

4.3.2 Results

The effective Young's modulus E for each model (both FEA and static testing) was calculated using **Equation 21**:

$$E = \frac{\sigma}{\varepsilon} = \frac{F}{A} \times \frac{\Delta L}{L} = \frac{F}{187.55 \times 1} \times \frac{234.43}{1} \qquad \textbf{Equation 21}$$

where σ is stress, ε is strain, F is the sum of the x-direction reaction forces at the nodes on the right-hand boundary of the model, A is the cross-sectional area of the model, L is the specimen length (width) and ΔL is the extension (= 1 μm). Since the models were assumed to behave in plane stress and hence had unit thickness, the cross sectional area was obtained by multiplying the specimen height by 1.

4.3.2.A **Mesh Convergence**

Nearly doubling the number of elements (187963 elements in the coarsest mesh, 369541 elements in the finest mesh) resulted in a change of approximately 0.7% in the predicted effective Young's modulus. The finest mesh was therefore judged to be adequate for the prediction of the effective Young's modulus.

4.3.2.B **Stress Distributions**

Plots of the von Mises stress distributions for representative models for each material are shown in Figure 4-27; Figure 4-28; and Figure 4-29. Stresses have been normalised to an applied load of 0.001 Newton (nominal stress 5.33 MPa) for the purposes of comparison.

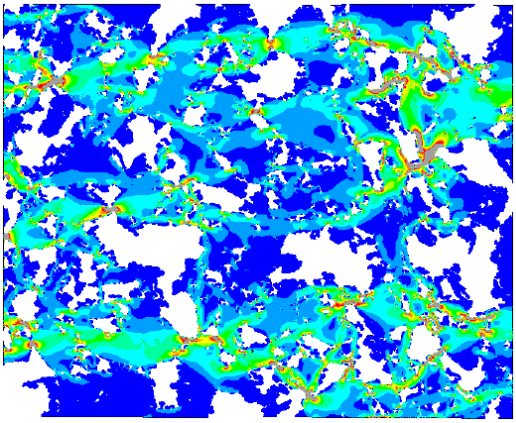

Figure 4-27 Plots of von Mises equivalent stress (MPa) in SiCaP-46G
Peak stresses are indicated in red, yellow and green regions.

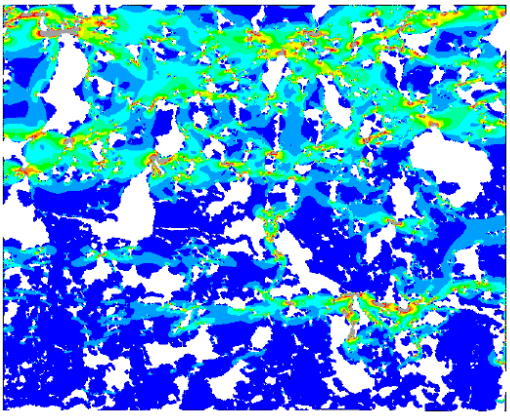

Figure 4-28 Plots of von Mises equivalent stress (MPa) in SiCaP-32G
Peak stresses are indicated in red, yellow and green regions.

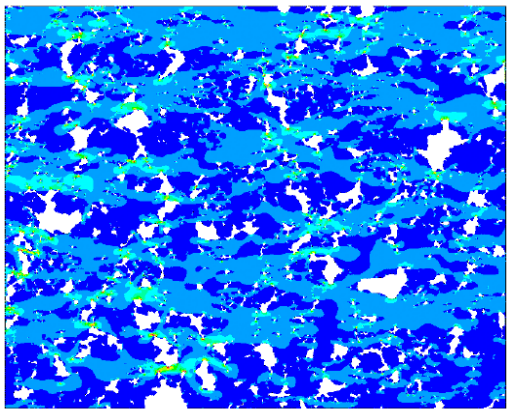

Figure 4-29 Plots of von Mises equivalent stress (MPa) in SiCaP-23G

Peak stresses are indicated in red, yellow and green regions.

4.3.2.C **Young's Modulus as a Function of Porosity**

A plot of the effective Young's modulus predicted by the finite element model as a function of strut porosity is shown in
Figure 4-30.

Table 4-5 Summary of uni-axial compression test data

Sample	Diameter (mm)	Young's Modulus (GPa)
1	5.081	3.497
2	5.075	4.556
3	5.080	2.921
4	5.077	3.910
5	5.068	4.943
6	5.048	3.758
7	5.062	5.822
8	5.081	3.304
9	5.076	3.629
10	5.079	5.179
	Mean	4.152
	StDev	0.930

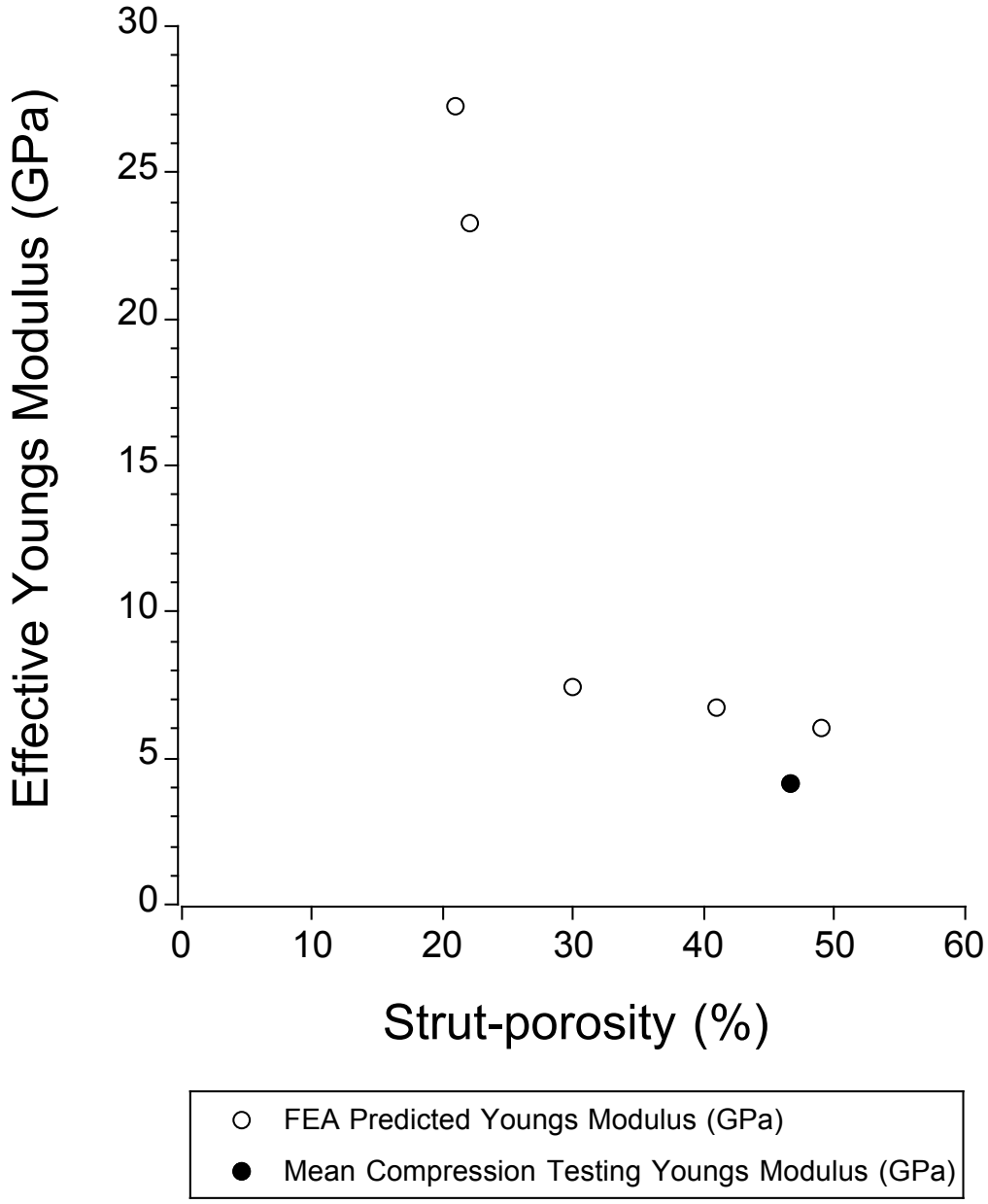

Figure 4-30 Plot of 2-Planar FEA model predicted Young's Modulus

A comparison of the measured Young's Modulus from static uni-axial testing with the 2-planar FEA model prediction and predictions according to empirical models developed for trabecular bone by Linde et al. (Linde, Norgaard et al. 1991, Rho, Hobatho et al. 1995) for materials of equivalent porosity (46.59%), is provided in Figure 4-31.

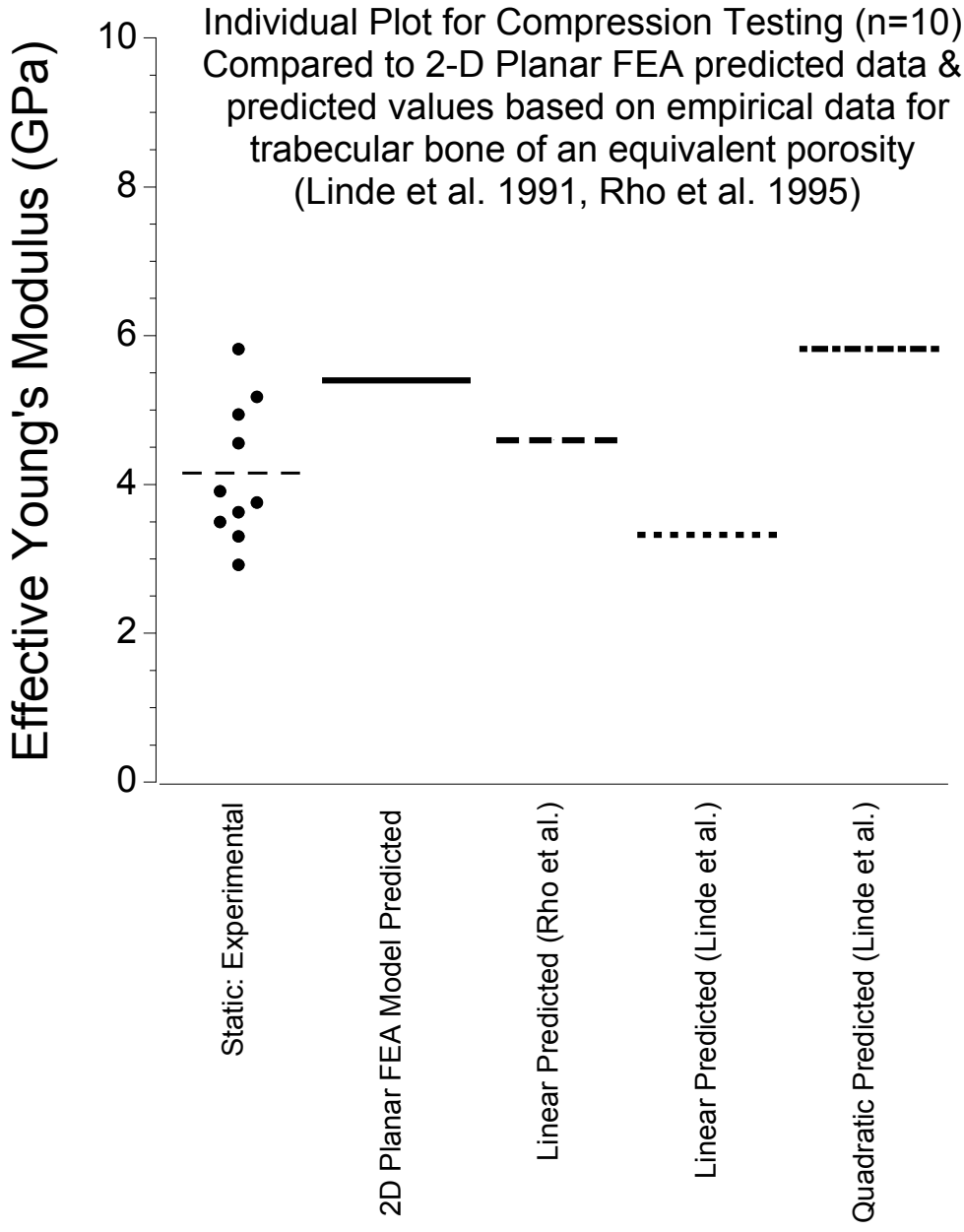

Figure 4-31 Individual plot for static uniaxial compression testing compared to FEA-predicted and literature-based predicted date

A comparison of the measured Young's Modulus from static uni-axial testing along with the 2-planar FEA model prediction and data reported from several studies in which calcium phosphate of varying density was tested for stiffness is provided in Figure 4-32. In this plot data is reproduced from studies in which a variety of mechanical testing techniques were used. These include static uni-axial testing (Akao, Aoki et al. 1981a, Charriere, Terrazzoni et al. 2001), ultrasonic testing (De With, van Dijk et al. 1981, Liu 1998), resonance testing (Arita, Wilkinson et al. 1995), and indenter testing (Patel 2003). All data reported from the literature was for stoichiometric hydroxyapatite containing various levels of porosity in the micropore size range. No comparative data for silicate-substituted calcium phosphate could be located in the literature.

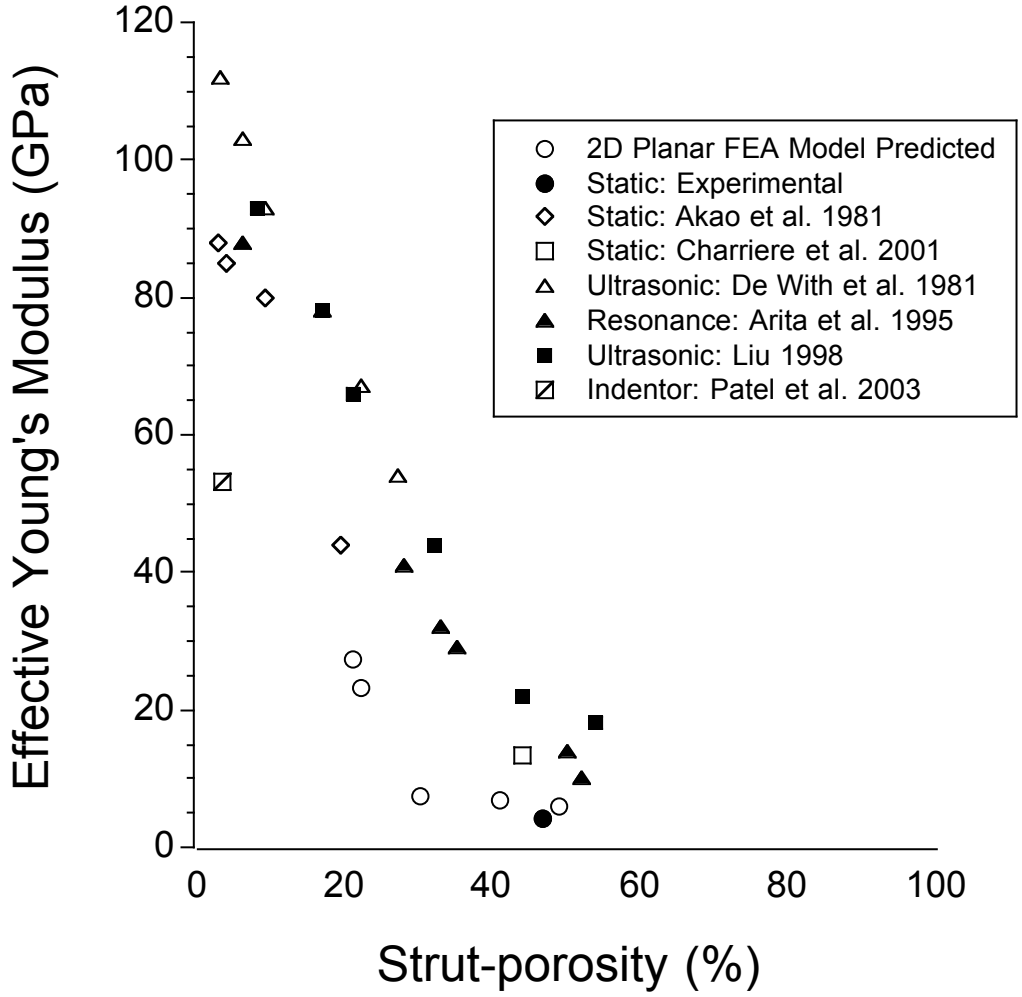

Figure 4-32 Plot of effective Young's modulus as a function of strut porosity

4.3.3 Discussion

The plots of von Mises stresses for the three test materials demonstrate that even in very low-loading situations (equivalent to 0.001N) there is a significant variation in stress distribution for materials of varying strut-porosity (Figure 4-27, Figure 4-28, Figure 4-29). In materials with a strut-porosity equivalent to 23% the stress is evenly distributed throughout the structure (Figure 4-29), whereas in materials with a greater amount of porosity the stresses appear concentrated at boundaries between adjacent pores (Figure 4-28, Figure 4-27). It is not unexpected that the materials would exhibit an increase in the frequency of stress-risers as the pore volume fraction increases, but it is interesting to note that there is a considerable shift in stress patterns over the range of porosity found within the test materials which are the subject of this thesis in other chapters.

Previous authors have examined the relationship between pore volume fraction and effective Young's Modulus in materials with a similar porous structure, such as trabecular bone (Linde, Norgaard et al. 1991, Rho, Ashman et al. 1993, Rho, Hobatho et al. 1995). In these studies the authors found that either a linear or quadratic equation led to the best fit to their experimental data. Our experimental data for a single batch of cylindrical test specimens with 46.59% porosity, as supplied by ApaTech Limited, UK, was in good agreement with the 2-D Planar FEA modelled prediction for a material with the same amount and morphology of porosity (Figure 4-31). We also compared this experimental data for silicate-substituted calcium phosphate with models generated from experimental data for trabecular bone. Rho et al., tested the mechanical properties of cortical and cancellous bone from eight human subjects using an ultrasonic transmission technique (Rho, Hobatho et al. 1995). In their study the predictive capabilities of linear and power models evaluated for cancellous bone alone were approximately equal. Similar to our own 2-D Planar FEA model, the power function gave a better fit of data at the low and high-density values. However, we found that the linear relationship described by Rho et al., was a good fit in the region of approximately 50% porosity with our own 2-D Planar FEA model and our experimental data. Our experimental data was also compared with work from Linde et al., who studied the effect of strain rate (epsilon) and apparent density (rho) on stiffness (E), strength (sigma u), and ultimate strain (epsilon u) was studied in 60 human trabecular bone specimens from the proximal tibia (Linde, Norgaard et al. 1991). Testing was performed by uniaxial compression to 5% specimen strain. Six different strain rates were used: 0.0001, 0.001, 0.01, 0.1, 1, and 10 s^{-1}. Apparent density ranged between 0.23 and 0.59 g cm^{-3}. Linear and non-linear regression analyses using strength, stiffness and ultimate strain as dependent

variables (Y) and strain rate and apparent density as independent variables were performed. Interestingly, the variations of strength and stiffness were explained equally well by the linear and the power function relationship to strain rate. The exponent was 0.07 in the power function relationship between strength and strain rate and 0.05 between stiffness and strain rate. This dependency of Young's Modulus on strain rate is important and should be considered for future studies. As per Rho's study, the variation of strength and stiffness was explained equally well by the linear, power function and quadratic relationship to apparent density. The cubic relationship between stiffness and apparent density showed a less good fit.

Figure 4-32 demonstrates that, compared to some previous studies for synthetic calcium phosphate, our finite element models under-predicted the effective Young's modulus of the ceramic materials by a factor of 2 to 3 (Akao, Aoki et al. 1981a, De With, van Dijk et al. 1981, Arita, Wilkinson et al. 1995, Liu 1998, Charriere, Terrazzoni et al. 2001). Other authors (Meille and Garboczi 2001) have found similar behaviour, albeit for materials made up of "particles" of much greater aspect ratio than those considered in this study. Interestingly, the difference between plane stress and plane strain two-dimensional models in Meille and Garboczi's study was much smaller than the difference between either two dimensional model and the three-dimensional model, suggesting that the plane stress approach taken in this study was not the source of the discrepancy between predicted and experimental results from other studies, rather that it was due to the limitations inherent in the reduction from three to two dimensions. Since both the two and three-dimensional models of Meille and Garboczi were generated from geometric models of hypothetical materials (rather than micrographs of real materials, as in the present study), they were able to compare other morphological parameters for both two and three dimensional models, and found that the percolation threshold (the simplest definition of the percolation threshold is that it is the value of porosity at which a large ("infinite") sample of a material becomes permeable) for their three-dimensional models was reached at about 80% porosity, whereas for the two-dimensional models it was at around 60% porosity, suggesting that for a given porosity, the three dimensional model would always show greater inter-particle connectivity and therefore be stiffer than the two-dimensional model.

4.4 Conclusions

In this chapter we sought to achieve two distinct objectives. These were (a) to use 3D finite element models to ascertain the mechanical environment of calcium phosphate

biomaterials in clinical applications; and (b) to develop a procedure for generating microstructural-level finite element models of calcium phosphate biomaterials from electron micrographs and to use the models to estimate the effective Young's modulus and the microstructural level stress and strain distribution under loading representative of the clinical mechanical environment.

Mechanical testing revealed silicate-substituted calcium phosphate to have similar mechanical behaviour to morcellised cancellous bone under similar test conditions. Furthermore, we discovered through the creation of novel 3D FEA models that bone grafts such as silicate-substituted calcium phosphate appear to be stress-shielded when applied in typical applications such as a tumour defect void or in a spinal fusion defect. We also learned through the use of novel 2D FEA models that there is an inverse exponential relationship between porosity and Young's Modulus which is similar to that described for trabecular bone and hydroxyapatite materials in previous studies.

Chapter Five: Effect of structure and chemistry on the Bioactivity of Calcium Phosphate Biomaterials

5.1 Introduction

Synthetic biomaterials designed for orthopaedic applications are no longer only considered safe and effective if they are inert and do not cause inflammatory reactions when implanted in the body. They must now also elicit a response from the body which favours the integration of the implant within the host bone (Osteointegration) whether the implant is intended for mechanical fixation, in the case of a pedicular metallic screw, or for repair; augmentation; or replacement of diseased or injured bone, in the case of bone graft extenders and substitutes. Since the early 1990's the potential for osteointegration of a material (its bioactivity) has been evaluated by examining the propensity of so-called 'bone-like apatite' to form on its surface after immersion in a simulated body fluid (SBF) with ion concentrations similar to those of human blood plasma (Kokubo, Ito et al. 1990). Although other solutions have been used to determine bioactivity, such as Dulbecco's phosphate buffered saline (DPBS) (Gandolfi, Ciapetti et al. 2009), the majority of researchers have applied the method described by Kokubo et. al.(Kokubo, Ito et al. 1990, Kokubo, Kushitani et al. 1990) Despite some controversy as to the methods reliability, its relevance to the understanding of mechanisms behind osteointegration, and the actual nature of the calcium-rich precipitate formed on materials Kokubo's SBF has been used to evaluate the bioactivity of numerous types of materials ranging from calcium phosphate ceramics and bioglasses through to Chitosan and natural Pearl (Table 5-1).

The objective of this study was to compare the bioactivity of calcium phosphate bone grafts of varying chemistry and strut-porosity through determining the rate of formation of hydroxycarbonate apatite (HCA) crystals on the material surface and the extent to which these crystals formed after the material was soaked in simulated body fluid for time periods ranging from 3 to 30 days.

Table 5-1 Examples of various materials tested for Bioactivity in Simulated Body Fluid

Ceramics :		Polymers :		Biologics / Metals :	
Diopside	(Miake, Yanagisawa et al. 1995)	Polysulfone	(Marcolongo, Ducheyne et al. 1997)	Collagen	(Li, Zheng et al. 1998)
Hydroxyapatite	(Weng, Liu et al. 1997, Kobayashi, Nakamura et al. 1998, Shirkhanzadeh and Azadegan 1998, Weng, Wang et al. 2002, Leng, Chen et al. 2003, Zhang, Chen et al. 2003, Yonggang, Wolke et al. 2007, Morejon-Alonso, Carrodeguas et al. 2008, Oliveira, Silva et al. 2009, Sanchez-Salcedo, Balas et al. 2009)	Polyethylene oxide/polybutylene terephthalate	(Du, Klasens et al. 2002)	Chitosan (with Calcium Phosphate)	(Zhang and Zhang 2002, Liu, Li et al. 2006, Leonor, Baran et al. 2008, Li, Yubao et al. 2009)
Tricalcium phosphate	(Kobayashi, Nakamura et al. 1998, Leng, Chen et al. 2003, Saint-Jean, Camire et al. 2005, Camire, Saint-Jean et al. 2006, Huan and Chang 2007, Morejon-Alonso, Carrodeguas et al. 2008, Hesaraki, Safari et al. 2009, Huan and Chang 2009, Sanchez-Salcedo, Balas et al. 2009, Vani, Girija et al. 2009)	Polycaprolactone	(Rhee, Choi et al. 2002, Jaakkola, Rich et al. 2004, Chouzouri and Xanthos 2007)	Starch (with Hydroxyapatite)	(Leonor, Ito et al. 2003) (Leonor and Reis 2003, Oliveira, Malafaya et al. 2003)
Wollastonite	(Kobayashi, Nakamura et al. 1998, Matsuoka, Akiyama et al. 1999, Greish and Brown 2001, Cortes, Medina et al. 2004, Zhang, Ye et al. 2009)	Polylactic-co-glycolic acid	(Lu, El-Amin et al. 2003)	Alginate	(Kokubo, Hanakawa et al. 2004)

Ceramics :		Polymers :		Biologics / Metals :	
Calcium silicate	(Siriphannon, Kameshima et al. 2000, Zhao, Wang et al. 2005, Ni, Chang et al. 2006, Huan and Chang 2007, Li, Shi et al. 2007, Zhao, Chang et al. 2007, Ni, Lin et al. 2008, Zhao, Chang et al. 2008, Coleman 2009, Coleman, Awosanya et al. 2009, Gandolfi, Ciapetti et al. 2009, Lin, Li et al. 2009, Ni and Chang 2009)	Poly(methyl methacrylate	(Miyazaki, Ohtsuki et al. 2003, Mori, Ohtsuki et al. 2005, Sugino, Miyazaki et al. 2008a, Lopes, Corbellini et al. 2009)	Cellulose (with carbonate hydroxyapatite)	(Yoshida, Miyazaki et al. 2006)
Silica	(Peltola, Jokinen et al. 2001, Izquierdo-Barbaa 2005, Heinemann, Heinemann et al. 2009, Mariappan, Yunos et al. 2009, Shi, Wang et al. 2009) (El-Ghannam, Ahmed et al. 2005)	Ultra-high molecular weight polyethylene (CaP coated)	(Leonor and Reis 2003)	Gelatin	(Yoon, Kim et al. 2008)
Calcium aluminate	(Oh, Choi et al. 2003)	Polyamide (CaP coated)	(Auclair-Daigle, Bureau et al. 2005, Kawai, Ohtsuki et al. 2007)	Pearl	(Shen, Zhu et al. 2006)
Silicon wafer	(Liu, Fu et al. 2004)	Polylactic-co-glycolic acid (45S5 bioglass additive)	(Lu, Tang et al. 2005)	Titanium (plasma sprayed)	(Ha, Eckert et al. 1997, Peltola, Jokinen et al. 1999, Takadama, Kim et al. 2001, Ning and Zhou 2002, de Medeiros, de Oliveira et al. 2008, de Souza, de Lima et al. 2011, Pattanayak, Yamaguchi et al. 2011)
Calcium metaphophate	(Kasuga, Ota et al. 2000)	Poly(lactic-co-glycolic acid) (Hydroxyapatite and bioglass additive)	(Huang and Miao 2007)	Tantalum	(Miyaza, Kim et al. 2002)

Ceramics :		Polymers :		Biologics / Metals :
Tobermorite	(Lin, Chang et al. 2007)	Poly-DL-lactic acid (45S5 bioglass additive)	(Chen and Boccaccini 2006, Maeda, Maquet et al. 2007)	
Calcium Carbonate	(Guo, Zhou et al. 2008, Kim and Park 2010)	Polymethylsiloxane (CaO-SiO_2 additive)	(Salinas, Merino et al. 2007)	
Octacalcium Phosphate	(Zhang, Leng et al. 2009, Orii, Masumoto et al. 2010, Yu, Yu et al. 2011)	Polyglutamic acid	(Sugino, Miyazaki et al. 2008b)	
Soda lime	(O'Donnell, Watts et al. 2009)	Poly(lactic acid) (b-TCP and Chitosan additive)	(Wang, Qu et al. 2008)	
Silicon carbide	(Will, Hoppe et al. 2010)	Hydroxyethylmethacrylate	(Miyazaki, Imamura et al. 2009)	
Silico Carnotite	(Lu, Duan et al. 2010)	Poly(lactic acid) (b-TCP additive)	(Kang, Yao et al. 2009)	

Ceramics :		Polymers :		Biologics / Metals :
Bioglass (Various systems incorporating CaO, SiO_2, TiO_2, P_2O_5, Na_2O, ZnO, CaF_2, MgO, SrO, K_2O, B_2O_3)	(Chen, Miyaji et al. 1999, Peltola, Jokinen et al. 1999, Vallet-Regi, Izquierdo-Barba et al. 1999, Chen, Miyata et al. 2000, Miyata, Fuke et al. 2002, Sepulveda, Jones et al. 2002, Fujibayashi, Neo et al. 2003, Oki, Parveen et al. 2004, Boyd and Towler 2005, Vakiparta, Forsback et al. 2005, Chen, Thompson et al. 2006, Kamitakahara, Ohtsuki et al. 2006, Pirhonen, Niiranen et al. 2006, Ni, Chang et al. 2008, Wren, Boyd et al. 2008, San Miguel, Kriauciunas et al. 2009, Seol, Kim et al. 2009, Towler, Boyd et al. 2009, Labbaf, Tsigkou et al. 2011, Wu, Hill et al. 2011)	Polyamide ($CaSiO_3$ treated)	(Leonor, Balas et al. 2009)	

5.2 Methods

5.2.1 Materials

Commercially available (Actifuse® Microgranules, ApaTech, Herts, UK) phase pure silicate-substituted (0.8 wt% Si) hydroxyapatite (SiCaP, $Ca_{10}(PO_4)_6(OH)_2$) material consisting of porous (80±2.5% total porosity), irregularly shaped microgranules (1–2 mm) with a strut-porosity of 22.5±2.5% (SiCaP-23) was tested. Two additional groups of SiCaP with strut-porosities of 32.0±2.5% and 46.0+2.5% were also included in the study (SiCaP-32 and SiCaP-46 respectively). A commercially available (Vitoss Scaffold Morsels, Orthovita, USA) porous beta-tricalcium phosphate (β-TCP, $Ca_3(PO_4)_2$) bone graft substitute consisting of porous (90% total porosity), irregularly shaped granules (1-4mm) was tested alongside the silicate-substituted calcium phosphate treatment groups.

5.2.2 Material Characterisation

Phase purity of the materials was confirmed by X-ray diffraction (XRD). The calcium, phosphorus, and silicon contents were determined by X-ray fluorescence (XRF). All chemical characterisation was performed as described previously. (Gibson, Best et al. 1999) Total porosity was confirmed according to a water immersion densitometry method. (Hing, Best et al. 1999) The strut-porosity was confirmed by mercury intrusion porosimetry in combination with helium pyconometry. The following conditions were used for the porosimetry measurement: an advancing contact angle of 140 degrees, a liquid-vapour interfacial free energy for mercury of 0.48 mJ/m^2, and a mercury density of 13.5 g/mL. The following conditions were used for the pyconometry measurement: a purge pressure of 19 Psi; both measurements were carried out at ambient temperature and pressure (20–25˚C and 1 atmosphere). The volume of closed strut pores, determined by the pyconometry, was added to the volume of open strut pores, determined by porosimetry, to give the total pore volume fraction of strut-porosity which is expressed as a percentage of the total strut volume (Equation 22). (Hing, Best et al. 1999) The surface area of the test materials was determined prior to this study by the BET method using a Micromeritics Tristar 3000 coupled with a Micromeritics FlowPrep 060.

$$\%\ Strut-porosity = \frac{Volume_{OPEN\ STRUT-POROSITY} + Volume_{CLOSED STRUT-POROSITY}}{Volume_{STRUT}} X\ 100\% \qquad \textbf{Equation 22}$$

5.2.3 Treatment in Simulated Body Fluid

The simulated body fluid (Table 5-2) was prepared according to the method described by Kokubo (Kokubo, Ito et al. 1990) and the assay validated through the analysis of negative controls in which blanks were checked for spontaneous formation of HCA. There is a great deal of disparity between studies investigating Bioactivity with regards the amount of material tested in any given volume of simulated body fluid (Table 5-3). The difference between the lowest concentration (Peltola, Jokinen et al. 2001) and the highest concentration (Sanchez-Salcedo, Balas et al. 2009) tested in the literature is some five orders of magnitude. This makes it extremely difficult for reviewers to compare across studies; particularly for studies investigating materials with varying surface morphologies. Since the study of Bioactivity is primarily concerned with the local effects occurring on a test materials' surface the most appropriate route to controlling exposure to the simulated body fluid is through normalising the amount of simulated body fluid for the measured surface area of the test material. Furthermore, the specific surface area of calcium phosphate ceramics is relatively low (<5 m^2g^{-1}) so the volume to surface ratio of SBF to scaffold is notably higher than for other scaffolds such as bioactive glasses so this must be compensated for when setting up the design of experiments. (Sanchez-Salcedo, Balas et al. 2009) The surface area results calculated for the materials tested in this study were used to calculate the volume of simulated body fluid required for each sample (Equation 23).

$$V_S = \frac{S_a}{10}$$ **Equation 23**

Where Vs is the volume of SBF (ml) and Sa is the apparent surface area of specimen (mm^2).

Table 5-2 Simulated body fluid

Order of addition to the vessel	Reagent	Amount	Purity (%)	MW
1	NaCl	8.035 g	99.5	58.4430
2	$NaHCO_3$	0.355 g	99.5	84.0068
3	KCl	0.225 g	99.5	74.5515
4	$K_2HPO_4.3H_2O$	0.231 g	99.0	228.2220
5	$MgCl_2.6H_2O$	0.311 g	98.0	203.3034
6	1.0M - HCl	39ml	-	-
7	$CaCl_2$	0.292 g	95.0	110.9848
8	Na_2SO_4	0.072 g	99.0	142.0428
9	Tris	6.118 g	99.0	121.1356
10	1.0M - HCl	0-5 ml	-	-

Table 5-3 Examples of various ratios of test material : SBF solution in the literature

As a concentration ($mgml^{-1}$) :		Per unit area of device (cm^{-1}) :	
0.20	(Peltola, Jokinen et al. 2001)	0.014	(Peltola, Jokinen et al. 1999)
0.50	(Shi, Wang et al. 2009)	0.020	(Will, Hoppe et al. 2010)
1.00	(Oki, Parveen et al. 2004, Li, Shi et al. 2007, Coleman 2009)	0.500	(San Miguel, Kriauciunas et al. 2009)
1.50	(Lin, Chang et al. 2007)	0.080	(Marcolongo, Ducheyne et al. 1997)
2.00	(Peltola, Jokinen et al. 1999)	1.000	(Lu, El-Amin et al. 2003)
10.0	(Sepulveda, Jones et al. 2002)	0.100	(Peltola, Jokinen et al. 1999, Lu, Tang et al. 2005, Zhao, Wang et al. 2005, Pirhonen, Niiranen et al. 2006, Chouzouri and Xanthos 2007, Huan and Chang 2007, Zhao, Chang et al. 2007, Morejon-Alonso, Carrodeguas et al. 2008, Ni, Chang et al. 2008, Ni, Lin et al. 2008, Zhao, Chang et al. 2008, Huan and Chang 2009, Lin, Li et al. 2009, Ni and Chang 2009, Towler, Boyd et al. 2009, Lu, Duan et al. 2010)
30.0	(Cortes, Medina et al. 2004)		
2.00 x 104	(Sanchez-Salcedo, Balas et al. 2009)		

The test described herein was carried out in duplicate for each test material and negative controls at every time-point. The calculated volume of SBF was pipetted into a tube (centrifuge) and heated to 36.5^{o}C. After heating the test materials were fully submerged in the SBF for various amounts of time prior to analysis.

Studies of Bioactivity described in the literature include testing the outcome measures at time-points varying from as little as thirty minutes (Sepulveda, Jones et al. 2002) through to sixty days (Oh, Choi et al. 2003, Izquierdo-Barbaa 2005, Sanchez-Salcedo, Balas et al. 2009). The primary objective of this study was to understand the effect of strut-porosity on the Bioactivity of calcium phosphate materials in order to determine the likely impact on the process of Osteointegration when implanted into bone. The test materials in this study were immersed in SBF for 3, 6, 9, 14, 18, 21, 25, and 30 days prior to analysis as this represents the critical phase following implantation but prior to woven bone formation *in vivo*.

In studies reported in the literature the SBF test is performed under static, semi-dynamic, or dynamic conditions. When performed under-semi-dynamic conditions the SBF solutions have been refreshed by investigators every 12 hours (Lin, Li et al. 2009), daily (El-Ghannam, Ahmed et al. 2005, Heinemann, Heinemann et al. 2009, Hesaraki, Safari et al. 2009), every 2 days (Ning and Zhou 2002, Vakiparta, Forsback et al. 2005, Shen, Zhu et al. 2006, Huang and Miao 2007, Morejon-Alonso, Carrodeguas et al. 2008, Wang, Qu et al. 2008), twice a week (Chen and Boccaccini 2006, Chen, Thompson et al. 2006), weekly (Cortes, Medina et al. 2004, Yonggang, Wolke et al. 2007), or every two weeks (Pirhonen, Niiranen et al. 2006). In the interest of allowing for cross-comparison of our study results with historical studies or studies conducted in the future our test was carried out under the static conditions described by Kokubo et. al, i.e. the SBF was not replenished for the duration of the study. (Kokubo, Ito et al. 1990, Kokubo, Kushitani et al. 1990)

5.2.4 Validation of Assay

The inner surfaces of the polypropylene sample containers used in this study were collected and examined with an Energy Dispersive X-Ray Analysis (EDX) detector coupled to a Scanning Electron Microscope (Stereoscan Model 360 SEM/Oxford Inca Energy 200 EDX, Cambridge Instruments, UK) at the end of the study to determine whether any HCA had spontaneously formed on surfaces other than the test article. A single used container from the 30 day group was examined in addition to one un-used container as negative control. A 10mm x 10mm sample of the container was cut out from an area which was exposed to SBF during the experiment, mounted inner-side-up on an SEM stub, and coated in approximately 4nm of Pt/Pd prior to analysis. The EDX spectra for the polypropylene samples were compared to a synthesised spectrum for hydroxy carbonated apatite.

5.2.5 Characterisation of Carbonated Crystalline Apatite

On removal from the SBF the granules were rinsed twice with approximately 2mls of MilliQ of distilled water. Excess water was then removed by glass pipette. Petri dishes were lidded and transferred to an oven set to 80°C for drying. The samples were mounted on SEM stubs, lightly coated in Pt/Pd then examined with Scanning Electron Microscopy (Cambridge S360, UK; Hitachi S4700, Japan). Images were captured at magnifications between 25 and 40,000 times.

5.2.6 Characterisation of SBF Ionic Composition

The ionic concentrations of Silicon, Calcium, and Phosphorus in all SBF samples were measured with inductively coupled plasma optical emission spectrometry (ICP-OES) using an IRIS Advantage Radial Plasma instrument installed with TEVA control software application (Thermo Scientific, USA). The instrument was calibrated using standard solutions made from traceable single-element stocks. Each unknown sample was measured against the calibration to give a concentration of the elements of interest in the sample. An instrument blank (identical to the calibration blank), and an instrument QC was run with and before each batch of samples. In the event any sample failed (i.e. the blank was outside ± the limit of detection or the QC was outside of ± 10% of the target value), the instrument was re-standardised against the top calibration standard and the calibration blank. Uncertainties for each element were estimated at 2% of the reported value.

5.3 Results

5.3.1 Energy Dispersive X-Ray Analysis

When compared to spectra for synthesised HCA (Figure 5-1a) and untreated specimen containers (Figure 5-1b) no calcium or phosphorus was detected on polypropylene specimen containers following exposure to SBF for 30 days (Figure 5-1c). Carbon and Oxygen were detected in expected quantities for a polypropylene material in addition to the Platinum-Palladium coating.

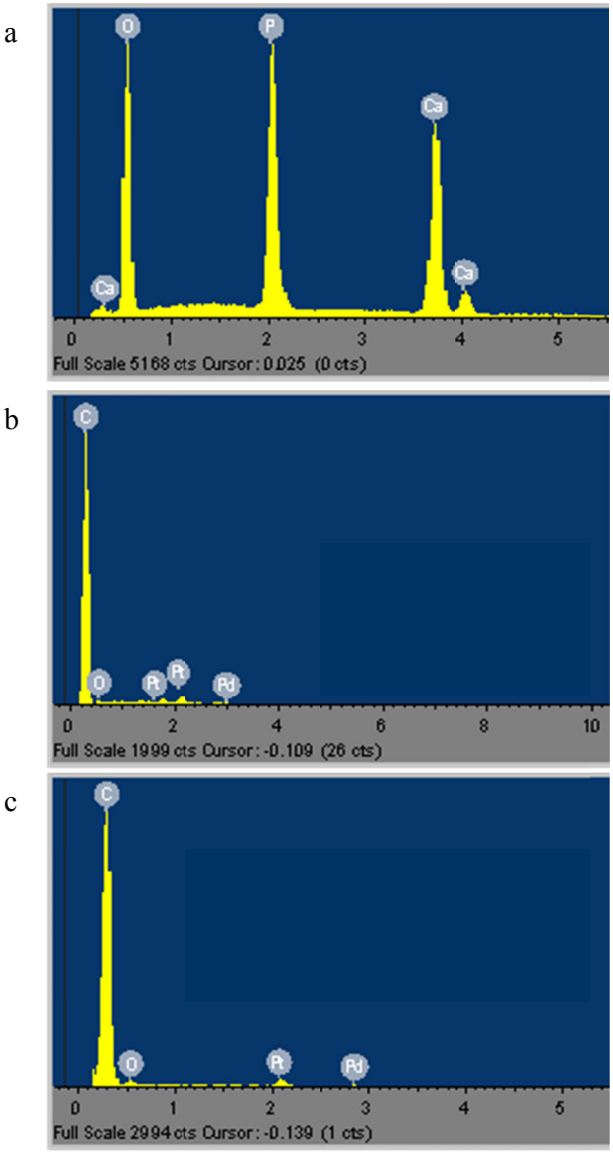

Figure 5-1 Energy Dispersive X-Ray Spectra

Energy Dispersive X-Ray spectra for (a) synthesised carboxyapatite; (b) untreated polypropylene specimen containers; and (c) polypropylene containers following exposure to SBF for 30 days

5.3.2 Scanning Electron Microscopy

There was no evidence of spontaneous formation of HCA crystals on the surface of the polypropylene containers in which the materials were tested. This was established by comparing samples from un-tested container with material from containers in which samples had been aged for 30 days.

All treatment groups comprised porous granules which when observed at low magnification under scanning electron microscope were found to be formed from highly interconnected ultra-macropores. In all groups micropores were visible in the walls of the macropores and were also highly interconnected, forming channels between the macropores (Figure 5-2a, b, c). At high magnification there was a clear difference between the treatment groups in the amount and the morphology of microporosity. The SiCaP-23; SiCaP-32; and SiCaP-46 groups were formed from crystallites of approximately 0.5 - 1.0 microns diameter fused together to form agglomerates of approximately 2.0 - 20 microns diameter (Figure 5-2b, c). The space formed between the packed and sintered agglomerates formed the microporosity with the level of porosity visible under the microscope increasing according to the following trend: SiCaP-23 < SiCaP-32 < SiCaP-46. The Vitoss group was formed from crystallites of approximately 2.0 - 5.0 microns diameter fused together to form the walls of the macropores (Figure 5-2a). The micropores in this material were formed between the crystallites themselves and not between agglomerated crystallites. The volume of microporosity observed in the Vitoss group was approximately equivalent to that observed in the SiCaP-46 group. A small number of surface contaminants of approximately 0.2 - 1.5 microns diameter were observed on all un-treated materials. This observation was attributed to particles being dislodged from surface during preparation and initial analysis before immersion in SBF. No HCA was present on the surface of the un-treated specimens.

Evidence of carbonate apatite formation was observed on the surface of all test materials as early as day 3 after being immersed in SBF. The mode of HCA formation for SiCaP-23; SiCaP-32; and SiCaP-46 was consistent between test groups. Formation of the HCA layer covered the entire surface of the material after only 3 days and was not localised to any one particular surface artefact (Figure 5-2e,f). In contrast, only very small crystals were formed on the Vitoss and the formation of HCA seemed to be localised to grain boundaries and defects or pits on the Vitoss material surface (Figure 5-2d). The morphology of the layer formed after 3 days varied between groups. HCA precipitated on Actifuse had a rod-like appearance (Figure 5-2e). The rods were approximately 0.2 microns in length, 0.05 microns in diameter, and formed a continuous coral-like matrix across the surface of the test material. The morphology of the HCA layer on SiCaP-32 and SiCaP-46 was lath-like and formed sheets of approximately 0.2 microns in length/depth and 0.01 microns in thickness (Figure 5-2f). The HCA formation on Vitoss was similarly lath-like but only in present in small quantities as spherical formations at grain boundaries (Figure 5-2d).

After 6 days, the rod-like structure observed on Actifuse at 3 days had matured into the lath-like structure observed on SiCaP-46 at the earlier time-point (Figure 5-3a) whilst the maturity of HCA on SiCaP-32 and SiCaP-46 had reached a state at which HCA began forming a secondary architecture above the primary surface layer of crystals resulting in a well-established crystal microstructure including pores and concavities (Figure 5-3b). The formation of the secondary layer of HCA on Actifuse was observed later in the experiment (day 14) (Figure 5-3c). There was no substantial change in the size or frequency of the spherical crystal formations observed on Vitoss between 3 and 14 days (Figure 5-2a and Figure 5-3d). Dissolution of the precipitated carbonate apatite layer was observed after 14 days for SiCaP-46 (Figure 5-3e) and 18 days for Actifuse (Figure 5-3f). A number of cracks and fissures were observed in the dried HCA layer as early as 14 days for SiCaP-46 (Figure 5-3e) and after 25 days for Actifuse (Figure 5-4a). This observation was absent for Vitoss as no continuous layer of HCA was formed on the surface over the course of the experiment although the number of spherical crystal formations observed did increase between days 18 (Figure 5-4b) and 30 (Figure 5-4c) and secondary structures were observed on the primary HCA crystals after 30 days (Figure 5-4c). After 30 days the precipitated HCA on Vitoss continued to form at defects or at grain boundaries on the material surface and did not appear to be present as a result of interactions (in the form of dissolution – precipitation) with the bulk material itself (Figure 5-4d). On the contrary after 30 days immersion all SiCaP groups were completely covered in an intimate layer of HCA (Figure 5-4e) with a tertiary structure consisting of lath-like sheets forming globular structures in between which pores were evident (Figure 5-4f).

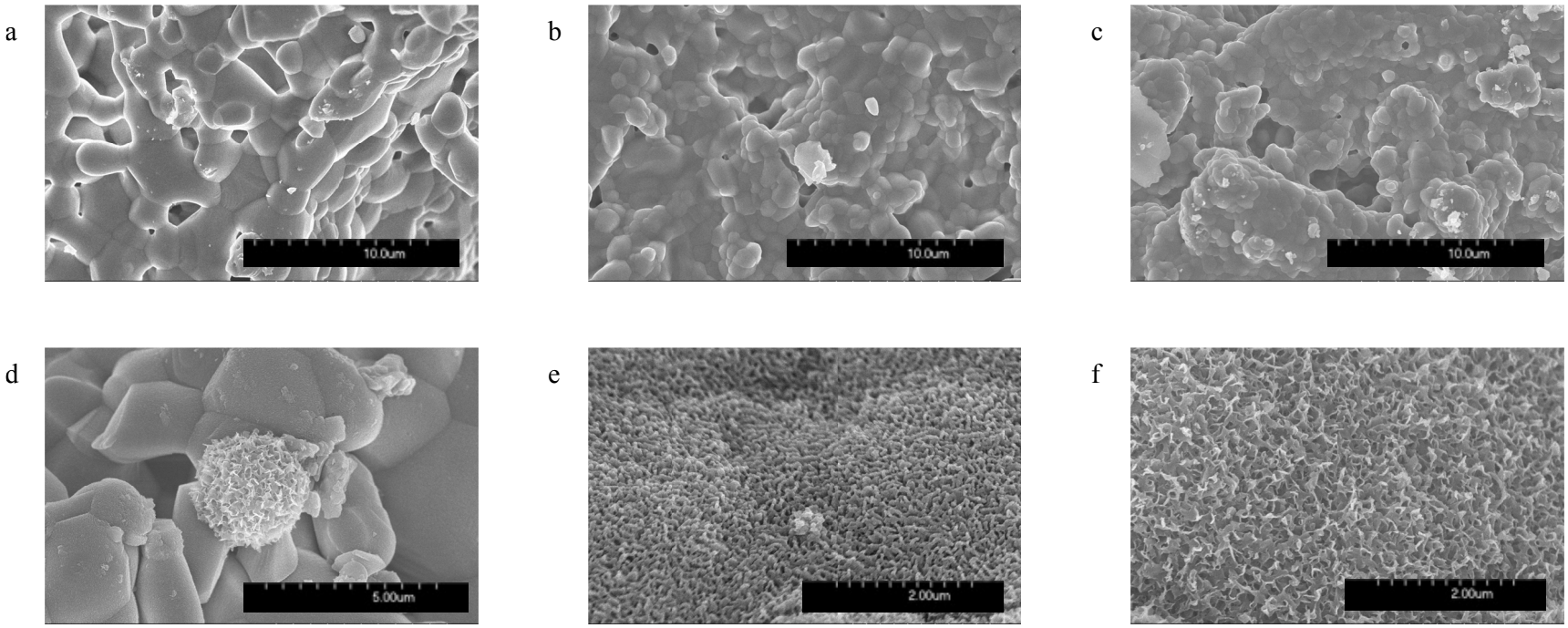

Figure 5-2 SEM micrographs:

Scanning electron micrographs at Day 0 (a-c) demonstrating all groups contain interconnected structures before being submerged in SBF - β-TCP (a) SiCaP-23 (b) and SiCaP-46 (c); Day 3 (d-f) Lath-like HCA formation present as spherical formations in small quantities at grain boundaries on β-TCP material (d), Rod-like HCA layer covering the entire surface observed on SiCaP-23 (e), and Lath-like formation of HCA layer covering the entire surface observed on SiCaP-46 (f).

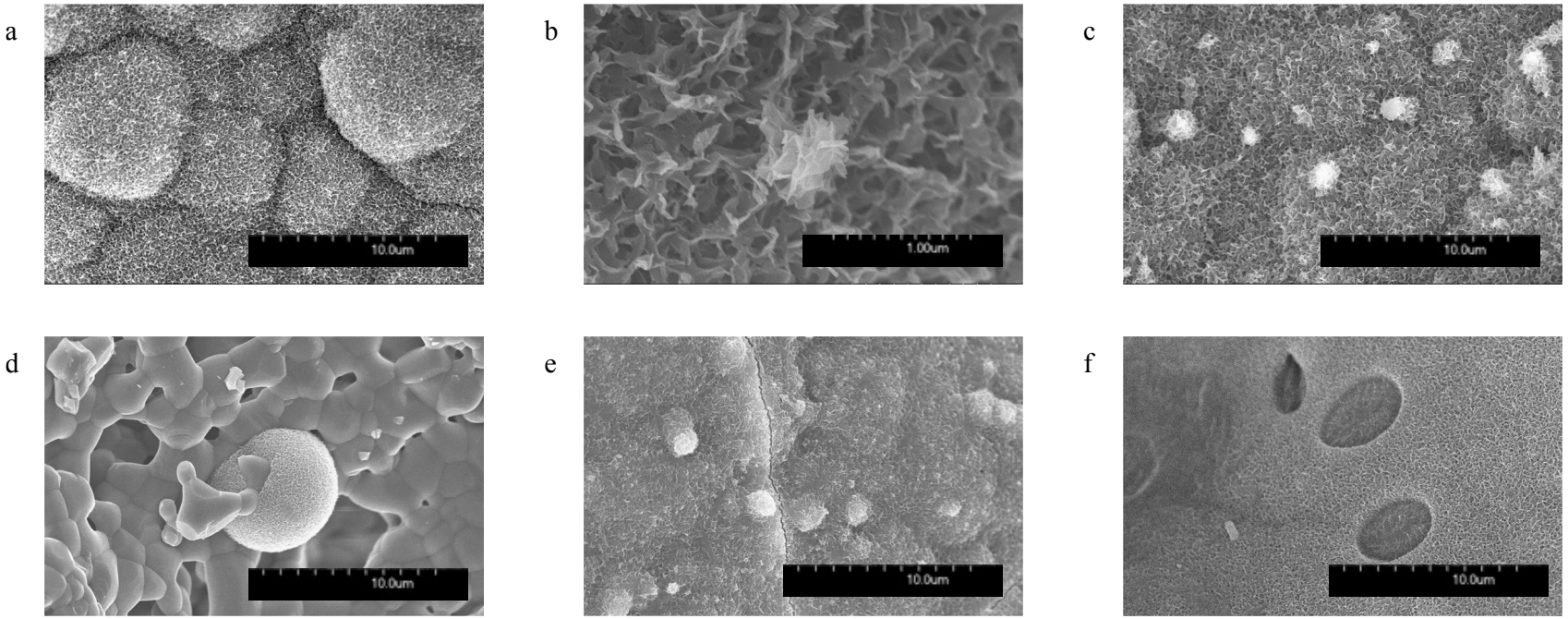

Figure 5-3 SEM micrographs

After 6 days the rod-like structure observed on SiCaP-23 had matured into the lath-like structure (a). At the same time-point the HCA formed on SiCaP-46 had matured to form a secondary architecture above the primary surface layer (b). This secondary architecture was observed on day 14 for the SiCaP-23 group (c). The spherical crystal formations observed on β-TCP at 14 days (d) were not substantially different from the 3 day time point. Dissolution of the precipitated carbonate apatite layer was observed after 14 days for SiCaP-46 (e) and 18 days for SiCaP-23 (f).

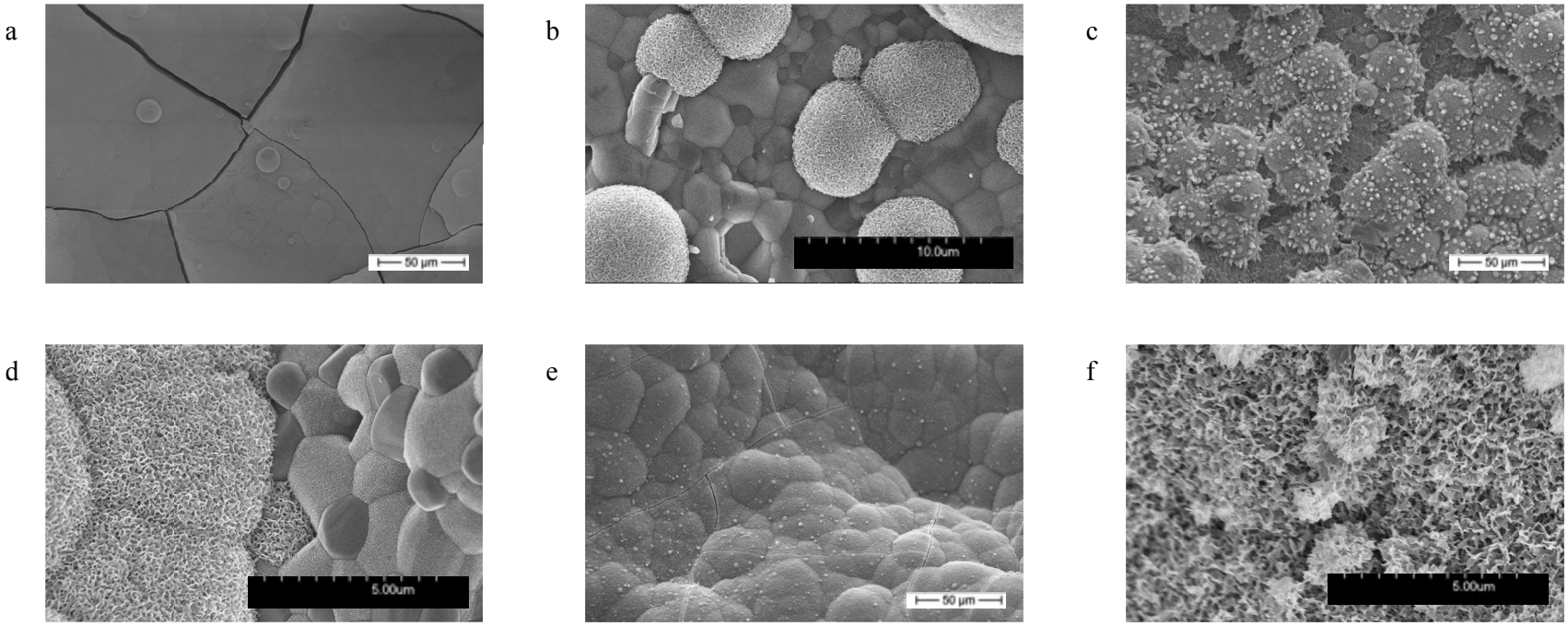

Figure 5-4 SEM micrographs

Cracks and fissures observed in the dried HCA layer after 25 days with SiCaP-23 (a). The number of spherical crystal formations observed increased in the β-TCP group between days 18 (b) and 30 days (c). After 30 days the precipitated HCA on β-TCP continued to form but did not interact with the bulk material itself (d) whereas after 30 days immersion, SiCaP-46 was completely covered in a tertiary structure of lath-like HCA sheets (e & f).

5.3.3 Inductively Coupled Plasma Optical Emission Spectrometry

There were no significant changes in silicon concentration over the 30 days of the study for any treatment group. There were substantial decreases in both calcium and phosphorus ions in the SBF from 0 to 30 days for all treatment groups (Figure 5-5a and b). There appeared to be a greater decrease in both ions for the SiCaP groups than the Vitoss group after 30 days immersion. Also of note was the amount of fluctuation in ion levels over the course of the experiment. Through integration of the decrease in calcium ion concentration (Figure 5-6a) and the phosphorus ion concentration (Figure 5-6b) with time it was apparent that the rate of both calcium and phosphorus loss from the solution was equivalent for all groups between day 0 and day 6. However, between days 6 and 9 the SBF solutions in which SiCaP-23 and SiCaP-32 were stored increased in calcium concentration but not for SiCaP-46 or Vitoss and the SBF solutions in which SiCaP-23; SiCaP-32; and Vitoss were stored increased in phosphorus concentration but not for SiCaP-46. Between days 9 and 14 both calcium and phosphorus ions decreased in concentration for all treatment groups apart from Vitoss. After 18 days there is a continued loss of calcium and phosphorus ions from the solution.

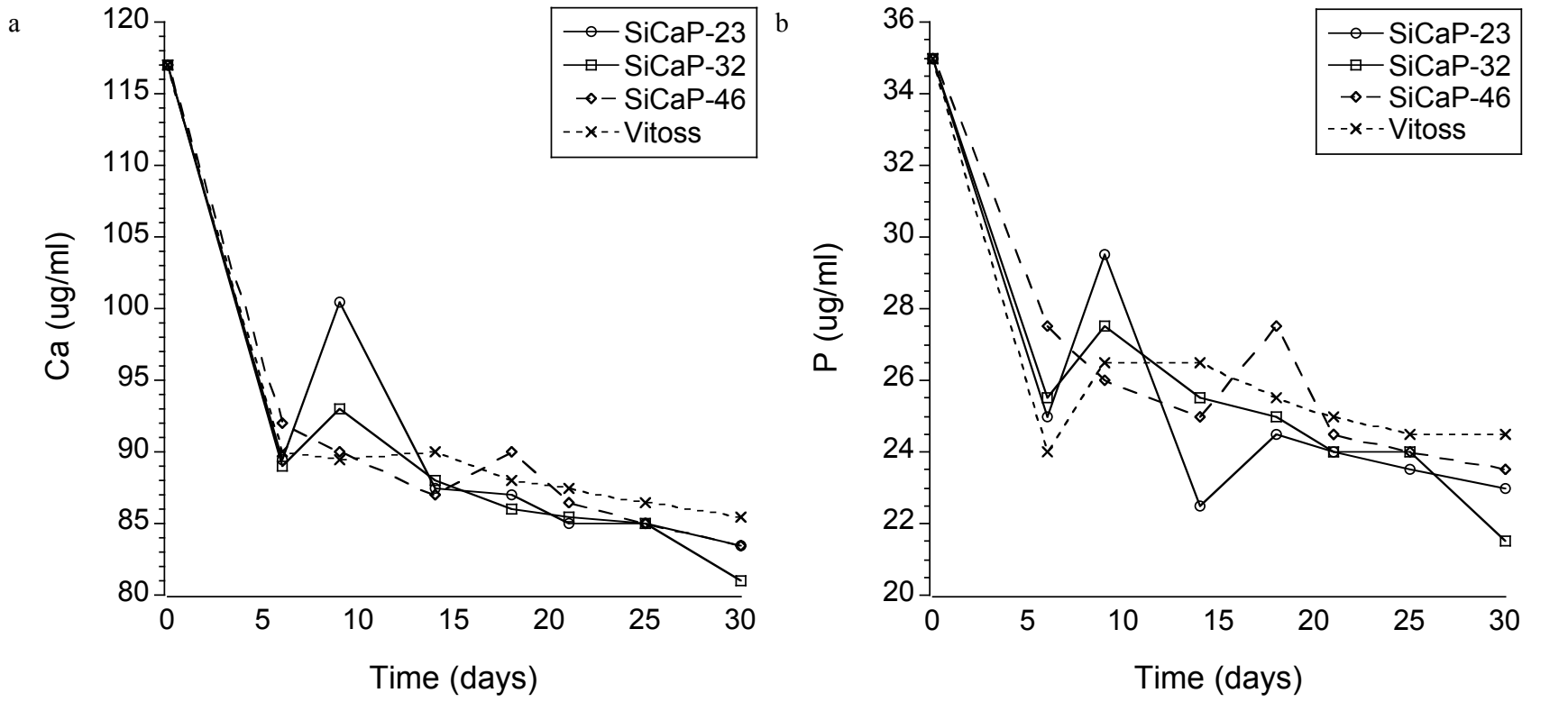

Figure 5-5 Concentration of Calcium ions in SBF across all groups between 0-30 days (a). Concentration of Phosphorous ions in SBF across all groups 0-30 days (b).

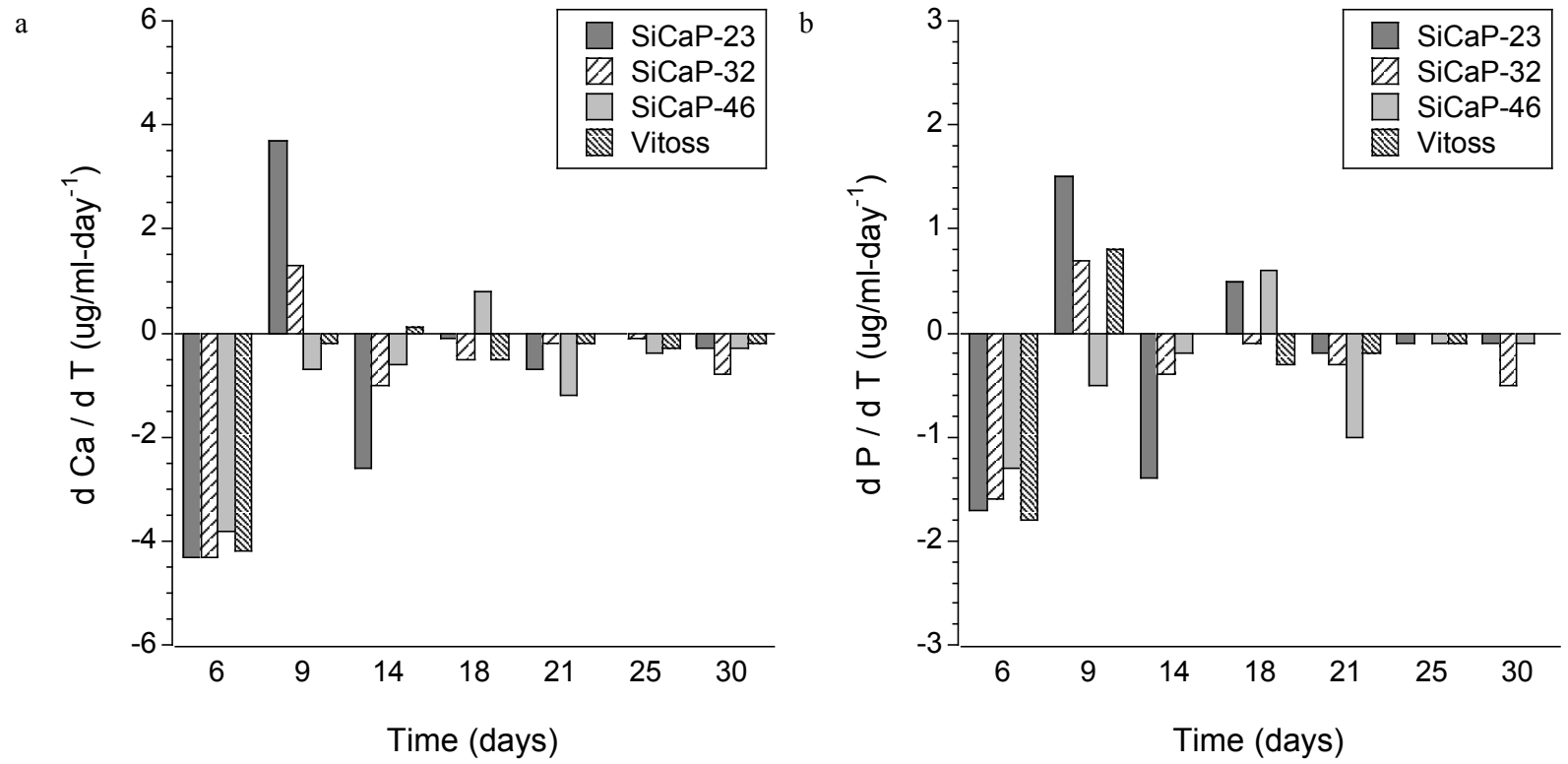

Figure 5-6 Change in concentration of Calcium ions per day across all groups 0-30 days (a). Change in concentration of Phosphorus ions per day across all groups 0-30 days (b).

5.4 Discussion

The number of clinical procedures performed in the USA in which bone graft was implanted was estimated at 1,109,000 in 2010 and is projected to reach 1,295,260 in 2015 (BioMedGPS 2012). This increasing demand for bone graft substitutes as a result of an ever-ageing population coupled with recent reports in the clinical literature of concerns regarding the safety of recombinant bone morphogenetic proteins such as rh-BMP-2 (Carragee, Ghanayem et al. 2011, Carragee, Hurwitz et al. 2011a, Carragee, Hurwitz et al. 2011b, Carragee, Mitsunaga et al. 2011) has led to an increased clinical interest in synthetic alternatives, such as porous calcium phosphate ceramics, to allograft; autograft; and recombinant growth factors. Whilst the preclinical and clinical efficacy of calcium phosphates is relatively well described in the scientific and clinical literature there is still a need to better understand the mechanisms behind their therapeutic action so that the next generation of synthetic bone graft substitutes can be developed with improved safety and efficacy. The effect of structure and chemistry on the *in vivo* performance of calcium phosphate bone graft substitutes in animals has been reported extensively in the scientific literature. (Hing, Best et al. 1998b, Hing, Gibson et al. 1998, Hing, Merry et al. 1999, Hing, Gibson et al. 2001, Hing 2004b, Hing 2004a, Hing, Saeed et al. 2004, Hing, Best et al. 2004, Hing 2005, Hing, Annaz et al. 2005, Hing, Revell et al. 2006, Hing, Wilson et al. 2007, Campion, Chander et al. 2011) For example, a recent study by this author investigated bone graft performance in an ovine critically-sized femur defect model and found that increasing the strut-porosity of silicate-substituted calcium phosphates enhances osteogenesis.(Campion, Chander et al. 2011) A gap in understanding currently exists between knowing how to manipulate the properties of such devices to elicit the desired biological response *in situ* and knowing by which mechanisms this manipulation takes effect. One way to reduce this knowledge gap is through the use of *in vitro* models. The test for bioactivity is one such assay and has been reported in the scientific literature for over 20 years. A large volume of scientific work investigating the bioactivity of biomaterials has preceded this study but only a handful of studies have used the assay described by Kokubo et. al. in 1990 as a means for comparing the impact of microstructure on the bioactivity of biomaterials and none have specifically investigated the effects of chemistry *and* structure on the bioactivity of porous calcium phosphate bone graft substitutes. One such study concluded that the induction period for HCA growth is a function of both composition and textural properties such as surface area, pore dimensions, density, and porosity (Coleman 2009). This study was designed to establish whether the microstructure or chemistry is the predominant factor in

determining a calcium phosphate ceramic bone graft substitute's bioactivity.

Our study was validated as being predictive for the assessment of *in vitro* HCA formation through the use of a negative control. We investigated whether a layer of HCA could spontaneously form on the surface of polypropylene containers over the 30 days of the study. Energy dispersive X-ray analysis and scanning electron microscopy of the surfaces of the polypropylene containers confirmed that no such spontaneous HCA layer formation occurs under the conditions of the study, therefore, any such HCA formation observed for the test materials could be presumed to be directly related to the material substrate and not super-saturation of the SBF fluid with calcium and phosphorus ions.

We demonstrated that when porous SiCaP ceramics are immersed in simulated body fluid a thick continuous layer of carbonate apatite crystals with a complex microstructural architecture forms over the surface of the material. The process of crystal growth appears multifarious as the layer continues to mature through several distinct phases of development. In the initial days following immersion small rod-like formations were present across the surface of the silicate-substituted materials with 23% strut-porosity whereas larger plate-like formations were observed across the surfaces of the silicate-substituted materials with 46% strut-porosity. This observation of two distinct morphologies of apatite crystal in the same system is consistent with the rod-like morphology of hydroxyapatite (HA) and blade-like morphology of octacalcium phosphate (OCP) observed in a study investigating the method of so-called central dark line formation. (Tseng, Mou et al. 2006) OCP and HA are structurally similar so OCP is proposed as a precursor in the development of biological apatite's *in vivo*. The presence in biological appetites of the central dark line, a crystallographic interference occurring at the interface between OCP and HA phases, is the evidence substantiating this theory. The hypothesis is further corroborated through comparison of dissolution profiles for calcium phosphates; OCP is the only phase with stability to dissolution approaching that of HA. (Heughebaert 1984) Hydroxyapatite forms more readily in solution at a pH of 7 or above(Akao, Aoki et al. 1981b) whereas OCP forms more readily as a pH of 6 or below. (Heughebaert 1984) In our study the pH of SBF was adjusted to ~7 by TRIS buffer so the fact that we observed both HA and OCP is not surprising. However, the rod-like morphology of HA was only observed at early time-points (3 days) and as a layer in intimate contact with the underlying SiCaP substrate. At all other time-points only crystals with the plate-like morphology of OCP were observed, thus, at pH ~7 the hydration of OCP to HA does not progress to any great extent and OCP

appears to be the more favourable phase.

Whilst on the subject of OCP and HA it is noteworthy that the need for caution to be exercised when claiming that precipitates on bioactive ceramics in SBF are "bone-like apatite" has been identified by other investigators in the past. A study using TEM crystal diffraction showed that precipitates on biphasic calcium phosphate (BCP) were neither bone-like or apatite (but OCP instead). (Leng, Chen et al. 2003) The significance of this *in vivo* is likely to be negligible as both HA and OCP are precursors for the formation of biological apatite, but this author proposes the term "precursor of biological apatite" as more appropriate than "bone-like apatite".

Far fewer crystals with the OCP characteristic and no HA-like crystals were observed on the β-TCP materials. After 3 days OCP was present in low quantities and only at surface artefacts such as grain boundaries or pore junctions. Other investigators have reported similar findings for β-TCP. (Juhasz, Best et al. 2008) Juhasz et. al. tested non-porous pressed disks of HA; β-TCP; and Brushite alongside each other and found that when β-TCP was placed in SBF there was slight dissolution on the surface and at the edges of individual grains of β-TCP, as well as the formation of small apatite crystals. In that study the materials were aged for 14 days and consequently most of the apatite crystals remained sub-micron sized although some grew into larger apatite clusters. The tendency of the porous β-tricalcium phosphate included in our study to develop infrequent HCA globules is, however, in contradiction to the majority of earlier reported findings. Most studies investigating β-TCP in this assay show no formation of HCA at all (Huan and Chang 2007, Hesaraki, Safari et al. 2009, Ni and Chang 2009); including an *in vivo* study in rats in which undecalcified sections of the interface between bone and β-TCP were examined with SEM-EPMA and no formation of surface apatite layer was observed despite there being a high mechanical bone-bonding strength.(Kotani, Fujita et al. 1991) The results of our study demonstrate that there is a much lower propensity for the formation of an OCP-like layer on β-TCP compared to SiCaP after immersion in SBF.

At the 6 day time-point a new phase of HCA development on SiCaP treatment groups which comprised both new crystal formation and dissolution into the SBF was observed in our study. This was evidenced through both our scanning electron microscopy of the material surface and ICP-OES analysis for ionic concentrations in the SBF supernatant. A large number of OCP-like globular crystals were observed by SEM forming over the initial HA-like HCA layer, an observation consistent with

those reported in the literature.(Siriphannon, Kameshima et al. 2000) In other studies the formation of this secondary layer was noted as proceeding much more readily than the initial layer formation although this was not corroborated by our own findings.(Saint-Jean, Camire et al. 2005) The formation of these crystals was accompanied by HCA dissolution; evidenced through the formation of pits in the initial HCA layer, an observation also consistent with findings of previous experiments.(Zhao, Wang et al. 2005, Huan and Chang 2007, Zhao, Chang et al. 2007) Further evidence for the counteracting processes of deposition and dissolution can be found in our analysis of the ionic composition of the SBF over the duration of the test. Calcium ion concentrations in SBF have been seen to fluctuate over time in a large number of previous experiments.(Peltola, Jokinen et al. 1999, Peltola, Jokinen et al. 2001, Takadama, Kim et al. 2001, Miyata, Fuke et al. 2002, Leonor and Reis 2003, Kokubo, Hanakawa et al. 2004, Kamitakahara, Ohtsuki et al. 2006, Chouzouri and Xanthos 2007, Guo, Zhou et al. 2008, Leonor, Baran et al. 2008, Coleman 2009, Leonor, Balas et al. 2009, Li, Yubao et al. 2009, Lopes, Corbellini et al. 2009) In our study there was a significant drop in calcium concentrations for all treatment groups between days 0 and 6. After day 6 the extent of fluctuation between dissolution and precipitation depended on the strut porosity of the material. The materials with low strut porosity (23%) gave rise to the most notable fluctuations between days 6 and 14 which then subsided thereafter whereas the materials with a higher strut porosity (32, 46%) resulted in less extreme fluctuations which continued through to day 30. The changes in phosphorus ion concentrations follow the same pattern as observed for calcium. These observations confirm that there is a structural dependence in the precipitation-dissolution dynamics of HCA formation in SBF.

Let us first consider the dependence of precipitation on substrate structure. The presence of pores has been demonstrated as important for the precipitation of HCA.(Izquierdo-Barbaa 2005, Li, Shi et al. 2007) Previous investigators have argued the size of HCA crystals is related to the number of available nucleation sites; the fewer the number of nucleation sites, the larger the spherical crystals can grow.(Zhang, Chen et al. 2003) Therefore, the morphology of the starting material surface can contribute nucleation sites for HCA crystallisation, more specifically the surface area of the substrate and the presence of micropores or microcracks in the surface of a bioactive substrate which can provide sites for HCA nucleation.(Saint-Jean, Camire et al. 2005) It is proposed that as the superposition of the surface potentials inside micropores increases the ionic concentration and degree of super-saturation of Ca and P ions, the precipitation of HCA is more likely to occur first inside the pores.(Pereira MM 1994) According to the literature pores of approximately 3

microns, such as those in the SiCaP treatment groups, are favourable to implant bioactivity, since the pores contribute to the anchorage of HA nuclei preceding the layer growing. (de Souza, de Lima et al. 2011) In one previous study nucleation of HCA began firstly on the surfaces of recessed regions and pores, or along micro cracks pre-existing in the surface prior to exposure to SBF which is consistent with this theory and with our own observations for the beta-TCP treatment group on which HCA was only associated with cracks or fissures in the surface of the material and the SiCaP groups on which the greatest overall amount of HCA deposition was observed (through SEM analysis) on the material with the greatest amount of strut-porosity.(Weng, Liu et al. 1997) The dependence of HCA layer dissolution on substrate structure will follow the same principle: the fewer the number of size of pores and cracks in the surface of the material, the lower the probability for any local increases in calcium and phosphorus in the SBF, and the greater the probability for dissolution. This may explain the greater fluctuation in the ionic concentrations of these ions in the SBF for materials with a lower strut-porosity.

5.5 Conclusions

The propensity for the formation of either HA or OCP as a continuous, un-broken layer over the implant surface immediately after implantation into bone is in theory likely to be significant to the processes of osteointegration; the greater the surface area covered by this layer the better the opportunity for interdigitation with host bone. In practice this assumption is still under debate as the *in vivo* studies in support of the outcomes of the bioactivity test are often contradictory. In our study formation of HCA was noted on all four test materials. The rates of formation and quantities of HCA varied among different materials. Under the conditions of the test, the fastest rate of HCA growth was observed on SiCaP-32 and SiCaP-46 followed by SiCap-23 (Actifuse). The quantity of HCA formed on Vitoss surface was much lower than the other three test materials. These results indicate that the strut-porosity of a material substrate should be increased to maximise the potential for formation of a precursor to bone-like apatite after implantation in osseous defects and further confirms previous reports that beta-tricalcium phosphate is much less bioactive than silicate-substituted hydroxyapatite and thus less likely to facilitate successful osteointegration when implanted in bone.

Chapter Six: Effect of Microstructure and Delivery Presentation on Osteoinductivity of Calcium Phosphate Bone Graft Substitute Biomaterials

6.1 Introduction

A considerable number of scientific articles have been published describing the osteoinductivity of calcium phosphate (CaP) based bone graft substitutes since the mid 1990's (Chan, Coathup et al. , Yang, Yuan et al. 1996, Yang, Yuan et al. 1997, Yuan, Yang et al. 1998, Yuan, Zou et al. 1998, Yuan, Kurashina et al. 1999, Yuan, Li et al. 2000, Eid, Zelicof et al. 2001, Yuan, De Bruijn et al. 2001a, Yuan, Yang et al. 2001, Gosain, Song et al. 2002, Barrere, van der Valk et al. 2003, Daculsi 2004, Fujibayashi, Neo et al. 2004, Habibovic, Yuan et al. 2005, Le Nihouannen, Daculsi et al. 2005, Habibovic, Sees et al. 2006, Habibovic, Yuan et al. 2006, Kondo, Ogose et al. 2006, Yuan, van Blitterswijk et al. 2006a, Yuan, van Blitterswijk et al. 2006b, Bodde, Cammaert et al. 2007, Li, Habibovic et al. 2007, Fellah, Gauthier et al. 2008, Habibovic, Gbureck et al. 2008, Habibovic, Kruyt et al. 2008, Cheng, Ye et al. 2009, van Gaalen 2009, Coathup, Samizadeh et al. 2011, Coathup, Hing et al. 2012). As a result of this extensive research a number of investigators have put forward hypotheses for the mechanisms for calcium phosphate derived osteoinductivity. These include Ripamonti who suggested that the concavities in the surfaces of such materials could lead to the condensation of elevated levels of bone morphogenetic proteins from the circulation and thus provide sites where there was a greater likelihood for stem cell differentiation down the osteoblastic lineage (Ripamonti 1996). After observing a difference in osteoinductive properties of calcium phosphates apparently according to their solubility, Habibovic later suggested that Osteoinductivity could be attributable to the formation of an apatite-like layer on the surface of substrates following a process of calcium and phosphorus dissolution and re-precipitation (Habibovic, van der Valk et al. 2004, Habibovic, Yuan et al. 2005). At the same time Le Nihouannen et al made a link between dissolution of calcium phosphates and the formation of particulate debris and subsequent bone formation in muscle pouches formed in sheep (Le Nihouannen, Daculsi et al. 2005). This group suggested that the local release of inflammatory cytokines as a result of macrophage activation might then stimulate circulating stem cells to differentiate into osteoblastic

cells producing bone tissue. This pathway, they argued, was corroborated by the absence of chondrocytes in these sites of new intramembranous bone formation. A useful summary of all proposed mechanisms for ectopic bone formation by calcium phosphate based ceramics is provided by Barrere et al. (Barrere, van der Valk et al. 2003). This group proposed that osteoinduction by porous calcium phosphate ceramics can be attributed to either (1) the incorporation and concentration of bone morphogenetic proteins (BMPs) by CaP crystals; (2) a low oxygen tension in the central region of the implant that triggers the pericytes of microvessels to differentiate into osteoblasts; (3) a rough surface produced by the 3D microstructure, which causes the asymmetrical division of mesenchymal cells that produce osteoblasts; (4) the surface charge of the substrate, which triggers cell differentiation; (5) the bone-like apatite layer formed in vivo that is recognized by mesenchymal cells; and/or (6) the local high level of free Ca^{2+} provided by the CaP material, which triggers cell differentiation and bone formation. However, despite what is known about calcium phosphate derived osteoinductivity there remains a great deal that is unknown. The primary objective of this chapter is to dig deeper into these mechanisms by comparing the results of our own osteoinductivity studies with those reported previously in the literature.

When used clinically calcium phosphate based bone graft substitutes are typically delivered in a carrier which provides the device the desired mouldability, cohesivity, and adhesivity to suit application by surgeons to irregularly shaped bone defects deep inside the human body. A recent study by Barbieri et al. investigated the influence of different polymeric gels on the ectopic bone forming ability of an osteoinductive biphasic calcium phosphate ceramic (Barbieri, Yuan et al.). This study concluded that the chemistry and dissolvability of aqueous based carriers can affect the osteoinductivity of biphasic calcium phosphates and that aqueous Poloxamer did not significantly reduce the amount of bone formed in muscle defects compared to a control biphasic calcium phosphate implanted without a carrier. A further study by the same group, however, proposes that the prolonged storage of tri-calcium phosphate (TCP) or biphasic (BCP) CaP ceramics in such aqueous carriers will eventually lead to their hydrolysis over time, which could ultimately be detrimental to the osteoinductivity of the TCP or BCP through changes to the biomaterial. As a secondary objective for this chapter we aim to investigate the long-term chemical stability of silicate-substituted calcium phosphate (SiCaP) stored in an aqueous carrier and to determine the effects of this carrier on the osteoinductivity of SiCaP when implanted *in vivo* in ectopic defects.

6.2 Methods

6.2.1 Materials

Phase pure silicate-substituted (0.8 wt% Si) hydroxyapatite (SiCaP, $Ca_{10}(PO_4)_6(OH)_2$) consisting of porous (80±2.5% total porosity), irregularly shaped microgranules (1–2 mm) with a strut-porosity of 23±2.5% (SiCaP-23), 32.0±2.5% (SiCaP-32), and 46±2.5% (SiCaP-46) was included in the study. The microgranules were tested alone (SiCaP-23G, SiCaP-32G, SiCaP-46G) and in combination with an aqueous (aq) Poloxamer carrier (SiCaP-23P, SiCaP-32P, SiCaP-46P).

6.2.2 Osteoinductivity

6.2.2.A Model design

Seventy two implants of each preparation were investigated, each being inserted into distinct regions along the left and right paraspinalis muscles of female commercially crossbred sheep weighing between 60 and 80 kg and aged between 2 and 5 years. The positions of each test material along the spine were rotated and in all, 6 implants per group were investigated at each time-point. All procedures were carried out by a qualified veterinary surgeon following local ethics approval and in compliance with UK's Home Office regulations (Animal Scientific Procedures Act 1986). This author attended all procedures.

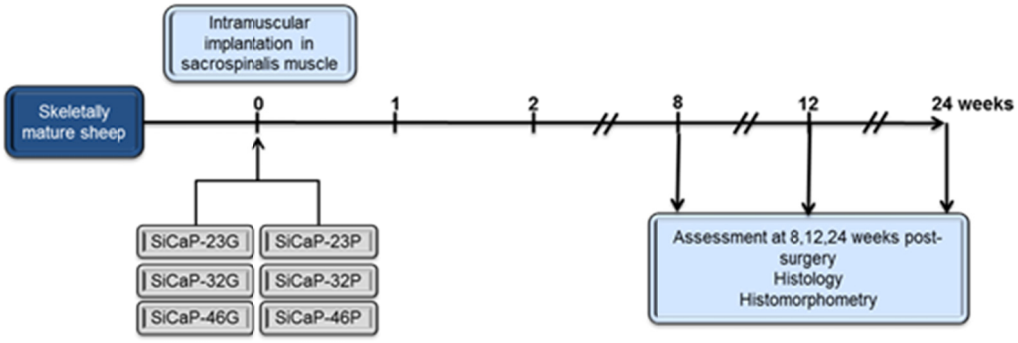

Figure 6-1 Model design

6.2.2.B **Surgical procedure**

Animals were placed in dorsal recumbency and longitudinal incisions measuring approximately 3 cm were made at the level of L2/L3, roughly 3 cm lateral to the spinal column. The fascia was split bilaterally to give access to intramuscular sites either side of the spine. The muscle was split by blunt dissection and the product inserted into the pouch (Figure 6-3). The granular groups (SiCaP-23G, SiCaP-32G, SiCaP-46G) were mixed with whole venous blood in a ratio of 6ml blood to 8ml granules. The mixture was left to clot for 15-20minutes and the resulting congealed mass was implanted (Figure 6-2).

Figure 6-2 Granules mixed with clotted blood

The wound was then carefully closed in layers. The procedure was then repeated and further incisions made resulting in a total of eight implants being inserted in each animal. Following surgery, animals were administered with routine prophylactic antibiotics and analgesia and were allowed to mobilise as tolerated. Antibiotic and analgesic prophylaxis was administered daily with subcutaneous injections of Baytril (Enrofloxacin 5 mg/kg; Bayer AG Leverkusen) and Finadyne (Flunixin Meglumine 2 mg/45 kg; Schering-Plough Ltd) for 3 days post-surgery. Animals were kept in individual pens for 1 week post operatively before being group housed. Implants remained in vivo for 8, 12 or 24 weeks.

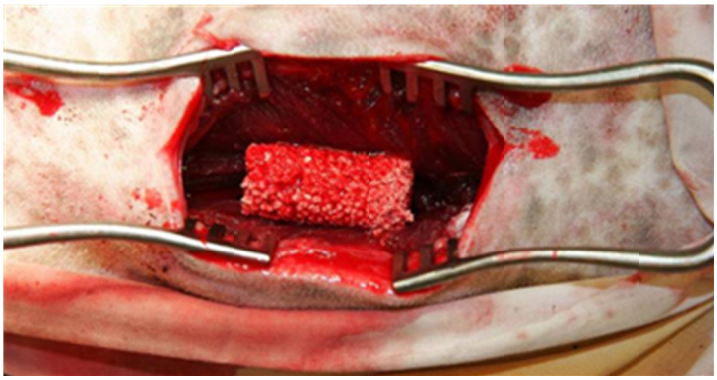

Figure 6-3 Implant site

6.2.2.C **Histological preparation and evaluation**

Implants remained *in vivo* for 8, 12 and 24 weeks and were then retrieved with the surrounding muscle. The samples were fixed and preserved using 4% paraformaldehyde for 3 days and were then processed for non-decalcified histology. After dehydration in a graded alcohol series and defatting using chloroform solution the samples were embedded in polyhydroxy-aromatic acrylic resin (LR White™ from The London Resin Company, Reading, United Kingdom). The specimens were cut longitudinally through the cranial/caudal plane and thin sections (~60 µm) were prepared using an EXAKT grinding system (EXAKT Corp, Norderstedt, Germany). Following polishing, sections were subsequently stained with Toluidine Blue (stains soft tissue) and Paragon (stains bone). The sections were examined histologically using light microscopy and examined under an objective magnification factor of five (Axiovision 4.5; Carl Zeiss, Jena, Germany).

6.2.2.D **Histomorphometry**

Bone formation within the bone graft substitute material was measured by selection of seven random regions of interest along the length of the implant. A line intercept method was employed to quantify bone formation and implant within each histological image. A mask of interconnecting lines measuring 10 × 12 mm was placed over each image and the type of material (mineralised bone, soft tissue or implant) at the intersection of each line was determined (total 225 intersect points per image). Bone was quantified only in pores > 50 µm. The percentage of bone was based on the overall area of the graft site. The percentage of bone-implant contact was also determined at the points where lines intersected with the SiCaP biomaterial surface.

6.2.3 Static Dissolution Testing of SiCaP

6.2.3.A **Sample storage**

Testing of SiCaP-23G and SiCaP-32G dissolution was performed in accordance with ISO 10993-14. Biological evaluation of medical devices – Part 14: Identification and quantification of degradation products from ceramics. Nominally five gram samples were stored in TRIS buffer at pH 7.4, in 500ml polypropylene bottles. Samples were placed in an oven set to 37±1^{o}C (Genlab, UK) for 120 hours.

6.2.3.B **Inductively coupled plasma optical emission spectrometry (ICP-OES)**

The ionic concentrations of Silicon, Calcium, and Phosphorus in the test solutions were measured with inductively coupled plasma optical emission spectrometry (ICP-OES) using an IRIS Advantage Radial Plasma instrument installed with TEVA control software application (Thermo Scientific, USA). The instrument was calibrated using standard solutions made from traceable single-element stocks. Each unknown sample was measured against the calibration to give a concentration of the elements of interest in the sample. An instrument blank (identical to the calibration blank), and an instrument QC was run with and before each batch of samples. In the event any sample failed (i.e. the blank was outside ± the limit of detection or the QC was outside of ± 10% of the target value), the instrument was re-standardised against the top calibration standard and the calibration blank. Uncertainties for each element were estimated at 2% of the reported value.

6.2.4 Long –term Stability of SiCaP with an aqueous carrier

6.2.4.A **Accelerated aging**

Samples of SiCaP-32P were irradiated using Gamma sterilisation and stored at elevated temperature for the equivalent of up to 5 years aging at room temperature, including 0.5, 1, 1.5, 2, 3, and 5 year equivalent time-points. An accelerated aging temperature (T_{AA}) of 45 °C was selected, on the basis that the choice of T_{AA} should be 10 °C lower than the transition temperature (T_M) for any of the component materials and should not be above 60 °C, as recommended in the international standard for accelerated aging of medical devices. Previous studies have indicated that storing Poloxamer at above its melting temperature can increase the rate of degradation, however, when stored at 50°C (5°C below its melting temperature) or

below, degradation proceeds as under normal conditions (Erlandsson 2002, Gallet 2002, Gallet and Erlandsson 2002). A room temperature (T_{RT}) of 22 °C was selected as being representative of the typical storage temperature for commercial bone graft substitutes. An accelerated aging factor of 4.92 was calculated using the Arrhenius equation (Equation 24) and a Q^{10} equal to 2 which is a common and conservative means of calculating the accelerated aging factor, where:

$$AAF = Q_{10}\left[{(T_{AA} - T_{RT})}/{10}\right] \qquad \textbf{Equation 24}$$

6.2.4.B **X-ray diffraction spectroscopy (XRD)**

XRD was used to qualitatively determine crystallinity and identify the phases present in the samples of SiCaP-32P before and after aging. Powdered specimens were prepared in a pestle and mortar prior to analysis. Diffraction patterns were obtained using a Siemens D5000 X-Ray Diffractometer in flat plate geometry between 2θ values of 20 and 40 θ, using a step size of 0.02 θ and a step time of 2.5 seconds. The ICDD standards for HA, TCP and CaO (ICCD: 9-432, 9-348, 37-1497 respectively) were used for identification of any crystalline phases.

6.2.4.C **X-ray fluorescence (XRF) spectroscopy**

The calcium, phosphorus, and silicon contents of SiCaP-32P samples were determined before and after aging by quantification of a range of metal oxides using X-ray fluorescence (XRF) spectroscopy on a Philips PW1606 spectrometer. Analyses were performed in accordance with the international standard ISO EN 12677:2003 – Chemical analysis of refractory products by XRF – Fused casting method. The ionic molar Ca/(P+Si) Ratio was calculated to the 2nd decimal place from the measured percentage weight (wt%) of calcium oxide (CaO) and phosphorus pentoxide (P_2O_5). The wt% silicon substitution in the samples was calculated from the measured silicon dioxide (SiO_2) content.

6.2.4.D **Fourier transform infrared spectroscopy (FTIR)**

Fourier transform infrared spectroscopy (FTIR) of SiCaP-32P before and after aging was used to confirm the absence of impurity groups or moieties within ceramics that exhibit vibrational frequencies in the 4,000 to 650 wavenumber range. Typically, this technique can determine such chemical moieties at levels down to 0.5% m/m.

FTIR spectra were obtained on a Thermo Nicolet Nexus spectrometer, using an MTech Photoacoustic 3000 cell. A background spectrum was collected at the beginning of the analysis and this was applied to all of the subsequent spectra. Samples were purged for 30 minutes in argon to (as far as possible) remove water and carbon dioxide. Spectra were collected at 4 cm^{-1} resolution, and 100 scans collected.

6.2.4.E **Statistics**

All statistical tests were performed using Minitab software (v15, Minitab Inc., USA). Parametric testing was utilised for all comparisons of analytical results for SiCaP-23G and SiCaP-32P. A Ryan-Joiner test for normality was performed using a significance value of p=0.05. Where data was confirmed as normal an f-test was performed to test for differences in variance with a significance value of p=0.10. A student t-test was performed to test for differences in the means for each group with a significance value of p=0.05. The non-parametric Mann-Whitney U test was used for statistical analysis between histomorphometrical experimental data where p values < 0.05 were considered significant.

6.3 Results

6.3.1 Histological evaluation

Histological evaluation identified a number of phenomena which did not appear to be strongly associated with any particular formulation of SiCaP. Remnants of the SiCaP granules were evident in the explanted tissue samples in all treatment groups at all time points but the amount of graft appeared to decline from 8 to 24 weeks post-implantation. Upon removal the implanted granules were found to be filled with both fibrocytes and chondrocytes forming loosely formed fibrous connective tissues as well as osteocytes trapped in a matrix of mature bone, with evidence of continuing bone formation throughout the 24 week period. There was no histopathological evidence of adverse fibrous reactions and no fibrous encapsulation was observed for any treatments.

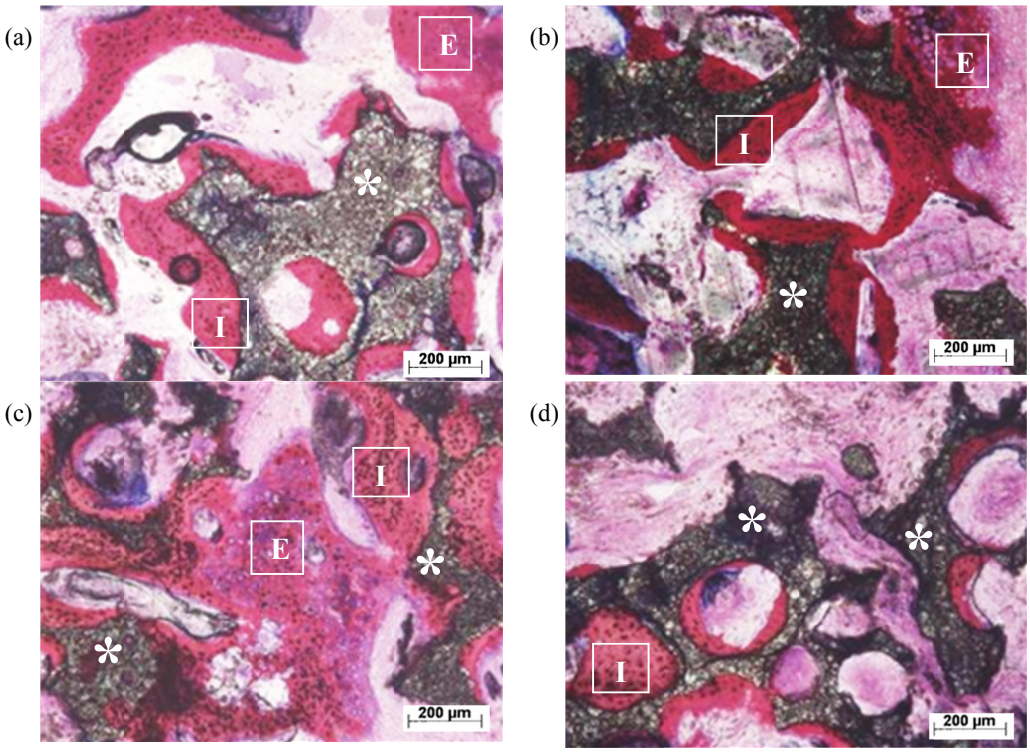

Figure 6-4 Micrographs of all groups at 12 weeks post-implantation
(a) SiCaP-32P (b) SiCaP-32G (c) SiCaP-46G (d) SiCaP-23G demonstrating close proximity of both endochondral [E] and intramembranous [I] bone formation in close contact with the graft surface (asterisks) and spanning between granules. Modified paragon histological stain.

Bone formation was most prevalent inside and between the implanted granules. This was in contrast to regions at the periphery of the implants - specifically, the interface between the granules and the overlying muscles - where less bone formation was observed. No substantial variation in bone morphology was noted between the four SiCaP treatment groups, although considerably less bone was observed in the SiCaP-23G materials compared to other groups at each of the 8, 12, and 24 week time-points. There appeared to be no preference for the location of bone formation in the central regions of the implanted granules, with islands of bone formation evenly distributed throughout.

In all treatment groups both intramembranous and endochondral bone formation were observed, often in very close proximity to one another (Figure 6-4a-c). Endochondral bone formation tended to occur in intra-granular spaces within the graft (Figure 6-5), whereas intramembranous bone formation tended to be closely associated with the surfaces of the graft (Figure 6-6a, Figure 6-8, Figure 6-7), although not exclusively so.

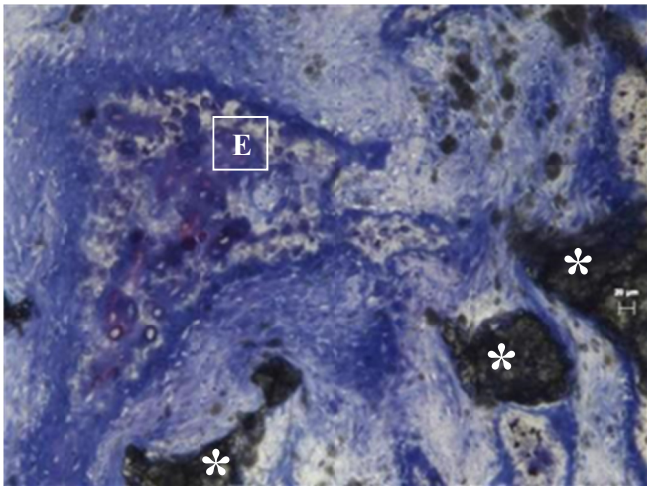

Figure 6-5 Endochondral bone [E] in the voids between granules of SiCaP-32G (asterisks) 12 weeks post-implantation. Toluidine blue histological stain.

The endochondral bone exhibited all the typical histological characteristics of bone formed via the endochondral ossification pathway. Zones of cartilage in reserve and undergoing proliferation as well as zones of hypertrophy and ossification were identifiable in the histology (Figure 6-6b). However, there were only sporadic signs of resorption in the endochondral regions of bone (Figure 6-6b) which is in contrast to the intramembranous bone where osteoclasts were much more active.

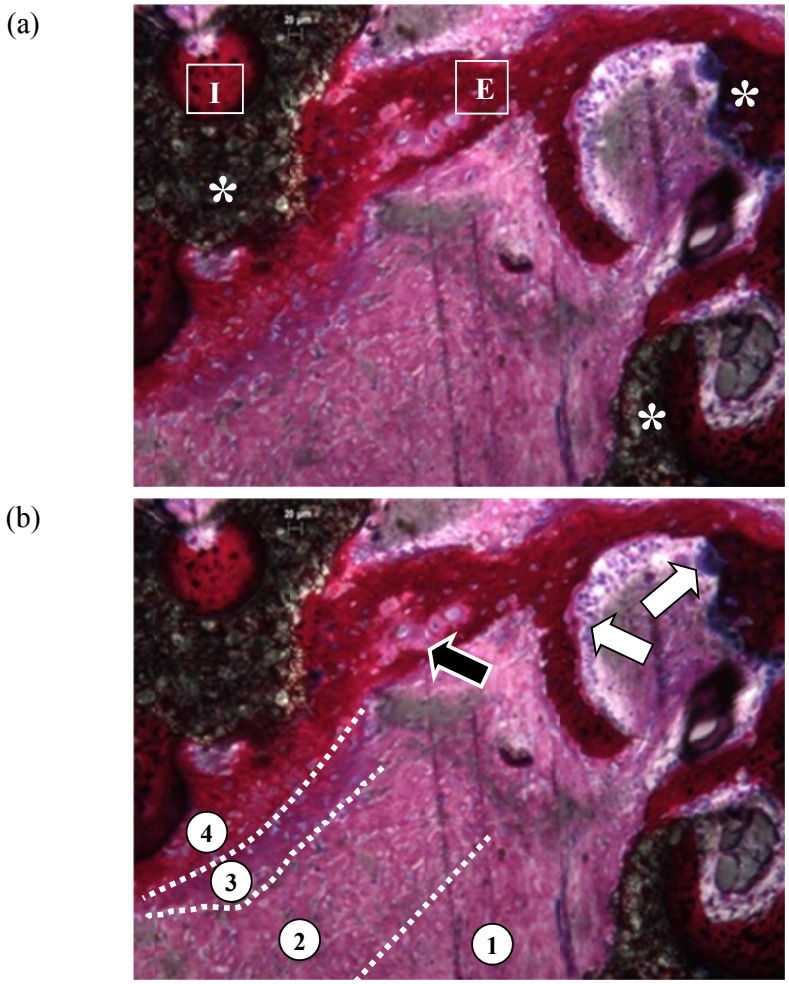

Figure 6-6 Endochondral bone histology

(a) Endochondral bone [E] in proximity to intramembranous bone [I] on SiCaP-32G (asterisks), (b) 1=Zone of reserve comprising fibrocartilage containing fibroblasts and quiescent chondrocytes, 2=Zone of hypertrophic chondrocytes, 3=Zone of calcifying chondrocytes, 4=Zone of ossified endochondral bone, white arrow=osteoblasts on surface of new bone, black arrow=voids characteristic of endochondral bone, hatched arrow=macrophage, likely to be an osteocyte. 12 weeks post-implantation. Modified paragon histological stain.

In the largest spaces between the granules the loose connective tissue surrounding regions of endochondral bone were characteristic of quiescent and proliferating chondrocytes which adopted a globular appearance as they grew in size. At regions closer to the front of ossification these cells became hypertrophic and spaces between them were evident, even at low magnification. This zone of hypertrophy took on a darker shade of pink in the histology as the dehydrated apoptised

chondrocytes began to calcify in regions closer to the centre of the forming bone. Eventually this boundary reached a deep, rich fuscia colour which indicated the zone of ossification and the presence of ossified tissue. This endochondral bone was clearly distinct from the intramembranous bone in the same defects due to the presence of circular voids formed as the chondrocytes became hypertrophic (Figure 6-6b). Endochondral bone formation is most typical at epiphyseal end plates or at sites of secondary fracture healing and thus the macroscopic morphology follows the necessary function of the preceding cartilaginous structure in these sites. The same was true in our studies in which the morphology of the endochondral bone matched the pre-existing spaces formed between the implanted granules into which fibrocartilagenous and cartilaginous tissues had infiltrated and colonised. The precise origin of these cartilaginous tissues was not evident using histological analysis as there were no signs of stromal cells at any of the 8, 12, or 24 week time-points.

Intramembranous bone formation exhibited all the expected traits for ossification via this pathway despite being formed in a non-bony site. The gradual layering down of new bone in a centripetal fashion on the surfaces of macropores was seen in all groups at all time-points (Figure 6-7a). Of interest was the observation that new bone formation took place in the smallest of the macropores, some measuring below 100microns (Figure 6-7b & Figure 6-7b). Layers of blue-staining cuboidal osteoblasts generated osteoid which was then mineralised to form pink-staining mature lamellar bone (Figure 6-7a-c). This new layer of mineralised tissue was usually found in intimate contact with the graft surface but also bridged between granules (Figure 6-7a & Figure 6-7c). Considerable numbers of osteocytes were located deep within the osteoid, evidently trapped in the mineralising tissues as the ossifying front increased in thickness layer by layer (Figure 6-7a-c). In sites of mature bone formation the development of Haversian-like systems in which neovessels penetrated through the osteoid matrix were also observed (Figure 6-7c). Osteoclasts were found located on the surfaces of the graft itself, indicating that some degree of cell-mediated resorption of the silicate-substituted calcium phosphate was taking place (Figure 6-7c).

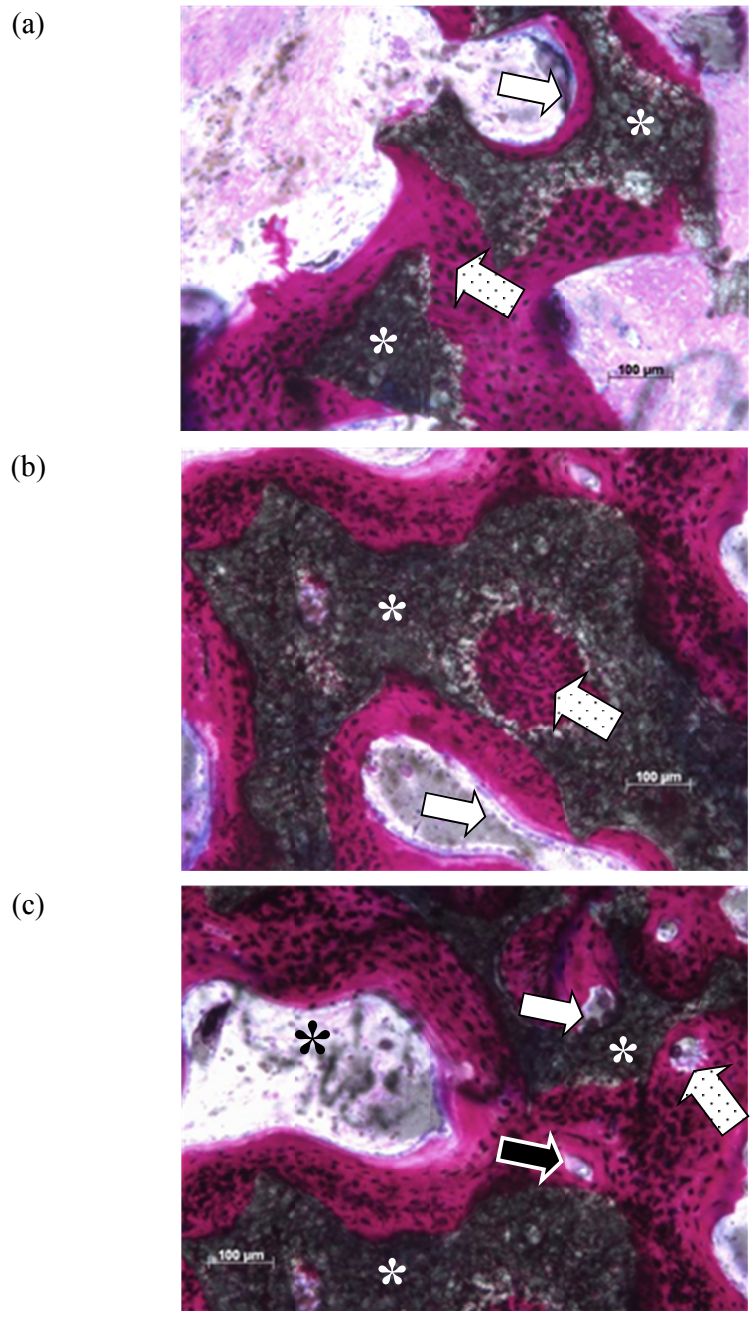

Figure 6-7 Histology micrographs of SiCaP-32

Micrographs of SiCaP-32G (white asterisks) showing typical intramembranous bone formation (a) Early-stage centripetal bone growth (white arrow) and bone bridging granules (hatched arrow) (b) Macropores filled with a high density of osteocytes (hatched arrow), layer of cuboidal osteoblasts (white arrow) (c) Haversian-like systems (black arrow), osteoclasts resorbing graft surface (white arrow), intramembranous bone formation in close proximity to particulate debris (black asterisk). All images 12 weeks post-implantation. Modified paragon histological stain.

In contrast to endochondral bone, the intramembranous bone tended to be more abundant in sites in which particles were present - presumably located there after pieces of the graft had dislodged from the material surface through dissolution or as a result of cell-mediated resorption. It's unclear whether this observation is significant or incidental since the intramembranous bone was typically associated with the graft surface which is where most particles would be expected to accumulate. In higher magnification micrographs it was possible to visualise striations formed from collagen fibres aligned perpendicular to the material surface in sites of new intramembranous bone formation. Osteoblasts at the front of ossification were clearly attached to these fibres and were subsequently being aligned in the direction of the collagen. Of note was that the collagen fibres tended to terminate at pockets of giant cells which had phagocytised particles of graft.

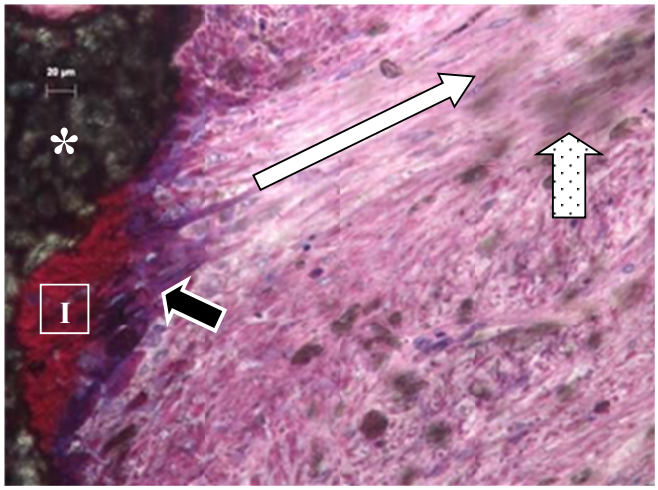

Figure 6-8 Histology micrographs of intramembranous bone formation
Intramembranous bone [I] formation on SiCaP-46G (asterisk). The geometry of the mineralising osteoblasts (black arrow) aligns with collagen fibres (white arrow). Also note collagen fibres terminate at a cluster of giant cells containing engulfed particles. 12 weeks post-implantation. Modified paragon histological stain.

High power micrographs revealed the walls of the macropores to be constructed of a mixture of spherical and acicular particles which were randomly stacked together to form a complex microstructure. A number of particles appeared to have a roughened or fenestrated surface texture. There was no trend to the location of these textured particles with respect to the walls of the macropores. The spaces formed between the particles, the micropores, were continuous with the material surface and were filled with tissues. These tissues stained in a similar manner to bone which was of

particular note in the SiCaP-23G treatment group since there was often very little, if any, bone within the macropores compared to materials in the other treatment groups (Figure 6-9).

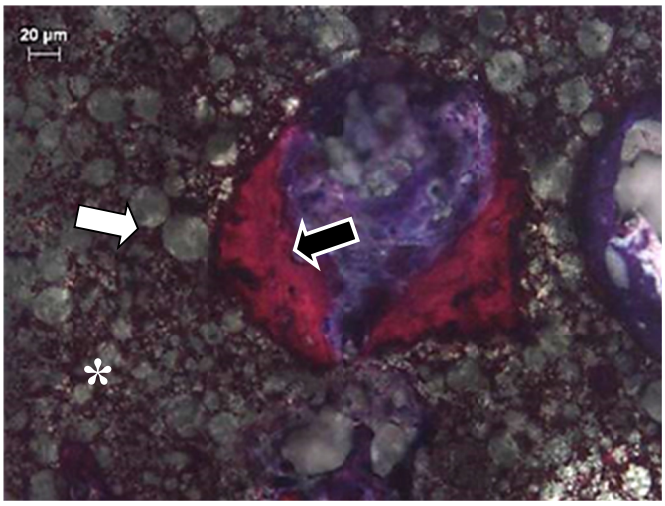

Figure 6-9 Histology of bone tissue inside microporosity
Bone tissue (white arrow) within the strut-porosity of SiCaP-23G (white asterisk). Bone tissue on the surface of the macro-pores. 12 weeks post-implantation. Modified paragon histological stain.

The intimate association between graft surface and new bone, in addition to the presence of mineralized tissue within the strut porosity was confirmed using back scattered electron microscopy (SEM) (Figure 6-10). SEM analysis revealed the extent of the number of osteocyte lacunae which appeared as dark voids in the layers of grey coloured mineralised bone tissue (Figure 6-10a-c). Some of these lacunae appeared to be located within the strut porosity (Figure 6-10b), suggesting that osteoblasts had migrated into the spaces in the walls of the macropores before differentiating into osteocytes. The layered appearance of mineralised osteoid which is so characteristic of intramembranous bone formation could clearly be identified from the SEM micrographs (Figure 6-10b). SEM analysis also confirmed the presence of intramembranous and endochondral bone in the same defect (Figure 6-10c). Similarly to histological characterisation the intramembranous bone was typically in close contact with the graft whilst endochondral bone was typically observed in the large open voids formed between granules.

(a)

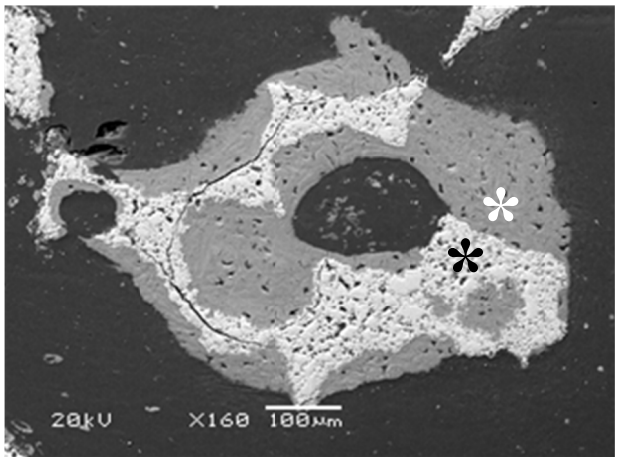

(b)

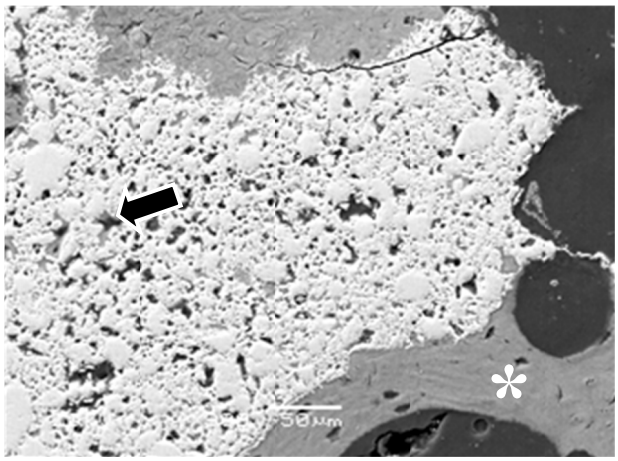

(c)

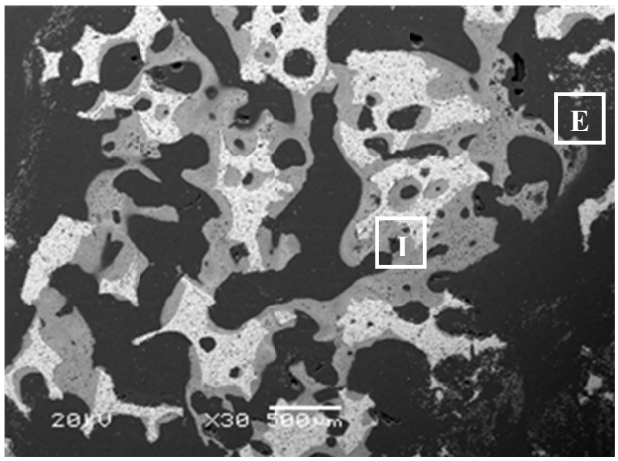

Figure 6-10 Back-scattered SEM of bone

Back-scattered scanning electron microscopy images demonstrating (a) intimate association of bone (white asterisk) and graft (black asterisk) (b) mineralised tissues within micropores (black arrow) and layered mineralised osteoid (white asterisk) (c) morphology of intramembranous [I] and endochondral [E] bone

By 24 weeks post-implantation there was a considerable amount of bone filling the defects in all treatments. The increase in bone volume corresponded with a decrease in graft volume as evidenced by the reduction in the macrostructure from an open and interconnected porous construct which spanned the defects to sporadic smaller-sized pieces of scaffold coated entirely by bone. The larger macropores in the graft and the larger spaces between granules assumed the histological characteristics of marrow spaces which were filled with large circular adipocyte cells (Figure 6-11).

(a)

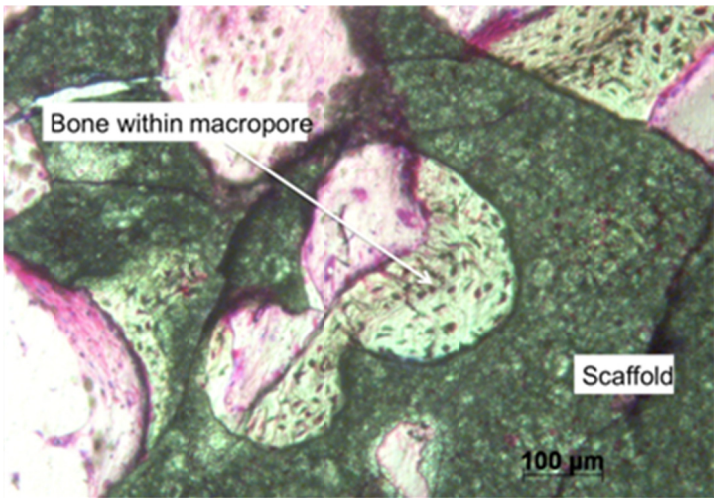

(b)

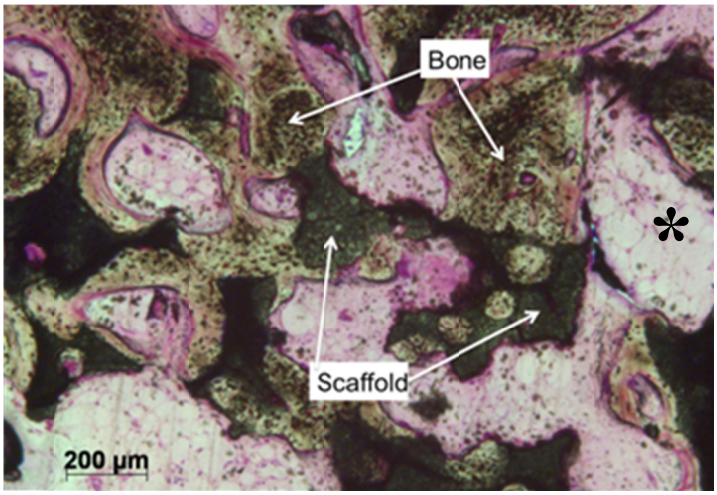

Figure 6-11 Histology micrographs of mature bone
(a) Mature intramembranous bone filling the macropores of the graft material (SiCaP-23G). (b) Bone filling the spaces between the granules of SiCaP-23G. Marrow space filled with adipocytes (asterisk). 24 weeks post-implantation. Modified paragon histological stain.

There was no substantial difference in the histological morphology between the four

treatment groups at 24 weeks. The new bone which was still being formed at 24 weeks (Figure 6-12b) comprised of long thin struts spanning the length of the defect which resembled the chancellors structure found in natural bone (Figure 6-12a). The extent of osteointegration was confirmed in higher resolution images in which it was almost impossible to differentiate between the pre-existing scaffold and the new bone (Figure 6-12b).

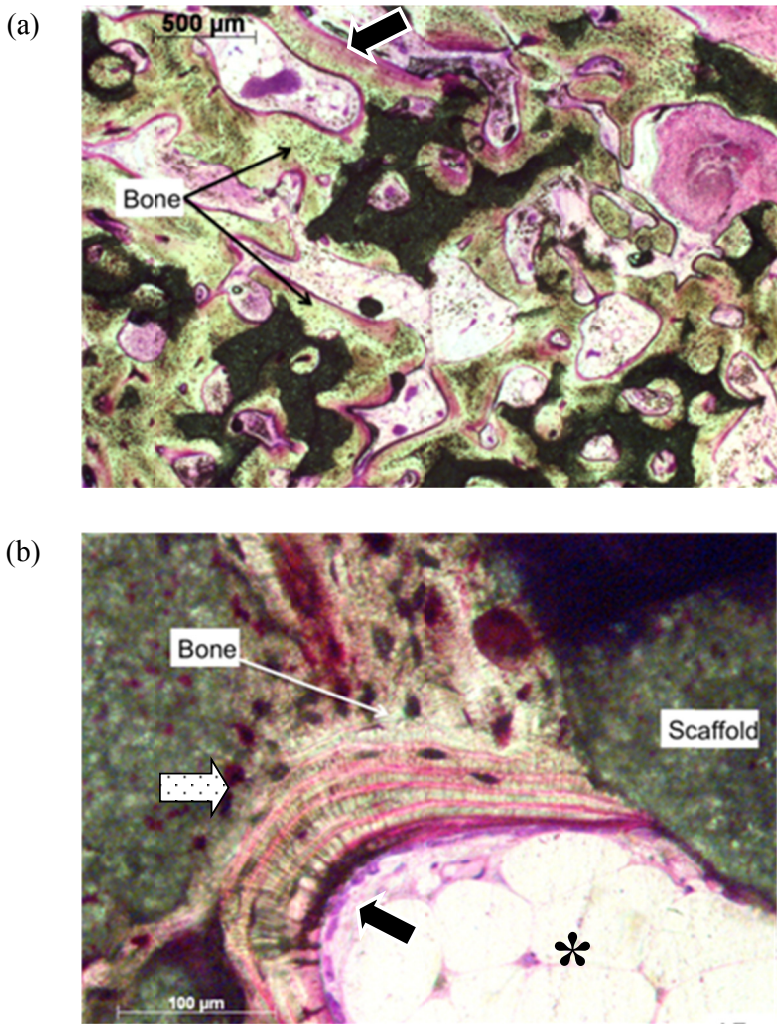

Figure 6-12 Histology micrographs of mature bone
(a) Mature intramembranous bone filling the macropores of the graft material (SiCaP-46G) and long thin struts of new bone (black arrow). (b) Marrow space (black asterisk) filling the void between two granules of SiCaP-46G. Zone of osteointegration (hatched arrow). Osteoblasts continuing to lay down new bone (black arrow). Modified paragon histological stain.

At all time-points throughout the study and for all treatments there was a consistent observation which merits some further discussion. Despite new bone formation

being found in most sites alongside graft degradation, some regions in the defects were completely devoid of bone and this appeared to correlate to areas in which the ceramic granules had undergone substantial graft dissolution and in which a large population of phagocytic cells had subsequently began to assemble (Figure 6-13a-cc). The approximate frequency for this observation was two to three granules from each defect site and there appeared to be no pattern to the distribution of these degraded granules with regard to location in peripheral or central regions of the defect. The infiltrated tissues in these granules were characterised by large numbers of macrophages containing graft particles. The engulfed particles appeared to be sub-micron in size and to have emanated from the material surface. The inflammatory response appeared to be predominantly mediated by degradation of the material surface and not caused by the presence of phagocytic cells. However, the presence of active osteoclast or macrophage like cells at the graft surface suggested that the degradation was at least in part cell-mediated (Figure 6-13a).

This characteristic degradation and associated mild inflammatory response was most apparent inside the macropores of the granules, where the highest numbers of macrophages were observed. It was not clear whether this was due to a greater amount of degradation occurring within the deeper macropores compared to external surfaces of the granules or whether this was attributed to there being less effective transport of particles away from these deeper pockets in the graft. Although not quantified with semi-quantitative histopathology there was an apparent trend for increasing graft degradation with increasing strut-porosity. There was no noticeable difference between the SiCaP-32G and SiCaP-32P treatment groups so the aqueous carrier did not appear to exacerbate the dissolution prior to implantation (Figure 6-13a & Figure 6-13b).

(a)

(b)

(c)

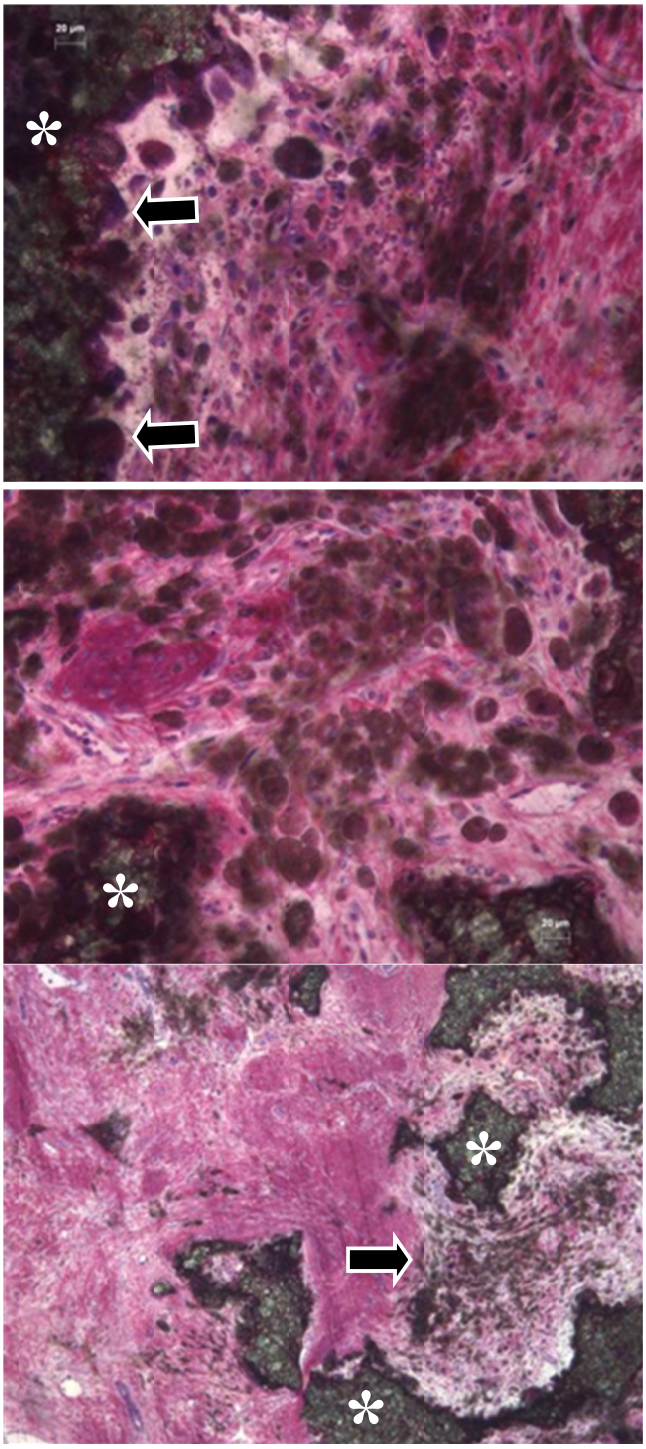

Figure 6-13 Examples of sample degradation

Examples of *in vivo* scaffold (asterisks) degradation (a) SiCaP-32P, black arrow indicates osteoclasts (b) SiCaP-32G (c) SiCaP-46G. Black arrow indicates macropores filled with degradants. Modified paragon histological stain.

6.3.2 Histomorphometry

The amount of bone (Bone Area) found in the defects increased from 8 to 24 weeks for all treatment groups, which reached statistical significance ($p<0.05$) for all treatment groups except for SiCaP-32G (Figure 6-14, Figure 6-15, Figure 6-16, Figure 6-17). Similarly the amount of bone attachment i.e. the proportion of the material surface covered with bone (Bone Contact) increased from 8 to 24 weeks for all treatment groups which reached statistical significance ($p<0.05$) for all groups excluding the SiCaP-32G group (Figure 6-14, Figure 6-15, Figure 6-16, Figure 6-17). Conversely the amount of graft (Graft Area) decreased from 8 to 24 weeks for all groups. This reached statistical significance ($p<0.05$) for all treatment groups (Figure 6-14, Figure 6-15, Figure 6-16, Figure 6-17).

At 8 weeks there was no statistical difference between the treatment groups with respect to the amount of bone detected in the defects (Figure 6-18). However, of note was the apparent presence of more bone in the SiCaP-32G group compared to all others. By 12 weeks post-implantation there was a trend for increasing bone formation with increasing strut-porosity although this only reached statistical significance ($p<0.05$) when comparing the treatment group with the lowest strut-porosity (SiCaP-23G) with the treatment group with the highest strut-porosity (SiCaP-46G). At 24 weeks post-implantation there was considerably more bone in the SiCaP-46G treatment groups compared with all other treatment groups but this did not reach statistical significance ($p>0.05$) due to the relatively high degree of variability from one animal to another within each treatment group. The amount of bone was approximately equal between groups SiCaP-23G and SiCaP-32P and lower for SiCaP-32G.

The amount of bone contact matched the patterns observed for bone area (Figure 6-19). At 8 weeks there was more bone in the SiCaP-32G treated defects compared to all other groups although this did not reach statistical significance ($p>0.05$). At 12 weeks there was a correlation between bone contact and the strut-porosity but statistical significance ($p<0.05$) was reached only when comparing data for SiCaP-23G and SiCaP-46G. At 24 weeks post-implantation there was approximately equivalent bone contact for SiCaP-32P and SiCaP-46G groups and less in the remaining groups although, again, this was not statistically significant ($p>0.05$).

There was no statistical difference ($p>0.05$) in graft area at any time-point when comparing between all groups (Figure 6-20). By trend there was less SiCaP-46G graft than the other three treatment groups at 8, 12, and 24 weeks.

(a)

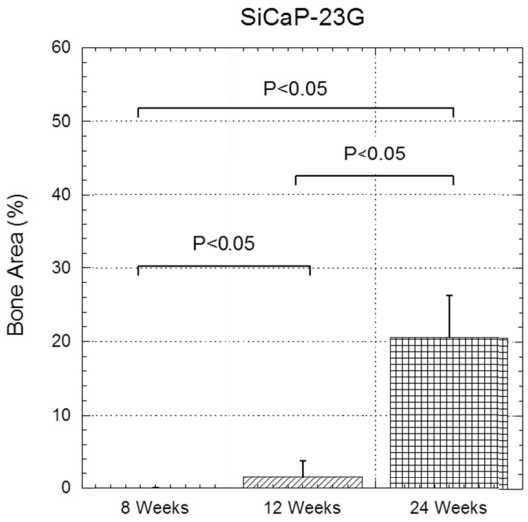

(b)

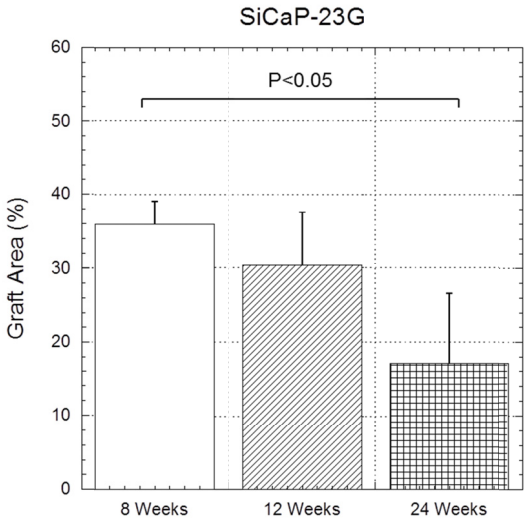

(c)

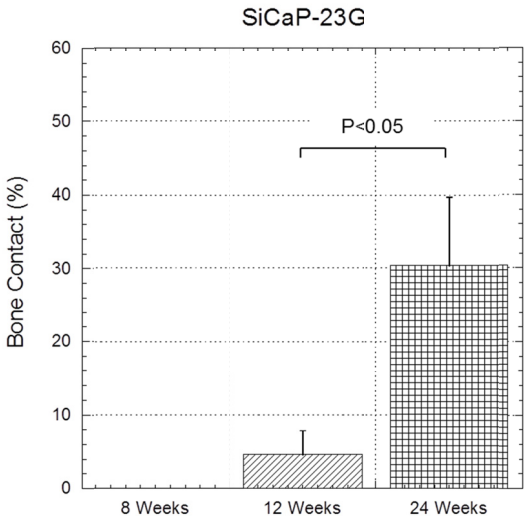

Figure 6-14 Summary data plot for SiCaP-23G
(a) Bone Area (b) Graft Area (c) Bone Contact

(a)

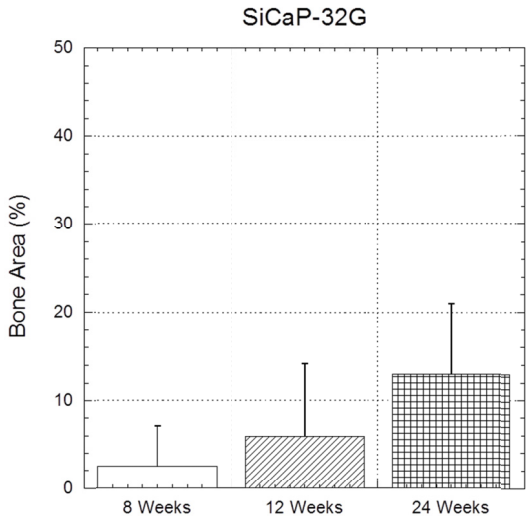

(b)

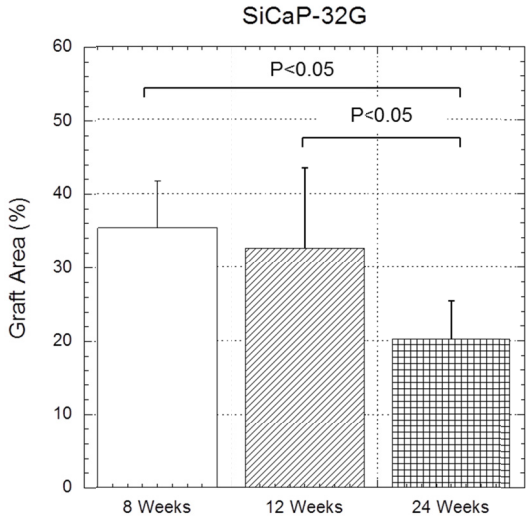

(c)

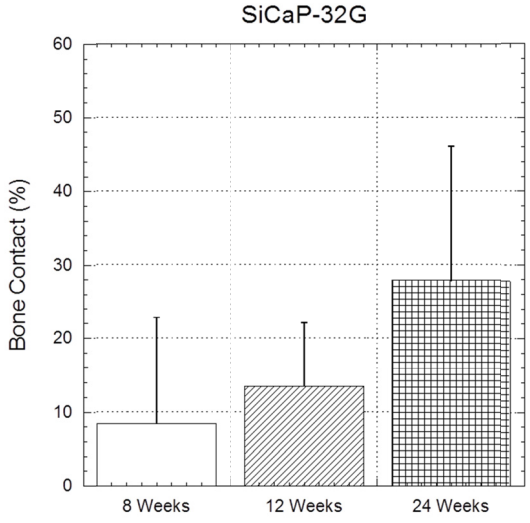

Figure 6-15 Summary data plot for SiCaP-32G
(a) Bone Area (b) Graft Area (c) Bone Contact

(a)

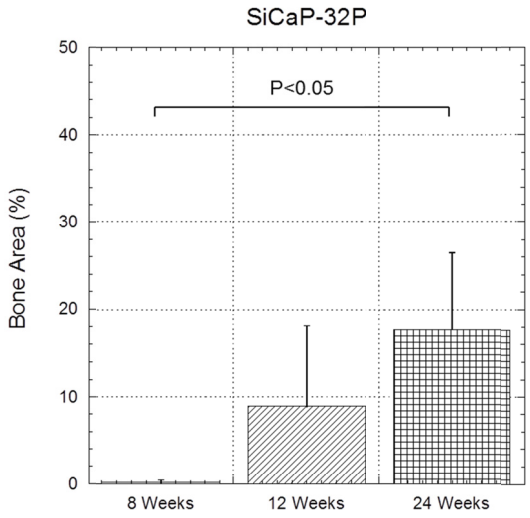

(b)

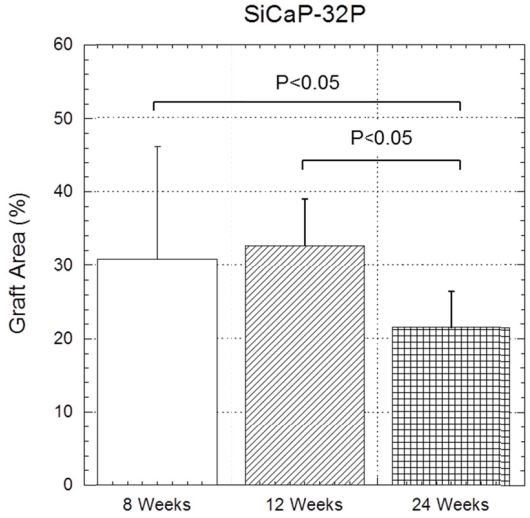

(c)

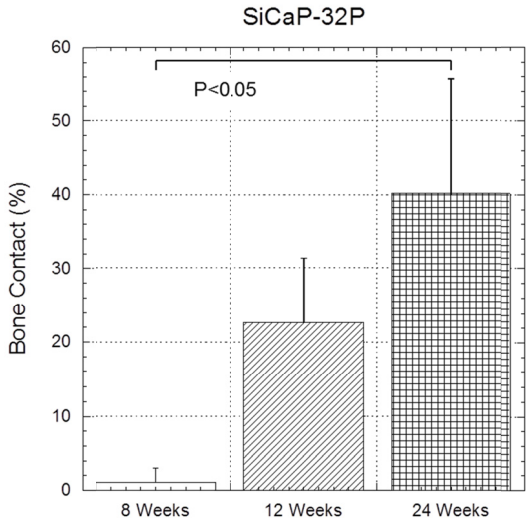

Figure 6-16 Summary data plot for SiCaP-32P
(a) Bone Area (b) Graft Area (c) Bone Contact

(a)

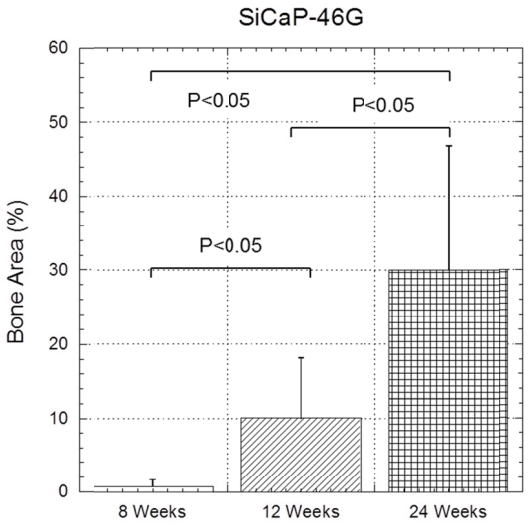

(b)

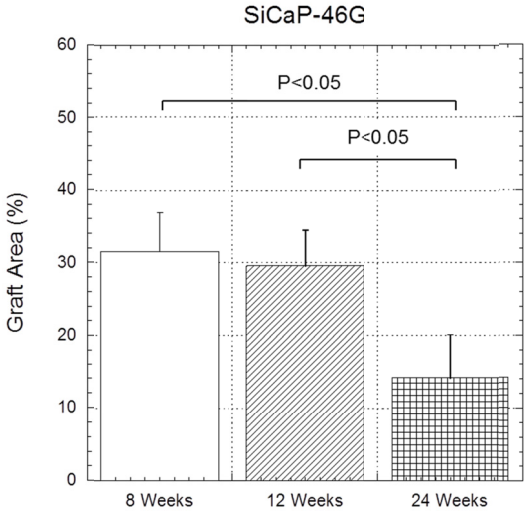

(c)

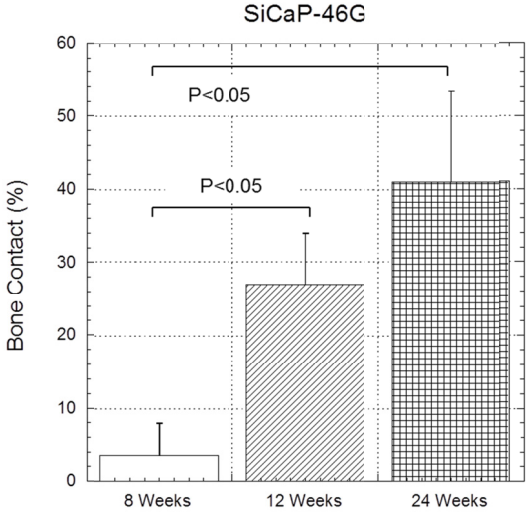

Figure 6-17 Summary data plot for SiCaP-46G
(a) Bone Area (b) Graft Area (c) Bone Contact

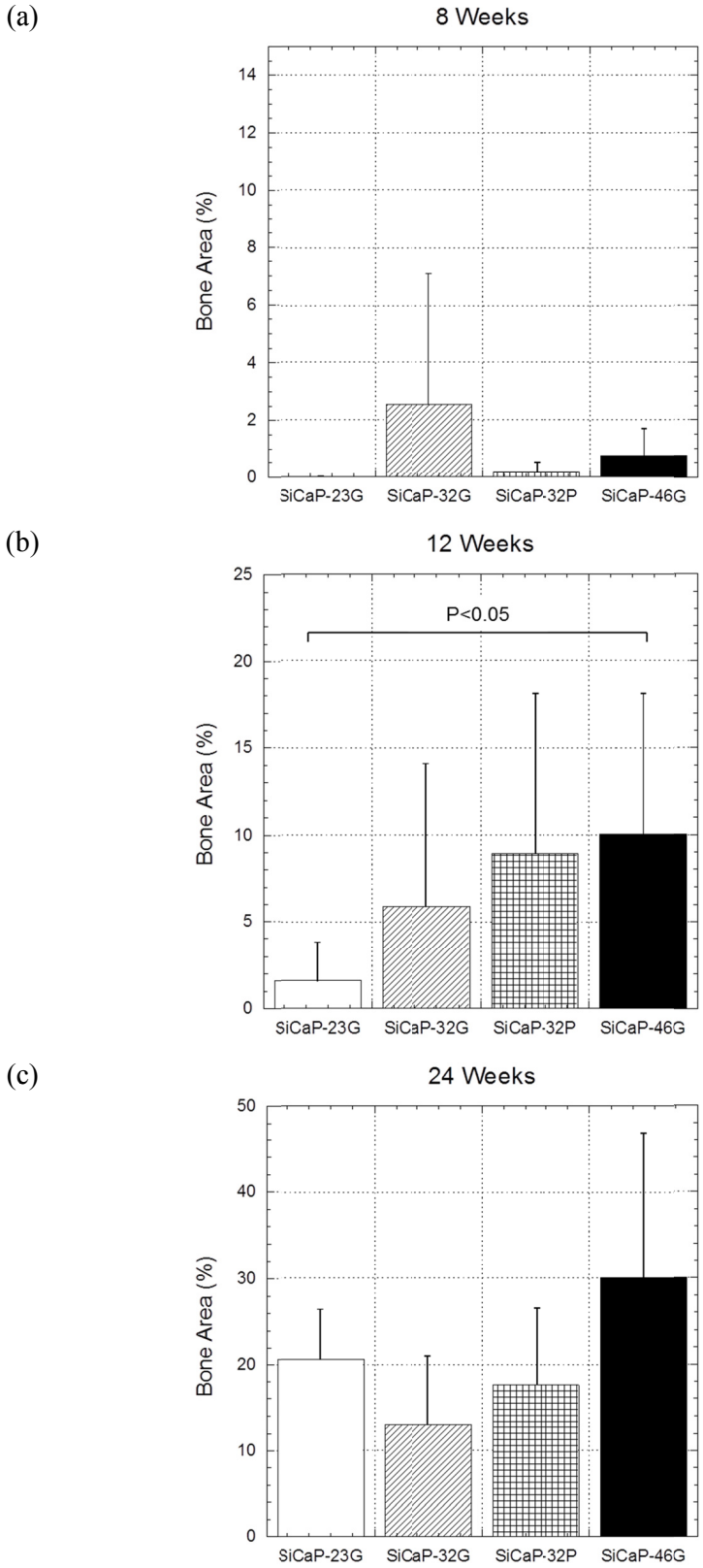

Figure 6-18 Summary data plot for Bone Area for all treatments at (a) 8 weeks (b) 12 weeks (c) 24 weeks

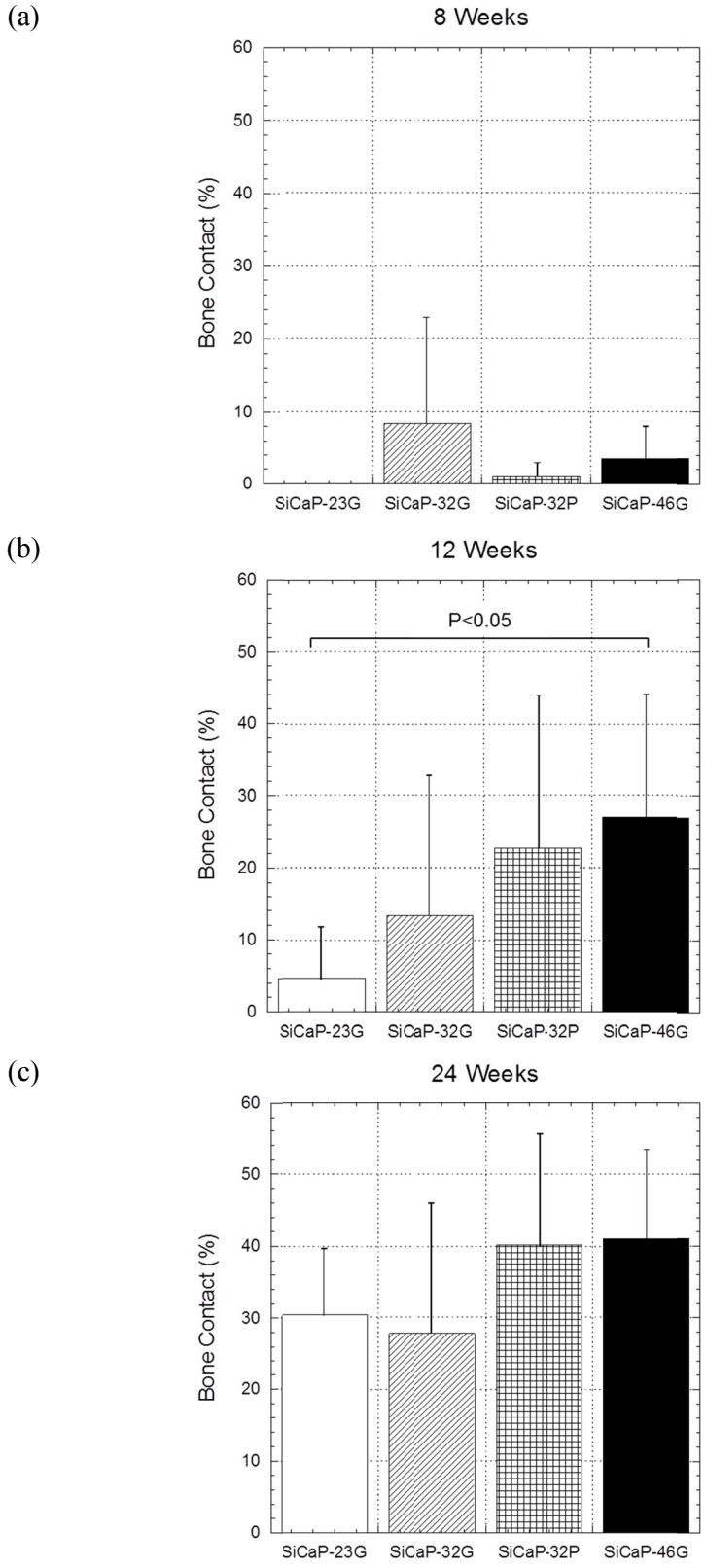

Figure 6-19 Summary data plot for Bone Contact for all treatments at (a) 8 weeks (b) 12 weeks (c) 24 weeks

(a)

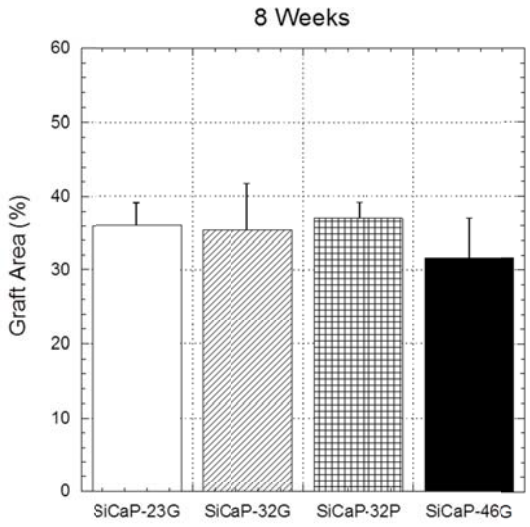

(b)

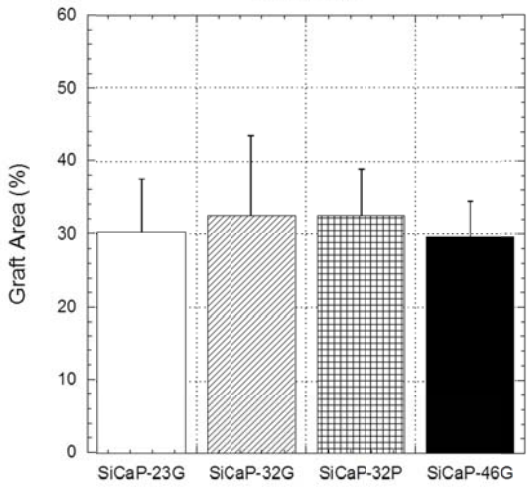

(c)

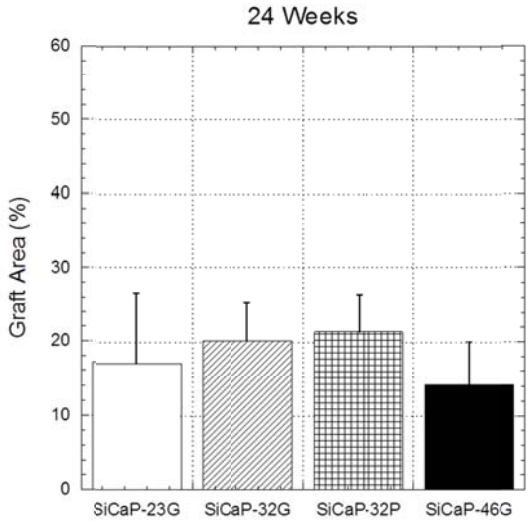

Figure 6-20 Summary data plot for Graft Area for all treatments at (a) 8 weeks (b) 12 weeks (c) 24 weeks

6.3.3 Inductively coupled plasma optical emission spectrometry (ICP-OES)

The levels of calcium (Ca), phosphorus (P), and silicon (Si) in the TRIS buffer soaking solution were measured with ICP-OES prior to and after the 120 hour dissolution period (Table 6-1). The amount of calcium, phosphorus, and silicon in the solution were significantly above the TRIS buffer baseline over the dissolution period.

Table 6-1 ICP-OES data for dissolution study

Test Group	Ca (mg/L)	P (mg/L)	Si (mg/L)
TRIS BUFFER	<0.05	<0.05	<0.1
SiCaP-23G	34.3 ± 2.5	1.2 ± 0.1	0.8 ± 0.1
SiCaP-32G	20.3 ± 3.8	2.2 ± 0.5	1.7 ± 0.3

6.3.4 X-ray Diffraction Spectroscopy (XRD)

Analysis of the crystalline composition all groups with X-Ray diffractometry demonstrated that all un-aged and aged materials were phase pure. All spectral peaks could be accounted for by the Hydroxyapatite powder diffraction file (9-432). The diffraction spectra showed narrow, high-resolution peaks and were consistent with highly crystalline material (Figure 6-21). There was no change in crystallinity over the aging period.

6.3.5 X-ray fluorescence (XRF) spectroscopy

X-Ray fluorescence spectroscopy showed all groups to have Ca/(P+Si) ratios in the expected range for phase pure Hydroxyapatite. There was no substantial change in Ca/(P+Si) ratio over the aging period (Figure 6-21). XRF also demonstrated that all samples were substituted with 0.80 ± 0.1 % silicon by weight. There was no substantial change in silicon content over the aging period (Figure 6-21).

6.3.6 Fourier transform infrared spectroscopy (FTIR)

All materials demonstrated the presence of the expected vibrational frequencies corresponding to hydroxyl (-OH) stretching and bending frequencies and the corresponding phosphate group (P=O) stretching frequencies. Additional peaks

were present at 891, 839 and 757 cm^{-1} as a result of the presence of SiO_4 groups in the structure (Figure 6-21). There was no change in spectra over the aging period.

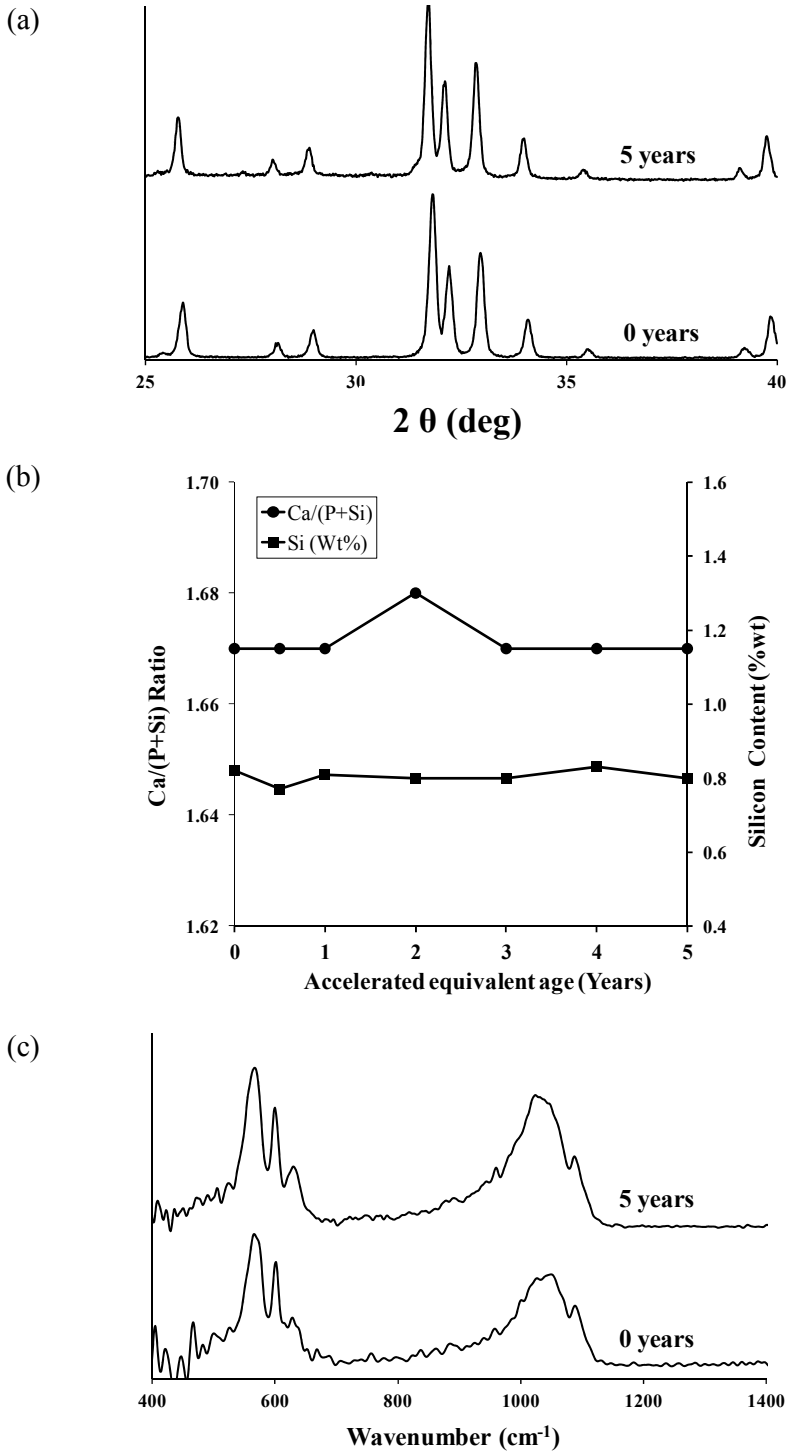

Figure 6-21 (a) XRD traces for aged and un-aged SiCaP-32P, (b) XRF data for aged and un-aged SiCaP-32P, (c) FTIR traces for aged and un-aged SiCaP-32P

6.4 Discussion

6.4.1 Factors in the Osteoinductivity of calcium phosphate biomaterials

The particular relevance of cellular colonisation of synthetic scaffolds in their osteogenic potential when implanted in ectopic sites is not a new concept. As far back as 1990 researchers found that by seeding calcium phosphates with osteoblast precursor cells, such as bone marrow derived stem cells, that a relatively inert macroporous structure could be engineered to be osteoinductive (Ohgushi, Okumura et al. 1990, Okumura, Ohgushi et al. 1991). This result was repeated later for more complex calcium phosphates with multi-scale hierarchical structures containing both microporosity and macroporosity (van Gaalen 2009). The same is true even for materials which have a surface chemistry even more remote to bone mineral than synthetic calcium phosphates - those such as titanium alloys, for example, which can be engineered to be osteoinductive when seeded with stem cells (Li, Habibovic et al. 2007). In Li et al.'s study the rate of incidence for bone formation in 55% porous titanium alloy substrates increased from 0% to 20% through the seeding of bone marrow derived stem cells onto the material substrate prior to implantation. The importance, therefore, of cellular attachment; differentiation; proliferation; and colonisation of synthetic scaffolds to their osteogenic potential in ectopic sites is irrefutable as demonstrated by the body of evidence available to-date. The extent of the role of structure and chemistry of synthetic scaffolds on their osteogenic potential in ectopic sites is also presented in scientific evidence. What still remains unclear is *how* these structural and chemical parameters give rise to a greater or lesser propensity of material substrates to encourage cell colonisation. In the following sub-sections we investigate the links between material parameters and osteogenic potential in ectopic bone formation.

6.4.1.A **Effect of strut-porosity on Osteoinductivity**

Micro-porosity, a term used interchangeably to describe strut-porosity, is the population of pores formed in the struts of macropores in ultramacroporous calcium phosphate biomaterials. The pores are formed between the particles which are fused together during sintering to form the walls of the macropores. These pores are typically open and interconnected with one another and the surface of the material, although not always so. The volume, equivalent circular diameter, interconnectivity, and geometry of these micropores can be manipulated through processing conditions during manufacture, the well-documented of which is the sintering temperature. The

amount of heat provided to a densifying green body during sintering will affect the amount of resultant porosity in the sintered product; the greater the amount of heat energy provided to the system during sintering, the greater amount of shrinkage and smaller the volume of voids (pores) found between the fusing particles. Yang et al. began investigating the impact of the amount of micro-porosity (manipulated through sintering) on the osteoinductivity of calcium phosphate ceramics in the mid 1990's (Yang, Yuan et al. 1996, Yang, Yuan et al. 1997). This group's observations in their initial research were of intramembranous bone formation in very close contact with the material surface after implantation in the dorsal muscle of dogs and under the dermal tissues of pigs. At fifteen days post-implantation they observed granulation-type fibroconnective tissue containing fibroblasts, macrophages, and newly formed vessels in the defects. After thirty days the fibroconnective tissue was well-organised parallel to the surface of the implanted material and polymorphic cell aggregates as well as multinucleated giant cells were observed. By forty five days the cell aggregation was more obvious and osteoblastic cell differentiation occurred directly within the polymorphic mesenchymal cell clusters which were evident at the pore surfaces. Woven bone was present by day sixty. The observations made by Yang et al. mirror our own study in which woven bone was found in direct contact with the implanted graft materials approximately sixty days post-implantation (Figure 6-18 & Figure 6-19).

Yang et al. also reported that at ninety and one hundred and twenty days post-implantation there were signs of osteoclasts and the development of trabeculated, remodelled bone. This observation is also corroborated by our own data as we also observed osteoclast-like cells on the surface of the graft (Figure 6-13) and also found evidence of cell-mediated resorption (Figure 6-7) as well as the development of a mature, trabeculated bony structure after nearly six months implantation (Figure 6-11 & Figure 6-12). Yang et al. proposed that (micro-cellular) environmental mechanisms for osteoinductivity are facilitated by: vessel ingrowth as a result of large, well-interconnected macropores; cellular adsorption and differentiation of cells as a result of the microporosity; crystallisation of apatite on the material surface; and increased localised calcium concentrations. Each of these mechanisms appears to be plausible based on our own observations in our present study but further interpretation of our own result is required to determine which mechanism is most influential.

The same group later published a study in which hydroxyapatite with and without microporosity, in addition to microporous alpha tricalcium phosphate, beta

tricalcium phosphate, biphasic calcium phosphate (HA/TCP), and titanium dioxide materials were implanted into the dorsal muscles of dogs (Yuan, Yang et al. 1998). The hydroxyapatite containing microporosity was sintered at 1100^{o}C or 1200^{o}C and thus two HA groups containing different levels of microporosity were implanted in total. In this important study the researchers found that there was no bone formation in any of the HA implants in which there was no microporosity whereas bone was observed in HA constructs with microporosity. The amount and quality of bone seemed to improve with increasing porosity i.e. more mature bone was found at earlier time-points in materials with greater levels of microporosity (those sintered at 1100^{o}C rather than 1200^{o}C). Yuan et al.'s study was the first to characterise and report the impact of amount of microporosity as a specific pore population on the osteoinductivity of calcium phosphates. The same group went on to publish a number of articles exploring the role of micro- and macro- porosity in ectopic bone formation (Yuan, Kurashina et al. 1999, Yuan, De Bruijn et al. 2001a, Yuan, de Bruijn et al. 2001b, Yuan, Yang et al. 2001, Habibovic, Yuan et al. 2005, Habibovic, Sees et al. 2006, Habibovic, Yuan et al. 2006, Yuan, van Blitterswijk et al. 2006a, Habibovic, Gbureck et al. 2008, Habibovic, Kruyt et al. 2008). Their continuing research, although confounded through the inclusion of a variety of calcium phosphate phases including alpha tricalcium phosphate; beta-tricalcium phosphate; hydroxyapatite; biphasic calcium phosphate amongst others, demonstrated a clear link between microporosity and the propensity of calcium phosphate scaffolds to form bone in non-bony defect sites. The data from their research closely matches the outcomes for our own study in which we observed a trend of increasing bone formation with increasing strut-porosity that reached statistical significance ($p<0.05$) at 12 weeks when comparing materials with 23% microporosity with materials with 46% microporosity (Figure 6-18). When plotting the Bone Area for each treatment against time on a scatter plot a pattern for more bone at earlier time-points in more microporous materials became apparent (Figure 6-22).

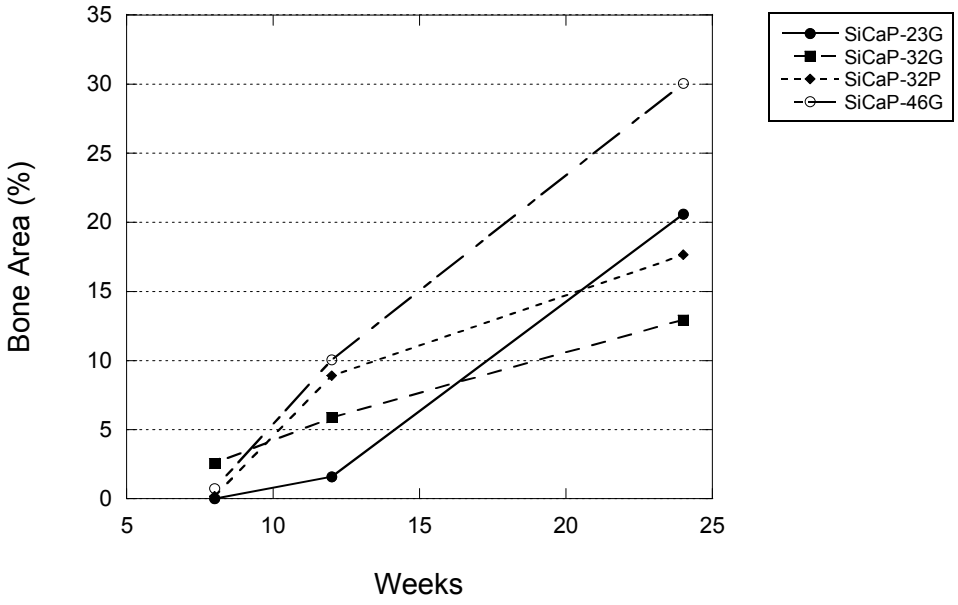

Figure 6-22 Summary of increase in Bone Area over time for each treatment group

Yuan et al. characterised osteoinductivity as a process in which osteogenic precursor cells became attached to the pore surface, aggregated, proliferated, differentiated, produced bone matrix, and ossified. Their team observed that bone formation started on the pore surface and proceeded to the pore centre in a centripetal fashion, much the same as might be expected in an orthotopic defect (Campion, Chander et al. 2011). We observed the same close association between the surface of the material and the integrating bone tissue (Figure 6-7, Figure 6-8, Figure 6-11, Figure 6-12). We also observed the same centripetal bone formation which started on the surface of macropores and grew layer by layer towards the centre of the pore (Figure 6-7). Perhaps uniquely, we also found bone cells attaching to the surface and infiltrating the graft itself (Figure 6-9 & Figure 6-10). This may go some way to explaining why we observed an apparent lag in the volume of bone forming in materials with less microporosity in these ectopic sites (Figure 6-22). This lag is even more apparent when examining the proportion of the material surface covered by bone (Figure 6-23).

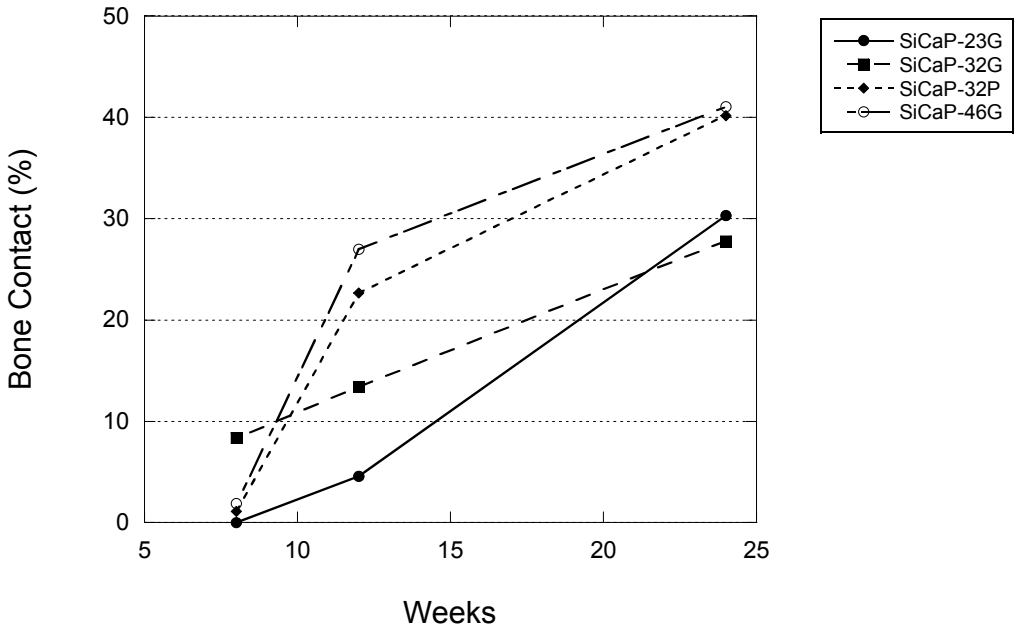

Figure 6-23 Summary of increase in Bone Contact over time for each treatment group

In our study there appeared to be a substantial improvement in the amount of bone-surface contact through the inclusion of more microporosity in the material substrate. It seems logical that providing a three-dimensional network of surface connecting pores - which are preferentially colonised by circulating osteoblastic precursor cells - would lead to a greater propensity for the material to form intramembranous bone on its surface. To further expand on this point – this may be preferential for more than just the obvious reason that more cell attachment leads to greater differentiation of precursor cells into osteoblasts. The cells which colonised the micro-pores in our study appeared to have the morphology of osteocytes, in that they were multi-dendritic and were in many cases connected to one another through these cellular extensions (Figure 6-12). Osteocytes have been well-characterised as the predominant bone cell phenotype responsible for modulating bone formation and remodelling through mechanotransduction, since an interconnected three-dimensional network is a very attractive structure for providing a mechano-sensing function and this is where osteocytes, which comprise >95% of the number of cells in bone, are located in physiological bone (Burger and Klein-Nulend 1999b). The lacunar-canalicular network in natural bone is an interconnected porous scaffold which allows for the transfer of fluid and small molecules from the surface to the centre of bone. This lacunar-canalicular porosity allows for the recruitment of new osteoblasts with anabolic paracrine factors excreted in the extracellular matrix by osteocytes, the mechanosensing cells of bone (Sikavitsas, Bancroft et al. 2003). In our study there was a continuous integration of the existing network of micro-pores

in the implanted substrate and the lacunar-canalicular network in the newly formed bone on its surface (Figure 6-12). Coupled with the observed colonisation of micro-pores by cells with an osteocyte-like morphology, the fact that the implanted and host microporous networks were continuous with each other appears to substantiate the importance of the role of osteocytes in the rate of bone formation in materials with microporosity and it seems logical that with more microporosity there is a greater opportunity for their role to be more influential.

6.4.1.B **Effect of scaffold persistence on Osteoinductivity**

The period over which bone is observed in calcium phosphate materials implanted in non-bony sites across the animal studies reported in the literature might perhaps give some indication as to which biological mechanism is responsible for osteoinduction in this family of bone graft substitutes. For instance, in the literature there is very little or no bone observed in test article treated defects within 21 days (Eid, Zelicof et al. 2001) or 8 weeks (Piecuch 1982, Ohgushi and Okumura 1990, Ripamonti 1996) of implantation. However, bone is generally observed in other studies at later time-points, including: 3 months (Ripamonti 1991, Yang, Yuan et al. 1996, Yuan, Kurashina et al. 1999); 4 months (Pollick, Shors et al. 1995); 5 months (Yuan, De Bruijn et al. 2001a); 1 year (Gosain, Song et al. 2002, Fujibayashi, Neo et al. 2004); and 2.5 years (Yuan, Yang et al. 2001). There exist some contradictions to these trends in that some investigators have reported observing bone as early as 45 days after treatment (Yuan, De Bruijn et al. 2001a), and at 60 days post-implantation (Yuan, Zou et al. 1998, Yuan, Li et al. 2000), although in these studies bone was observed only in a small number of pores (Yuan, Li et al. 2000, Yuan, De Bruijn et al. 2001a) or the study was performed in a pig rather the more typical sheep or goat model (Yuan, Zou et al. 1998). In our study bone was observed as early as 8 weeks post-implantation but in much lower quantities than that seen at 12 or indeed 24 weeks (Figure 6-18). The apparent 8 week minimum period required for the osteoinductive potential of calcium phosphate biomaterials to take effect would support some of the theories proposed by Barrere et al. in that one might expect a delay would be observed for adsorption of the necessary concentration of BMP's to stimulate osteogenesis or for the development of a low oxygen tension local to the defect site (Barrere, van der Valk et al. 2003). It might also correspond to the time required for a sufficient number of circulating stem cells to reach the defect site, attach to the surface, and to differentiate into osteoblasts before producing bone matrix.

When combined, the amount of graft and new bone in the defects characterised in our study appeared to reach equilibrium at between 35-40% defect area for all groups at all time-points excluding SiCaP-46G (Figure 6-24a-c). In contrast, for the SiCaP-46G group there was a trend for increasing overall area occupied by graft and new bone (Figure 6-24d). At 24 weeks post-implantation this had reached approximately 45% of the total defect area. There is variation in the reported literature as to how much bone is observed in biomaterials at relatively longer time-points post-implantation. Bone and graft material were absent at only 150 – 168 days post-implantation for TCP (Yuan, De Bruijn et al. 2001a) and OCP (Barrere, van der Valk et al. 2003). Whereas bone and graft were present after 1 - 2.5 years for HA (Yuan, Yang et al. 2001, Gosain, Song et al. 2002) and after a similar amount of time in Titanium materials (Fujibayashi, Neo et al. 2004). This indicates that graft stability and the sustained presence of a scaffold may be important in the long-term osteoinductive effect of biomaterials. In our study there was clear evidence of dissolution of the graft over time (Figure 6-24). This reduction in graft volume was at least in part through cell mediated mechanisms, but with the extent of graft dissolution observed, chemical dissolution must also have contributed to this trend. However, even at 24 weeks post-implantation the scaffold was present in all defects analysed and despite the SiCaP-46G generally having a lower amount of scaffold remaining at 24 weeks compared to the other groups the graft still occupied approximately 15% of the area of analysed sections on average. This reduction in graft volume over time corresponded to an increase in contact between new bone and graft surface so clearly the graft continues to be of utility to ongoing bone growth and remodelling even after nearly six months implantation in these ectopic sites. This again points to the importance of the provision of a three-dimensional network and scaffold to the formation of bone in ectopic sites. There is no better evidence for this than the fact that resorbable grafts such as TCP and OCP do form bone in ectopic sites but as soon as they dissolve, as they inevitably do, the bone resorbs whereas for non-resorbable grafts, such as HA and Titanium, bone is present for as long as the graft remains in situ.

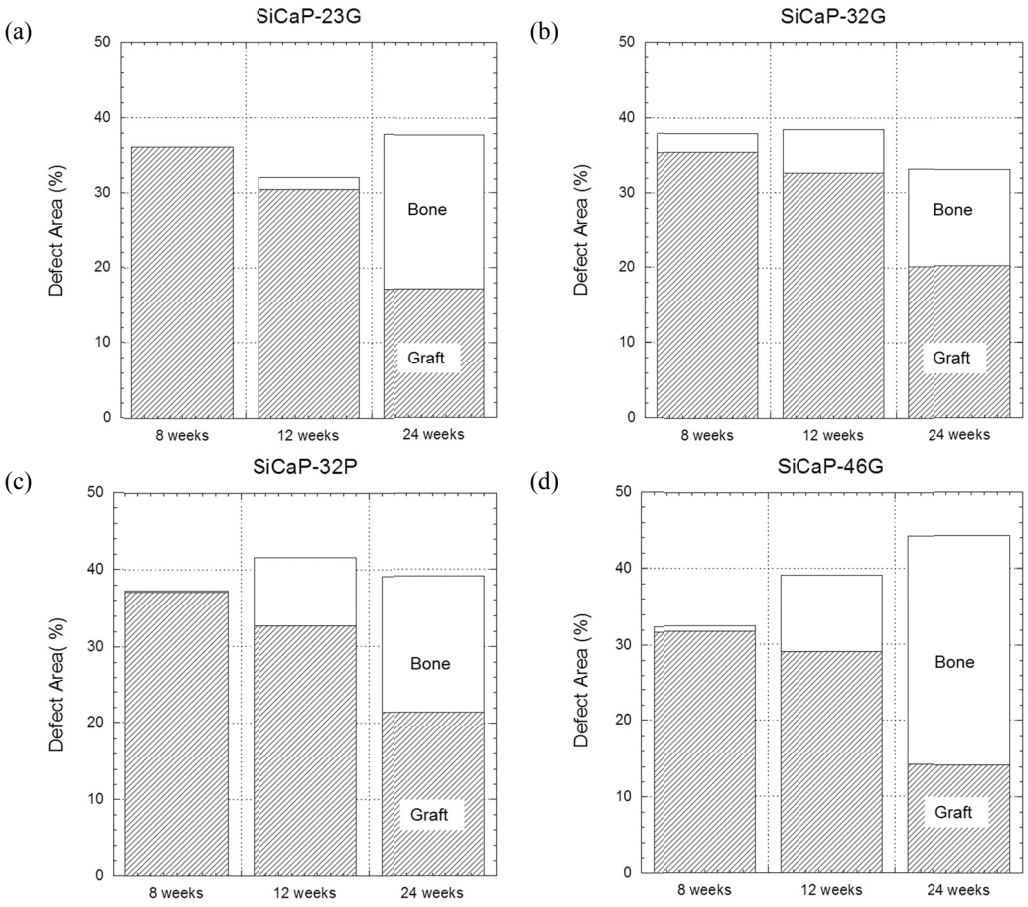

Figure 6-24 Stacked column plots showing Graft and Bone Area for all groups at 8, 12, and 24 weeks post-implantation (a) SiCaP-23G (b) SiCaP-32G (c) SiCaP-32P (d) SiCaP-46G

6.4.1.C **Role of macrophages in Osteoinductivity**

Of particular note in our own study was the complete absence of bone in regions of the defect where there was considerable scaffold degradation (Figure 6-13). This degradation was not accompanied by a gross rejection of the graft through fibrous encapsulation which would be expected to prevent bone infiltration, rather, the degraded regions tended to contain a greater number of macrophages which were clearly filled with engulfed particulate debris collected from the material surface. Macrophages with an osteoclast-like morphology were also evident on the material surface. Le Nihouannen et al. postulated that the presence of an elevated number of macrophages might be responsible for bone formation in non-bony sites since they are often observed with osteoclast-like morphology on the surface of the material as well as in the surrounding tissue matrix (Le Nihouannen, Daculsi et al. 2005). Le Nihouannen argued that micro-particles are phagocytised by macrophages but are degraded with difficulty and therefore might cause cell death and tissue inflammation. Since studies have shown that monocytes cultured in the presence of

hydroxyapatite particles produce abundant quantities of cytokines (Laquerriere, Grandjean-Laquerriere et al. 2003, Lu, Blary et al. 2004), Le Nihouannen et al., suggested that these cytokines might be responsible for regulating the differentiation of stem cells down the osteoblastic lineage. This hypothesis was further corroborated, they argued, by two additional facts: one, in physiological bone there is a close association between macrophages (which are recruited to sites of bone fracture to clean up bone debris and lysed cells) and stem cells which differentiate down the osteoblast lineage; and two, the predominant pathway for bone healing following fracture is intramembranous bone formation which corresponds to the type of bone formation found in calcium phosphates. Like Le Nihouannen et al. we did find macrophages in the matrix and osteoclast-like cells on the material but in the presence of a large number of particulates these cells did not appear to recruit stem cells as no bone was observed in these regions. It may be that these cells do play a role in ectopic bone formation but our study suggests that this is counteracted in the most severe cases of graft degradation through another process. Furthermore, unlike Le Nihouannen and many other researchers, we found endochondral bone formation as well as intramembranous bone formation, often in close proximity to one another (Figure 6-6), thus demonstrating that not only a macrophage-induced inflammatory trigger for stem cell differentiation is responsible for bone formation in ectopic defects.

6.4.1.D **Effect of calcium and phosphorus dissolution on Osteoinductivity**

Many researchers have suggested a primary factor in the formation of bone in ectopic implantation sites is the ability of the material to form a bone-like-apatite on its surface once *in situ* (Yang, Yuan et al. 1997, Yuan, Yang et al. 1998, Yuan, De Bruijn et al. 2001a, Barrere, van der Valk et al. 2003, Le Nihouannen, Daculsi et al. 2005, Habibovic, Sees et al. 2006). These groups have suggested, as a direct result of their findings, that a calcium phosphate phase with a greater propensity to chemically dissolve, such as beta-tricalcium phosphate (as compared hydroxyapatite), will more readily form a bone-like-apatite on its surface and therefore lead to a greater level of stem cell differentiation either directly through an interaction between the stem cells and the apatite surface or indirectly by forming a layer which will more preferentially adsorb circulating bone morphogenetic proteins. Most of these groups have also linked the surface area contributed to by microporosity as being influential in the subsequent formation of an apatite-like layer. Thus overall with these two material parameters (dissolution profile and surface area) combined an HA with a low surface area will have a much lower

propensity to form a bioactive layer than a tricalcium phosphate with a high surface area.

One fundamental finding in our study seems to dispel the theory that the propensity of materials to form bone in ectopic sites is almost entirely linked to their surface area. In a scenario where a layer of bone-promoting material is formed on the surface of an implant of fixed volume but with varying surface area, the ***proportion*** of bone contact would be expected to remain constant with increasing surface area (as surface area increases the amount of sites available for bone growth increases proportionally) but the relative volume of bone in the graft would increase with surface area (as the absolute amount of bone forming within the fixed volume would increase with more bone nucleation sites). Hypothetical representations of this are provided in Figure 6-25.

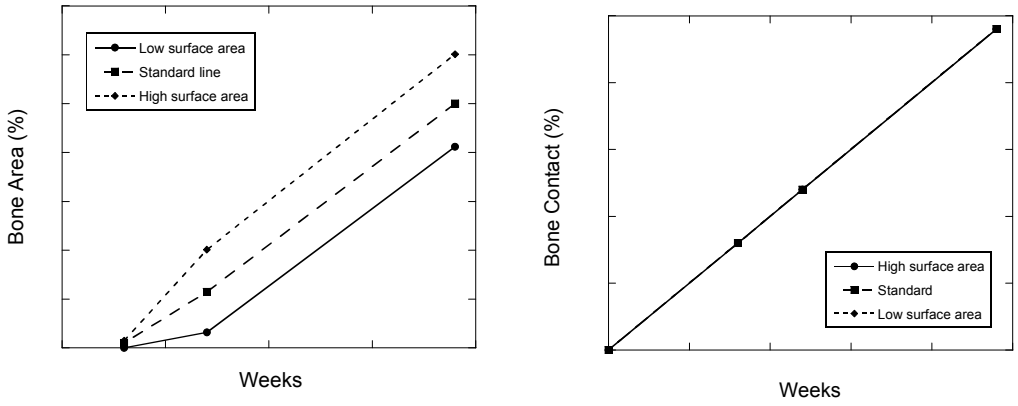

Figure 6-25 Hypothetical schematics for increase in bone contact and bone area over time with varying surface area

In our study however, whilst the contribution of surface area to amount of bone present in the voids was as expected (Figure 6-22 c.f. Figure 6-25) the surface area also contributed to the proportion of surface area covered by new bone (Figure 6-23 c.f. Figure 6-25). In fact, there was a greater lag for bone contact than for bone volume. This hints at the involvement of factors other than surface area in the rate of bone development.

In addition to our observations, there exist a substantial number of articles which contradict the notion that dissolution-reprecipitation reactions govern bone formation in ectopic sites. In a previous study microporous hydroxyapatite materials which were implanted into fatty tissues and intraperitoneal sites of hamsters were shown to be covered by a new inorganic phase which was significantly different from

hydroxyapatite in terms of (a) morphology (size and shape) of crystals; (b) the intimate association of the new inorganic phase with the surrounding organic tissues; (c) inclusion of carbonate (CO_{3-}) groups; (d) electron diffraction pattern which in contrast to phase pure stoichiometric hydroxyapatite shared the same peaks as natural bone mineral (Heughebaert, LeGeros et al. 1988). Heughebaert et al. also reported that the same inorganic layer was observed on materials implanted in both anatomical sites so the process behind this formation was, to a large extent, independent of cellular and acellular microenvironment. However, despite the formation of bone-like mineral in these sites mature bone itself was not observed. This may be a result of a genetic disposition of hamsters which, like other small animals such as rodents and rabbits, are reported not to tolerate bone formation in calcium phosphates implanted in ectopic sites – a common theme in the available scientific literature. However, despite hydroxyapatite being widely reported as a highly bioactive substrate, readily capable of forming an apatite-like layer on its surface (Weng, Liu et al. 1997, Kobayashi, Nakamura et al. 1998, Shirkhanzadeh and Azadegan 1998, Weng, Wang et al. 2002, Leng, Chen et al. 2003, Zhang, Chen et al. 2003, Yonggang, Wolke et al. 2007, Morejon-Alonso, Carrodeguas et al. 2008, Oliveira, Silva et al. 2009, Sanchez-Salcedo, Balas et al. 2009, Campion, Ball et al. 2013), microporous hydroxyapatite has been reported as having a low osteoinductivity by the researchers supporting the theory connecting apatite-layer formation and osteoinductivity (Habibovic, Yuan et al. 2005, Habibovic, Kruyt et al. 2008, Yuan, Fernandes et al. 2010). Perhaps even more remarkable is a study in which macroporous Bioactive glass (45S5) was implanted into the thighs of dogs wherein bone was found throughout the graft but more preferably in regions where an apatite-like layer was *not* present (Yuan, de Bruijn et al. 2001b). This study highlights the potential role of silicon in the upregulation of attached osteoblast cells instead of having a role in the development of an apatite-like layer on the surface of the biomaterial. The mechanisms for the direct role of silicon in upregulation of osteoblasts are described in section 2.5.3.A. The same researchers have reported a high-level of osteoinductivity for pure beta-tricalcium phosphate (Yuan, Fernandes et al. 2010) despite beta-tricalcium phosphate having been found previously to have a very low propensity to form a bioactive layer of bone-like apatite on its surface (Huan and Chang 2007, Juhasz, Best et al. 2008, Hesaraki, Safari et al. 2009, Campion, Ball et al. 2013).

The data substantiating the importance of calcium and phosphorus dissolution and re-precipitation on the osteoinductivity of calcium phosphates is thus unclear from the literature. In this study we found abundant levels of bone in direct contact with

phase pure hydroxyapatite but there were no obvious signs of a boundary layer between the hydroxyapatite and the newly formed bone. The zone of integration appeared to be continuous from the synthetic phase to the physiological phase of mineral (Figure 6-12). In our own study the pre-requisite for a bone-like apatite to form on the surface in order for bone formation to take place was not apparent. In contrast to these observations for calcium phosphate materials, the need for a bone-like apatite layer to form on the surface of other material types before osteoinduction can take place is well documented in the literature.

6.4.1.E **Effect of graft perfusion on Osteoinductivity**

Endochondral ossification was not expected, but was seen in most granule masses where significant bone formation was observed, including the carrier-containing formulation. In the largest spaces between the granules the loose connective tissue surrounding regions of endochondral bone were characteristic of quiescent and proliferating chondrocytes which adopted a globular appearance as they grew in size. These chondrocytes can only have been differentiated from circulating mesenchymal stem cells since no cartilaginous tissue was present in the tissues surrounding the defect. This observation was not due to the presence of clotted venous blood but must be associated with the environment provided by the granule masses in the critical bone formation period (presumed from histomorphometry to be between 9-12 weeks). Data from previous mechanistic studies suggests that oxygen levels play an active role in the regulation of hypertrophic differentiation of hyaline chondrocytes (Leijten, Moreira Teixeira et al. 2012). Normoxia stimulates hypertrophic differentiation evidenced by the expression of hypertrophic differentiation related genes. In contrast, hypoxia suppresses hypertrophic differentiation of chondrocytes, which might be at least partially explained by the induction of GREM1, FRZB and DKK1 expression.

In our study the packing density of the granules appeared somewhat lower compared to observations from studies reported in the literature (Coathup, Samizadeh et al. 2011). It was also felt that the level of bone interconnection (between regions of bone that had formed around distinct granules) was lower in the ectopic specimens as compared to that previously observed in orthotopic sites (Campion, Chander et al. 2011). This may either reflect the higher area of bone normally found in an orthotopic site at a similar time point, the effect of local biomechanical and biochemical stimuli associated with an orthotopic site on local bone morphology, or it may be related to the lower packing density as a result of the relative containment

in the varying sites (an orthotopic defect is constrained on three sides by osseous tissue and one side by soft tissues whereas an ectopic defect is constrained only by soft tissues in all axes). This latter proposal may explain why we observed endochondral bone formation in the ectopic defects since there would be expected to be a greater amount of perfusion through the graft bed in sites with a lower packing density of granules. In regions of greater perfusion there would be expected to be conditions of Normoxia. However, the evidence is slightly contradictory in our study as we observed both intramembranous and endochondral bone formation in very close proximity to one another (Figure 6-6) suggesting anoxia or vascularisation was not always a factor in determining the mechanism of bone formation.

6.4.2 Utility of aqueous carriers for osteoinductive biomaterials

6.4.2.A **Dissolution profile**

The measured ion release concentrations of the test material in TRIS buffer were consistent with resorbable calcium-phosphate bone grafts that have limited solubility at pH 7, and were lower than those detected previously for porous hydroxyapatite (HA) (Klein, de Blieck-Hogervorst et al. 1990, Hench 1993, Fazan and Marquis 2000, Chun, Na et al. 2002). For comparison, Fazan et al reported values of approximately 40-50 mg/L for Ca and 10-15 mg/L for P released into TRIS buffer after soaking of plasma-sprayed HA coating (Fazan and Marquis 2000). The discrepancy between Fazan's observations and our own may be explained by differences in surface area, crystallinity, phase purity, or porosity of the two materials studied. We used the standard test for dissolution of calcium phosphate ceramics to determine whether it was likely that there would be any substantial loss of calcium, phosphate, or silicon ions from the calcium phosphate when packaged in an aqueous based carrier over an aging period of five years. Our testing demonstrated that even at elevated temperature ($37^{o}C$) the rate of chemical dissolution in TRIS buffer is very low for silicate-substituted calcium phosphate. Under room temperature conditions, typically approximated to $22^{o}C$ for bone graft substitutes when stored in air conditioned warehousing, the rate of dissolution can be expected to be even lower. Furthermore, in a commercial product containing calcium phosphate and aqueous Poloxamer the rate of dissolution would be slowed by the lack of free mobility of the solvent water ions as the aqueous Poloxamer is a gel at room temperature.

6.4.2.B **Long-term stability**

Physical and chemical characterisation of the un-aged test materials revealed the samples to be phase-pure, highly crystalline, silicate-substituted hydroxyapatite with a Ca/P+Si ratio of 1.67 and 0.80% silicon by weight substituted into the crystal lattice. This is consistent with all previous research for materials manufactured by the same novel foaming route (Gibson, Best et al. 1999, Hing, Best et al. 1999). The presence of hydroxyapatite as a highly crystalline phase is consistent with other bone graft substitutes characterised by the same techniques (Tadic and Epple 2004). We aged the calcium phosphate at elevated temperature to determine whether there were any noticeable changes in the chemical stability of the composite over the period of the equivalent of five years aging at room temperature. The results show that for period up to and including five years the predominant (>99%) phase present in the ceramic component was hydroxyapatite and that the ceramic component remains highly crystalline over the aging period, as demonstrated by the narrow spectral bands matching the hydroxyapatite library file. We also used X-Ray fluorescence spectroscopy to detect changes in the metal oxide content of the ceramic components. Specifically, we measured the ratio of calcium to phosphorus and silicon which is a sensitive and quantitative means to pick up changes in phase composition in the calcium phosphate. All samples were found to be within the expected ratio 1.67±0.10 for a hydroxyapatite, indicating that no decomposition into tricalcium phosphate had occurred over the aging period. XRF was also used to detect any changes in silicon ion substitution in the hydroxyapatite crystalline lattice, as any significant dissolution of the ceramic might be expected to affect this parameter over the period of aging. There was some variation from time-point to time-point but all samples were measured as having the expected 0.80±0.10 weight percentage silicon and there was no trend for silicon loss or adsorption over the period of aging. Fourier transform infrared spectroscopy analysis of control and aged samples revealed no differences in chemical profile, thus confirming the absence of any degradation moieties in the aged samples, the presence of which might be expected if the ceramic had undergone any substantial hydrolysis after being irradiated and stored at elevated temperature in aqueous Poloxamer carrier. Our chemical analyses confirm that over the period of accelerated aging equivalent to five years aging at room temperature there were no changes in chemical composition of silicate-substituted hydroxyapatite ceramic when combined with an aqueous Poloxamer gel.

6.5 Conclusions

Our study corroborates the findings in the literature that the mechanism for calcium phosphate derived osteoinductivity is not likely to be closely associated with any biological reactions to the graft which take place in the first twenty four hours after implantation. Coupled with the observed colonisation of micro-pores by cells with an osteocyte-like morphology, the fact that the implanted and host microporous networks were continuous with each other appears to substantiate the importance of the role of osteocytes in the rate of bone formation in materials with microporosity and it seems logical that with more microporosity there is a greater opportunity for their role to be more influential.

Our data substantiates the importance of the provision of a three-dimensional network and scaffold to the formation of bone in ectopic sites. There is no better evidence for this than the fact that resorbable grafts such as TCP and OCP do form bone in ectopic sites but as soon as they dissolve, as they inevitably do, the bone resorbs whereas for non-resorbable grafts, such as HA and Titanium, bone is present for as long as the graft remains in situ.

Unlike Le Nihouannen and many other researchers, we found endochondral bone formation as well as intramembranous bone formation, often in close proximity to one another, thus demonstrating that not only a macrophage-induced inflammatory trigger for stem cell differentiation is responsible for bone formation in ectopic defects.

We found abundant levels of bone in direct contact with phase pure hydroxyapatite but there were no obvious signs of a boundary layer between the hydroxyapatite and the newly formed bone. The zone of integration appeared to be continuous from the synthetic phase to the physiological phase of mineral. In our study the pre-requisite for a bone-like apatite to form on the surface in order for bone formation to take place was not apparent.

Our chemical analyses confirm that over the period of accelerated aging equivalent to five years aging at room temperature there were no changes in chemical composition of silicate-substituted hydroxyapatite ceramic when combined with an aqueous Poloxamer gel.

Chapter Seven: Effect of Strut-porosity on the Performance of Calcium Phosphate Biomaterials in an Orthotopic Bone Defect Study

7.1 Introduction

The structural characteristics of synthetic bone graft materials are also pivotal to the extent to which they can elicit a positive cellular response to their implantation. The microenvironment within the graft appears to influence the process of osteogenesis. One of the key features of synthetic bone grafts is the level of macroporosity (where macroporosity can be considered as pores >50 μm in size) and strut (micro) porosity (pores <50 μm in size) which play an important role in vascularisation of the bone graft, which supports the proliferation and differentiation of osteoblasts and the ingrowth of new bone into the graft itself (Hing 2004b). In common research terms, microporosity and strut porosity are used interchangeably. Strut pores are formed from the interconnected spaces existing between particles of calcium phosphate which have been sintered together to form the struts in the scaffold of calcium phosphate biomaterials. The term 'strut-porosity' is used to describe the average pore volume fraction within the struts that form the walls around the macropores. Studies conducted with various different bone graft materials suggest a greater degree and faster rate of bone penetration as the macroporosity of the scaffold increases (Klawitter, Bagwell et al. 1976, Holmes, Mooney et al. 1984, Eggli, Muller et al. 1988, Kuhne, Bartl et al. 1994, Hing, Best et al. 2004). Increased levels of strut porosity also appear to promote the faster apposition of greater volumes of new bone demonstrating a more dense morphology within time points up to 24 weeks post-implantation (Hing 2004b, Hing, Annaz et al. 2005). Similarly, the degree of structural interconnectivity between the pores of the graft material appears to influence the speed and extent of the development of the vascular network vital for new bone formation (Eggli, Muller et al. 1988, Rubin, Popham et al. 1994).

The primary purpose of the current study was to investigate the potential benefits of increasing the strut porosity in synthetic bone graft substitutes on osteogenesis bone graft implants in an ovine critical-sized intraosseus defect model. The first study (Study A) validated the ovine critical defect model and its capacity for repair using microporous synthetic bone graft substitutes. The biological response of empty defect (control) sites was compared with bone graft materials consisting of a porous

silicate-substituted HA matrix (SiCaP; 0.8 wt% Si) that has previously been shown to be effective in healing osseous defects in lapine and ovine models when compared with HA (Patel, Best et al. 2002, Hing, Saeed et al. 2004, Patel, Brooks et al. 2005). The second study (Study B) examined the biological responses and graft stability to different test bone graft materials that comprised of SiCaP matrices (0.8 wt% Si) with varying interconnected strut porosity ranging from 32% to 46%.

7.2 Methods

Two studies were conducted: Study A and Study B were conducted with the same contract research organisation and at the same facility (Biomatech, France). Study A was conducted to validate the ovine critical defect model. The study assessed the intraosseous implantation of SiCaP materials with a strut porosity level of 23% into the distal femoral epiphyses of sheep (Ovis aries) and compared the healing of the defect site with non-implanted empty defect (control) sites. Study B assessed the intraosseous implantation of SiCaP test materials with strut porosity levels of 32%, 32% or 46% using the same ovine model. In both studies, sheep were euthanised at either 8 weeks or 12 weeks and samples were retrieved for assessment using histological and micro-computerised tomography (CT).

The study protocols were reviewed and approved by the Ethical Committee of the contract research organisation conducting the studies (and conformed to NF EN ISO 10993 standard (2006 and 2007) (Organisation 2006).

7.2.1 Implants

In Study A, the SiCaP material (Actifuse® Microgranules, ApaTech, Herts, UK) consisted of porous (80-82.5% total porosity), irregularly shaped microgranules (1–2 mm) of phase pure SiCaP (0.8 wt% Si) with a strut porosity of 23% (SiCaP-23G) and granules in an aqueous poloxamer carrier with a strut porosity of 23% (SiCaP-23P) which were compared with non-implanted empty (control) defect sites.

In Study B, the test materials also consisted of porous (80-82.5% total porosity), phase pure SiCaP (0.8 wt% Si) (ApaTech, Herts, UK) but also comprised of the following: microgranules (1-2mm) with a strut porosity of 32% (SiCaP-32G); microgranules in an aqueous poloxamer carrier with a strut porosity of 32% (SiCaP-32P; microgranules with a strut porosity of 46% (SiCaP-46G) and microgranules in an aqueous poloxamer carrier with a strut porosity of 46% (SiCaP-46P).

7.2.2 Surgical Procedure

Fifty-four (Study A; n = 18; Study B; n = 36) skeletally mature adult ewes aged between 2 and 5 years underwent bilateral surgery on the distal femur with two defects being generated on each side of the femur. In both studies, the locations in which synthetic bone graft materials were implanted and the allocation of animals to treatment groups was conducted according to randomisation schedules that were created prior to the start of the surgical procedure. All animals were kept under the conditions required by EC Directive 86/609 (Directive 1986).

Animals were fasted for 24 to 72 h before undergoing the surgical implantation procedure. At the time of implantation, pre-medication and anaesthesia was achieved by intravenous injection of a mixture of thiopental (Nesdonal®, Merial SAS, Lyon, France) and pentobarbital mixture (CEVA Santé animale, Libourne, France) followed by atropine (Aguettant Santé SA, Lyon, France) and subsequent inhalation of an O2–isoflurane mixture (1–4% isoflurane; Aeranne®, Baxter SAS, Maurepas, France). Pre-operatively, each animal received two analgesics intramuscularly: flunixine 2 mL/50 kg (Meflosyl®, Fort Dodge Santé Animale, Tours, France) and butorphanol 0.05 mL/kg (Torbugesic®, Fort Dodge Santé, Animale, Tours, France). The animal's legs were clipped free of wool and the exposed skin was scrubbed with povidone iodine (Vetedine®, Vetoquinol, France).

Implantation was conducted under standard aseptic surgical conditions. A cutaneous incision was made on the medial face of the knee followed by blunt dissection of the subcutaneous tissue and of the fascia lata. The condyle, slightly upper to the collateral medial ligament insertions, was exposed by partial M. vastus medialis and capsular section. A pneumatic drill was then used to drill holes 8 mm in diameter and 15 mm deep in the distal femoral epiphysis (two per side). The defects were drilled under constant irrigation with saline solution (0.9% w/v). Defects were filled with test formulations so that the graft material was in close contact with all internal surfaces of the defect, or left empty in control operations. Filling was achieved by gradually loading from bottom to top and the test formulations were slightly packed down gently with a metal spatula so as not to damage the brittle porous granules. The incisions were then closed by suturing both capsule and muscles with absorbable thread (PDS® (polydioxane sutures) II, 1, Ethicon Inc., Somerville, NJ, USA) and the subcutaneous layer was closed with absorbable thread (Vicryl® 2 or Vicryl® 1, Ethicon Inc., Somerville, NJ, USA). The skin layer was closed using surgical staples.

7.2.3 Specimen Retrieval

At the appropriate time point (8 weeks or 12 weeks post-implantation), the animals were administered an injection of ketamine (Ketamine 1000®, Virbac, France) with xylazine (Rompun®, Bayer Pharma, France). Animals were then euthanised with a lethal injection of barbiturate (Dolethal®, Vetoquinol, France). Soft tissues surrounding the implant site were dissected to allow access. Tissues were assessed to see if the granules had migrated from the defect site. The distal femoral epiphyses were harvested and identified.

7.2.4 Histological Evaluation

Retrieved samples were labelled and fixed in a solution of 10% formalin. Each implant site and the surrounding tissue was initially isolated using a band saw and then cut in two about the central longitudinal section. These samples were dehydrated in alcohol solutions of increasing concentration and cleared in xylene.

Specimens were prepared for embedding in poly methyl methacrylate using the ExaktTM system (Exakt Medical Instruments, Oklahoma City, OK, USA). One longitudinal histological section per site, immediately parallel to the central plane, was obtained using a micro cutting and grinding technique similar to that described previously (Donath and Breuner 1982). Sections were then stained using modified paragon staining. For paraffin embedding, one longitudinal histological section per site was cut to a thickness of 5–7 μm using a microtome (Mircom®, Thermo Fisher Scientific Inc., Walldorf, Germany). Sections were stained with Masson's trichrome.

Semi-quantitative analysis was performed on both types of embedded sub-specimen in accordance with the International Standard ISO 10993 Biological evaluation of medical devices – Part 6: Tests for local effects after implantation (Organisation 2006). The sub-specimens were analysed and graded according to signs of infection, necrosis, fibrinous exudate, tissue degeneration, polymorphonuclear leukocyte cells, lymphocytes, macrophages, giant cells, osteoblastic cells, fibrocytes and fibroconnective tissue, osteolysis and signs of bone remodelling. Particular attention was paid to: quality of the neoformed bone, inflammatory response; presence of fibrosis; biodegradation and possible graft or debris migration. A semi-quantitative scoring system was adopted, with the following reaction grades: 0 = absent; 1 = slight; 2 = moderate; 3 = marked; 4 = severe. 'Empty' regions in paraffin sections were considered to correspond to the implanted material. Attention was also paid to

the morphology and maturity of bone ingrowths in addition to neovascularization within the graft macro-structure. Microphotographs were taken of representative sites illustrating histological observations.

7.2.5 Histomorphometry

Histomorphometry assessments were conducted on samples embedded in PMMA resin from both Study A and Study B. One longitudinal section was taken parallel to the central plane and approximately 1–2 mm away from the central plane and analysis performed within a 13 mm^2 region of interest located to include a complete cross section of the defect at a standardised depth using high-resolution digital images taken from each histological slide using an axioscope microscope (Carl Zeiss AG, Oberkochen, Germany) coupled with a Samba version 4.27 image analyser systems (Bossa Nova Technologies, Venice, CA, USA). Histomorphometric parameters measured included: bone volume ($^{HISTO}BV$) and total defect volume ($^{HISTO}TV$). These parameters were then used to calculate percentage absolute bone volume $^{HISTO}ABV$ ($^{HISTO}BV/^{HISTO}TV$) (Hing, Best et al. 1998a).

7.2.6 Micro Computerised Tomography

In Study A Micro CT-imaging and morphometrical analysis was conducted by Animage (Lyon, France) whereas for Study B Micro CT-imaging and morphometrical analysis was conducted by ETH (Zurich, Switzerland). To correct for the volume of implant in the defect (Study A only), a normalised volume of bone ingrowth (^{CT}NBV) was calculated as: $^{CT}NBV = {}^{CT}BV/({}^{CT}TV - {}^{CT}GV)$, where total volume ($^{CT}TV$) was defined as the volume of the defect into which the material was implanted and ^{CT}GV was the total graft volume within the defect [22]. To verify implant stability (Study B only), a quantification of absolute graft volume, ^{CT}AGV ($^{CT}GV/^{CT}TV$) of each defect was performed following micro-CT acquisition (Hing, Best et al. 1998b).

The capacity of the SiCaP matrix to undergo resorption was also assessed. Based on small amounts of implant resorption observed in previous studies it was proposed that the test material with the greatest porosity (SiCaP-46G and SiCaP-46P) would be that most predisposed to resorption because of the larger predicted surface area available for dissolution (Hing, Wilson et al. 2007). Morphometric and visual assessment was performed on micro CT images of the SiCaP-46G and SiCaP-46P graft sites at weeks 8 and 12.

7.2.7 Statistical Analysis

Histomorphometrical data (^{HISTO}ABV) from 8 weeks and 12 weeks post-implantation were analysed using analysis of variance (ANOVA) to compare the test treatments using a pair-wise comparison, with *P* values of less than 0.05 being considered statistically significant (Analyze-IT Version 2.12, Analyze-IT Software Ltd, UK).

Micro CT data (^{CT}NBV and ^{CT}AGV) at 8 and 12 weeks post-implantation was analysed by ANOVA to compare the empty defect (control) site with test treatments SiCaP-23G and SiCaP-23P and to assess SiCaP-46G and SiCaP-46P graft degradation with time, using a pair-wise comparison, with *P* values of less than 0.05 being considered statistically significant (Analyze-IT Version 2.12, Analyze-IT Software Ltd, UK).

7.3 Results

7.3.1 Histology Findings

In Study A, there was only histological evidence of creeping edge repair in untreated (control) defects and no bone tissue in the centre at 8 weeks (Figure 7-1). The central regions of control defects were entirely filled with loosely vascularised fibro-connective tissue. Defects treated with SiCaP-23G and SiCaP-23P showed development of a neo-vascular network penetrating through the graft macrostructure into the centre of the defect. In addition, osseous repair was observed in the centre of the defect and characterised by regions of centripetal bone growth within the macropores (Figure 7-2). There appeared to be remnant evidence of a mild inflammatory response, consistent with that expected following a surgical procedure, in the form of graft infiltration by macrophages, giant cells and lymphocytes. The empty (control) sites continued to show poor signs of bone regeneration at 12 weeks with no evidence of bone ingrowth in the centre of the defect validating this size of defect as a being critically-sized and an appropriate test control under the conditions of the study (Figure 7-3). In contrast, evidence of bone remodelling was observed for both SiCaP-23 materials and associated with thicker more organised layers of bone at week 12 than at the week 8 time point. At both 8 and 12 weeks, the level or volume of bone apposition appeared similar for SiCaP-23G and SiCaP-23P (Figure 7-2 and Figure 7-4).

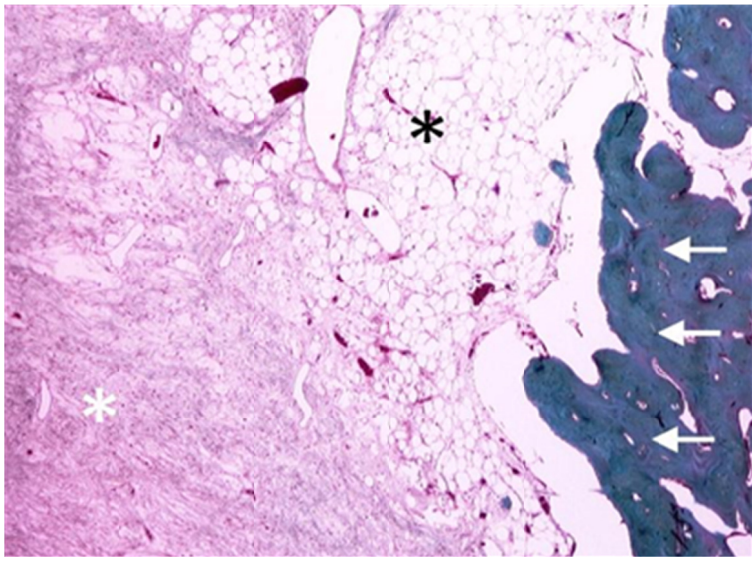

Figure 7-1 Control X 2 Mag Masson's trichrome staining.
Paraffin-embedded histology specimen (x2 magnification; Masson's trichrome stain) for an empty (non-implanted) control defect at 8 weeks, showing early signs of creeping edge repair (white arrows). The centres of the defects were filled with fibrous tissue (white asterisk) and bone marrow (black asterisk).

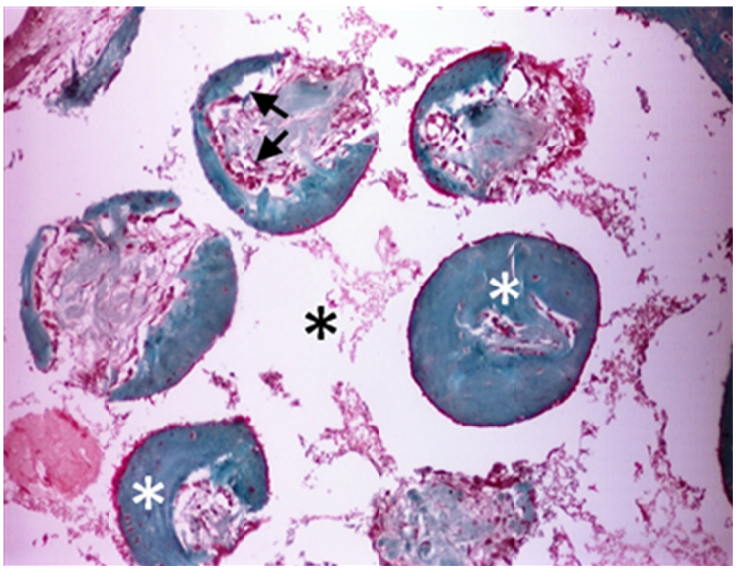

Figure 7-2 SiCaP-23P X 10 Masson's trichrome staining.
Paraffin-embedded histology specimen (x10 magnification; Masson's trichrome stain) for SiCaP-23P at 8 weeks showing bone growth (white asterisks) throughout the implanted material (black asterisk) in the centre of the defect after 8 weeks implantation. Woven bone formed centripetally in the macropores of the material (black arrows).

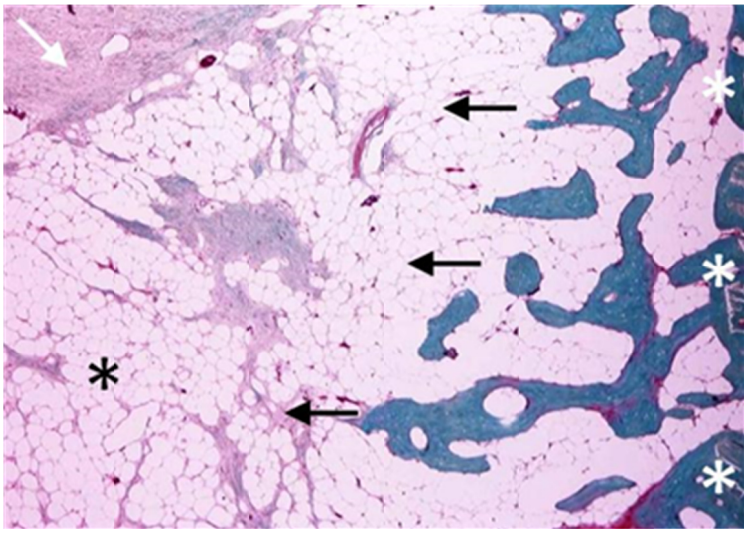

Figure 7-3 Control X 2 Mag Masson's trichrome staining
Paraffin-embedded histology specimen (x2 magnification; Masson's trichrome stain) for an empty (non-implanted) control defect at 12 weeks, showing creeping edge repair at the edges of the defect (white asterisks) towards the centre of the defect (black arrows). The centre of the defects were filled with fibrous tissue (white arrow) and bone marrow (black asterisk).

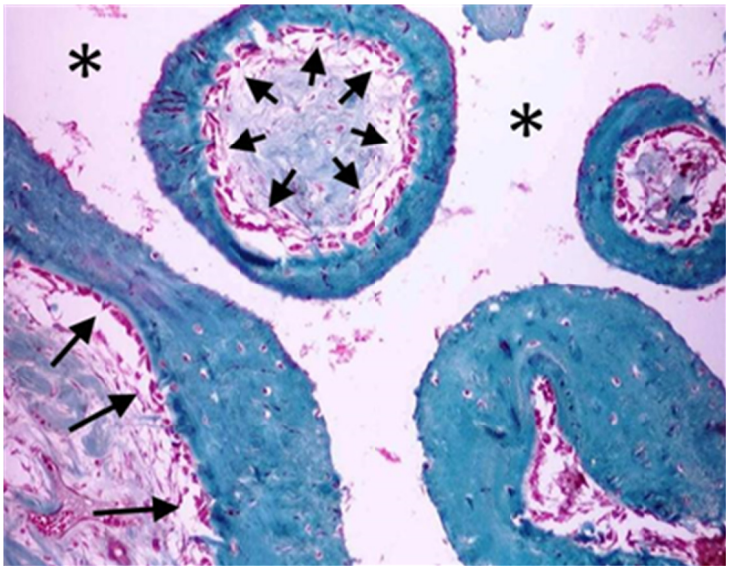

Figure 7-4 SiCaP-23G X 10 Mag Masson's trichrome staining.
Paraffin-embedded histology specimen (x10 magnification; Masson's trichrome stain) for SiCaP-23G (black asterisk) at 12 weeks, showing centripetal bone growth in direct apposition to the material surface by osteoblasts (black arrows).

In Study B, at 8 weeks, examination of the defect sites treated with all the test materials demonstrated the presence of a neo-vascular network penetrating into the

centre of the defect similar to that observed with the SiCaP-23 materials, but appearing more established in the higher strut porosity (32-46%) test materials (Figure 7-5 and Figure 7-6). A mild inflammatory response was also observed consistent with that observed for SiCaP-23 (Figure 7-5).

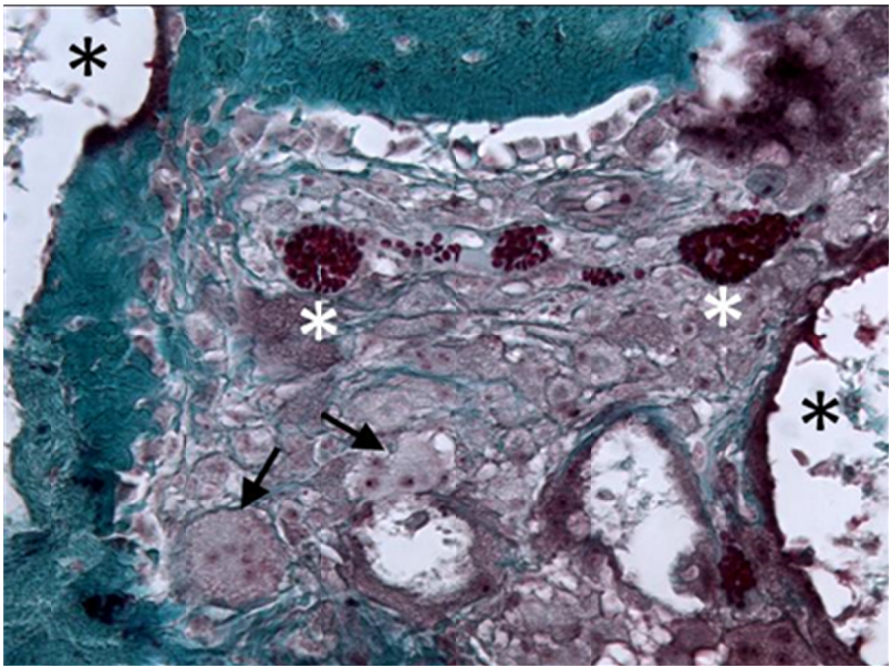

Figure 7-5 SiCaP-46P X 20 Mag Masson's trichrome staining
Paraffin-embedded histology specimen (x20 magnification; Masson's trichrome stain) for SiCaP-46P (black asterisks) at 8 weeks, showing presence of neovascularisation (white asterisks); bone (green regions); and giant cells (black arrows).

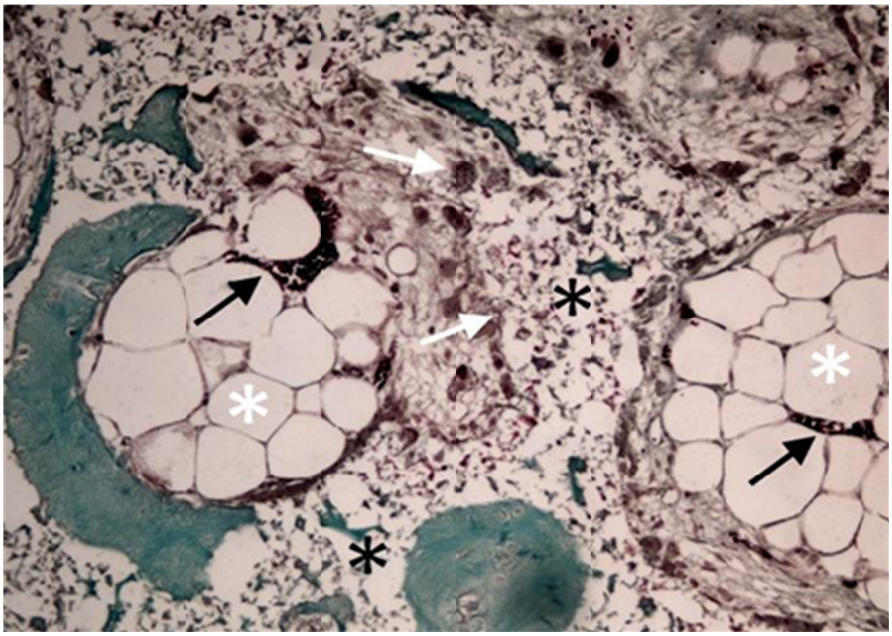

Figure 7-6 SiCaP-32G X 10 Mag Masson's trichrome staining.
Paraffin-embedded histology specimen (x10 magnification; Masson's trichrome stain) for SiCaP-32G at 8 weeks, showing presence of neovascularisation (black arrows); marrow (white asterisks); green staining de novo mineralised bone within the strut porosity (black asterisk); and osteoclast resorption pits (white arrows).

Bone apposition was well advanced in all four test materials with evidence of cell-mediated remodelling at 8 weeks (Figure 7-6 and Figure 7-7) and the characteristic centripetal bone growth with direct apposition of woven bone onto SiCaP granule macropore surfaces (Figure 7-7). The structural morphology of this new bone appeared most advanced with SiCaP-46G versus the other components of Study B; with evidence of direct apposition of lamellar bone within central regions of the defect and a more interpenetrating network of new bone within the graft macroporosity (Figure 7-8).

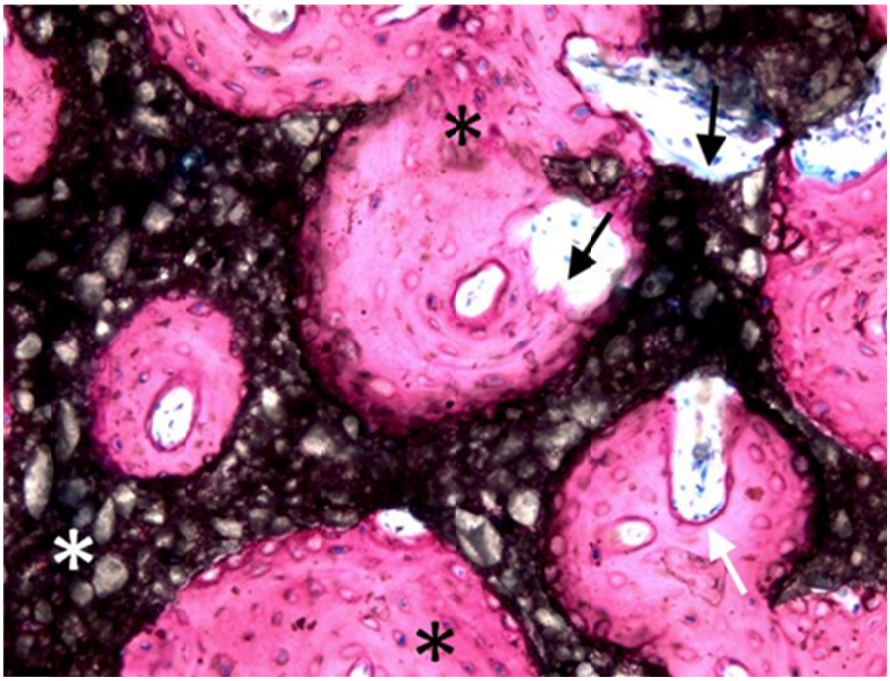

Figure 7-7 SiCaP-32G X 10 Mag Modified Paragon staining.
Resin-embedded histology specimen (x10 magnification; modified Paragon stain) for SiCaP-32G (white asterisk) at 8 weeks showing centripetal bone growth (pink regions); ruffled areas of osteoclastic resorption of bone and material strut (black arrows); a remodelling osteoclastic cutting cone (white arrow); and osteocytes trapped in de novo bone (black asterisks).

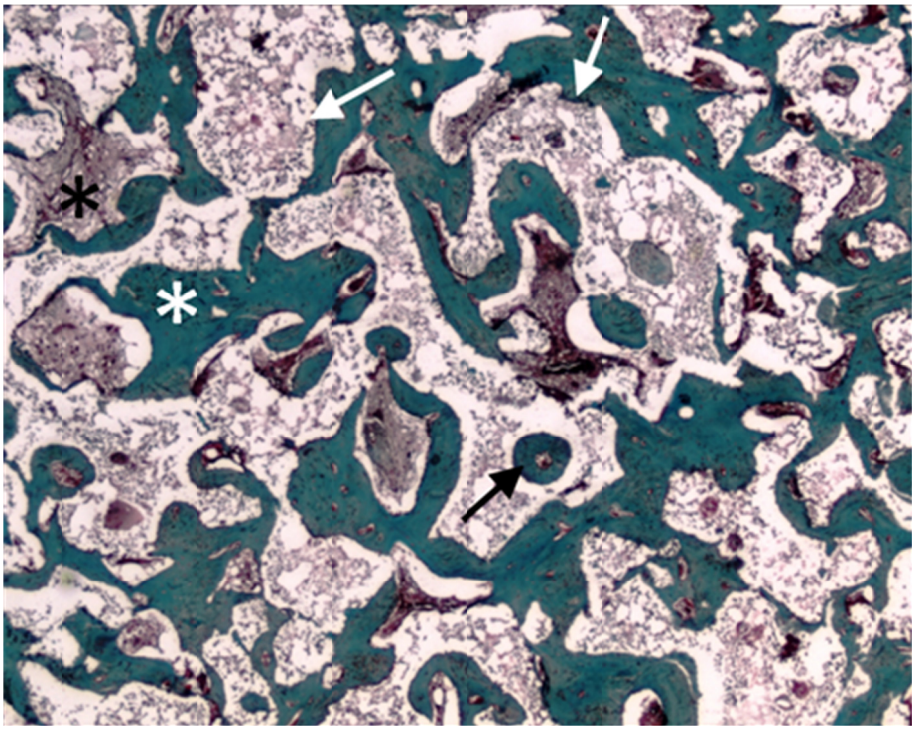

Figure 7-8 SiCaP-46P X 2.5 Masson's trichrome staining.
Paraffin-embedded histology specimen (x2.5 magnification; Masson's trichrome stain) for SiCaP-46P at 8 weeks showing bone growth (white asterisks) throughout the implanted material (white arrows) in the centre of the defect after 8 weeks implantation. Bone filled the macropores of the material in the centre of the treatment site (black arrow). Some regions contained fibro-connective tissues (blast asterisk) which were less prevalent at 12 weeks post implantation.

Histological examination of the test material sites at 12 weeks showed a diminished inflammatory response compared with that seen at 8 weeks (also observed for SiCaP-23 materials). In addition, there was a reduction in the amount of fibrous connective tissue and fibrocartilage along with an increase in the amount of bone marrow (again also observed with SiCaP-23 materials). However, there was a marked increase in the extent and maturity of the bony network within all test materials at 12 weeks compared with 8 weeks, especially within the SiCaP-46G and SiCaP-46P graft sites where there was clearly an increase in the amount of bone tissue in contact with the graft material (Figure 7-9). Signs of bone remodelling, such as the presence of thicker layers of mineralised bone and osteoclast pits, were more prominent for all test materials at 12 weeks than that at 8 weeks (Table 7-1) and semi-quantitative histological examination indicated that the capacity for osteogenesis was slightly greater for SiCaP-46G than for SiCaP-32G.

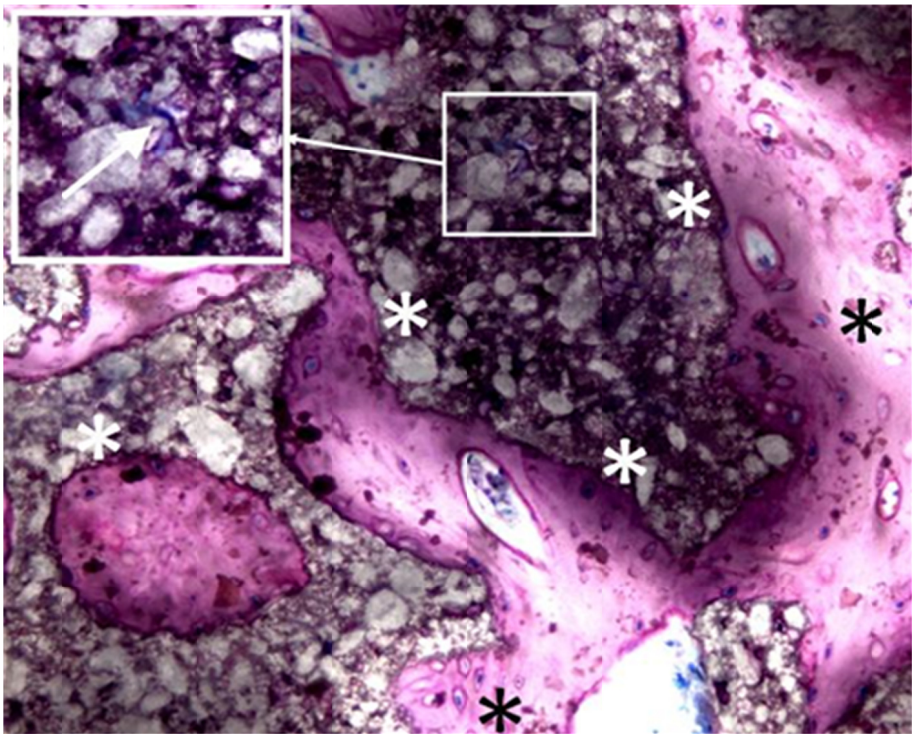

Figure 7-9 SiCaP-46P X 10 Mag Modified Paragon staining.
Resin-embedded histology specimen (x10 magnification; modified Paragon stain) for SiCaP-46P at 12 weeks showing direct bone apposition covering a high proportion of the materials surface (white asterisks): osteocytes trapped in de novo bone (black asterisks); and blue-staining bone cells in the strut porosity (white arrow).

There was no evidence of graft migration outside the defect sites, impairment in bone healing, abnormal bone healing, premature resorption or osteolysis (Table 7-1) in the vicinity of any of the graft treated defects during the 12-week assessment period. Histological observations were consistent in both the non-decalcified (paraffin) and the decalcified (resin) samples.

Table 7-1 Mean values of semi-quantitative histological assessment (resin slides)

	SiCaP-23G (n = 6)	SiCaP-23P (n = 6)	SiCaP-32G (n = 6)	SiCaP-32P (n = 6)	SiCaP-46G (n = 6)	SiCaP-46P (n = 6)
Osteolysis						
8 weeks	0	0	0	0	0	0
12 weeks	0	0	0	0	0	0
Implant migration						
8 weeks	0	0	0.5	0.1	0.6	0.3
12 weeks	0	0	0.3	0	0.2	0.3
Signs of bone remodelling						
8 weeks	1	1	1.2	1.1	1.2	1
12 weeks	2	2.3	2	1.7	2.2	2.2
Bone density						
8 weeks	2	2.7	2.2	2.4	2.3	2.8
12 weeks	2.2	2.2	2.8	3	2.8	3.2
Bone contact						
8 weeks	2.2	2.8	2.2	3.0	2.5	2.4
12 weeks	2.7	2.8	2.0	3.0	2.8	2.8

7.3.2 Histomorphometry Results

Histomorphometry of graft treated defect sites at 8 weeks demonstrated a trend towards greater mean values for the volume of newly formed bone (^{HISTO}ABV) in the higher strut porosity graft treated defect sites, but the differences did not achieve statistical significance ($P > 0.05$ for all comparisons) (Figure 7-10). 12 weeks after implantation there were no significant differences in the ^{HISTO}ABV of SiCaP-23G and SiCaP-23P treated defect sites (Figure 7-11). In contrast, graft materials with higher strut porosity (32%–46%) demonstrated statistically significantly higher ^{HISTO}ABV values than those for SiCaP-23G and SiCaP-23P ($P < 0.05$) in all cases (Table 7-2).

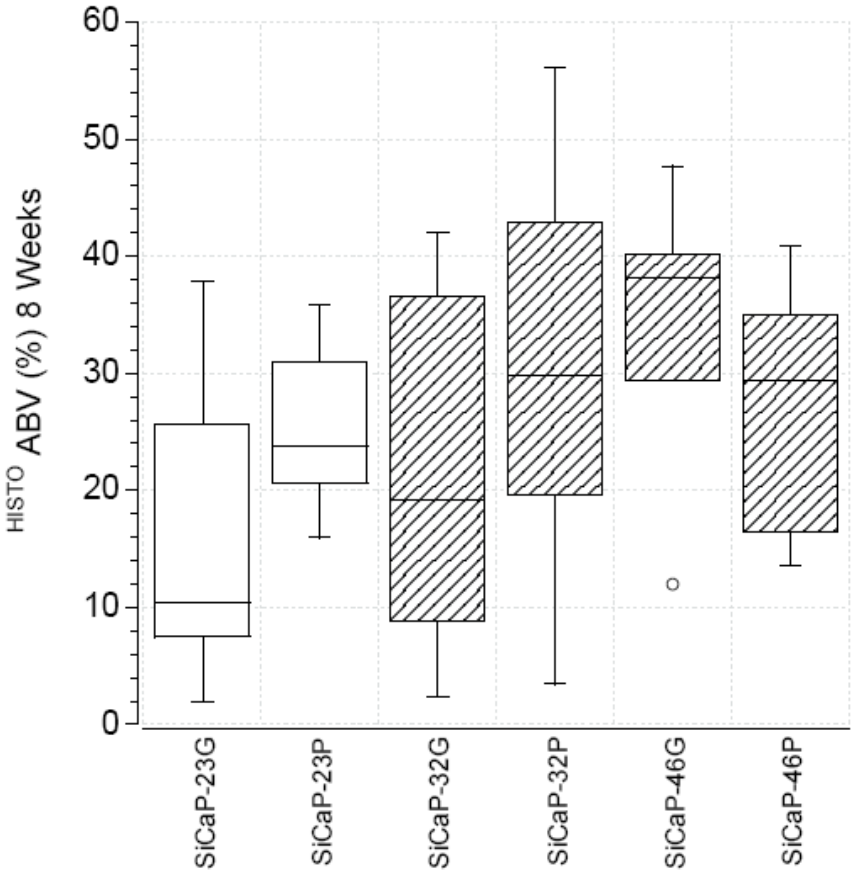

Figure 7-10 Mean percentage absolute bone volume (histology) at 8 weeks

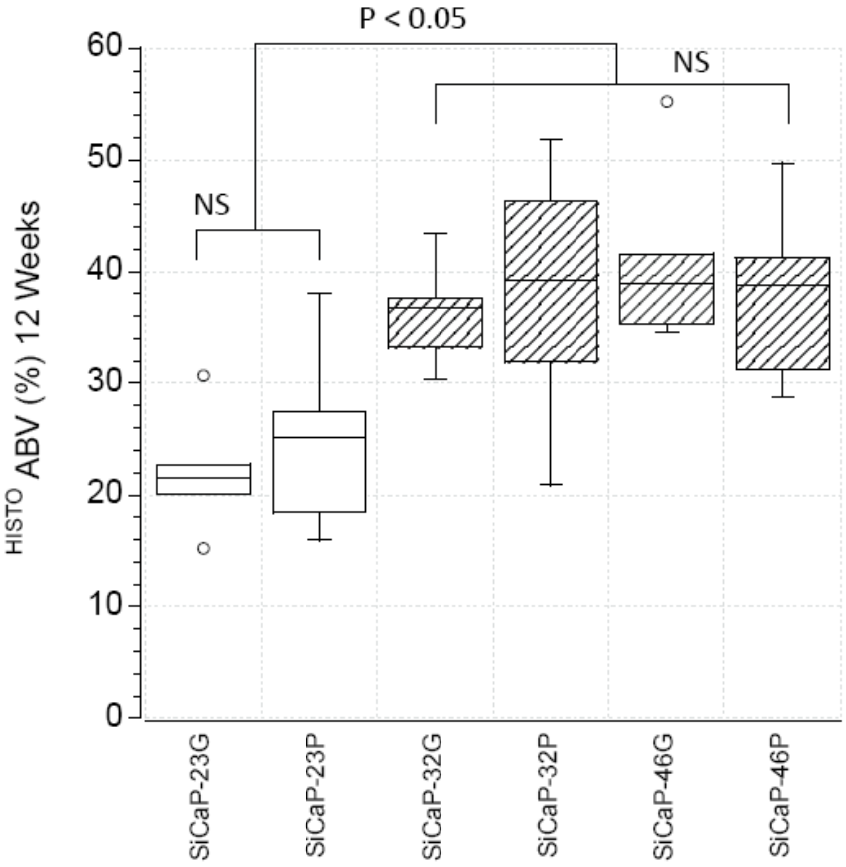

Figure 7-11 Mean percentage absolute bone volume (histology) at 12 weeks

Table 7-2 Histomorphometric results

	Mean ^{HISTO}ABV (SD)					
	SiCaP-23G (n = 6)	SiCaP-23P (n = 6)	SiCaP-32G (n = 6)	SiCaP-32P (n = 6)	SiCaP-46G (n = 6)	SiCaP-46P (n = 6)
8 weeks	15.6 (12.30)	25.2 (6.80)	21.40 (15.45)	30.63 (18.15)	33.50 (13.67)	27.45 (10.61)
12 weeks	22.00 (4.60)	25.0 (7.10)	36.33 (4.41)	38.23 (11.22)	40.75 (7.69)	38.10 (7.48)

7.3.3 Micro Computerised Tomography Results

At 8 and 12 weeks, defects treated with 23% strut porosity bone grafts (SiCaP-23G and SiCaP-23P) contained significantly more bone (^{CT}NBV) than that observed in the empty defect (control) sites ($P < 0.05$) (Figure 7-12). Moreover there was no significant difference in ^{CT}NBV with time for either control, SiCaP-23G or SiCaP-23P treated defects.

Assessment of the absolute graft volume (^{CT}AGV) in SiCaP-46G and SiCaP-46P treated defects by micro CT indicated that there was a reduction in ^{CT}AGV from 8 to 12 weeks but these differences were not statistically significant (Figure 7-13).

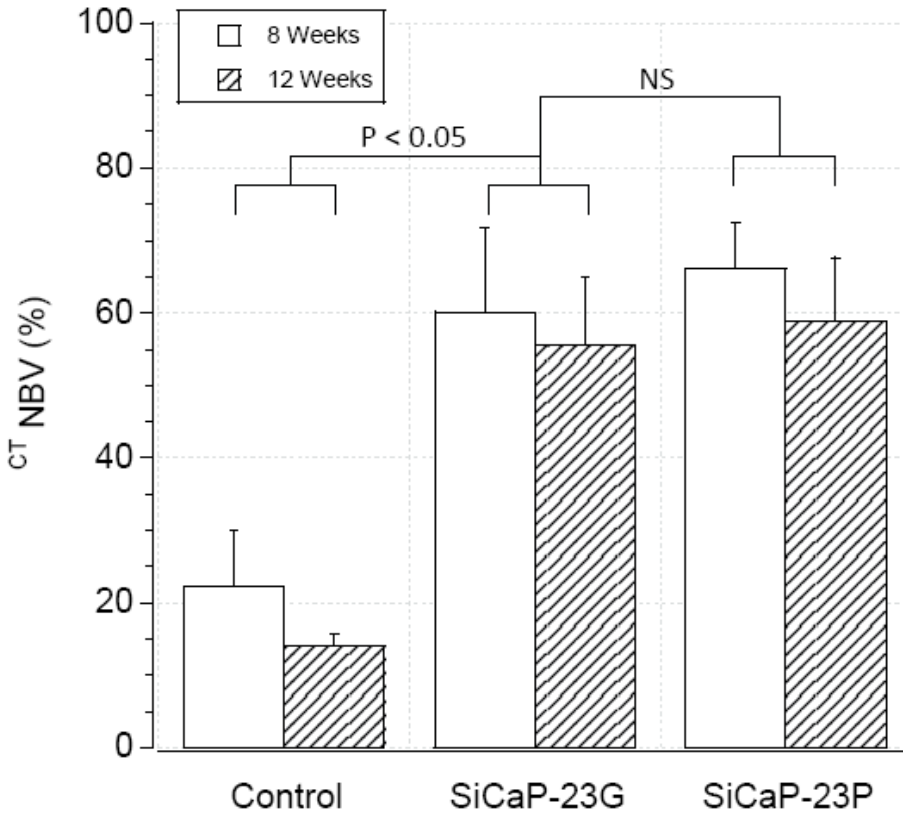

Figure 7-12 Mean percentage normalised bone volume (micro CT) for SiCaP-23G and SiCaP-23P over 12 weeks

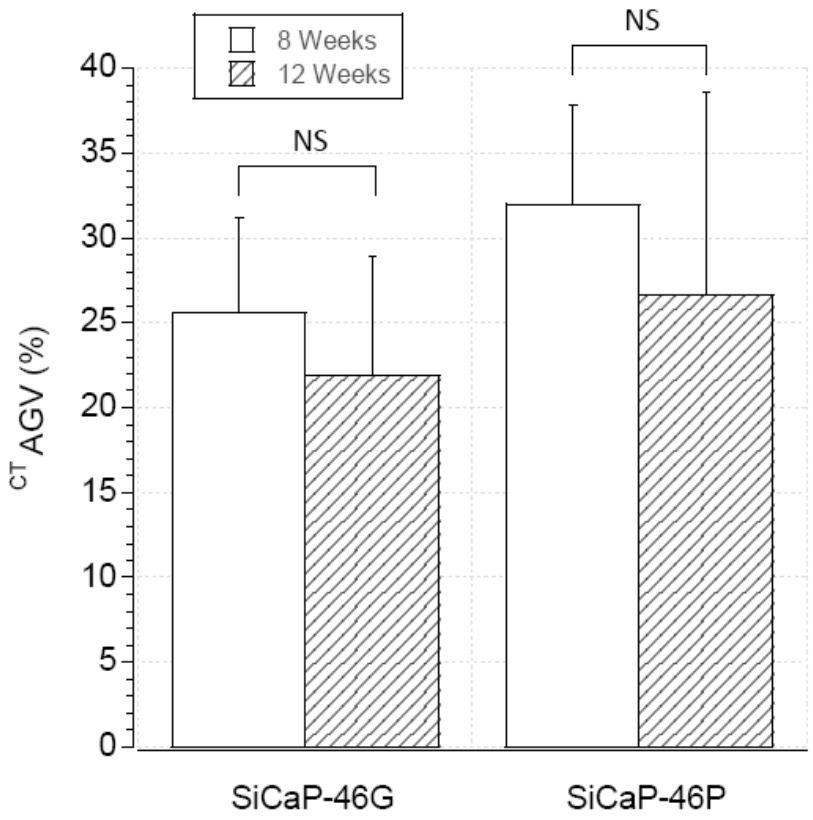

Figure 7-13 Mean percentage absolute graft volume (micro CT)
For SiCaP-46G and SiCaP-46P over 12 weeks

7.4 Discussion

Synthetic bone graft substitutes are utilised for a number of indications including spinal fusion procedures. The various synthetic bone graft substitutes available for clinical use appear to differ somewhat in their bone forming properties (Patel, Brooks et al. 2005, Hing, Wilson et al. 2007). The physiochemical properties of these materials appear to be critical to the potential for osteogenesis observed under pre-clinical settings. For example, in previous studies, we have highlighted the importance of silicate ion incorporation into a hydroxyapatite scaffold (SiCaP) on the bone forming properties of synthetic bone graft substitutes (Patel, Brooks et al. 2005, Samizadeh, Coathup et al. 2007). In this study, we evaluated how the strut porosity of the scaffold material may affect the osteogenic response of synthetic bone graft substitutes. We modified the strut porosity of SiCaP and determined the osteogenic properties (or capacity) of six SiCaP test materials in the ovine cancellous defect model. The critical defect model represents controlled injurious environments

that preclude spontaneous healing by physiologic repair processes that are ideal for testing the *in vivo* properties of synthetic bone graft materials (Schmitz and Hollinger 1986, Hollinger and Kleinschmidt 1990). The ovine model has been used successfully in other studies to assess the osteogenic capacity of calcium phosphate-based implants (Simmons 1976 , Patel, Brooks et al. 2005). The rationale for selecting this model was based on the similarity between bone metabolism in sheep and that in humans (Staller, Richardson et al. 1995) and the fact that sheep support their body weight post surgery on treated limbs (Nunamaken 1998, Flautre, Delecourt et al. 1999), and the size of the animal permits the creation of a practically-sized defect (Patel, Best et al. 2002). We made metaphyseal defects in the medial femoral condyle as this site bears more weight and so would be expected to encourage mechanical stimulation around the implant, thus encouraging bone ingrowth and remodelling. The site is also physiologically challenging since it is only constrained at the lateral aspect by a loose muscle fascia and thus also tests for graft migration from the defect.

The findings from Study A supported previous validations of this model as a critically-sized defect model, where spontaneous bone formation did not occur in untreated (control) defects over the study time period and demonstrated that both SiCaP-23 graft materials were osteogenic. Study B was conducted to compare the influence of varying levels of strut porosity on the osteogenic properties of SiCaP synthetic bone graft substitutes and to also evaluate the effect of increasing strut porosity on graft degradation or resorption over the study time period of 12 weeks by assessing graft volume at 8 and 12 weeks post implantation of the most porous test materials. None of the formulations investigated displayed any histological evidence of osteolysis, nor did the most porous formulation (SiCaP-46G and SiCaP-46P) show a significant level of degradation over the test period, although a slight trend in graft resorption was noted (Figure 7-13).

Our findings are in agreement with previous observations that the level of strut porosity markedly affects the post-implantation response in porous HA scaffolds (Hing 2004b, Hing, Annaz et al. 2005)and Habibovic and co-papers!. The combined findings from Study A and B support the concept that the phase pure SiCaP scaffold is osteogenic. Increasing the strut porosity of the scaffold appeared to promote bone apposition (percentage ^{HISTO}ABV) without significantly affecting the stability of the graft (percentage ^{CT}AGV). There was little evidence of excessive inflammation, osteolysis or other tissue reactions that could have adversely affected the success of the graft. In previous studies investigating the effect of calcium phosphate cements

implanted in an ovine model reported the formation of fibrous capsules around the site of implantation thus impeding repair (Annaz, Hing et al. 2004c). In contrast, there was no evidence of the formation of a fibrous capsule with any the formulations used in this study.

In terms of the mechanism(s) leading to enhanced bone formation with higher strut porosity (32%–46%), it is possible that increasing the permeability of struts within the scaffold increased physical accessibility of nutrients to support infiltration and proliferation of cells. An increase in surface area may also have affected the overall protein binding capacity, thus promoting osteogenic protein adsorption and cell anchorage that could lead to more rapid bone apposition (McFarland, Thomas et al. 2000, Hing, Annaz et al. 2005). The protein species that are adsorbed to the graft immediately on implantation and the subsequent change in structural conformation are critical in promoting osteogenic cell attachment (Green, Davies et al. 1999, Guth, Campion et al. 2010a), spreading (Rouahi, Champion et al. 2006), proliferation (Kilpadi, Chang et al. 2001) and morphology (Rouahi, Gallet et al. 2006). Establishing the cellular and micro environmental infrastructure for subsequent neovascularization is accepted as an essential precursor step prior to successful and sustained bone apposition (Stevenson, Emery et al. 1996).

Histological assessment showed that the patterns of *in vivo* tissue responses to all the test materials were similar, all exhibiting the formation of a neo-vascular network, centripetal bone growth and direct bone apposition. The magnitude of the tissue response depended on the levels of strut porosity. Evidence suggests that the more rapid and greater degree of vascularisation seen in the test materials with increased strut porosity (32%–46%) facilitated an increase in volume of new bone tissue ingrowth into the graft at 8 weeks. It was, however, difficult to differentiate further between the test materials (32% versus 46%) or the carrier (microgranules or aqueous poloxamer). Further evidence that increased strut porosity enhances the osteogenic capacity of the graft material was observed at 12 weeks where, although thicker layers of mineralised bone was more prominent for all graft materials compared with that at 8 weeks, a higher strut porosity (32%–46%) was associated with a larger area of more mature bone tissue in contact with the graft.

These findings indicate that all test material-treated sites had achieved an equilibrium level of bone formation throughout the defect site by 12 weeks, i.e. the volume of bone within the defect had reached a dynamic steady state, as modulated by the combination of local host and graft-related environmental and biomechanical

factors (Hing, Best et al. 2004, Hing, Annaz et al. 2005, Hing, Revell et al. 2006). However, the equilibrium level of absolute bone volume was greater in both 32% and 46% strut porosity grafts, moreover, evidence of earlier neo-vascularisation and greater levels of bone-graft contact suggested more rapid attainment of an equilibrium bone volume within these more microporous grafts, as has previously been observed with stoichiometric HA (Hing, Annaz et al. 2005). Augmentation (both temporal and volumetric) of the dynamic healing processes would offer particular clinical benefits to patients with either conditions or under therapeutic treatments associated with impaired bone repair. In otherwise healthy patients, it may also reduce healing times. Clearly, further investigations are required to discover whether our *in vivo* findings can be extrapolated to a clinical setting.

7.5 Conclusions

In conclusion, bone formation in the critically-sized defect confirmed the clinically relevant osteogenic properties of a porous silicate-substituted (0.8 wt% Si) calcium phosphate bone graft substitute with a strut porosity of 23% when applied either as granules or in an aqueous poloxamer carrier. Increasing the strut porosity appeared to augment the osteogenic potential of the matrix in terms of encouraging earlier neovascularization and increasing the absolute equilibrium volume of bone growth within the graft.

Chapter Eight: Critical Review

With this research we tested the hypothesis that modifying the micron-scale physical structure of a hierarchical porous calcium phosphate based biomaterial influences its functional performance *in vitro*, which can be applied to improve its performance outcomes in ectopic and orthotopic treatment sites *in vivo*. In order to test this hypothesis the literature was examined, computational models were applied, experimental tests were performed, and clinically relevant research models were executed. The outcomes of which are perhaps best examined in totality by asking the following four questions:

1. Does changing the micron-scale physical properties of calcium phosphate biomaterials change their physiochemical response to acellular tissue fluids and is this relevant to biological performance in vivo?
2. Do computational finite element analysis models correspond to empirical studies of calcium phosphate biomaterial physical properties and can they be used to predict cellular responses in vitro and in vivo?
3. Is osteoinductivity a suitable predictor for orthotopic performance of calcium phosphate biomaterials?
4. Are we any closer to understanding the mechanisms leading to osteogenic potential in calcium phosphate biomaterials?

In the following sections these questions will prompt a discussion of the prior art in respect of this research, an examination of the relevance of the outcomes to the research hypothesis, an assessment of the novelty of the work, and lastly proposals for future research in the field.

8.1 Does changing the micron-scale physical properties of calcium phosphate biomaterials change their physiochemical response to acellular tissue fluids *in vitro* and is this relevant to biological performance *in vivo*?

The propensity for the formation of either HA or OCP as a continuous, un-broken layer over the implant surface immediately after implantation into bone is in theory likely to be significant to the processes of osteointegration; the greater the surface area covered by this layer the better the opportunity for interdigitation with host bone. In practice this assumption is still under debate as the *in vivo* studies in support

of the outcomes of the bioactivity test are often contradictory. Many researchers have suggested a primary factor in the formation of bone in ectopic implantation sites is the ability of the material to form a bone-like-apatite on its surface once *in situ* (Yang, Yuan et al. 1997, Yuan, Yang et al. 1998, Yuan, De Bruijn et al. 2001a, Barrere, van der Valk et al. 2003, Le Nihouannen, Daculsi et al. 2005, Habibovic, Sees et al. 2006). These groups have suggested, as a direct result of their findings, that a calcium phosphate phase with a greater propensity to chemically dissolve, such as beta-tricalcium phosphate (as compared hydroxyapatite), will more readily form a bone-like-apatite on its surface and therefore lead to a greater level of stem cell differentiation either directly through an interaction between the stem cells and the apatite surface or indirectly by forming a layer which will more preferentially adsorb circulating bone morphogenetic proteins. Most of these groups have also linked the surface area contributed to by microporosity as being influential in the subsequent formation of an apatite-like layer. Thus overall with these two material parameters (dissolution profile and surface area) combined an HA with a low surface area will have a much lower propensity to form a bioactive layer than a tricalcium phosphate with a high surface area.

In our study we examined the formation of HCA on materials of varying strut-porosity (23%; 32%; 46%) and chemistry (SiCaP and beta tricalcium phosphate). Formation of HCA was noted on all four of the test materials. The rates of formation and quantities of HCA varied among different materials. Under the conditions of the test, the fastest rate of HCA growth was observed on SiCaP-32 and SiCaP-46 followed by SiCap-23. The quantity of HCA formed on the beta tricalcium phosphate surface was much lower than the other three test materials. These results indicate that the strut-porosity of a material substrate should be increased to maximise the potential for formation of a precursor to bone-like apatite after implantation in osseous defects and further confirms previous reports that beta-tricalcium phosphate is much less bioactive than silicate-substituted hydroxyapatite. These results appear, in part, to contradict the theory that a layer of a precursor to bone-like apatite is a prerequisite to ectopic bone formation. Beta tricalcium phosphate is reported to have a low bioactivity (Huan and Chang 2007, Hesaraki, Safari et al. 2009, Ni and Chang 2009), yet has been claimed to have a high osteoinductive potential (Yang, Yuan et al. 1997, Yuan, Yang et al. 1998, Yuan, De Bruijn et al. 2001a, Barrere, van der Valk et al. 2003, Le Nihouannen, Daculsi et al. 2005, Habibovic, Sees et al. 2006).

Moreover, we found in our studies of osteoinductivity abundant levels of bone in

direct contact with phase pure silicate-substituted calcium phosphate with no obvious signs of a boundary layer or dark line between the silicate-substituted calcium phosphate and the newly formed bone. The zone of integration appeared to be continuous from the synthetic phase to the physiological phase of mineral. In this part of our study the pre-requisite for a bone-like apatite to form on the surface in order for bone formation to take place was not apparent.

A large volume of scientific work investigating the bioactivity of biomaterials has preceded this study but only a handful of studies have used the assay described by Kokubo et. al. in 1990 as a means for comparing the impact of microstructure on the bioactivity of biomaterials and few had specifically investigated the effects of chemistry *and* structure on the bioactivity of porous calcium phosphate bone graft substitutes. In this respect our study was novel, however no new techniques for characterisation were developed during the course of our experimentation. The limitations of our own studies of bioactivity were that the test was performed under static conditions and that submersion was performed in simulated body fluid without the addition of the proteins that one would expect the biomaterial to be exposed to *in vivo*. Both of these experimental conditions may have elicited a modified response in bioactivity from the test materials. Future studies should consider the use of dynamic conditions and the use of serum-based simulated body fluids.

In summary, we found that the bioactivity of a calcium phosphate based biomaterial, that is the propensity of the material to form a layer of a precursor to a bone-like apatite on its surface after submersion in simulated body fluid, is influenced by the structure and chemistry of the biomaterial. This is a novel finding, however, we found no evidence that this dictated the subsequent biological performance in orthotopic and ectopic implantation sites *in vivo*.

8.2 Do computational finite element analysis models correspond to empirical studies of calcium phosphate biomaterial physical properties and can they be used to predict cellular responses *in vitro* and *in vivo*?

To characterise the mechanical properties of hierarchical porous silicate-substituted calcium phosphate we used a “Jenike” or “cam shear” testing rig which has previously been used by researchers to characterise the shear properties of allograft bone (Bolland, Partridge et al. 2006). This mechanical testing revealed porous silicate-substituted calcium phosphate to have similar mechanical behaviour to

morcellised cancellous bone under similar test conditions. Moreover, we discovered through the creation of novel 3D FEA models that bone grafts such as silicate-substituted calcium phosphate appear to be stress-shielded when applied in typical applications such as a tumour defect void or in a posterolateral spinal fusion defect. Previous research has used mechanical testing in combination with finite element analysis to predict the behaviour of bone grafts in clinical applications such as for impaction grating of uncemented femoral hips (Wong, New et al. 2005, Bolland, Partridge et al. 2006, Tilley, Bolland et al. 2006, Bolland, Tilley et al. 2007, Bolland, New et al. 2008, Leung, Browne et al. 2008, Dopico-Gonzalez, New et al. 2009, Dopico-Gonzalez, New et al. 2010) and in the spine for posterior lumbar interbody fusions (Zander, Rohlmann et al. 2002), but this is the first time, to this authors knowledge, that this combined approach has been used to study the expected mechanical environment experienced by a bone graft following implantation in an instrumented posterolateral fusion site in the lumbar spine. The fact that the graft is shielded to the extent that it is only exposed to stresses close to 22kPa is an interesting one. Immediately after implantation this would be advantageous to a certain extent, as the surgeon would want the spinal motion segment to be mechanically stable for as long as the fusion mass is remodelled to mature bone, and this can only be achieved by the implanted metalwork. However, from a bone remodelling consideration this low level of stress may in fact cause slower than desired bone formation according to Wolff's law. There exist a vast array of technical and engineering solutions to stabilising a spinal motion segment following posterolateral fusion, with tens of commercial systems being available across the world. Our model could find use in the future as a tool to determining the stresses experienced by a bone graft in posterolateral fusion dependent upon the design of the metalwork implanted alongside it for immediate post-operative motion segment stability.

There were limitations to the present model, as it did not take into account the stress-dependence of the Young's modulus of the silicate-substituted calcium phosphate. An improved model would include a treatment of this behaviour. While in the femur model stresses were sufficiently low compared to those in the surrounding bone that changes in the Young's modulus of the silicate-substituted calcium phosphate as a result of the imposed stresses could be neglected, this might not be the case where the silicate-substituted calcium phosphate would be expected to carry greater loads, for example if it were considered for use in impaction bone grafting in joint replacement. An improved material model could in these cases be essential. Furthermore, *in vivo*, the spine is subject to a wide variety of loading conditions

reflecting the wide variety of daily activities. In the present study only one load case has been considered. Further load cases to simulate the effects of a greater range of activities, for example flexion-extension, lateral bending, axial torsion should be considered to more fully characterise the mechanical environment of the silicate-substituted calcium phosphate in clinical application. Lastly, the effects of soft tissue constraint on the silicate-substituted calcium phosphate have not been included. An improved model would take the effects of soft tissue constraint into account. This could be implemented either by applying pressure loads to the silicate-substituted calcium phosphate surface (simpler but cruder) or by explicitly modelling the soft tissues (more complex and computationally expensive but potentially more realistic).

We also learned through the use of novel 2D Planar FEA models that there is an inverse exponential relationship between porosity and Young's Modulus that is similar to that described for trabecular bone and hydroxyapatite materials in previous studies (Akao, Aoki et al. 1981a, De With, van Dijk et al. 1981, Linde, Norgaard et al. 1991, Arita, Wilkinson et al. 1995, Rho, Hobatho et al. 1995, Liu 1998, Charriere, Terrazzoni et al. 2001, Patel 2003). Our experimental results were in agreement with our 2D-Planar finite element analysis model and with values predicted using empirically derived model equations from two previous research studies for trabecular bone (Linde, Norgaard et al. 1991, Rho, Hobatho et al. 1995). There was less agreement (usually an under-prediction) between our own results and with previous studies of calcium phosphate materials (Akao, Aoki et al. 1981a, De With, van Dijk et al. 1981, Arita, Wilkinson et al. 1995, Liu 1998, Charriere, Terrazzoni et al. 2001), although there was good agreement to an indenter study of a similar silicate-substituted calcium phosphate material (Patel 2003). These outcomes suggest that it is important to use mechanical testing of investigative materials wherever possible in building finite element analysis models. The difference between our own data and that of previous studies could be explained by the difference in manufacturing methods used to produce the test materials (e.g. slip casting versus uniaxial pressing of HA powders) or by variations in the way in which the samples were mechanically tested (e.g. uniaxial compression versus ultrasonic or shear rates of $0.03s^{-1}$ versus a shear rate of $0.001s^{-1}$). The limitation of taking a 2D Planar approach is that a three dimensional model will always show greater inter-particle connectivity and therefore be stiffer, and perhaps more accurate, than the two-dimensional model. Future studies may improve on the accuracy of FEA modelling of silicate-substituted calcium phosphates by taking a 3D approach.

The finite element analysis model was very insightful when it came to visually

comparing the relative stress distributions in the micron-scale structure as a result of the application of load to the test materials. We learned that the distribution of von Mises stress for materials with low porosity was relatively uniform throughout the micron-scale structure but higher porosity led to stress-risers at the point of pore-pore boundaries. We were not able to investigate the likely stress-distributions under physiological loading due to time constraints during the study; however, this analysis could prove significant in determining the variation in stress experienced by cells at a micron-scale. Based on all of the research highlighted in the survey of literature provided in Chapter 2, this FEA model could prove useful in comparing the relationship between known levels of stress activation in osteocytes, as determined through empirical cellular studies, and the predicted stress in the region of cell attachments as a result of substrate strain at a micron scale after a substrate is loaded with a physiologically representative load pattern. An alternative and extremely novel approach, which this author is keen to investigate in future studies, would be to run similar FEA analysis of histological images in which osteoblasts and osteocytes are clearly identifiable, such as those in Chapter 7. This would permit the comparison of cell location and morphology with the points of likely stress concentration within the construct.

In summary, we found that computational 2D Planar and 3D finite element analysis models do correspond with empirical data, albeit with some discrepancy likely due to manufacturing process and analysis technique variations. We have put forward several ideas as to how these models might be used to predict *in vitro* and *in vivo* behaviour of silicate-substituted calcium phosphate biomaterials. For our own purposes these models have shown that our experimental materials behave similarly to trabecular bone of a similar porosity and that the stress distribution within the micro-scale structure does vary considerably with porosity.

8.3 Is osteoinductivity a suitable predictor for orthotopic performance of calcium phosphate biomaterials?

Our research was not the first to perform concurrent ectopic and orthotopic models for calcium phosphate based biomaterials (Urist 1965, Pollick, Shors et al. 1995, Yuan, Li et al. 2000, Habibovic, Yuan et al. 2006, Yuan, van Blitterswijk et al. 2006a, Li, Habibovic et al. 2007, Habibovic, Gbureck et al. 2008, Habibovic, Kruyt et al. 2008, Cheng, Ye et al. 2009, van Gaalen 2009). Urist found a good agreement between his ectopic (Rectus abdominus) and orthotopic (ulna defect) results for demineralised rabbit bone (Urist 1965). In that study incidence of bone formation

was 98% in ectopic sites and 90% in orthotopic sites. Pollick et al., were the first group to use quantitative histomorphometric techniques to compare the results from ectopic (vastus lateralis & subcutaneous sites in the dorsum) and orthotopic (lateral femur) implantation sites (Pollick, Shors et al. 1995). In their study bone was observed in all defects but there was considerably more bone in the orthotopic sites than in the subcutaneous sites, and more in the subcutaneous sites than in the intramuscular sites. The outcomes were similar when measuring both bone area and bone contact. This is in contrast to more recent studies which have generally noted a higher level of bone in intramuscular sites compared to subcutaneous sites (Habibovic, Sees et al. 2006). Yuan et al., compared the bone formation of biphasic calcium phosphate and hydroxyapatite in ectopic and orthotopic sites in dogs over a long time period (up to 360 days) (Yuan, van Blitterswijk et al. 2006a).

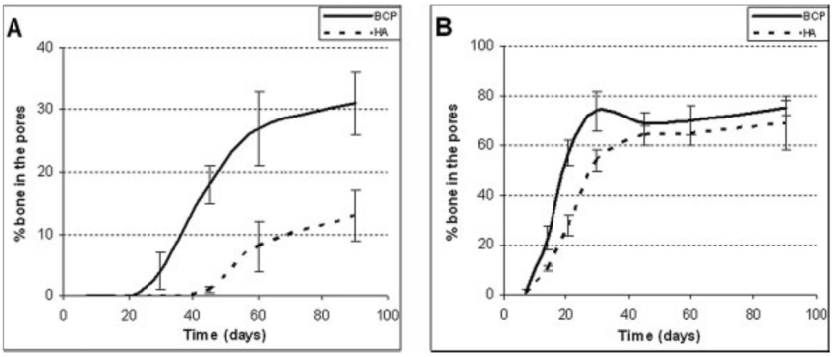

Figure 8-1 Bone area (%) in biphasic calcium phosphate (BCP) and hydroxyapatite (HA) after implantation in muscle (A) and bone (B). Faithfully reproduced from (Yuan, van Blitterswijk et al. 2006a)

In their study Yuan et al., found agreement between the performance of the test materials in ectopic and orthotopic sites in terms of bone incidence, but not in terms of time to bone formation or resultant bone area in the defects (Figure 8-1). We observed very similar behaviour for our own test materials. For comparison the data described in Chapters 6 & 7 has been adapted and is provided below in Figure 8-2. In both studies a latent period exists before bone formation begins in the ectopic sites as compared to the orthotopic sites. However, the amount of bone in the ectopic and orthotopic sites in our study better converges at the final endpoint for implantation compared to the findings of Yuan et al. The existence of this artefact is of interest, since it elucidates to the mechanisms behind osteoinductivity, however these will be discussed in the following section. For this discussion it is noteworthy that there is a discrepancy between ectopic and orthotopic implantation sites and this should be

understood and appreciated by researchers prior to using ectopic data to predict osteogenic potential in orthotopic application.

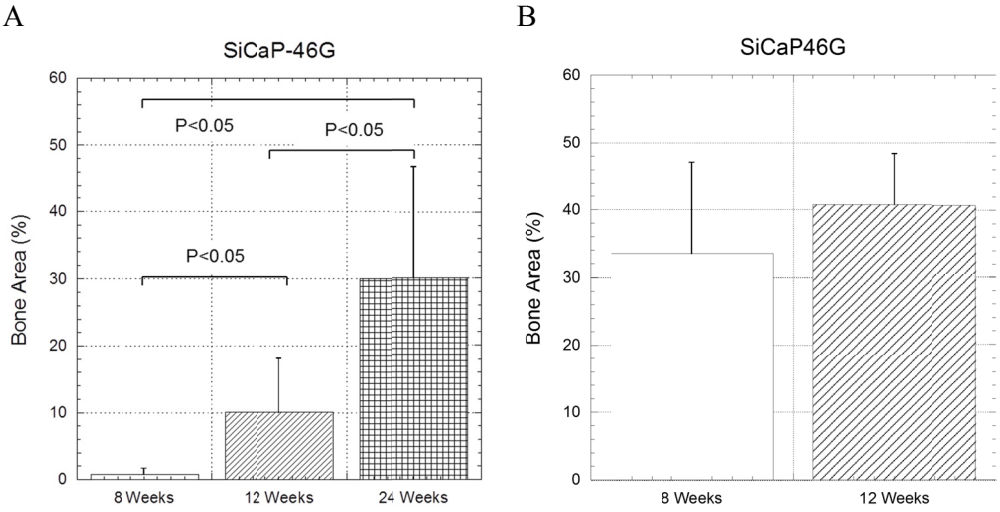

Figure 8-2 Bone area (%) in silicate-substituted calcium phosphate after implantation in muscle (A) and bone (B). Adapted from (Campion, Chander et al. 2011)

Habibovic et al., reported correlating ectopic (intramuscular) performance to orthotopic (iliac crest) sites in a study in goats (Habibovic, Yuan et al. 2006). However, this was only statistically significant in the central zones of the orthotopic sites. In their study the two test groups were claimed to have been of the same macroporosity based on terms of volume fraction. However, on review of the micrographs it appears that test group which faired less favourably in the orthotopic central zones was of a more closed porous structure relative to the test group that elicited greater amounts of bone. This would be expected to reduce the amount of osteoconduction in central regions. Nevertheless the same research group have since repeated similar studies for different test materials and demonstrated a link between osteoinductivity and orthotopic performance in goats (Habibovic, Gbureck et al. 2008, Habibovic, Kruyt et al. 2008).

Interestingly the most recent study to compare ectopic and orthotopic outcomes did not find much correlation between the two implantation sites. Indeed this research group found that the test materials they studied did form bone in the ectopic (paraspinalis) sites but not in the orthotopic (decorticated posterolateral fusion) sites (van Gaalen 2009). However, the authors proposed that the mobile setting of the posterolateral spine (the fusion was non-instrumented with intact facet joints) in comparison to the solidly enveloped area intramuscularly in addition to the relatively loose packing of cell- seeded constructs could be part of the explanation for the

approximately 100-fold difference in bone scaffold contact length between the two locations.

There were limitations in our researching of the ectopic and orthotopic performance of silicate-substituted calcium phosphate. For example, our orthotopic study did not extend to the full 24 weeks studied for ectopic outcomes. In addition, both studies involved implanting multiple test groups within a single test subject. This is the only ethically acceptable approach to performing such studies but does provide a confounding variable, particularly for ectopic studies in which the exact mechanisms of osteoinductivity have not yet been elucidated. There is a very small chance that systemic effects caused in one implantation site lead to an over estimation or underestimation of osteogenic potential in an adjacent defect site. This would be particularly likely if, for example, the inflammatory system was discovered to have a significant role in osteoinductivity. Despite these limitations, from the data presented above and in the preceding chapters it seems reasonable to assume that osteoinductive propensity is indeed a marker for expected orthotopic performance. The rate of onset of bone formation and the eventual amount of bone formation does vary between ectopic and orthotopic defect sites for a given material, but on the whole our own research and the research of others teaches us that if a material forms bone in an ectopic implantation site it is more likely to lead to successful healing in an orthotopic site than a material which does not form bone in ectopic sites.

8.4 Are we any closer to understanding the mechanisms leading to osteogenic potential in calcium phosphate biomaterials?

It's at this point that this author wishes he were studying for a doctorate in the study of logic, since with so many confounding variables across the studies, both in the literature and in our own research, it is challenging to pull out common threads of data which can irrevocably substantiate the mechanisms behind biomaterial-derived osteoinductivity. Several authors have attempted to decipher the plethora of proposals in the literature but none have achieved the ultimate goal. Several logical arguments will follow which are based on the review of the literature and the observations of our own empirical research:

- **Osteoinductivity is dependent on the species of the test subject.** A common theme is apparent in the literature: osteoinductivity of calcium phosphate biomaterials is more frequently observed in larger animals, such as rabbits; dogs; and goats, than in smaller animals, such as rodents (Urist 1965,

Urist and Strates 1971, Piecuch 1982, Heughebaert, LeGeros et al. 1988, Okumura, Ohgushi et al. 1991, Ripamonti 1991, Yang, Yuan et al. 1996, Gosain, Song et al. 2002, Daculsi 2004, Yuan, van Blitterswijk et al. 2006b, Bodde, Cammaert et al. 2007, Li, Habibovic et al. 2007).

- **Osteoinductivity is dependent upon the strain of the test subject.** In a recent study the investigators screened mice from 11 different inbred mouse strains for their responsiveness to subcutaneous implantation of osteoinductive tricalcium phosphate (TCP). In only two strains (FVB and 129S2) the ceramic induced bone formation, and in particularly, in FVB mice, bone was found in all the tested mice (Barradas, Yuan et al. 2011).

- **Osteogenic materials i.e. those containing a cellular component tend to be more osteoinductive.** Cell-seeding can increase osteogenic potential of calcium phosphate based materials (Ohgushi and Okumura 1990, Ohgushi, Okumura et al. 1990, Okumura, Ohgushi et al. 1991, van Gaalen 2009) and non calcium phosphate based materials (Li, Habibovic et al. 2007).

- **Microporosity plays a fundamental role in osteoinduction.** This is demonstrated by studies in which authors report no bone formation for non-porous materials whereas bone is observed in equivalent constructs containing microporosity (Yuan, Yang et al. 1998). Recent studies have demonstrated that the size and morphology of the surface substructure are critical parameters to osteoinduction (Davison, Luo et al. 2014, Zhang, Barbieri et al. 2014, Zhang, Luo et al. 2014).

- **Ectopic bone formation tends to occur via the intramembranous route and in a centripetal diction to the pore surface, although not exclusively so:** (Yuan, Kurashina et al. 1999, Yuan, De Bruijn et al. 2001a, Yuan, de Bruijn et al. 2001b, Yuan, Yang et al. 2001, Habibovic, Yuan et al. 2005, Habibovic, Sees et al. 2006, Habibovic, Yuan et al. 2006, Yuan, van Blitterswijk et al. 2006a, Habibovic, Gbureck et al. 2008, Habibovic, Kruyt et al. 2008). In our study In all treatment groups both intramembranous and endochondral bone formation were observed, often in very close proximity to one another. Endochondral bone formation tended to occur in intra-granular spaces within the graft, whereas intramembranous bone formation tended to be closely associated with the surfaces of the graft.

- **Anoxia and vascularisation is not always a determining factor in osteoinductive bone formation.** As we observed both intramembranous and endochondral bone formation in very close proximity to one another, we propose anoxia or vascularisation was not always a factor in determining the mechanism of bone formation. Furthermore, recent studies in which TCP was implanted subcutaneously in FVB strain mice with and without local treatment of VEGF demonstrated there to be very little direct effect of the application of VEGF on the incidence of bone formation or the amount observed in the graft (Barradas, Yuan et al. 2012).

- **Osteocytes are likely to be involved in osteoinductivity.** We observed cells of the osteocyte morphology colonising the microporosity of the graft. This lacunar-canalicular-like porosity might potentially allow for the recruitment of new osteoblasts with anabolic paracrine factors excreted in the extracellular matrix by osteocytes, the mechanosensing cells of bone (Sikavitsas, Bancroft et al. 2003).

- **Bone formation in ectopic sites does not begin until week 8 post-implantation in larger animals**. In the literature there is very little or no bone observed in test article treated defects within 21 days (Eid, Zelicof et al. 2001) or 8 weeks (Piecuch 1982, Ohgushi and Okumura 1990, Ripamonti 1996) of implantation. However, bone is generally observed in other studies at later time-points, including: 3 months (Ripamonti 1991, Yang, Yuan et al. 1996, Yuan, Kurashina et al. 1999); 4 months (Pollick, Shors et al. 1995); 5 months (Yuan, De Bruijn et al. 2001a); 1 year (Gosain, Song et al. 2002, Fujibayashi, Neo et al. 2004); and 2.5 years (Yuan, Yang et al. 2001).

- **Macrophages may play a role in osteoinductivity but are not the sole initiators of the process.** In our study there was a complete absence of bone in regions of the defect where there was considerable scaffold degradation. It may be that these cells do play a role in ectopic bone formation but our study suggests that this is counteracted in the most severe cases of graft degradation through another process. Furthermore, unlike Le Nihouannen and many other researchers, we found endochondral bone formation as well as intramembranous bone formation, often in close proximity to one another, thus demonstrating that not only a macrophage-induced inflammatory trigger for stem cell differentiation is responsible for bone formation in ectopic defects.

- **The formation of a precursor to bone-like-apatite is not a prerequisite to osteoinductive bone formation.** Perhaps the best evidence for this is a study in which macroporous Bioactive glass (45S5) was implanted into the thighs of dogs wherein bone was found throughout the graft but more preferably in regions where an apatite-like layer was *not* present (Yuan, de Bruijn et al. 2001b). In addition, the same researchers have reported a high-level of osteoinductivity for pure beta-tricalcium phosphate (Yuan, Fernandes et al. 2010) despite beta-tricalcium phosphate having been found previously to have a very low propensity to form a bioactive layer of bone-like apatite on its surface (Huan and Chang 2007, Juhasz, Best et al. 2008, Hesaraki, Safari et al. 2009, Campion, Ball et al. 2013).

After summarising the key facts in the story of biomaterial-derived osteoinductivity it becomes clear that there is one common thread to these logical scenarios: the fundamental needs of cells, in particular pre-osteoblasts; osteoblasts; osteocytes; and osteoclasts. What seems the most logical explanation for species-dependency, strain-dependency, and anatomical dependency of osteoinductivity is the number of circulating stem cells available for the colonisation of the graft. The fact that in orthotopic sites most bone is formed within 8 weeks whereas in ectopic sites bone is not formed until 12-24 weeks points heavily towards a cellular influence on proceedings, as does the fact that pre-seeding biomaterials with osteoprogenitor cells also gives the process a kick-start. The role of macrophages, surface apatite, anoxia/hypoxia environments, VEGF, BMP, and substrate nano-structure are likely to be secondary to the fundamental need of circulating stem cells, which is to find a structure on which to attach and differentiate. The impact of various microstructures is well described in the literature and in our research. However, what isn't described is a study of the availability of circulating stem cells in various species of test subject and anatomical locations within those subjects. Further work should investigate the availability of circulating stem cells in osseous and non-osseous tissues within a variety of species, including humans.

Our research has provided us with some novel insight into the role of physiochemical parameters on the osteogenic of calcium phosphate biomaterials. We have learned that the propensity to form a precursor to bone-like apatite on its surface is a low driver for osteoinductivity. We have also reported for the first time, as far as this author can discover, the presence of both intramembranous and endochondral bone formation alongside each other in an ectopic site following

implantation of a calcium phosphate based biomaterial. We have also observed the presence of osteocytes deep inside the microporosity of biomaterials implanted in ectopic sites.

8.5 Concluding remarks

With this research we tested the hypothesis that modifying the micron-scale physical structure of a hierarchical porous calcium phosphate based biomaterial influences its functional performance *in vitro*, which can be applied to improve its performance outcomes in ectopic and orthotopic treatment sites *in vivo*. Our research has confirmed our hypothesis; small changes in the micron-scale structure of silicate calcium phosphates can have a big impact on their osteogenic potential, which can be successfully predicted using *in vitro* and ectopic *in vivo* models.

After having traveled a significant journey over the last eight years, perhaps what emanates in my own mind as the bigger question at stake is: *how relevant is it to use ectopic animal models to predict orthotopic outcomes in humans?* We have discovered through analysis of the literature that a variety of osteoinductive bone grafts are commercially marketed around the world. The claims for these products are supported through the use of *in vitro* and *in vivo* tests, which are conducted for every batch sold. However, the tests conducted tend to be performed in small animals such as mice or rats (Bacterin , Etex , Synthes , Zhang, Powers et al. 1997b, Zhang, Powers et al. 1997a, Edwards, Diegmann et al. 1998, Coulson and Lalor 2000, Takikawa, Bauer et al. 2003, Kay 2004, Honsawek, Powers et al. 2005, Boyan, Ranly et al. 2006a). This is in spite of other research studies, which demonstrate a substantial amount of species-related dependency when it comes to measuring osteoinductivity for a given material (Urist 1965, Ripamonti 1996, Yuan, van Blitterswijk et al. 2006b, Barradas, Yuan et al. 2012). It is not ethically viable to correlate human ectopic and orthotopic implantation performance prior to bone graft products being marketed. However, many of these commercially available products are now supported by published clinical data. It would benefit the clinical community if future studies investigated the correlation of osteoinductivity of these commercial products, as determined with *in vitro* and *in vivo* studies, with the reported performance outcomes *in vivo* in humans.

Appendix I: Literature for Mechanotransduction Studies

Table 9-1 A historical review of in vitro studies of fluid flow and mechanical strain –induced upregulation of fibroblasts, osteoblasts, osteocytes and osteoclasts

Author	Year	Cell type	Material type	Mechanical stimuli	Response	Observations
(Roelofsen, Klein-Nulend et al. 1995)	1995	Murine primary OPR and differentiated OB	Culture plate (PS)	Intermittent hydrostatic compression. Compression of CO2 gas phase in a closed chamber. Maximum pressure = 13kPa above ambient. Pulse frequency was 0.3Hz. The maximum pressure rate was 32.5kPa/sec. Controls were run in same chamber without IHC.	DNA content / AP activity / protein content	IHC did not affect the growth of OB's and OPR's as shown by DNA and protein content. IHC had no adverse effects on cell viability or proliferation. IHC increased AP mRNA levels. IHC upregulated COL-1 and actin expression in Obs
(Klein-Nulend, Semeins et al. 1995)	1995	Chicken calvarial osteocytes and fibroblast. Murine differentiated osteoblasts	Polylysine-coated glass slide	Pulsating fluid flow. 5Hz with a fluid shear stress of 0.5±0.02Pa and the peak shear stress rate 0.4 Pa/sec. Samples were analysed after 5,10,15,30,45,60 mins	NO production using Greiss reagent; PGE2 was measured sung enzyme immunoassay (EIA)	Purified Osteocytes produced higher basal and PFF-stimulated levels of NO than mixed bone cells; whilst Fibroblasts did not respond to flow at all. The characteristic osteocytic morphology is restored in vitro. PFF also increased PGE2 production. PGE2 production was delayed but continued throughout the hour whilst NO production was transient and only occurred for the first 5 mins.
(Klein-Nulend, van der Plas et al. 1995)	1995	Osteocytes, Osteoblasts, Fibroblasts derived from embryonic chicken calvariae	Culture dish	Intermittent hydrostatic compression. Compression of CO2 gas phase in a closed chamber. Maximum pressure = 13kPa above ambient. Pulse frequency was 0.3Hz. The maximum pressure rate was 32.5kPa/sec. Controls were run in same chamber without IHC / Pulsating fluid flow. 5Hz with a fluid shear stress of 0.5±0.02Pa and the peak shear stress rate 0.4 Pa/sec.	PGE2 / PGI2 production	For IHC Osteocytes responded by an increase in PGE2 after 6/24 hours and an increased PGI2 after 24hours. Osteoblasts only showed a significant increase after 6hours. Periosteal fibroblasts didn't respond at all. PFF stimulated release of PGE2 from Osteocytes but not from Osteoblasts or from fibroblasts. No effect was found for PGI2 in any cell group after PFF treatment. Osteocytes response was sustained 1hour after flow whereas Osteoblasts/fibroblasts did not respond after 5 mins after flow.
(Klein-Nulend, Roelofsen et al. 1997)	1997	Primary osteoblasts (OB) and proliferating and differentiating	Culture chamber	Intermittent hydrostatic compression. Compression of CO2 gas phase in a closed chamber. Maximum pressure = 13kPa above ambient. Pulse	Osteopontin	In 1o osteoblasts (OB) OPN expression decreased in the control but increased for the treatment group. OPN expression was higher in the differentiating culture than in the proliferating culture. The 44kDa type of OPN expressed

Author	Year	Cell type	Material type	Mechanical stimuli	Response	Observations
		M3T3-E1		frequency was 0.3Hz. The maximum pressure rate was 32.5kPa/sec. Controls were run in same chamber without IHC. 2 wks culture		during bone formation was observed. IHC upregulated OPN protein production in both differentiating and proliferating groups, but was most noticeable in the differentiated cell population. OPN is functional in cell adhesion.
(Pavalko, Chen et al. 1998)	1998	M3T3-E1	Culture chamber (Cytodyne, CA, USA)	Fluid shear stress using perfusion chamber (Cytodyne, CA, USA). 18ml/min equivalent to 12 dyn/cm2. 1hr treatment. 37C.	B-integrin ; A-actin ; Cox2 ; c-fos upregulation	Application of fluid shear induces development of actin stress fibers and formation of focal adhesions containing B-integrins and A-actinin. Osteoblasts upregulate Cox-2 and c-fos expression in response to fluid shear. Disruption of microfilaments with cytochalasin D inhibits fluid shear induced increases in Cox-2 protein expression. Microinjection of the integrin binding domain of a-actinin inhibits linkage of actin filaments to integrins and blocks fluid shear induced cytoskeletal reorganisation and gene expression.
(Sterck, Klein-Nulend et al. 1998)	1998	Mature human osteoblasts	Glass slide	Pulsating fluid flow 5Hz. Mean shear stress 0.7±0.03Pa with a peak shear rate of 12.2Pa/s. 1 hour treatment. 37C	NO production using Greiss reagent; PGE2 was measured sung enzyme immunoassay (EIA); TGF-ß1 measured by ELISA; Protein content	PGE2 release was marked after 24 hours post-incubation for the non-osteoporotic group. PFF did not induce PGE2 release in any of the 5 OP cultures. All OP donors were treated with Vit D which cannot be excluded from findings although the cell cultures had been growing for 4-5wks pre treatment so external factors were considered unlikely. NO production was increased whilst TGF-B1 was inhibited during treatment but increased after 3 days.
(Klein-Nulend, Helfrich et al. 1998)	1998	Mature human osteoblasts	Polylysine-coated glass slide	Pulsating fluid flow 5Hz. Mean shear stress 0.7±0.03Pa with a peak shear rate of 12.2Pa/s. 1 hour treatment. 37C	NO production was determined with Greiss reagent; RT-PCR for mRNA content; protein content	Mechanical stimulation of cells resulted in increased NO production. Maximum levels were detected after 5 mins indicating the presence of constitutive NOS activity. The ecNOS isoform of NOS was most active.

Author	Year	Cell type	Material type	Mechanical stimuli	Response	Observations
(Ajubi, Klein-Nulend et al. 1999)	1999	Chicken calvarial osteocytes	Glass slide	Pulsating fluid flow 5Hz. Mean shear stress 0.7±0.03Pa with a peak shear rate of 12.2Pa/s. 1 hour treatment. 37C	PGE2 with non-radioactive enzyme immunoassay system; DNA content	Cellular deformation as a result of fluid flow induced stresses leads to actin dependent opening of Ca2+ - permeable, gadolinium sensitive ion channel. Ca2+ influx near surface membrane stimulates PLC, which generates secondary Ca2+ responses from internal stores. DAG (byproduct of PLC) and Ca2+ activate PKC which enhances PLA sensitivity to Ca2+, leading eventually to increased AA release. This together with NO production mediated COX-2 activation leads to PG synthesis.
(Westbroek, Ajubi et al. 2000)	2000	Fetal chicken Calvarial OBMix; Osteoblasts; Osteocytes	Chicken osteoblast conditioned medium-coated glass slides	Pulsating fluid flow. 5Hz; shear stress 0.7±0.03Pa with a peak stress 12Pa/sec. 15 minute treatment	PGE2 with non-radioactive enzyme immunoassay system; PHGS-2 expression via DNA	Osteoblasts and Osteocytes do exhibit inducible PGHS-2 activity, therefore, observations made regarding effects of PFF are linked to mechanosensitivity of OB's and OCY's and not ability to express PGHS-2. OCY's are more sensitive to fluid shear stress than OB's, as measured by PHGS-2 expression. Klein-Nulend may have observed PGE2 expression in OB's due to presence of OCYs in the culture of the state of differentiation in the relatively mature neonatal murine cell culture.
(Joldersma, Burger et al. 2000)	2000	Mature human osteoblasts	Polylysine-coated glass slide	Pulsating fluid flow 5Hz. Mean shear stress 0.7±0.02Pa with a peak shear rate of 12.2Pa/s. 1 hour treatment. 37C	PGE2; PGI2; PGF2 were measured sung enzyme immunoassay (EIA) / COX-2 mRNA expression was measured with RT-PCR	PGE2 and PGI2 were upregulated following PFF treatment. PGF2 was upregulated for 1 hour only. Treatment with PFF increased COX-2 but not COX-1 expression. Shear stress-induced responses were independent of species and anatomical location. The levels of prostaglandin production varied significantly between donors and was related to the variation in osteocyte population numbers. A correlation analysis showed no relationship between age and bone cell sensitivity.
(Bakker, Soejima et al. 2001)	2001	Mature Osteoblasts	Polylysine-coated glass slide	Low PFF (3Hz; 0.39Pa; amplitude 0.12Pa; peak shear stress 2.26Pa/s) / Medium PFF (5Hz; 0.64Pa; amplitude 0.127Pa; peak shear stress 8.40Pa/s) / High PFF (9Hz; 1.20Pa; amplitude 0.37Pa; peak shear stress	NO production using Greiss reagent; PGE2 was measured sung enzyme immunoassay (EIA)	Bone cells respond to flow in a dose-dependent manner. Increasing viscosity also increases responses. Increasing the viscosity will simultaneously heighten the mean shear stress and the amplitude of the pulsatile shear stress - the exact mode of upregulation was not determined. Bone cells are sensitive to low flow rates (0.20±0.06ml/s)

Author	Year	Cell type	Material type	Mechanical stimuli	Response	Observations
				20.90Pa/s) / Dextran PFF (3Hz; 1.20Pa; amplitude 0.0.37Pa; peak shear stress 6.97Pa/s)		
(Di Palma, Douet et al. 2003)	2003	MG-63 Osteosarcoma cell line	HA Plasma sprayed Ti-4Al-4V discs. Ca/P 1.663-1.697/purity > 99%. Surface roughness 7.85±0.23µm; controls of Ti-4Al-4V and polystyrene. Gamma sterilised	piezoelectric induced strain for 15 mins 3 times a day for 1,3,5 days at 0.25Hz and 600µstrain	Cell number, cell adhesion and spreading and ALP were measured	Cellular adhesion takes longer (48 hours) but is more effective on rougher (HA group) surfaces than smoother (controls) surfaces. Mechanical regimen was important - short repeated deformations increased ALP after 5 days but not continuous 24 hours deformation. MG-63 cells expressed mechano-sensitivity by increasing differentiation not proliferation. Human osteoblasts responded in an opposite trend and so it was postulated that the state of confluence of the cells governs their response to mechanical strain
(Wang, Uemura et al. 2003)	2003	Bone Marrow Derived Osteoblastic cells (BMO) from rats. Primarily stromal cells	B-TCP (Olympus Optical, Japan). 75% porosity; pores 100-400um.Heat sterilised	Perfusion chamber (minucells, Germany). 2mL/h. 37C. 1,2,3,4 weeks	ALP activity and Osteocalcin content	ALP and Osteocalcin was increased in perfused samples compared to control (n=12 ; p<0.01)
(Sikavitsas, Bancroft et al. 2003)	2003	Marrow stromal rat Osteoblastic cells	Titanium meshes (Bekaert, Belgium) vol porosity of 86% and fibre diameter of 40µm. The average pore size was ~250µm.	Fluid flow @ 0.3ml/min. 37C	DNA / AP / Ca-deposition	Addition of dextran to the media increased viscosity and increased mineralised matrix deposition. AP was significantly higher for fluid sheared cells. Upregulation from a change in fluid shear stress modulated by viscosity and not flow rate indicates that the rate of chemotransport is not a factor in the upregulation of Osteoblastic cells in response to increased fluid shear.
(Bakker, Joldersma et al. 2003)	2003	M3T3-E1	Polylysine-coated glass slide	Pulsating fluid flow 5Hz. Mean shear stress 0.6Pa with a pulse amplitude of 0.3Pa and peak stress rate of 8.4Pa/s 37C	NO production using Greiss reagent; PGE2 was measured sung enzyme immunoassay (EIA)	Treatment with PTH without shear stress stimulated PGE2 production but not NO production. When PTH was added <1min before shear stress treatment it blocked NO production. PTH inhibits NOS (ecNOS) in bone cell production of NO.

Author	Year	Cell type	Material type	Mechanical stimuli	Response	Observations
(Nagatomi, Arulanandam et al. 2003)	2003	Mature rat osteoblasts	Polystyrene or etched glass	Cyclic pressure in the range 10-40kPa at 1Hz for 1 hour daily for 5,12,19 days.	Gene expression by RT-PCR; Total RNA; Collagen; Total DNA; Calcium	Expression of Transforming growth factor-ß1 mRNA was not different across the groups; total DNA was not different between groups. Amount of acid-soluble collagen and calcium in osteoblasts exposed to cyclic pressure was significantly higher after 19days culture.
(Bakker, Klein-Nulend et al. 2003)	2003	Murine and human mature osteoblasts	Polylysine-coated glass slide	Pulsating fluid flow 5Hz. Mean shear stress 0.6Pa with a pulse amplitude of 0.3Pa and peak stress rate of 8.4Pa/s 37C	PGE2 was measured sung enzyme immunoassay (EIA); Total RNA and protein; COX-1 and COX-2 Mrna	PGE2 was completely inhibited when COX-1 and COX-2 were blocked. PFF induced COX-2 mRNA expression. PGE2 production dependent on COX-2 not COX-1 expression. 1hour PFF stimulated COX-2 mRNA expression. COX-2 mRNA expression continued for 24 hours post=treatment
(McGarry and Prendergast 2004)	2004	Bone Derived Osteoblastic cells (BO) from Humans	Culture plate (PS)	Fluid shear stress (0.6±0.3 Pas; 5Hz) for 1hr in a laminar flow plate perfusion chamber / Substrate strain (1000µstrain; 1Hz) for 1 hr using 4-point bending apparatus	NO production using Greiss reagent ; PGE2 using enzyme immunoassay ; Collagen type I as measured by Western blot analysis. Wilcoxon signed rank test (NO/PGE2) and Linear model (Collagen type I)	FEA modeling revealed that fluid flow effected on all cell model components whereas strain only effected the cell attachments. Fluid flow (not strain) increases PGE2 due to upregulation of Cox2 and re-organization of actin. Mechanically induced NO production results from activation of ecNOS in the plasma membrane and is affected most by fluid-shear. Collagen production was upregulated by strain and not fluid shear. Applied strain induces cell behaviour associated with the Osteoblastic phenotype. Whereas, fluid-shear does not illicit responses of the osteoblast phenotype. Instead increased cell signaling molecules (NO/PGE2) are reported. Both of which are thought to be involved in osteocyte mediation.
(Bacabac, Smit et al. 2004)	2004	MC3T3-E1 Osteoblasts	Polylysine-coated glass slide	Fluid shear stress with a Parallel-plate flow chamber. Steady shear stress (0.70Pa) ; High/Low amplitude (0.70±0.31 / 0.70±0.70 Pa) AND High/Low frequency (5/9 Hz) shear stress and static controls were used.	NO production using Greiss reagent	Bone cell response to fluid shear stress is rate-dependent. Increasing amplitude or frequency without changing average stress enhanced NO production. NO production is rapid (<15mins). NO production is linearly dependent on the rate of fluid shear stress.

Author	Year	Cell type	Material type	Mechanical stimuli	Response	Observations
(Mauney, Sjostorm et al. 2004)	2004	Human Bone Marrow Stromal Cells	Bovine partially demineralised bone scaffolds	Four point bending induced strain. Mean tensile strain of 505 ± 196 µstrain and -521 ± 216 µstrain in compression	Cell number; ALP activity; Total RNA; Mineralized matrix production	ALP transcript levels were significantly higher after mechanical stimulation compared to the static controls. OPN transcript levels of mRNA were increased in response to mechanical stimulation. Mechanically stimulated OPN expression was dexamethasone dependent which was attributed to be an effect of BMPs in the DBM. Osteocalcin levels were not significantly affected by mechanical stimulation. Mineralised matrix production was substantially increased in mechanically stimulated specimens compared to static controls.
(Tanaka, Sun et al. 2005)	2005	MC3T3-E1 Osteoblasts	HA deposited on 3D porous collagen network (Collacote, Centeroulse Dental, CA, USA) Pores 89±28µm/22±7µm	piezoelectric induced strain for 3mins (1Hz ; 0-3000 µstrain) Fluid flow was measured with 3µm polystyrene microspheres (Polysciences, USA)	RT-PCR was used to determine the mRNA levels of selected load-sensitive genes c-fos, egr1, cox2, Osteopontin	Amplitude and velocity of fluid flow was greatest in fine pores. Strain induced flow was greater stimulus than strain alone on the expression of load-induced genes. Strain alone elevated c-fos/Osteopontin mRNA. Strain-induced flow upregulated all gene mRNA
(McGarry, Klein-Nulend et al. 2005)	2005	MC3T3-E1 Osteoblasts and Osteocytic MLO-Y4	Polylysine-coated glass slide	Pulsatile fluid flow-derived shear stress. 0.39Pa @ 3Hz / 0.64Pa @5Hz for 10mins. 37C	NO production using Greiss reagent; PGE2 was measured sung enzyme immunoassay (EIA)	Cytoskeleton modulates PFF-induced NO response in OB and involves stress fiber formation and alignment. The enhanced PGE2 response in OB is related to pulsatile fluid flow stimulation of focal adhesions formed when the cytoskeleton is disrupted. In OCY modulation of NO production occurs by cytoskeleton disruption. Inhibition of PFF-induced PGE2 response in OCY with cytoskeleton disruption indicates a high dependence of OCYs on actin-rich cytoskeleton. It is also possible that the PGE2 response is governed by shear/stretch sensitive ion channels which are known to be dominant in OCY response to mechanical loading.
(Bacabac, Smit et al. 2005)	2005	M3T3-E1	Polylysine-coated glass slide	Fluid shear stress with a Parallel-plate flow chamber. Steady shear stress (0.70Pa;0PaHz) ; low amplitude (0.70±0.31Pa) at 2 frequencies (5Hz;9.70PaHz / 9Hz;17.5PaHz) ; high amplitude (0.70±0.70 Pa) at 1 frequency (5Hz;22.0PaHz)	NO production using Greiss reagent	Bone cell response to fluid stress is rate dependent, but an initial stress kick is required for the cells to respond. Cytoskeletal arrangement during a pretreatment phase may explain the lack of response without a stress kick. Cellular sensitivity to stress occurs in under 1 min. However, cells were not affected by a short stress kick (10s; 0.7Pa) so the effect of stress on NO production occurs between 10s - 1min.

Author	Year	Cell type	Material type	Mechanical stimuli	Response	Observations
(Di Palma, Guignandon et al. 2005)	2005	MG-63 Osteosarcoma cell line	(1) Ti-6Al-4V blasted with glass balls (2) Ti-6Al-4V sandblasted (3) Alumina (>80%)	piezoelectric induced strain for 15 mins 3 times a day for 1,3,5 days at 0.25Hz and 600μstrain	ALP activity; cell number; Fibronectin; Vincullin; N-cadherin; Fibronectin	IMS had no effect on cell number for any treatment group. Osteoblastic cells upregulate ALP activity in response to stain irrespective of the surface stiffness. FN synthesis was increased for Ti-Al by 60% but not for other groups. Surface topography differences or perhaps a delayed response for the other groups were attributed to this observation. There was no difference in the total amount of Vincullin for any groups over all timepoints. Surface roughness is determinant for the up-regulation of N-cadherin by mechanical stretch. FN and N-cadherin probably act as mechanosensors.
(Ignatius, Blessing et al. 2005)	2005	Human fetal Osteoblastic cell line Hfob 1.19	Type I collagen gel	Cylindrical stretching at 1Hz with a strain of 10,000μstrain. Gels were stretched for 30mins a day for 3 weeks.	RNA by RT-PCR	Static forces promoted both cell proliferation and AP/OC expression whereas dynamic stresses slightly stimulated OC expression but inhibited cell growth and AP expression.
(Sikavitsas, Bancroft et al. 2005)	2005	Rat Bone Marrow Stromal Cells	Poly(L-lactic acid) nonwoven scaffolds (Denkendorf, Germany). Thickness = 1.7mm; vol porosity = 99%; fibre diameter 17μm	Fluid flow @ 0.6ml/min. 37C	DNA content / AP activity / Calcium deposition / μct	PLLA nonwoven scaffolds allowed the attachment, growth and differentiation towards Osteoblastic phenotype of rat MSCs seeded on them. Treatment with fluid flow allowed for (i) accelerated proliferation at 7days (ii) enhanced mineral deposition at 16 days (iii) enhanced spatial distribution of deposited ECM compared to static controls

Appendix II: Literature for Biomaterial-related Osteoinductivity

Table 10-1 Biomaterial related osteoinductivity

Author	Title	Material	Model	Summary
(Urist 1965)	Bone: Formation by Autoinduction	Acellular, devitalized, decalcified, bone matrix.	Samples of HCl-decalcified homogenous diaphyseal bone from rabbits; laboratory animals; or humans were implanted into (i) a pouch in the belly of either the rectus abdominus, quadriceps, or erector spinae muscles of approximately 250 rabbits, 20 rats, 10 mice, and 5 guinea pigs; (ii) a defect in the ulna in 10 rabbits or a bed of bone on the lumbar vertebrae in 3 dogs; (iii) a defect in a bone in various skeletal system disorders in 21 human beings.	>90% success new bone formation inside decalcified bone matrix. First use of term 'osteogenesis by auto***induction***'. Bone formation seen in well-vascularised regions at 4-6 weeks. Endochondral bone formation seen between 8-16 weeks. Wherever bone induction occurred there was a pool of stem cells, osteoprogenitor cells, and small capillaries, surrounded by palisades of deeply basophilic plump osteoblasts. Lamellar bone formation was evidenced by appositional formation of new bone, layers of osseous tissue with intermediate cement lines were deposited on the surface of decalcified dead matrix. The deposits were always enclosed in excavation chambers, either within the external surface or deep inside the old matrix; new bone never extended outside the implant.
(Winter 1970)	Heterotopic Bone Formation in a Synthetic Sponge	Polyhydroxyethyl-methacrylate (polyHEMA: Hydron),	Sponge was implanted in the fatty tissue under the dermis in the skin of pigs of the age 15-30 weeks. Implants were retrieved 9 weeks later.	Bone was present in the implants from 6 animals. All implants retrieved at 60 days post-implantation were ossified.
(Urist and Strates 1971)	Bone Morphogenetic Protein	Acellular, devitalized, decalcified, bone matrix.	The diaphyseal segment of long bones of 200 adult rats, Sprague-Dawley strain, were decalcified and implanted for 4 weeks in the muscle ovxczlogeneic rats.	After a period of two weeks after implantation and exposure to the enzymes of the recipient muscle, the implanted matrix gradually lost the cross-banded structure of collagen fibrils and the interfibrillar lacelike conformation of proteoglycans. Although calcification occurred as soon as osteoblasts differentiated and new bone matrix was deposited on the surface of the implanted matrix, the bulk of the old bone collagen did not recalcify.
(Piecuch 1982)	Extraskeletal implantation of a porous hydroxyapatite ceramic	Based on the skeleton of a common reef-building coral, porous hydroxyapatite ceramic was produced by hydrothermal conversion of the coral's aragonite ($CaCO_3$) structure. The resulting coralline replamineform hydroxyapatite (RHAP) was characterized by uniform interconnecting pores having a diameter of	Twelve identical 5 x 5 x 10 mm blocks of porous hydroxyapatite were implanted in a subcutaneous pocket in twelve adult, male, laboratory-bred beagle dogs. Implants were retrieved and evaluated histologically eight weeks following placement.	The results of this study suggest that porous hydroxyapatite ceramic does not act as a bone-inducing agent. The implant material is well-tolerated by host tissues, and was rapidly infiltrated by connective tissue. No evidence of rejection was observed. Likewise, no bone or osteoid was seen within any of the specimens. This was felt to be a significant finding, despite the short time frame (eight wk) of the study, since previous work had shown considerable bony ingrowth as early as six

Author	Title	Material	Model	Summary
		140-160 μm.		wk after subperiosteal implant placement. The author suggests that osseous ingrowth is apparently dependent on contact of the implant with bone.
(Heughebaert, LeGeros et al. 1988)	Physicochemical characterization of deposits associated with HA ceramics implanted in nonosseous sites	Pellets of well-characterized microporous hydroxyapatite (HA) ceramic	Pellets of well-characterized microporous hydroxyapatite (HA) ceramic were implanted in hamsters in two nonosseous sites: (1) in the fatty tissue of the gingival crease, far from bony tissue and (2) in intraperitoneal sites. The implants in site 1 were placed directly in contact with tissues, cells, and extracellular fluids while the implants in site 2 were placed in special chambers made of plexiglass cylinders covered in both ends with millipore filters, preventing contact with tissues and cells, but not with extracellular fluids. The hamsters were sacrificed and the implants recovered after 8, 16, 30, 150, and 365 days. The pellets were characterized using x-ray diffraction, infrared absorption, thermogravimetry, scanning and transmission electron microscopy, and calcium and phosphate analyses before and after implantation.	Physicochemical analyses of HA ceramic implants before and after implantation demonstrated the formation of new material which was significantly different from the HA ceramic in terms of the following: (a) morphology (size of shape) of crystals; (b) intimate association of the inorganic phase of the new material with an organic phase similar to inorganic/organic association in bone; (c) the inorganic phase of the new material is a CO3-apatite, similar to that of bone, while the HA in ceramic is CO3-free; (d) electron diffraction of apatite of new material is similar to that of bone apatite. This study also demonstrated that the new material associated with the HA ceramics implanted in two different nonosseous sites were identical in spite of the differences in their microenvironment (cellular and acellular).
(Ohgushi and Okumura 1990)	Osteogenic capacity of rat and human marrow cells in porous ceramics. Experiments in athymic (nude) mice	Replaniformed Coralline Porous hydroxyapatite (HA) and tricalcium phosphate (TCP), ceramic discs were implanted with or without rat marrow cells, The discs of HA and TCP had identical microstructures: pore size was 190-230 microns, porosity was 50-60%, and they were fully interconnected.	Porous hydroxyapatite ceramics, alone and combined with rat marrow cells, were implanted subcutaneously in 22 nude mice.	The ceramics alone were invaded by fibrovascular tissue without any bone formation. In contrast, all the ceramics combined with marrow cells had bone formation in the pores 4 to 8 weeks after implantation. The bone formation began on the surface of the ceramic with direct bonding of the bone to the ceramic and proceeded to the center of the pores. The ceramics were also combined with bone marrow cells from 7 humans and implanted in nude mice. In five experiments, bone formation occurred after implantation. In addition, the ceramics were combined with in vitro cultured fibroblastic cells, resulting in bone formation in 2/6 cases.
(Ohgushi, Okumura et al. 1990)	Marrow cell induced osteogenesis in porous hydroxyapatite and tricalcium phosphate: a comparative histomorphometri	Replaniformed Coralline Porous hydroxyapatite (HA) and tricalcium phosphate (TCP), ceramic discs were implanted with or without rat marrow cells, The discs of HA and TCP had identical microstructures: pore size was 190-230 microns, porosity was 50-60%, and they were fully interconnected.	Ceramic discs were implanted with or without rat marrow cells into subcutaneous sites in syngeneic rats.	Implants without marrow cells (discs themselves) did not show bone formation, whereas implants with marrow cells showed bone formation in the pores of the ceramics. The bone formation of both HA and TCP occurred initially on the surface of the ceramic and progressed towards the center of the pore. The de novo bone was quantitated from decalcified serial sections of the implants. One month after implantation with marrow cells, the percentage fractions of the pore area filled with bone for implanted HA and TCP were 16.9 and

Author	Title	Material	Model	Summary
	c study of ectopic bone formation			15.1, respectively. At 2 months after implantation with marrow cells, the fractions of bone were 34.3 and 30.9, respectively.
(Okumura, Ohgushi et al. 1991)	Bonding osteogenesis in coralline hydroxyapatite combined with bone marrow cells	Replaniformed Coralline Porous hydroxyapatite (HA) and tricalcium phosphate (TCP), ceramic discs were implanted with or without rat marrow cells, The discs of HA and TCP had identical microstructures: pore size was 190-230 microns, porosity was 50-60%, and they were fully interconnected.	Coralline hydroxyapatite ceramics alone (control) and the ceramics combined with rat marrow cells were implanted subcutaneously in the backs of syngeneic Fischer rats and harvested at 1,2,3,4,6,8 and 24 wk after surgery.	None of the control ceramics (without marrow) showed bone formation. However, ceramics combined with marrow cells showed consistent new bone formation in the pore regions. Histometrical results revealed increased new bone formation over time. Undecalcified sections of the ceramics studied by fluorochrome labelling showed that the osteogenesis began directly on the surface of the ceramic and proceeded centripetally towards the centre of the pores (bonding osteogenesis). SEM-EPMA analysis of the bone-ceramic interface also revealed direct bonding of bone to the ceramic surface.
(Ripamonti 1991)	The morphogenesis of bone in replicas of porous hydroxyapatite obtained from conversion of calcium carbonate exoskeletons of coral	Replicas of porous hydroxyapatite that had been obtained after hydrothermal conversion of the calcium carbonate exoskeleton of coral (genus Goniopora)	Samples were implanted intramuscularly in twenty-four adult male baboons (Papio ursinus). Samples were retrieved after 3, 6, and 9mnths	Sections showed that initially the formation of fibrous connective tissue was characterized by a prominent vascular component and by condensations of collagen fibers assembled at the interface of the hydroxyapatite. The morphogenesis of bone was intimately associated with the differentiation of the connective-tissue condensations. Bone formed without an intervening endochondral phase. Although the amount of bone varied considerably, in several specimens extensive bone developed, filling large portions of the porous spaces and culminating in total penetration by bone within the implants. The mean volume fraction composition of the specimens was 20.8±1.0% for bone, 17.3 ± 1.7% for connective-tissue condensation, 31.9 ± 1.0 % for fibrovascular tissue, 6.4 ± 0.6 % for bone marrow, and 34.6 ± 0.5 % for the hydroxyapatite framework. The amount of bone and marrow increased at each time-period, and the hydroxyapatite framework was significantly reduced between six and nine months. Linear regression analysis showed a negative correlation between the hydroxyapatite framework and the magnitude of bone formation within the porosities of the hydroxyapatite ($p = 0.0001$). The hydroxyapatite substratum may have functioned as a solid-phase domain for anchorage of bone morphogenetic proteins.
(Ripamonti, Ma et al. 1992)	Osteogenin, a bone	Replicas of porous hydroxyapatite that had been obtained after hydrothermal	After exposure of the calvaria, 64 cranial defects, 25 mm in diameter, were prepared in 16 adult male baboons	Histomorphometry on decalcified sections prepared on days 30 and 90 showed superior osteogenesis in osteogenin-treated

Author	Title	Material	Model	Summary
	morphogenetic protein, adsorbed on porous hydroxyapatite substrata, induces rapid bone differentiation in calvarial defects of adult primates.	conversion of the calcium carbonate exoskeleton of coral (genus Goniopora)	(Papio ursinus). Defects were implanted with disks of porous nonresorbable and resorbable hydroxyapatite substrata obtained after hydrothermal conversion of calcium carbonate exoskeletons of corals. In each animbal, one disk of each hydroxyapatite preparation was treated with osteogenin isolated and purified from baboon bone matrix after sequential chromatography on heparin-Sepharose, hydroxyapatite, and Sephacryl S-200 gel filtration columns. The remaining two defects were implanted with one disk of each hydroxyapatite preparation without osteogenin as control.	nonresorbable hydroxyapatite specimens as compared with controls. On day 90, substantial bone formation also had occurred in control nonresorbable hydroxyapatite specimens.
(Pollick, Shors et al. 1995)	Bone formation and implant degradation of coralline porous ceramics placed in bone and ectopic sites	Replaniformed Corraline Hydroxyapatite derived from Porites (180-230µm pores; 45-55% porosity) and Goniopora (270-550µm pores; 60-70% porosity) a.k.a Interpore 200 and Interpore 500 respectively	Two adult dogs received a total of 56 implants placed in the femur, skeletal muscle, and subcutaneous tissues. Lateral approach to femur for orthotopic implantation. Blunt dissection of vastus lateralis muscle to create muscle pouches. Subcutaneous implantation was performed through 1.5cm incisions in dorsum. Implants were retrieved at 4 months	Degradation of implant was statistically significant in intraosseous sites (16.7-24.4%) but not in intramuscular (4.9-10.1%) or in subcutaneous (5.0-9.7%) sites. ORTHOTOPIC SITES: Bone area in osseous sites was 18.4-43.1%. Soft tissues accounted for 15-32.0% area. Implant accounted for 13.6-24.7% area. Bone contact (percentage area of implant surface covered by bone) was 81.3±10.8%. INTRAMUSCULAR SITES: Bone area was 3.3-4.3%. Bone contact (percentage area of implant surface covered by bone) was 17.8±32.3%. SUBCUTANEOUS SITES: Bone area was 5.5-6.6%. Bone contact (percentage area of implant surface covered by bone) was 22.7-35.0%. Degradation was greatest in the osseous sites and so it is assumed that degradation of calcium-rich implants is, in large part, a biological phenomenon. Bone formation was found in the centre of the defect rather than the periphery.
(Ripamonti 1996)	Osteoinduction in porous hydroxyapatite implanted in heterotopic sites of different animal models	Replicas of porous hydroxyapatite that had been obtained after hydrothermal conversion of the calcium carbonate exoskeleton of coral (genus Goniopora)	A total of 40 hydroxyapatite rods were m, implanted bilaterally in intramuscular pouches created by sharp and blunt dissection in the rectus abdominis, four rods per animal: four clinically healthy outbred Chacma baboons (Papio ursinus) with normal haematological and biochemical profiles; two adult inbred beagles; and four adult rabbits were of the New Zealand white strain.	Implants harvested from rabbits and dogs were less vascularised than hose from Baboons at the macroscopic level. Bone area in Rabbits was 0.5±0.3%; in Dogs was 0.79±0.49%; and in Baboons was 11.3±3.02%. The amount of bone did vary considerably between specimens. Author speculates that Osteoinductivity is not inherent but that BMP's bind preferentially to the surface (based on previous binding studies). Bone differentiation occurred after 60days implantation. No bone formation after 30 days implantation so

Author	Title	Material	Model	Summary
				author speculates that this indicates that a critical level of endogenous BMP is required to be adsorbed to the surface to start the bone formation cascade. Bone formation was not via the Endochondral route.
(Yang, Yuan et al. 1996)	Osteogenesis in extraskeletally implanted porous calcium phosphate ceramics: variability among different kinds of animals	Biphasic ceramic consisted of 65% hydroxyapatite (HA) and 35% b-tricalcium phosphate (b-TCP) with 61% porosity and an average pore size of 402 µm. Micropores were 2-5µm in size and found on the walls of macropores of 200-600µm in size.	4 dogs, 2 pigs, 2 goats, 6 rabbits and 10 rats were implanted either in dorsal muscle (dogs) or under abdomen skins (pigs, goats, rabbits, rats) or in leg muscle (rats).n=6. Specimens were harvested at 15 (only for dogs and rabbits), 30 (only for dogs and rabbits), 45, 60, 90 and 120 days after implantation	DOGS AND PIGS: Bone observed in some defects after 45 days. Bone observed in all implants after 60/90 days. Woven bone formed via intramembraneous route. After 12 days extensive amount of trabeculated non-lamelar bone present. Bone was intimate with pores but also formed in periphery of graft. Bone was remodelled. After 15 days this appeared to be granulation type fibroconnective tissue, containing fibroblasts, macrophages and newly formed vessels. At 30 days fibroconnective tissue was organised parallel to the surface of the graft, polymorphic cell aggregates (ALP+), and multinucleated giant cells were present. At day 45, cell aggregation was more obvious Osteoblast differentiation occurred directly within the polymorphic mesenchymal cell clusters aggregated at the pore inner surface. Woven bone was in direct contact with the graft at 60 days. De novo bone was formed via intramembraneous route not Endochondral. Trabeculated, remodeled bone present at 90,120 days. Bone was formed inside the graft and not in periphery. Multi-nucleated giant cells in contact with material surface resembled osteoclasts. GOATS, RABBITS, AND RATS: No bone was observed in any defect at any timepoint.At early timepoints (15-60 days) the graft was full of loosely packed fibroconnective tissue.
(Yang, Yuan et al. 1997)	Osteogenic responses to extraskeletally implanted synthetic porous calcium phosphate ceramics: an early stage histomorphological study in dogs	Biphasic ceramic consisted of 65% hydroxyapatite (HA) and 35% b-tricalcium phosphate (b-TCP) with 61% porosity and an average pore size of 402 µm. Micropores were 2-5µm in size and found on the walls of macropores of 200-600µm in size.	A total of 28 cylinders (diameter, 4 mm; length, 5 mm) of porous HA*D*TCP ceramics were prepared for implantation. Cylinders were implanted in the dorsal muscles of 4 dogs, all far from osseous tissues (n=4). Implants retrieved at 7, 15, 30, 45, 60, 90 and 120 days	After 7 days pores were filled with clotted blood. After 15 days this appeared to be granulation type fibroconnective tissue, containing fibroblasts, macrophages and newly formed vessels. At 30 days fibroconnective tissue was organised parallel to the surface of the graft, polymorphic cell aggregates (ALP+), and multinucleated giant cells were present. At day 45, cell aggregation was more obvious Osteoblast differentiation occurred directly within the polymorphic mesenchymal cell clusters aggregated at the pore inner surface. Woven bone was in direct contact with the graft at 60 days. De novo bone was formed via intramembraneous route

Author	Title	Material	Model	Summary
				not Endochondral. Trabeculated, remodeled bone present at 90,120 days. Bone was formed inside the graft and not in periphery. Multi-nucleated giant cells in contact with material surface resembled osteoclasts. Proposed environmental mechanisms are facilitated vessel ingrowth (macroporosity) > favourable adsorption/differentiation of cells (microporosity) >crystallization of HA on the surface of material > increased calcium concentration (surface area/dissolution characteristics)bb
(Yuan, Zou et al. 1998)	Bone morphogenetic protein and ceramic-induced osteogenesis	TCP/HA (30TCP/70HA, porosity, 50-70%, average pore size 400 µm) rods (diameter 5 mm x 6 mm)	4 rods implanted into the dorsal muscle of one pig. 15 days later another 4 rods implanted on the other side of the dorsal muscle of the same animal. All implants retrieved after 45 days from start of study.	Bone formation could be detected inside the ceramics implanted in the dorsal muscle of the domestic pig at 45 d, while no bone formation could be observed at 30 d At 30 d, however, the organic matrix and polymorphic cells on the pore surface of the implants and some cells in the pores stained positively by bBMP-McAb compared to a negative control.
		Calcium phosphate ceramics with the same porosity (50%) but different chemical constitution (Cl, HA; C2, 22TCP/78HA; C3, 37TCP/63HA) were selected. Ceramic rods with the same size (diameter 12 mm] 8 mm) were used.	Each ceramic rod was placed in a rubber tube (diameter 10 mm) and connected in a cycle system in which 10 ml bovine BMP solution (300 lg bBMP/ml 4 MGu-HCl) circulated at a rate of 50 ml h~1. The bBMP concentration in the circulating solution was measured by fluorescene specto-photometry (scanning:150-600 nm) at different time periods. After 2 h, the ceramic column with the absorbed bBMP was taken out and washed in the cycle system with 10 ml distilled water or 0.1% CaCl2 or phosphate buffer for 1 h. The bBMP in the evaluate was measured by UV-spectrophotometry (scanning: 220-320 nm).	Calcium phosphate ceramics had a strong ability to absorb bBMP from the solution. At 30 min, a large amount of bBMP was absorbed by ceramic rods. In 2 h, most of bBMP in the solution was absorbed by the ceramic rods. Among the three types of calcium phosphate ceramics, HA has the stronger adsorption ability than 22TCP/78HA than 37/68HA .
(Yuan, Yang et al. 1998)	Osteoinduction by calcium phosphate biomaterials	HA with no microporosity (Mitsubishi); HA with microporosity on surface of macropores at 2 levels (sintered at 1100/1200C);TCP/HA (Ca/P=1.60) with microporosity; a-TCP with microporosity; B-TCP with microporosity; Calcium phosphate cement (mixing powders containing a-TCP, DCPD and a small amount of HA with phosphate solution containing N+ and K+); TiO2 with microporosity. All implants except	All materials were implanted into the dorsal muscle (excluding the cement paste which was implanted in the thigh muscle) and retrieved at 30; 37; 45; 60; 90; 150; 180 days	No bone formation was found in any implants of HA without micropores, TiO2 ceramic and a-TCP. Only bone-like tissue could be detected in HA sintered at 1200degC at 90 and 180 days, while bone formation could be found in HA sintered at 1100 *deg*C as early as 30 days. Bone formation could be found at 45 d post-operatively in TCP/HA. Bone formation could also be found in pores and deep rugged surface of cement, both implanted as prehardened form and paste. Bone formation in b-TCP started before 45 d, while, at longer time implantation, the induced bone in b-TCP ceramic demineralized at the

Author	Title	Material	Model	Summary
		cements were rods (3.5 mm x 8.5 mm to 5 mm x6 mm)		interface between bone tissue and ceramic. Factors impacting Osteoinduction noted as: Microporosity; sintering temperature; rate of dissolution; porosity; CaP *A bonding osteogensis process, in which the osteogenic precursor cells became attached to the pore surface, aggregated, proliferated, differentiated, produced bone matrix and ossified, could be observed in calcium phosphate-induced osteogenesis. Bone formation started from the pore surface and proceeded to the pore center; the induced bone bonded to calcium phosphate materials and no chondrocyte could be detected during the osteoinduction.*
(Yuan, Kurashina et al. 1999)	A preliminary study on osteoinduction of two kinds of calcium phosphate ceramics	Hydroxyapatite ceramic rods, 3.5x8.5 mm, provided by Mitsubishi average pore size of 200µm, a porosity of 70%, and was sintered at 1200degC. S-HA: Hydroxyapatite ceramic rods, 5x6 mm, average pore size 400 µm, porosity 60-70%, sintered at 1100degC, prepared by Sichuan Union University (Chengdu, China). S-HA contained interconnected microporosity in the walls of the macroporosity	Materials were implanted into 4 dogs. After disclosing the dorsal muscles, parallel incisions were made by scalpel in the dorsal muscle bundles (*longissimus dorsi*) and one ceramic implant, which was parallel to the muscle bundles, was loaded into each incision. Four ceramic rods were implanted into the dorsal muscles of each dog, two J-HA implants and two S-HA implants.	Bone formation in all S-HA implants (4/4 at 3 months); (4/4 at 6 months) and no bone formation in any J-HA implants (0/4 at 3 months), (0/4 at 6 months). Gross observation showed more bone at 6 months than that at 3 months in S-HA implants. No bone tissue could be histologically detected in all J-HA implants at both 3 months and 6 months only fibrous tissues, blood vessels and blood cells were in the pores. Interestingly the author comments that an insufficient number of tests were conducted to perform quantitative analysis. However, the number of animals tested was 4 and the materials were tested in duplicate.
(Yuan, Li et al. 2000)	Tissue responses of calcium phosphate cement: a study in dogs	HA powder, a-TCP powder and DCPD powder were mixed in the desired ratios of 5 : 55 : 40% (in weight) to obtain calcium phosphate cement powder. Cement solution consisted of 15.0 g K2HPO4.3H2O, 15.0 g NaH2PO4.H2O and 70 ml distilled water. The cement paste was prepared by mixing the cement powder with sterile cement solution in the	7 male dogs were used in the study. Cement paste was implanted in the femora and dorsal muscles of 4 dogs. 2 animals wee sacrificed after 3 months and 2 after 6 months. Pre-hardened cement cylinders were implanted into the thigh muscles of the remaining dogs. One animal was sacrificed at 1, 2, and 6 months post-operation.	ORTHOTOPIC SITES: After 3 months the cement surface had become irregular and was covered by bone. In some areas bone tissue had grown into the cement. After 6 months there was evidence of resorption lacunae. Osteoclast-like cells were present containing cement particles. Direct apposition between bone and cement was apparent. Cement had undergone chemical dissolution.

Author	Title	Material	Model	Summary
		ratio of 2.2 g : 1 ml, 2 min before implantation.		INTRAMUSCULAR SITES: At 1 month macrophages were attached to the surface of the cement. At longer time-periods giant cells containing cement particles were observed. Bone formation was seen on the deep rugged surfaces of the cements as well as in some pores. Bone was in intimate contact with the cement. A seam of secretary osteoblasts on the surface of the cement was observed. Osteocyte lacunae were also evident with back scattered electron microscopy. Bone was not found in all treated defects (approximately 50%). The detachment of weakly bound cement particles was seen as a short-coming for use in clinical practice.
(Yuan, Yang et al. 2001)	Bone Induction by Porous Glass Ceramic Made from Bioglass (45S5)	Porous glass ceramic, which was prepared from Bioglasst powder (45S5, U.S.Biomaterials). Pores ranged from 100–600 μm	16 healthy adult dogs (1–5 years old, 10–15 kg, 14 male and 2 female). A longitudinal incision was made and the thigh muscle was exposed by blunt separation. Longitudinal incisions were made by scalpel and blunt separation, and then the glass ceramic cylinders were implanted in the muscle pouches.	Bone was formed on crystal layers and where pathological calcification had occurred. Bone formation was greatest in pores where neither of these phenomena existed. The de novo bone contained osteoblasts and osteocytes. Bone formation was intimate with the surface of the implant and progressed inwards into pores. Implant area was 32±4% and bone area was 3±2%. Clear morphological distinction between pathological calcification and de novo bone formation. No Phosphorus was found in the crystallized layers on the surface of the material. The excavated centres of Bioglass granules provided a nucleation site for mesenchymal cells to differentiate into osteoblasts. First reference to the term osteoinduction. Bone formation was via the intramembraneous route and therefore not related to BMP's alone.
(Eid, Zelicof et al. 2001)	Tissue reactions to particles of bone-substitute materials in intraosseous and heterotopic sites in rats: discrimination of osteoinduction, osteocompatibility, and inflammation	Particles of various materials: HA (250-450/75-250μm), β-TCP (300-400μm), BCP (HA:TCP 65:35), Polyethylene (70-250μm), Polymethylmethacrylate (70-250μm)	Bilateral subcutaneous pockets were prepared by blunt dissection over the thoracic area in male rats (28-day-old). 50mg implants of nrCP, rCPs, PE, or PMMA deposited in the cephalad ends of the pockets. Implants were retrieved up to 3 weeks later.	Fibrous reaction to the implantation HA at day 7. Each particle was enclosed by layers of fibrous connective tissue. With the exception of an occasional multinucleated cell, neither acute nor chronic inflammatory cells were evident. No bone or cartilage was present. TCP/BCP generated a fibrous tissue reaction, with TCP showing partial resorption after 7 days. The particles were surrounded by TRAP-negative foreign body giant cells. PMMA was surrounded with fibrous tissue and a few foreign body giant cells, which were rarely TRAP-positive.

Author	Title	Material	Model	Summary
				Each particle of PE was surrounded by large, multinucleated giant cells. The interstitial space was composed of connective tissue with small blood vessels and cells resembling fibroblasts, mononuclear cells, and occasional polymorphonuclear granulocytes. The multinucleated cells around PE did not stain strongly for TRAP.
(Yuan, De Bruijn et al. 2001a)	Bone formation induced by calcium phosphate ceramics in soft tissue of dogs: a comparative study between porous alpha-TCP and beta-TCP	Microporous and Macroporous a-TCP and B-TCP sintered ceramic bodies. No details as to pore classification data provided. The author claims the pore geometries are equivalent but the electron micrographs appear to show a difference in the quantity of microporosity between the two materials.	In four dogs the muscle bundles of longissimus dorsi in both sides were disclosed by blunt separation. One ceramic rod was inserted into each of two incisions. Two a-TCP ceramic rods were implanted in one side and two b-TCP ceramic rods in the other side of each dog. 2 animals at each of 30, 45, and 150 days were sacrificed and the implants retrieved.	No bone formation was observed in any defect treated with a-TCP at any time point. Macrophages and giant cells were not present in large numbers. In the B-TCP implants polymorph cells were observed as aggregated in the pores and on the surface of the material. After 45 days bone was observed in some pores. Bone was in intimate contact with the pore surface. Osteoblast and Osteocyte lineage were obvious. At 150 d, the bone tissues inside the pores of b-TCP implants were no longer normal; no bone marrow tissue, no bone remodeling process, no osteoblast lineage, even no obvious osteocytes could be observed, only a small amount of calcified tissue with less osteocytes could be found in the center of pores. The tissues between the pore surface and calcified tissue seemed to be demineralized bone. Direct bonding between bone and b-TCP ceramic was hardly observed at 150 d. The author speculates that the dissolution rate of implants could affect the rate at which an apatite-like layer is formed on the surface of the material, thus affecting the rate of de novo bone formation. The author also comments that it is the dissolution properties of B-TCP which eventually leads to the degeneration of bone in the defect at longer time periods as the concentrations of calcium and phosphorus reach a detrimental level.
(Yuan, Yang et al. 2001)	Material-dependent bone induction by calcium phosphate ceramics: a 2.5-year study in dog	Two ceramics with macropores between 100 and 1000 μm in size and micropores 0.1–10 μm on their macropore surface. The HA samples have a macroporosity of 52 % while BCP has a macroporosity of 40%. A trace of TCP presents in HA, while BCP contains 38%weight TCP.	1 adult male dog. n=4 of each material was implanted in the dorsal muscle of the dog and retrieved 2.5 years after implantation.	All implants were tracelable and none had completely been dissolved/remodelled. Mature bone containing osteoblasts, osteocytes, and osteoclasts was observed in all treated defects apart from ¾ of the a-TCP group. In HA implants 48±4% pore area was occupied by bone and in BCP implants bone filled 41±2% pore area.
(Gosain, Song et	A 1-Year Study of	Disc shapes measuring 16.8 mm in	10 adult female sheep. Intramuscular pockets were created	There was no bone formation in the cements.

Author	Title	Material	Model	Summary
al. 2002)	Osteoinduction in Hydroxyapatite-Derived Biomaterials in an Adult Sheep Model: Part I	diameter by 5mm Ceramics (45% porous; 200-300µm): Interpore and BCP (HA:TCP 60:40) Cements (45-55% porous; 2-5nm): Bonesource, BCP (HA:TCP 60:40) paste, BCP (HA:TCP 20:80) paste	on RHS and subcutaneous on LHS. All implants were retrieved 1 year post-op. Autogeneous bone was harvested from the cranium (full thickness) and implanted.	Mean bone replacement ranged from 6.6±1.4 percent to 11.7 ± 1.17 percent within both composites of ceramic hydroxyapatite implants, with no significant difference in bone formation noted between the intramuscular and subcutaneous sites.
(Barrere, van der Valk et al. 2003)	Osteogenecity of octacalcium phosphate coatings applied on porous metal implants	Dense titanium alloy (Ti6Al4V surgical grade, Smitford Staal BV, The Netherlands) and porous tantalum cylinders (Hedrocel™, Implex Corporation, USA). The OCP coating was 100% crystalline and was composed of octacalcium phosphate crystals [OCP, Ca8(HPO4)2(PO4)4 . 5H2O that grew perpendicularly to the substrate. The BCA coating was 65% crystalline and was composed of a carbonate apatite closely similar to bone mineral	14 Dutch milk goats. Grafts were implanted (n=2x2) intramuscularly in the spine with 2 un-coated and 2 coated implants per side. Implants were retrieved 12 and 24 weeks post-implantation.	OCP coatings were all but dissolved in all retrieved implants. No bone was found intramuscularly in any of the un-coated implants. Only ¼ of the implants contained bone for the OCP-coated Ti6Al4V (intramembraneous route) whereas ¾ of the OCP-coated tantalum cyclinders contained bone at 12 weeks. Interestingly at 24 weeks no bone was found but a calcified matrix was found. Hedrocel had a higher surface area than Ti6Al4V so the author suggests that this led to greater free Ca and more BMP adsorption to the surface. Bone formation not found orthotpically in un-coated Ti6Al4V. OCP-coated Ti6Al4V consistently conducted bone right the way through the defect. BCA-coated Ti6Al4V only conducted bone at the periphery of the defect.
(Fujibayashi, Neo et al. 2004)	Osteoinduction of porous bioactive titanium metal	(1) Porous blocks (5x5x7mm3, porosity=40–60%, pore size=300–500 µm) (2) fibre mesh cylinders (diameter= 4 mm, length=11 mm, porosity=40–60%, pore size=50–450 µm)	Materials were implanted into the dorsal muscles of 6 mature beagle dogs for either 3 or 12 months before retrieval.	Bone was only formed in the porous Ti constructs which had been thermally and chemically treated after 12 months implantation.16.27 ± 7.5% new bone had formed in the pores that covered 23.27±5.5% of implant area.
(Daculsi 2004)	Osteoinductive Properties of Micro Macroporous Biphasic Calcium Phosphate Bioceramics	The material used was a mixture of hydroxyapatite (HA) and beta tricalcium phosphate (b-TCP) with a weight ratio of 60/40 % HA/b- TCP, 30 % of microporosity of less than 1 micron and a specific surface area of the crystal of 4±0.02 m^2/g. The macroporosity was 50 % with a range of macropores of 150 to 700 with a mean of 400 microns (TriositeTM Zimmer, MBCPTM Biomatlante, France)	Small animals (36 Rats and 72 rabbits) and large animals (24 dogs, 2 cats). The materials were calibrated cylinders or granules implanted in subcutaneous areas or in paravertebral muscles.	No bone formation in any of the rats or rabbits. Bone formation was found at 3-7months after implantation in cats and dogs. Bone was formed in the centre of the pores. The range of bone formation was 1-6%. Bone growth was related to the formation of biological apatite layer on the surface of the biomaterial.
(Habibovic, Yuan et al. 2005)	3D micro-environment as essential Element for osteoinduction	Porous HA and porous HA/TCP ceramic cylinders (4 different groups). Macroporosity of between 46-54 (%). Mean macropore diameter between 243-	10 dutch goats were implanted (n=10) in the lumbar region of the back on the left handside at 0 weeks and right handside at 6 weeks and then sacrificed at 12 weeks. The author notes that other implants not disclosed in the	Bone contact of >2% considered measure of effect. Bone induction: (BCP1100, BCP1150)4(BCP1200, HA1150)4HA1250 (no induction at all). Bone induction in individual animals: 42% bone contact in 20% of animals after

Author	Title	Material	Model	Summary
	by biomaterials	380 (μm). Specific surface area of between 0.07-1.60 (m2/g). Chemical composition: 88 wt% HA/12 wt% b-TCP in BCP versus 100 wt% HA.	paper were implanted at the same time.	6 weeks and in goats 70% after 12 weeks of implantation. Hardly any bone induction in 30% goats. No bone was observed on the outside of the implants. Bone formation was limited to inside the pores. Significant variation between animals. Interestingly the incidence of bone was reported in the article but the absolute volume measured was not, despite being cited as being measured.
(Le Nihouannen, Daculsi et al. 2005)	Ectopic bone formation by microporous calcium phosphate ceramic particles in sheep muscles	(MBCP) granules of 1–2 mm composed of hydroxyapatite and beta-tricalcium phosphate (60/40) had macropores of 450 (100-600) μm, micropores of 0.43 (0.1-0.5) μm, and a specific surface area of 1.8 m2/g. Total porosity was 70% of which 45% was Macroporosity. Macroporosity was not always interconnected.	8 female sheep. Sinus lift augmentation was also performed in the same animals. 2cm3 Implants were grafted in intramuscular space in the lumbar region. Implantation was performed bilaterally. Implants were retrieved after 6 months.	Bone was mature and mineralised and bridged between granules in the intramuscular site. Osteocytes were trapped within the bone, formed via the intramembraneous route. Bone was in direct contact with the MBCP granules surface and was present throughout the graft site. A zone with an electron density similar to that of mineralized bone, but lacking osteocytes and remodelling lacunae, was observed on the surface of the MBCP Granules. Author postulates that this acellular envelope might be caused by the precipitation of biological apatite on the surface of MBCP granules. Ceramic and bone density by image analysis 26.9 and 10.2% respectively. Ceramic and bone density by Micro-CT analysis 20.8 and 14.3% respectively. The # and thickness of bone trabeculae was similar to natural bone in MBCP treated defects.
(Kondo, Ogose et al. 2006)	Osteoinduction with highly purified b-tricalcium phosphate in dog dorsal muscles and the proliferation of osteoclasts before heterotopic bone formation	The porosity of the block was 75% and the surface area was 1.4m2/g. The b-TCP block contained macropores of 100–500 μm and micropores of less than 5 μm. Nearly all macropores were interconnected via 100–200 mm pores. Five-millimeter cubic blocks of b-TCP were used in the study.	Twelve-month-old female beagle dogs were used in the study. Materials were implanted in the perivertebral muscle in each dog and extracted at 14, 28, 42, 56, 112 and 168 days post-implantation.	New bone formed in the implants between 42 and 56 days. The TCP area decreased over the time-course from 10.4 to 2.4mm^2. The bone area increased from 0.18 to 0.68%. NB bone area was quoted as % of TCP area.
(Habibovic, Sees et al. 2006)	Osteoinduction by biomaterials: Physico-chemical and structural	Porous Biphasic and carbonate apatite cylinders (4xBCP and 1xCA groups). Macroporosity for all implants was 53-53%. The macropore diameter of ¾ BCP	Materials were implanted in 10 goats in the paraspinalis muscle by blunt dissection. Subcutaneous implantations of the same materials was performed after 8, 10, and 11 weeks. Animals were sacrificed at 12 weeks and the	Bone in 9/10 of implants (HA/TCP 80/20) with microporosity of 17% and SA of 1m^2/g. Bone in 6/10 of implants (HA/TCP 70/30) with 24% microporosity and SA of 1.4m2/g. No bone in any other treatment group or for materials implanted

Author	Title	Material	Model	Summary
	influences	groups was 400µm whilst CA group had smaller pores and the remaining BCP had even smaller pores. Microporosity ranged between 4-24% across the groups. Surface area ranged 0.2-9.7m2/g. Microporosity had a diameter of approx 1µm in all groups.	implants retrieved.	subcutaneously. Macroporosity was considered 2o factor as increased solubility (SA/TCP content) did not correlate with incidence/amount of bone. Macropores in more effective material were 400µm whilst macropores in less effective material were 100um. Fragments of material were found in the less effective group – this coincided with a lack of bone formation. This was attributed to a less stable graft and micromotion. CA spontaneously dissolved and prevented bone formation. Implant size had an effect (larger implants [10mm L] performed better than smaller implants [5mm L]). Dissolution-precipitation reaction is proposed because there is significantly more organic comounds and carbonate found on the surface of implants with a higher SA/microporosity.
(Yuan, van Blitterswijk et al. 2006a)	A comparison of bone formation in biphasic calcium phosphate (BCP) and hydroxyapatite (HA) implanted in muscle and bone of dogs at different time periods	Two ceramics with macropores between 100 and 1000 µm in size and micropores 0.1–10 µm on their macropore surface. The HA samples have a macroporosity of 52 % while BCP has a macroporosity of 40%. A trace of TCP presents in HA, while BCP contains 38%weight TCP.	Ceramic cylinders were implanted in both femurs of dogs. Four BCP cylinders were implanted in muscles and 2 BCP cylinders in femoral cortical bone in one femur; four HA cylinders in muscles and 2 HA cylinders in cortical bone in the other femur. Animals were sacrificed at 7, 14, 21, 30, 45, 60, 90, 180, and 360 days after implantation.	Bone was present after 30 days for BCP (8/8) and 45 days for HA (8/8). Bone area increased from 1% at 45 days to 21±4% at 360 days for HA. For BCP the bone area increased from 4% at 30 days to 34±9% after 360 days. The authors claim that osteoinductive potential is reflected in the orthotopic defect sites.
(Habibovic, Yuan et al. 2006)	Relevance of osteoinductive biomaterials in critical-sized orthotopic defect	Biphasic (80%TCP:20%HA) cylinders (17x6mm3) of 50-60% Macroporosity; 68 or 76% total porosity. One group had more microporosity (17%/0.7um diameter/1.0m^2/g) than the second group (3%/1.0um diameter/0.2m^2/g).	Materials were implanted in orthotopic (iliac wing) and ectopic (paraspinalis muscles) sites of 10 goats. Animals were sacrificed at 12 weeks.	ECTOPIC SITES: Bone formed in the more porous implants in all sites after 6 weeks. Bone area varied considerably between animals (0.05-6%: mean = 1.5±2.0%). Bone contact also varied considerably (0.5-10%=: mean = 2.9±3.8%). No bone was observed in the less porous implants. ORTHOTOPIC SITES: Bone was observed in all defects but more was present in more porous materials. Bone formation started before 8 weeks in porous materials and after 8 weeks in less porous materials. No significant diference in bone area (15.2±4.2% vs. 13.5±5.1%), but a significant difference in bone contact area (13.9±3.1% vs.8.1±3.6%).
(Yuan, van	Cross-species	Two ceramics with macropores between	8 dogs, 4 rabbits, 8 rats, and 16 mice were included in the	Bone incidence in animals dogs (8/8), rabbits (4/4), rat (0/8),

Author	Title	Material	Model	Summary
Blitterswijk et al. 2006b)	comparison of ectopic bone formation in biphasic calcium phosphate (BCP) and hydroxyapatite (HA) scaffolds	100 and 1000 μm in size and micropores 0.1–10 μm on their macropore surface. The HA samples have a macroporosity of 52 % while BCP has a macroporosity of 40%. A trace of TCP presents in HA, while BCP contains 38%weight TCP.	study. Materials were implanted in the gluteal muscles of dogs, thigh muscles of rabbits & rats, and dorsal subcutaneous pouches in the mice. All implants were left in situ for 90 days.	and mice (3/16). For materials retrieved from dogs, bone volume was 14±5% in HA implants and 30±6% in the BCP implants. Bone volume was only seen in BCP implants in rabbits but at <5%. Bone area was quoted normalised to pore volume. No bone was seen in any materials implanted in rats and only 3/16 materials implanted in mice. Bone found in the materials implanted in dogs was mature with trapped osteocytes, an osteoblast line, mineralised osteoid and osteoclast-like cells.
(Bodde, Cammaert et al. 2007)	Investigation as to the Osteoinductivity of Macroporous Calcium Phosphate Cement in Goats	The total porosity of the cement was 59.8%, with a macroporosity (pore diameter 10–300 μm, average 150 μm) of 20.2% and microporosity (pore diameter <10 μm) of 39.6%.	Four mature (age 2–4 years) female Saanen goats, weighing about 45 kg were used as experimental animals.	After 3 months only 35% of the graft was remaining after the a-TCP phase had completely dissolved. The macrostructure was completely lost after this amount of time post-implantation. There was present a fibrous capsule with few inflammatory cells. After 6 months only 25% of the graft remained. There was no change to the fibrous capsule of cell types observed. No bone or cartilage was observed in any of the defects at any time-point.
(Li, Habibovic et al. 2007)	Biological performance in goats of a porous titanium alloy-biphasic calcium phosphate composite	Porous Ti6Al4V scaffolds. The diameter and space between fibres was 400 μm. Porosity was 55%. Permeability, elastic modulus, and young's modulus were comparable to cancellous bone. Composites of Ti6Al4V and BCP were also implanted. Both Ti6Al4V only and composite grafts were implanted alone or seeded with BMSC. BCP was 80:20 HA:TCP; 60% porous with macropores 100-800 microns. Micropores were present on the surface sized <10μm	Ten Dutch goats. Intramuscular defects were created in the paraspinalis muscle at T8-L3. Orthotopic sites were created on the top of the transverse processes at L4-L5. Implants were retrieved and examined after 12 weeks. Bone area was normalised for available pore space.	ECTOPIC SITES: No bone formation with Ti6Al4V only scaffolds which were filled solely with fibrous connective tissue. 2/10 of the BMSC seeded Ti6Al4V implants contained bone. Bone was formed between 6-9 weeks (xylenol orange fluorochrome label) in one implant and after 9 weeks in the other. In the composites bone was preferentially found in the pores of the BCP. For cell-seeded composites bone was found in 8/10 implants: 3DFT and BMSC 3DFT 2–3% total implant area 3DFT+BCP and BMSC 3DFT+BCP implants about 8–10% total implant area and approximately 0-18% of available pore volume ORTHOTOPIC SITES: 3DFT and BMSC 3DFT 2–7% of available pore volume 3DFT+BCP and BMSC 3DFT+BCP implants about 3–16% of available pore volume Bone formation was prominent at interface between Ti6Al4V and BCP components rather than the middle of the BCP component suggesting that nutrient and oxygen supply are

Author	Title	Material	Model	Summary
				important.
(Habibovic, Gbureck et al. 2008)	Osteoconduction and osteoinduction of low-temperature 3D printed bioceramic implants	The brushite surface consisted of unreacted particles with a diameter of 10–20 mm, embedded in a matrix of tabular crystals (2–5 mm). The monetite structure was similar to that of brushite, however the surface contained more micropores with a diameter of 10–20 µm. The microporosity of brushite and monetite was 38% and 44% and the specific surface area was 3.60 and 6.09m^2/g, respectively.	Intramuscular pockets were created in the T8-L3 paraspinal muscles of goats. Materials were also implanted in decorticated regions of T4-T5. A separate un-reported material was also screwed to the transverse process. Implants were retrieved 12 weeks after surgery.	Both implant types were considerably resorbed at retrieval. Bone incidence was 45% in Brushite implants and 73% in Monetite. Generally, a layer of bone with a thickness of about 100 µm was found in close contact with the implant surface. Most bone formed where the implant had resorbed. This was in contrast to the pattern of growth in orthotopic sites. The bone formed was woven, immature bone. Bone markers were only present at 9 weeks, suggesting bone growth starting between 6&9 weeks. In some animals markers were not present even at 9 weeks, suggesting bone growth after that time-point.
(Fellah, Gauthier et al. 2008)	Osteogenicity of biphasic calcium phosphate ceramics and bone autograft in a goat model	(MBCP) granules of 1–2 mm composed of hydroxyapatite and beta-tricalcium phosphate (60/40) had macropores of 450 (100-600) µm. BCP1050 had micropores of 0.36µm diameter, SFA=2.66m^2/g and total porosity of 65%. BCP1125 had micropores of 0.45µm, SFA=1.45m^2/g and total porosity of 65%. BCP1200 had no microporosity, SFA=0.67m^2/g and total porosity of 55%.	4 intramuscular sites were created in the paraspinalis muscle of goats. Explants were retrieved at 6 and 12 weeks post-implantation. Materials were implanted within a porous PTFE clinder.	ORTHOTOPIC SITES: For BCP1050 the amount of bone increased from 1.01 to 5.6% over the period 6-12 weeks. For BCP1125 the amount of bone increased from 2.05-9.6% over the same period. For BCP1200 bone was present only at 0.85-1.5% over the period 6-12weeks. Graft resrpotion was related to sintering profile and microstructure. Graft resorption reduced the graft volume from 30% to 25% by 12 weeks for all material types. ECTOPIC SITES: No bone formation see in autograft or test articles at any time-point.
(Habibovic, Kruyt et al. 2008)	Comparative in vivo study of six hydroxyapatite-based bone graft substitutes	BCPA = 80:20 B-TCP/HA, 75% total porosity, 1.5m^2/g; BCPB = 80:20 B-TCP/HA, 70% total porosity, 0.2m^2/g BCPC = 70:30 B-TCP/HA, 80% total porosity, 1.8m^2/g BCPC+ = 70:30 B-TCP/HA, 80% total porosity, 1.8m^2/g (+PLA) HA = 80% total porosity, 1.9m^2/g CA = 80% total porosity, 8.6 m^2/g	Intramuscular sites were created in the paraspinalis muscles of 12 goats. Orthotpic implantations were also performed over decorticated regions of the lumbar spine. All anials were euthanized at 12weeks after implantation.	ECTOPIC SITES: Bone incidence: BCPA (9/11), BCPB (0/11), BCPC (9/11), BCPC+(4/11), HA (0/11), CA (0/11). Bone area of pore: BCPA (2.83), BCPC (2.80), BCPC+ (0.54) Bone markers were only evident after 6 weeks implantation.
(van Gaalen 2009)	Goat Bone Tissue Engineering: Comparing an intramuscular	Biphasic (80%TCP:20%HA) of 50-60% Macroporosity; microporosity (17%/0.7um diameter/1.0m^2/g)	Materials were implanted in the paraspinalis muscles of 8 goats. Posterolateral fusions were also performed over L1-L2 and L4-L5. Materials were retrieved 12 weeks post-implantation. Half of the materials were seeded with cells	8/8 of cell-seeded implants grow bone in the ectopic defect sites. 4/8 of control (un-seeded) implants grew bone in ectopic sites. All samples were well vascularised. In animals treated with cell-seeded implants bone markers were evident at 4

Author	Title	Material	Model	Summary
	with a posterolateral lumbar spine location		cultured from bone marrow aspirate.	weeks whereas in animals treated with control implants the marker was evident until 8 weeks post-implantation. There was very little effect of cell-seeding when the same materials were implanted in the PLF location.
(Cheng, Ye et al. 2009)	Osteoinduction of hydroxyapatite/b-tricalcium phosphate bioceramics in mice with a fractured fibula	Biphasic (60%HA:40% TCP) of 50% porosity, with pores 300-500 microns. SEM images seem to show low level of microporosity in the surfaces of the macropores.	In 30 mice the left fibula was fractured and materials implanted in both the left and right leg muscles (groups 1 and 2). In a further 15 mice the materials were implanted subcutaneously in bilateral pouches (group 3). Implants were retrieved at weeks 2, 4, 6, 8, and 12.	No bone was found in any of the subcutaneous defect sites. Bone formed in the muscle pouches of the uninjured legs after 8 weeks. Bone formed in the muscle pouches of injured legs after week six. At week 6 the percentage was 6.7 ± 1.25 in group 1; at week 8 the percentage was 35.8 ± 1.65 in group 1 and 8.5 ± 0.98 in group 2; at week 12 the percentage was 42.6 ± 1.86 in group 1 and 35.8 ± 1.32 in group 2; no new bone tissue was observed in group 2 at week 6 or in group 3 at any time point.
(Barradas, Yuan et al. 2012)	The influence of genetic factors on the osteoinductive potential of calcium phosphate ceramics in mice	HA sintered at 1250ºC; BCP sintered at 1150ºC and 1300ºC; TCP sintered at 1050ºC. All machined to 4x4x4mm blocks.	Subcutaneous implantation in mice of varying strains. Strains included: - C3H/HeNHsd - DBA/10laHsd - DBA/20laHsd - CBA/CaOlaHsd - BALB/cOlaHsd - C57BL/6JOlaHsd - FVB/NCrl - 129S2/SvPasCrl - SKL/JOrlCrl - CB17/Icr-prkdc^{scid}/IcrCrl - A/J Implants were retrieved 12 weeks after implantation.	Bone formation only detected in FVBand 129S2 strains.Bone was mostly observed at the periphery of the implanted ceramic block, but in contact with the scaffold.Bone formation was via intramembraneous pathway as eveidenced by osteocytes trapped in osteoid. Bone marrow filled cavities. No observations for endochondral bone formation or cartilage formation. Incidence of bone formation was 6/6 for FVB and 4/5 for 129S2. Bone architecture in the treated animals (bone volume; connectivitydensity; structural model index; trabecular separation; trabecular thickness) was found to be equivalent across FVB and 129S2 groups. Supplemental VEGF did not induce more bone formation. The study concludes that the genetic background of the individuals is a key element in the osetogenic response to synthetic materials.

Bibliography

Ahmad, M., M. B. McCarthy and G. Gronowicz (1999). "An in vitro model for mineralization of human osteoblast-like cells on implant materials." Biomaterials **20**(3): 211-220.

Ajubi, N. E., J. Klein-Nulend, M. J. Alblas, E. H. Burger and P. J. Nijweide (1999). "Signal transduction pathways involved in fluid flow-induced PGE2 production by cultured osteocytes." Am J Physiol **276**(1 Pt 1): E171-178.

Akao, M., H. Aoki and K. Kato (1981a). "Mechanical properties of sintered hydroxyapatite for prosthetic applications." Journal of Materials Science **16**: 809-812.

Akao, M., H. Aoki and K. Kato (1981b). "Mechanical properties of sintered hydroxyapatite for prosthetic applications." J Mater Sci **16**: 809-812.

Alberts, B., D. Bray, J. Lewis, M. Raff, K. Roberts and J. D. Watson (1994). Molecular Biology of the Cell. New York, Garland Publishing.

Annaz, B. (2003). in-vitro Assessment of the Biological Role of Microporosity in Synthetic porous Hydroxyapatite PhD, Queen Mary University London.

Annaz, B., K. Hing, M. Kayser, T. Buckland and L. Di Silvio (2004a). "Porosity Variations in Hydroxyapatite and Osteoblast Morphology: A Scanning Electron Microscopy Study." The Royal Microscopical Society - Journal of Microscopy **215**: 100-110.

Annaz, B., K. A. Hing, M. Kayser, T. Buckland and L. Di Silvio (2004b). "Porosity variation in hydroxyapatite and osteoblast morphology: a scanning electron microscopy study." J Microsc **215**(Pt 1): 100-110.

Annaz, B., K. A. Hing, M. Kayser, T. Buckland and L. Di Silvio (2004c). "An ultrastructural study of cellular response to variation in porosity in phase-pure hydroxyapatite." J Microsc **216**(Pt 2): 97-109.

Anon. (2010). "GeotechniCAL Reference." Retrieved 05/03/2010, 2010.

Anselme, K. (2000). "Osteoblast Adhesion on Biomaterials." Biomaterials **21**: 668-680.

Aoki, H. (1994). Medical Applications of Hydroxyapatite, Takayama Press, System center co. INC.

Aoki, M. (1991). Science and Medical Applications of Hydroxyapatite. Tokyo, Takayama Press System Center Co., Inc.

Arita, I. H., D. S. Wilkinson, M. A. Mondragon and V. M. Castano (1995). "Chemistry and sintering behaviour of thin hydroxyapatite ceramics with controlled porosity." Biomaterials **16**(5): 403-408.

Athanasiou, K. A., C. Zhu, D. R. Lanctot, C. M. Agrawal and X. Wang (2000). "Fundamentals of biomechanics in tissue engineering of bone." Tissue Eng **6**(4): 361-381.

Auclair-Daigle, C., M. N. Bureau, J. G. Legoux and L. Yahia (2005). "Bioactive hydroxyapatite coatings on polymer composites for orthopedic implants." J Biomed Mater Res A **73**(4): 398-408.

Bacabac, R. G., T. H. Smit, M. G. Mullender, S. J. Dijcks, J. J. Van Loon and J. Klein-Nulend (2004). "Nitric oxide production by bone cells is fluid shear stress rate dependent." Biochem Biophys Res Commun **315**(4): 823-829.

Bacabac, R. G., T. H. Smit, M. G. Mullender, J. J. Van Loon and J. Klein-Nulend (2005). "Initial stress-kick is required for fluid shear stress-induced rate dependent activation of bone cells." Ann Biomed Eng **33**(1): 104-110.

Bacterin Osteosponge brochure. Bacterin. Belgrade, MT, USA.

Bae, H., L. Zhao, D. Zhu, L. E. Kanim, J. C. Wang and R. B. Delamarter (2010). "Variability across ten production lots of a single demineralized bone matrix product." J Bone Joint Surg Am **92**(2): 427-435.

Bakker, A. D., M. Joldersma, J. Klein-Nulend and E. H. Burger (2003). "Interactive effects of PTH and mechanical stress on nitric oxide and PGE2 production by primary mouse osteoblastic cells." Am J Physiol Endocrinol Metab **285**(3): E608-613.

Bakker, A. D., J. Klein-Nulend and E. H. Burger (2003). "Mechanotransduction in bone cells proceeds via activation of COX-2, but not COX-1." Biochemical and Biophysical Research Communications **305**(3): 677-683.

Bakker, A. D., K. Soejima, J. Klein-Nulend and E. H. Burger (2001). "The production of nitric oxide and prostaglandin E(2) by primary bone cells is shear stress dependent." J Biomech **34**(5): 671-677.

Balas, F., J. Perez-Pariente and M. Vallet-Regi (2003). "In vitro bioactivity of silicon-substituted hydroxyapatites." J Biomed Mater Res A **66**(2): 364-375.

Barbieri, D., H. Yuan, F. de Groot, W. R. Walsh and J. D. de Bruijn "Influence of different polymeric gels on the ectopic bone forming ability of an osteoinductive biphasic calcium phosphate ceramic." Acta Biomater **7**(5): 2007-2014.

Barr, T., A. J. McNamara, G. K. Sandor, C. M. Clokie and S. A. Peel (2010). "Comparison of the osteoinductivity of bioimplants containing recombinant human bone morphogenetic proteins 2 (Infuse) and 7 (OP-1)." Oral Surg Oral Med Oral Pathol Oral Radiol Endod **109**(4): 531-540.

Barradas, A. M., H. Yuan, C. A. van Blitterswijk and P. Habibovic (2011). "Osteoinductive biomaterials: current knowledge of properties, experimental models and biological mechanisms." Eur Cell Mater **21**: 407-429; discussion 429.

Barradas, A. M., H. Yuan, J. van der Stok, B. Le Quang, H. Fernandes, A. Chaterjea, M. C. Hogenes, K. Shultz, L. R. Donahue, C. van Blitterswijk and J. de Boer (2012). "The influence of genetic factors on the osteoinductive potential of calcium phosphate ceramics in mice." Biomaterials **33**(23): 5696-5705.

Barrere, F., C. M. van der Valk, R. A. Dalmeijer, G. Meijer, C. A. van Blitterswijk, K. de Groot and P. Layrolle (2003). "Osteogenecity of octacalcium phosphate coatings applied on porous metal implants." J Biomed Mater Res A **66**(4): 779-788.

Bergmann, G. (2009). "Orthoload." 2010.

Betz, R. R. (2003). "Limitations of autograft and allograft: new synthetic solutions." Orthopedics **25**(5 Supplement): S561-S570.

Bignon, A., J. Chouteau, J. Chevalier, G. Fantozzi, J. P. Carret, P. Chavassieux, G. Boivin, M. Melin and D. Hartmann (2003). "Effect of micro- and macroporosity of bone substitutes on their mechanical properties and cellular response." J Mater Sci Mater Med **14**(12): 1089-1097.

BioMedGPS (2012). Bone - Market Overview. BioMedGPS, BioMedGPS LLC.

Birchall, J. (1993). "Dissolved Silica and the bioavailability of aluminium." The Lancet **342**.

Blitterswijk, C. A. v., D. Bakker, S. C. Hesseling and H. K. Koerten (1991). "Reactions of Cells at Implant Surfaces." Biomaterials **12**: 187-193.

Bodde, E. W., C. T. Cammaert, J. G. Wolke, P. H. Spauwen and J. A. Jansen (2007). "Investigation as to the osteoinductivity of macroporous calcium phosphate

cement in goats." J Biomed Mater Res B Appl Biomater **83**(1): 161-168.
Bolland, B. J., A. M. New, G. Madabhushi, R. O. Oreffo and D. G. Dunlop (2008). "The role of vibration and drainage in femoral impaction bone grafting." J Arthroplasty **23**(8): 1157-1164.
Bolland, B. J., K. Partridge, S. Tilley, A. M. New, D. G. Dunlop and R. O. Oreffo (2006). "Biological and mechanical enhancement of impacted allograft seeded with human bone marrow stromal cells: potential clinical role in impaction bone grafting." Regen Med **1**(4): 457-467.
Bolland, B. J., S. Tilley, A. M. New, D. G. Dunlop and R. O. Oreffo (2007). "Adult mesenchymal stem cells and impaction grafting: a new clinical paradigm shift." Expert Rev Med Devices **4**(3): 393-404.
Boyan, B. D., T. W. Hummert, D. D. Dean and Z. Schwartz (1996). "Role of material surfaces in regulating bone and cartilage cell response." Biomaterials **17**(2): 137-146.
Boyan, B. D., D. M. Ranly, J. McMillan, M. Sunwoo, K. Roche and Z. Schwartz (2006a). "Osteoinductive ability of human allograft formulations." J Periodontol **77**(9): 1555-1563.
Boyan, B. D., D. M. Ranly and Z. Schwartz (2006b). "Use of growth factors to modify osteoinductivity of demineralized bone allografts: lessons for tissue engineering of bone." Dent Clin North Am **50**(2): 217-228, viii.
Boyd, D. and M. R. Towler (2005). "The processing, mechanical properties and bioactivity of zinc based glass ionomer cements." J Mater Sci Mater Med **16**(9): 843-850.
Boyne, P. J. (1970). "Autogenous Cancellous Bone and Marrow Transplants." Clinical Orthopaedics and Related Research **73**: 199-209.
Brown, E. T., J. W. Bray and F. J. Santarelli (1989). "Influence of stress-dependent elastic moduli on stresses and strains around axisymmetric boreholes." Rock Mechanics and Rock Engineering **22**(3): 189-203.
Buckwalter, J. A., T. A. Einhorn, M. E. Bolander and R. L. Cruess (1996). Healing of the Musculoskeletal Tissue. Fracture in Adults. R. C.A., G. D.P., B. R.W. and H. J.D. Philadelphia, Lippincott-Raven**:** 261-304.
Buckwalter, J. A., M. J. Glimcher, R. R. Cooper and R. Recker (1996a). "Bone biology. I: Structure, blood supply, cells, matrix, and mineralization." Instr Course Lect **45**: 371-386.
Buckwalter, J. A., M. J. Glimcher, R. R. Cooper and R. Recker (1996b). "Bone biology. II: Formation, form, modeling, remodeling, and regulation of cell function." Instr Course Lect **45**: 387-399.
Burger, E. H. and J. Klein-Nulend (1999a). "Mechanotransduction in Bone- Role of the Lacunocanalicular Network." FASEB **13 Supplement**: S101-S112.
Burger, E. H. and J. Klein-Nulend (1999b). "Mechanotransduction in bone--role of the lacuno-canalicular network." Faseb J **13 Suppl**: S101-112.
Burger, E. H., J. Klein-Nulend and T. H. Smit (2003). "Strain-derived canalicular fluid flow regulates osteoclast activity in a remodelling osteon--a proposal." J Biomech **36**(10): 1453-1459.
Cameron, K., P. Travers, C. Chander, T. Buckland, C. Campion and B. Noble (2013). "Directed osteogenic differentiation of human mesenchymal stem/precursor cells on silicate substituted calcium phosphate." J Biomed Mater Res A **101**(1): 13-22.
Cameron, K., P. Travers, C. Chander, T. Buckland, C. Campion and B. Noble (In Press). "Directed osteogenic differentiation of human mesenchymal

stem/precursor cells on silicate substituted calcium phosphate." J Biomed Mater Res A.

Camire, C. L., S. J. Saint-Jean, C. Mochales, P. Nevsten, J. S. Wang, L. Lidgren, I. McCarthy and M. P. Ginebra (2006). "Material characterization and in vivo behavior of silicon substituted alpha-tricalcium phosphate cement." J Biomed Mater Res B Appl Biomater **76**(2): 424-431.

Campion, C. R., S. L. Ball, D. L. Clarke and K. A. Hing (2013). "Microstructure and chemistry affects apatite nucleation on calcium phosphate bone graft substitutes." J Mater Sci Mater Med **24**(3): 597-610.

Campion, C. R., C. Chander, T. Buckland and K. Hing (2011). "Increasing strut porosity in silicate-substituted calcium-phosphate bone graft substitutes enhances osteogenesis." J Biomed Mater Res B Appl Biomater **97**(2): 245-254.

Cao, W. and L. L. Hench (1996). "Bioactive Materials." Ceramics International **22**: 493-507.

Carlisle, E. M. (1970). "Silicon: a possible factor in bone calcification." Science **167**(916): 279-280.

Carlisle, E. M. (1972). "Silicon: an essential element for the chick." Science **178**(61): 619-621.

Carlisle, E. M. (1974). "Proceedings: Silicon as an essential element." Fed Proc **33**(6): 1758-1766.

Carlisle, E. M. (1975). "Silicon." Nutr Rev **33**(9): 257-261.

Carlisle, E. M. (1976). "In vivo requirement for silicon in articular cartilage and connective tissue formation in the chick." J Nutr **106**(4): 478-484.

Carlisle, E. M. (1980a). "Biochemical and morphological changes associated with long bone abnormalities in silicon deficiency." J Nutr **110**(5): 1046-1056.

Carlisle, E. M. (1980b). "A silicon requirement for normal skull formation in chicks." J Nutr **110**(2): 352-359.

Carlisle, E. M. (1981). "Silicon: a requirement in bone formation independent of vitamin D1." Calcif Tissue Int **33**(1): 27-34.

Carlisle, E. M. (1982). "The nutritional essentiality of silicon." Nutr Rev **40**(7): 193-198.

Carlisle, E. M. (1986). "Silicon as an essential trace element in animal nutrition." Ciba Found Symp **121**: 123-139.

Carlisle, E. M. (1988). "Silicon as a trace nutrient." Sci Total Environ **73**(1-2): 95-106.

Carragee, E. J., A. J. Ghanayem, B. K. Weiner, D. J. Rothman and C. M. Bono (2011). "A challenge to integrity in spine publications: years of living dangerously with the promotion of bone growth factors." Spine J **11**(6): 463-468.

Carragee, E. J., E. L. Hurwitz and B. K. Weiner (2011a). "A critical review of recombinant human bone morphogenetic protein-2 trials in spinal surgery: emerging safety concerns and lessons learned." Spine J **11**(6): 471-491.

Carragee, E. J., E. L. Hurwitz, B. K. Weiner, C. M. Bono and D. J. Rothman (2011b). "Future directions for The spine journal: managing and reporting conflict of interest issues." Spine J **11**(8): 695-697.

Carragee, E. J., K. A. Mitsunaga, E. L. Hurwitz and G. J. Scuderi (2011). "Retrograde ejaculation after anterior lumbar interbody fusion using rhBMP-2: a cohort controlled study." Spine J **11**(6): 511-516.

Carter, D. R. and W. C. Hayes (1976). "Bone compressive strength: the influence of

density and strain rate." Science **194**(4270): 1174-1176.
Chan, O., M. J. Coathup, A. Nesbitt, C. Y. Ho, K. A. Hing, T. Buckland, C. Campion and G. W. Blunn "The effects of microporosity on osteoinduction of calcium phosphate bone graft substitute biomaterials." Acta Biomater.
Charriere, E., S. Terrazzoni, C. Pittet, P. H. Mordasini, M. Dutoit, J. Lemaitre and P. H. Zysset (2001). "Mechanical characterization of brushite and hydroxyapatite cements." Biomaterials **22**(21): 2937-2945.
Chen, Q., F. Miyaji, T. Kokubo and T. Nakamura (1999). "Apatite formation on PDMS-modified CaO-SiO2-TiO2 hybrids prepared by sol-gel process." Biomaterials **20**(12): 1127-1132.
Chen, Q., N. Miyata, T. Kokubo and T. Nakamura (2000). "Bioactivity and mechanical properties of PDMS-modified CaO-SiO(2)-TiO(2) hybrids prepared by sol-gel process." J Biomed Mater Res **51**(4): 605-611.
Chen, Q. Z. and A. R. Boccaccini (2006). "Poly(D,L-lactic acid) coated 45S5 Bioglass-based scaffolds: processing and characterization." J Biomed Mater Res A **77**(3): 445-457.
Chen, Q. Z., I. D. Thompson and A. R. Boccaccini (2006). "45S5 Bioglass-derived glass-ceramic scaffolds for bone tissue engineering." Biomaterials **27**(11): 2414-2425.
Cheng, L., F. Ye, R. Yang, X. Lu, Y. Shi, L. Li, H. Fan and H. Bu (2009). "Osteoinduction of hydroxyapatite/beta-tricalcium phosphate bioceramics in mice with a fractured fibula." Acta Biomater.
Chouzouri, G. and M. Xanthos (2007). "In vitro bioactivity and degradation of polycaprolactone composites containing silicate fillers." Acta Biomater **3**(5): 745-756.
Chun, S., S. Na, J. Lee, J. Chung, I. Ryu and S. K. Kim (2002). "Biodegradation Study of Potassium Calcium Metaphosphate in the SBF and Tris-Buffer Solution." Key Engineering Materials **218 - 220**: 149-152.
Coathup, M. J., K. A. Hing, S. Samizadeh, O. Chan, Y. S. Fang, C. Campion, T. Buckland and G. W. Blunn (2012). "Effect of increased strut porosity of calcium phosphate bone graft substitute biomaterials on osteoinduction." J Biomed Mater Res A **100**(6): 1550-1555.
Coathup, M. J., S. Samizadeh, Y. S. Fang, T. Buckland, K. A. Hing and G. W. Blunn (2011). "The osteoinductivity of silicate-substituted calcium phosphate." J Bone Joint Surg Am **93**(23): 2219-2226.
Coleman, N. J. (2009). "Aspects of the in vitro bioactivity and antimicrobial properties of Ag(+)- and Zn (2+)-exchanged 11 A tobermorites." J Mater Sci Mater Med **20**(6): 1347-1355.
Coleman, N. J., K. Awosanya and J. W. Nicholson (2009). "Aspects of the in vitro bioactivity of hydraulic calcium (alumino)silicate cement." J Biomed Mater Res A **90**(1): 166-174.
Cortes, D. A., A. Medina, J. C. Escobedo, S. Escobedo and M. A. Lopez (2004). "Effect of wollastonite ceramics and bioactive glass on the formation of a bonelike apatite layer on a cobalt base alloy." J Biomed Mater Res A **70**(2): 341-346.
Coulson, R. and P. Lalor (2000). Osteoinductivity of human demineralized bone matrix by in vivo and in vitro assays., GenSci
Cowin, S. C. and S. Weinbaum (1998). "Strain amplification in the bone mechanosensory system." Am J Med Sci **316**(3): 184-188.
Cowles, E. A., L. L. Brailey and G. A. Gronowicz (2000). "Integrin-mediated

signaling regulates AP-1 transcription factors and proliferation in osteoblasts." J Biomed Mater Res **52**(4): 725-737.

Cowles, E. A., M. E. DeRome, G. Pastizzo, L. L. Brailey and G. A. Gronowicz (1998). "Mineralization and the expression of matrix proteins during in vivo bone development." Calcif Tissue Int **62**(1): 74-82.

Daculsi, G. (2004). "Osteoinductive Properties of Micro Macroporous Biphasic Calcium Phosphate Bioceramics." Key Engineering Materials **254-256**: 1005-1008.

Dark, G. (1997, 24 Mar 2004). "On-Line Medical Dictionary." from http://cancerweb.ncl.ac.uk/cgi-bin/omd?On-line+Medical+Dictionary

Das, B. M. (2009). Fundamentals of Geotechnical Engineering, CL-Engineering.

Davison, N. L., X. Luo, T. Schoenmaker, V. Everts, H. Yuan, F. Barrere-de Groot and J. D. de Bruijn (2014). "Submicron-scale surface architecture of tricalcium phosphate directs osteogenesis in vitro and in vivo." Eur Cell Mater **27**: 281-297; discussion 296-287.

De Godoy, R. F., S. Hutchens, C. Campion and G. Blunn (2015). "Silicate-substituted calcium phosphate with enhanced strut porosity stimulates osteogenic differentiation of human mesenchymal stem cells." J Mater Sci Mater Med **26**(1): 5387.

de Medeiros, W. S., M. V. de Oliveira, L. C. Pereira and M. C. de Andrade (2008). "Bioactive porous titanium: an alternative to surgical implants." Artif Organs **32**(4): 277-282.

de Souza, G. B., G. G. de Lima, N. K. Kuromoto, P. Soares, C. M. Lepienski, C. E. Foerster and A. Mikowski (2011). "Tribo-mechanical characterization of rough, porous and bioactive Ti anodic layers." J Mech Behav Biomed Mater **4**(5): 796-806.

De With, G., H. J. A. van Dijk, N. Hattu and K. Prijs (1981). "Preaparation, microstructure, and mechanical properties of dense polycrystalline hydroxyapatite." Journal of Materials Science **16**.

Degasne, I., M. F. Basle, V. Demais, G. Hure, M. Lesourd, B. Grolleau, L. Mercier and D. Chappard (1999). "Effects of roughness, fibronectin and vitronectin on attachment, spreading, and proliferation of human osteoblast-like cells (Saos-2) on titanium surfaces." Calcif Tissue Int **64**(6): 499-507.

Di Palma, F., M. Douet, C. Boachon, A. Guignandon, S. Peyroche, B. Forest, C. Alexandre, A. Chamson and A. Rattner (2003). "Physiological strains induce differentiation in human osteoblasts cultured on orthopaedic biomaterial." Biomaterials **24**(18): 3139-3151.

Di Palma, F., A. Guignandon, A. Chamson, M.-H. Lafage-Proust, N. Laroche, S. Peyroche, L. Vico and A. Rattner (2005). "Modulation of the responses of human osteoblast-like cells to physiologic mechanical strains by biomaterial surfaces." Biomaterials **26**(20): 4249-4257.

Dinopoulos, H., R. Dimitriou and P. V. Giannoudis (2012). "Bone graft substitutes: What are the options?" Surgeon **10**(4): 230-239.

Directive, E. (1986). "EC Directive 86/609. Available at : http://www.ecbr.eu/pdf/86-609-eec_en.pdf. Accessed 14 December 2009.".

Donath, K. and G. Breuner (1982). "A method for the study of undecalcified bones and teeth with attached soft tissues. The Sage-Schliff (sawing and grinding) technique." J Oral Pathol **11**(4): 318-326.

Dopico-Gonzalez, C., A. M. New and M. Browne (2009). "Probabilistic analysis of an uncemented total hip replacement." Med Eng Phys **31**(4): 470-476.

Dopico-Gonzalez, C., A. M. New and M. Browne (2010). "A computational tool for the probabilistic finite element analysis of an uncemented total hip replacement considering variability in bone-implant version angle." Comput Methods Biomech Biomed Engin **13**(1): 1-9.

Du, C., P. Klasens, R. E. Haan, J. Bezemer, F. Z. Cui, K. de Groot and P. Layrolle (2002). "Biomimetic calcium phosphate coatings on Polyactive 1000/70/30." J Biomed Mater Res **59**(3): 535-546.

Edwards, J. T., M. H. Diegmann and N. L. Scarborough (1998). "Osteoinduction of human demineralized bone: characterization in a rat model." Clin Orthop Relat Res(357): 219-228.

Eggli, P. S., W. Muller and R. K. Schenk (1988). "Porous hydroxyapatite and tricalcium phosphate cylinders with two different pore size ranges implanted in the cancellous bone of rabbits. A comparative histomorphometric and histologic study of bony ingrowth and implant substitution." Clin Orthop Relat Res(232): 127-138.

Eid, K., S. Zelicof, B. P. Perona, C. B. Sledge and J. Glowacki (2001). "Tissue reactions to particles of bone-substitute materials in intraosseous and heterotopic sites in rats: discrimination of osteoinduction, osteocompatibility, and inflammation." J Orthop Res **19**(5): 962-969.

Einhorn, T. A. (2003). Basic Science of Bone Graft Substitutes. Boston, Massachusetts, Department of Orthopaedic Surgery,.

Einhorn, T. A. and L. C. Gerstenfeld (2015). "Fracture healing: mechanisms and interventions." Nat Rev Rheumatol **11**(1): 45-54.

El-Ghannam, A., K. Ahmed and M. Omran (2005). "Nanoporous delivery system to treat osteomyelitis and regenerate bone: gentamicin release kinetics and bactericidal effect." J Biomed Mater Res B Appl Biomater **73**(2): 277-284.

Elliott, J. (1994). Structure and Chemistry of the Apatites and Other Calcium Orthophosphates, Elsevier.

Erlandsson, B. (2002). "Stability-indicating changes in poloxamers: the degradation of ethylene oxide-propylene oxide copolymers at 25 and 40C." Polymer Degradation and Stability **78**: 571-575.

Etex Osteoinductivity Certification of Equivabone. Etex. Cambridge, MA, USA.

Fazan, F. and P. M. Marquis (2000). "Dissolution behavior of plasma-sprayed hydroxyapatite coatings." J Mater Sci Mater Med **11**(12): 787-792.

Fellah, B. H., O. Gauthier, P. Weiss, D. Chappard and P. Layrolle (2008). "Osteogenicity of biphasic calcium phosphate ceramics and bone autograft in a goat model." Biomaterials **29**(9): 1177-1188.

Flautre, B., C. Delecourt, M. C. Blary, P. Van Landuyt, J. Lemaitre and P. Hardouin (1999). "Volume effect on biological properties of a calcium phosphate hydraulic cement: experimental study in sheep." Bone **25**(2 Suppl): 35S-39S.

Fritsch, A., L. Dormieux, C. Hellmich and J. Sanahuja (2009). "Mechanical behavior of hydroxyapatite biomaterials: an experimentally validated micromechanical model for elasticity and strength." J Biomed Mater Res A **88**(1): 149-161.

Fujibayashi, S., M. Neo, H. M. Kim, T. Kokubo and T. Nakamura (2003). "A comparative study between in vivo bone ingrowth and in vitro apatite formation on Na2O-CaO-SiO2 glasses." Biomaterials **24**(8): 1349-1356.

Fujibayashi, S., M. Neo, H. M. Kim, T. Kokubo and T. Nakamura (2004). "Osteoinduction of porous bioactive titanium metal." Biomaterials **25**(3): 443-450.

Gallet, G. (2002). "Thermal degradation of poly(ethylene oxide-polypropylene

oxide-ethylene oxide) triblock copolymer: comparative study by SEC/NMR, SEC/MALDI-TOF and SPME/GC-MS." Polymer **43**: 1081-1094.

Gallet, G. and B. Erlandsson (2002). "Thermal oxidation of poly(ethylene oxide-propylene oxide-ethylene oxide) triblock copolymer: focus on low molecular weight degradation products." Polymer Degradation and Stability **77**: 55-66.

Gandolfi, M. G., G. Ciapetti, F. Perut, P. Taddei, E. Modena, P. L. Rossi and C. Prati (2009). "Biomimetic calcium-silicate cements aged in simulated body solutions. Osteoblast response and analyses of apatite coating." J Appl Biomater Biomech **7**(3): 160-170.

Gao, T., H. T. Aro, H. Ylanen and E. Vuorio (2001). "Silica-based bioactive glasses modulate expression of bone morphogenetic protein-2 mRNA in Saos-2 osteoblasts in vitro." Biomaterials **22**(12): 1475-1483.

Garcia, A. J., P. Ducheyne and D. Boettiger (1998). "Effect of surface reaction stage on fibronectin-mediated adhesion of osteoblast-like cells to bioactive glass." J Biomed Mater Res **40**(1): 48-56.

Gauthier, O., J. M. Bouler, E. Aguado, P. Pilet and G. Daculsi (1998). "Macroporous biphasic calcium phosphate ceramics: influence of macropore diameter and macroporosity percentage on bone ingrowth." Biomaterials **19**(1-3): 133-139.

Giannoudis, P. V., H. Dinopoulos and E. Tsiridis (2005). "Bone substitutes: an update." Injury **36 Suppl 3**: S20-27.

Gibson, I., J. Huang, S. Best and W. Bonfield (1999). "Enhanced In Vitro Cell Activity and Surface Apatite Layer Formation on Novel Silicon-Substituted Hydroxyapatites." Bioceramics **12**: 191-194.

Gibson, I. R., S. M. Best and W. Bonfield (1999). "Chemical characterization of silicon-substituted hydroxyapatite." J Biomed Mater Res **44**(4): 422-428.

Gibson, L. J. (1985). "The mechanical behaviour of cancellous bone." J Biomech **18**(5): 317-328.

Gosain, A. K., L. Song, P. Riordan, M. T. Amarante, P. G. Nagy, C. R. Wilson, J. M. Toth and J. L. Ricci (2002). "A 1-year study of osteoinduction in hydroxyapatite-derived biomaterials in an adult sheep model: part I." Plast Reconstr Surg **109**(2): 619-630.

Green, R. J., M. C. Davies, C. J. Roberts and S. J. Tendler (1999). "Competitive protein adsorption as observed by surface plasmon resonance." Biomaterials **20**(4): 385-391.

Greenspan, D. (1999). "Bioactive ceramic implant materials." CURRENT OPINION IN SOLID STATE & MATERIALS SCIENCE **4**(4): 389-393.

Greish, Y. E. and P. W. Brown (2001). "Characterization of wollastonite-reinforced HAp--Ca polycarboxylate composites." J Biomed Mater Res **55**(4): 618-628.

Gunzburg, R., M. Szpalski, N. Passuti and M. Aebi (2001). "Biomaterials: the new frontiers in spine surgery." Eur Spine J **10 Suppl 2**: S85.

Guo, Y., Y. Zhou and D. Jia (2008). "Fabrication of hydroxycarbonate apatite coatings with hierarchically porous structures." Acta Biomater **4**(2): 334-342.

Guth, K., C. Campion, T. Buckland and K. Hing (2010a). "Effect of Silicate-Substitution on Attachment and Early Development of Human Osteoblast-Like Cells Seeded on Microporous Hydroxyapatite Discs " Advanced Engineering Materials **12**(1-2): Pages B26 - B36.

Guth, K., C. Campion, T. Buckland and K. Hing (2010b). "Surface physiochemistry affects protein adsorption to stoichiometric and silicate substituted microporous hydroxyapatites." Advanced Biomaterials **In press**.

Ha, S. W., K. L. Eckert, E. Wintermantel, H. Gruner, M. Guecheva and H. Vonmont

(1997). "NaOH treatment of vacuum-plasma-sprayed titanium on carbon fibre-reinforced poly(etheretherketone)." J Mater Sci Mater Med **8**(12): 881-886.

Habibovic, P., U. Gbureck, C. J. Doillon, D. C. Bassett, C. A. van Blitterswijk and J. E. Barralet (2008). "Osteoconduction and osteoinduction of low-temperature 3D printed bioceramic implants." Biomaterials **29**(7): 944-953.

Habibovic, P., M. C. Kruyt, M. V. Juhl, S. Clyens, R. Martinetti, L. Dolcini, N. Theilgaard and C. A. van Blitterswijk (2008). "Comparative in vivo study of six hydroxyapatite-based bone graft substitutes." J Orthop Res **26**(10): 1363-1370.

Habibovic, P., T. M. Sees, M. A. van den Doel, C. A. van Blitterswijk and K. de Groot (2006). "Osteoinduction by biomaterials--physicochemical and structural influences." J Biomed Mater Res A **77**(4): 747-762.

Habibovic, P., C. M. van der Valk, C. A. van Blitterswijk, K. De Groot and G. Meijer (2004). "Influence of octacalcium phosphate coating on osteoinductive properties of biomaterials." J Mater Sci Mater Med **15**(4): 373-380.

Habibovic, P., H. Yuan, M. van den Doel, T. M. Sees, C. A. van Blitterswijk and K. de Groot (2006). "Relevance of osteoinductive biomaterials in critical-sized orthotopic defect." J Orthop Res **24**(5): 867-876.

Habibovic, P., H. Yuan, C. M. van der Valk, G. Meijer, C. A. van Blitterswijk and K. de Groot (2005). "3D microenvironment as essential element for osteoinduction by biomaterials." Biomaterials **26**(17): 3565-3575.

Han, D., X. Sun, X. Zhang, T. Tang and K. Dai (2008). "Ectopic osteogenesis by ex vivo gene therapy using beta tricalcium phosphate as a carrier." Connect Tissue Res **49**(5): 343-350.

Healy, K. E., C. H. Thomas, A. Rezania, J. E. Kim, P. J. McKeown, B. Lom and P. E. Hockberger (1996). "Kinetics of bone cell organization and mineralization on materials with patterned surface chemistry." Biomaterials **17**(2): 195-208.

Heinemann, S., C. Heinemann, R. Bernhardt, A. Reinstorf, B. Nies, M. Meyer, H. Worch and T. Hanke (2009). "Bioactive silica-collagen composite xerogels modified by calcium phosphate phases with adjustable mechanical properties for bone replacement." Acta Biomater **5**(6): 1979-1990.

Heiple, K. G., V. M. Goldberg, A. E. Powell, G. D. Bos and J. M. Zika (1987). "Biology of Cancellous Bone Grafts." Orthopedic Clinics of North America **18**(2): 179-185.

Hench, L. L. (1993). An Introduction to Bioceramics, World Scientific Publishing.

Hesaraki, S., M. Safari and M. A. Shokrgozar (2009). "Development of beta-tricalcium phosphate/sol-gel derived bioactive glass composites: physical, mechanical, and in vitro biological evaluations." J Biomed Mater Res B Appl Biomater **91**(1): 459-469.

Heughebaert, J. (1984). "Kinetics of Crystallization of Octacaicium Phosphate." J. Phys. Chem. **88,** : 2478-2481.

Heughebaert, M., R. Z. LeGeros, M. Gineste, A. Guilhem and G. Bonel (1988). "Physicochemical characterization of deposits associated with HA ceramics implanted in nonosseous sites." J Biomed Mater Res **22**(3 Suppl): 257-268.

Hing, K. (2004a). "Bone Development is Sensitive to Silicon Level in Substituted Apatites." 7th World Biomaterials Congress: 108.

Hing, K. (2004b). "Microporosity affects Bioactivity of Macroporous HA Bone Graft Substitutes." Bioceramics - Key Engineering Materials **16**.

Hing, K. (2005). "Bioceramic Bone Graft Substitutes: Influence of Porosity and Chemistry." International Journal of Applied Ceramic Technology **2**(3): 184-199.

Hing, K., S. Saeed, B. Annaz, T. Buckland and P. Revell (2004). Silicate substitution alters the progression of bone apposition within porous hydroxyapatite bone graft substitutes. Orthop Res Soc San Francisco, CA.

Hing, K. A. (2004c). "Bone repair in the twenty-first century: biology, chemistry or engineering?" Philos Transact Ser A Math Phys Eng Sci **362**(1825): 2821-2850.

Hing, K. A., B. Annaz, S. Saeed, P. A. Revell and T. Buckland (2005). "Microporosity enhances bioactivity of synthetic bone graft substitutes." J Mater Sci Mater Med **16**(5): 467-475.

Hing, K. A., S. M. Best and W. Bonfield (1999). "Characterization of porous hydroxyapatite." J Mater Sci Mater Med **10**(3): 135-145.

Hing, K. A., S. M. Best, K. E. Tanner, W. Bonfield and P. A. Revell (2004). "Mediation of bone ingrowth in porous hydroxyapatite bone graft substitutes." J Biomed Mater Res A **68**(1): 187-200.

Hing, K. A., S. M. Best, K. E. Tanner, P. A. Revell and W. Bonfield (1998a). "Histomorphological and Biomechanical Characterisation of Calcium Phosphate in the Osseous Environment." Process Institution of Mechanical Engeneering **212**: 437-451.

Hing, K. A., S. M. Best, K. E. Tanner, P. A. Revell and W. Bonfield (1998b). "Histomorphological and biomechanical characterization of calcium phosphates in the osseous environment." Proc Inst Mech Eng [H] **212**(6): 437-451.

Hing, K. A., I. R. Gibson, L. Di-Silvio, S. M. Best and W. Bonfield (1998). "Effect of Variation in Ca:P Ratio on Cellular Response of Primary Human Osteoblast like Cells to Hydroxyapatite Based Ceramics." Bioceramics **11**: 293-296.

Hing, K. A., I. R. Gibson, P. A. Revell, S. M. Best and W. Bonfield (2001). "Influence on Phase Purity on the in vivo Response to Hydroxyapatite." Bioceramics **13**: 373-376.

Hing, K. A., J. C. Merry, I. R. Gibson, L. Di-Silvio, S. M. Best and W. Bonfield (1999). "Effect of Carbonate Content on the Response of Human Osteoblast-Like Cells to Carbonate Substituted Hydroxyapatite." Bioceramics **12**: 195-198.

Hing, K. A., P. A. Revell, N. Smith and T. Buckland (2006). "Effect of silicon level on rate, quality and progression of bone healing within silicate-substituted porous hydroxyapatite scaffolds." Biomaterials **27**(29): 5014-5026.

Hing, K. A., L. F. Wilson and T. Buckland (2007). "Comparative performancve of three ceramic bone graft substitutes." Spine J **In Press**.

Hodgskinson, R. and J. D. Currey (1990). "The effect of variation in structure on the Young's modulus of cancellous bone: a comparison of human and non-human material." Proc Inst Mech Eng [H] **204**(2): 115-121.

Hollinger, J. O. and J. C. Kleinschmidt (1990). "The critical size defect as an experimental model to test bone repair materials." J Craniofac Surg **1**(1): 60-68.

Holmes, R., V. Mooney, R. Bucholz and A. Tencer (1984). "A coralline hydroxyapatite bone graft substitute. Preliminary report." Clin Orthop Relat Res(188): 252-262.

Honsawek, S., R. M. Powers and L. Wolfinbarger (2005). "Extractable bone morphogenetic protein and correlation with induced new bone formation in an in vivo assay in the athymic mouse model." Cell Tissue Bank **6**(1): 13-23.

Huan, Z. and J. Chang (2007). "Novel tricalcium silicate/monocalcium phosphate monohydrate composite bone cement." J Biomed Mater Res B Appl Biomater **82**(2): 352-359.

Huan, Z. and J. Chang (2009). "Novel bioactive composite bone cements based on the beta-tricalcium phosphate-monocalcium phosphate monohydrate composite cement system." Acta Biomater **5**(4): 1253-1264.

Huang, X. and X. Miao (2007). "Novel porous hydroxyapatite prepared by combining H2O2 foaming with PU sponge and modified with PLGA and bioactive glass." J Biomater Appl **21**(4): 351-374.

Huggins, C. B. (1931). "The phosphatase activity of transplants of the epithelium of the urinary bladder to the abdominal wall producing heterotopic ossification." Biochem J **25**(3): 728-732.

Hunter, A., C. W. Archer, P. S. Walker and G. W. Blunn (1995). "Attachment and proliferation of osteoblasts and fibroblasts on biomaterials for orthopaedic use." Biomaterials **16**(4): 287-295.

Ignatius, A., H. Blessing, A. Liedert, C. Schmidt, C. Neidlinger-Wilke, D. Kaspar, B. Friemert and L. Claes (2005). "Tissue engineering of bone: effects of mechanical strain on osteoblastic cells in type I collagen matrices." Biomaterials **26**(3): 311-318.

Izquierdo-Barbaa, R.-G., C. Doadrioa, González-Calbetb, Vallet-Regí (2005). "Tissue regeneration: A new property of mesoporous materials." Solid State Sciences **7**(8): 983-989.

Jaakkola, T., J. Rich, T. Tirri, T. Narhi, M. Jokinen, J. Seppala and A. Yli-Urpo (2004). "In vitro Ca-P precipitation on biodegradable thermoplastic composite of poly(epsilon-caprolactone-co-DL-lactide) and bioactive glass (S53P4)." Biomaterials **25**(4): 575-581.

Jarcho, M. (1981). "Calcium Phoshpate Ceramics as Hard Tissue Prosthetics." Clinical Orthopaedic Related Research **157**: 259.

Joldersma, M., E. H. Burger, C. M. Semeins and J. Klein-Nulend (2000). "Mechanical stress induces COX-2 mRNA expression in bone cells from elderly women." J Biomech **33**(1): 53-61.

Juhasz, J. A., S. M. Best, A. D. Auffret and W. Bonfield (2008). "Biological control of apatite growth in simulated body fluid and human blood serum." J Mater Sci Mater Med **19**(4): 1823-1829.

Kamitakahara, M., C. Ohtsuki, H. Inada, M. Tanihara and T. Miyazaki (2006). "Effect of ZnO addition on bioactive CaO-SiO2-P2O5-CaF2 glass-ceramics containing apatite and wollastonite." Acta Biomater **2**(4): 467-471.

Kang, Y., Y. Yao, G. Yin, Z. Huang, X. Liao, X. Xu and G. Zhao (2009). "A study on the in vitro degradation properties of poly(L-lactic acid)/beta-tricalcuim phosphate (PLLA/beta-TCP) scaffold under dynamic loading." Med Eng Phys **31**(5): 589-594.

Kasuga, T., Y. Ota, M. Nogami and Y. Abe (2000). "Surface modification of calcium metaphosphate fibers." J Mater Sci Mater Med **11**(4): 223-225.

Kawai, T., C. Ohtsuki, M. Kamitakahara, K. Hosoya, M. Tanihara, T. Miyazaki, Y. Sakaguchi and S. Konagaya (2007). "In vitro apatite formation on polyamide containing carboxyl groups modified with silanol groups." J Mater Sci Mater Med **18**(6): 1037-1042.

Kay, J. F. (2004). In vivo osteoinductivity assessment of a DBM-based carrier, Isotis.

Keller, T. S. (1994). "Predicting the compressive mechanical behavior of bone." J Biomech **27**(9): 1159-1168.

Kilpadi, K. L., P. L. Chang and S. L. Bellis (2001). "Hydroxylapatite binds more serum proteins, purified integrins, and osteoblast precursor cells than titanium or steel." J Biomed Mater Res **57**(2): 258-267.

Kilpadi, K. L., A. A. Sawyer, C. W. Prince, P. L. Chang and S. L. Bellis (2004). "Primary human marrow stromal cells and Saos-2 osteosarcoma cells use different mechanisms to adhere to hydroxylapatite." J Biomed Mater Res **68A**(2): 273-285.

Kim, D. H., R. Rhim, L. Li, J. Martha, B. H. Swaim, R. J. Banco, L. G. Jenis and S. G. Tromanhauser (2009). "Prospective study of iliac crest bone graft harvest site pain and morbidity." Spine J **9**(11): 886-892.

Kim, H., H. Arakawa, T. Osada and A. Ikai (2003). "Quantification of cell adhesion force with AFM: distribution of vitronectin receptors on a living MC3T3-E1 cell." Ultramicroscopy **97**(1-4): 359-363.

Kim, S. and C. B. Park (2010). "Mussel-inspired transformation of CaCO3 to bone minerals." Biomaterials **31**(25): 6628-6634.

Klawitter, J. J., J. G. Bagwell, A. M. Weinstein and B. W. Sauer (1976). "An evaluation of bone growth into porous high density polyethylene." J Biomed Mater Res **10**(2): 311-323.

Klein, C. P., J. M. de Blieck-Hogervorst, J. G. Wolke and K. de Groot (1990). "Studies of the solubility of different calcium phosphate ceramic particles in vitro." Biomaterials **11**(7): 509-512.

Klein-Nulend, J., M. H. Helfrich, J. G. Sterck, H. MacPherson, M. Joldersma, S. H. Ralston, C. M. Semeins and E. H. Burger (1998). "Nitric oxide response to shear stress by human bone cell cultures is endothelial nitric oxide synthase dependent." Biochem Biophys Res Commun **250**(1): 108-114.

Klein-Nulend, J., J. Roelofsen, C. M. Semeins, A. L. Bronckers and E. H. Burger (1997). "Mechanical stimulation of osteopontin mRNA expression and synthesis in bone cell cultures." J Cell Physiol **170**(2): 174-181.

Klein-Nulend, J., C. M. Semeins, N. E. Ajubi, P. J. Nijweide and E. H. Burger (1995). "Pulsating fluid flow increases nitric oxide (NO) synthesis by osteocytes but not periosteal fibroblasts--correlation with prostaglandin upregulation." Biochem Biophys Res Commun **217**(2): 640-648.

Klein-Nulend, J., A. van der Plas, C. M. Semeins, N. E. Ajubi, J. A. Frangos, P. J. Nijweide and E. H. Burger (1995). "Sensitivity of osteocytes to biomechanical stress in vitro." Faseb J **9**(5): 441-445.

Knabe, C., G. Berger, R. Gildenhaar, J. Meyer, C. R. Howlett, B. Markovic and H. Zreiqat (2004). "Effect of rapidly resorbable calcium phosphates and a calcium phosphate bone cement on the expression of bone-related genes and proteins in vitro." J Biomed Mater Res **69A**(1): 145-154.

Knott, L. and A. J. Bailey (1998). "Collagen cross-links in mineralizing tissues: a review of their chemistry, function, and clinical relevance." Bone **22**(3): 181-187.

Kobayashi, M., T. Nakamura, Y. Okada, A. Fukumoto, T. Furukawa, H. Kato, T. Kokubo and T. Kikutani (1998). "Bioactive bone cement: comparison of apatite and wollastonite containing glass-ceramic, hydroxyapatite, and beta-tricalcium phosphate fillers on bone-bonding strength." J Biomed Mater Res

42(2): 223-237.

Kokubo, T., M. Hanakawa, M. Kawashita, M. Minoda, T. Beppu, T. Miyamoto and T. Nakamura (2004). "Apatite-forming ability of alginate fibers treated with calcium hydroxide solution." J Mater Sci Mater Med **15**(9): 1007-1012.

Kokubo, T., S. Ito, Z. T. Huang, T. Hayashi, S. Sakka, T. Kitsugi and T. Yamamuro (1990). "Ca,P-rich layer formed on high-strength bioactive glass-ceramic A-W." J Biomed Mater Res **24**(3): 331-343.

Kokubo, T., H. Kushitani, S. Sakka, T. Kitsugi and T. Yamamuro (1990). "Solutions able to reproduce in vivo surface-structure changes in bioactive glass-ceramic A-W." J Biomed Mater Res **24**(6): 721-734.

Kondo, N., A. Ogose, K. Tokunaga, H. Umezu, K. Arai, N. Kudo, M. Hoshino, H. Inoue, H. Irie, K. Kuroda, H. Mera and N. Endo (2006). "Osteoinduction with highly purified beta-tricalcium phosphate in dog dorsal muscles and the proliferation of osteoclasts before heterotopic bone formation." Biomaterials **27**(25): 4419-4427.

Kotani, S., Y. Fujita, T. Kitsugi, T. Nakamura, T. Yamamuro, C. Ohtsuki and T. Kokubo (1991). "Bone bonding mechanism of beta-tricalcium phosphate." J Biomed Mater Res **25**(10): 1303-1315.

Kuhne, J. H., R. Bartl, B. Frisch, C. Hammer, V. Jansson and M. Zimmer (1994). "Bone formation in coralline hydroxyapatite. Effects of pore size studied in rabbits." Acta Orthop Scand **65**(3): 246-252.

Labbaf, S., O. Tsigkou, K. H. Muller, M. M. Stevens, A. E. Porter and J. R. Jones (2011). "Spherical bioactive glass particles and their interaction with human mesenchymal stem cells in vitro." Biomaterials **32**(4): 1010-1018.

Landis, W. J., K. J. Hodgens, M. J. Song, J. Arena, S. Kiyonaga, M. Marko, C. Owen and B. F. McEwen (1996). "Mineralization of collagen may occur on fibril surfaces: evidence from conventional and high-voltage electron microscopy and three-dimensional imaging." J Struct Biol **117**(1): 24-35.

Laquerriere, P., A. Grandjean-Laquerriere, E. Jallot, G. Balossier, P. Frayssinet and M. Guenounou (2003). "Importance of hydroxyapatite particles characteristics on cytokines production by human monocytes in vitro." Biomaterials **24**(16): 2739-2747.

Laurencin, C. T. (2003). Bone Graft Substitutes. Bridgeport, ASTM international.

Le Nihouannen, D., G. Daculsi, A. Saffarzadeh, O. Gauthier, S. Delplace, P. Pilet and P. Layrolle (2005). "Ectopic bone formation by microporous calcium phosphate ceramic particles in sheep muscles." Bone **36**(6): 1086-1093.

Lee, K. J., J. G. Roper and J. C. Wang (2005). "Demineralized bone matrix and spinal arthrodesis." Spine J **5**(6 Suppl): 217S-223S.

LeGeros, R. Z. (2002). "Properties of osteoconductive biomaterials: calcium phosphates." Clin Orthop Relat Res(395): 81-98.

Leijten, J. C., L. S. Moreira Teixeira, E. B. Landman, C. A. van Blitterswijk and M. Karperien (2012). "Hypoxia inhibits hypertrophic differentiation and endochondral ossification in explanted tibiae." PLoS One **7**(11): e49896.

Leng, Y., J. Chen and S. Qu (2003). "TEM study of calcium phosphate precipitation on HA/TCP ceramics." Biomaterials **24**(13): 2125-2131.

Leonor, I. B., F. Balas, M. Kawashita, R. L. Reis, T. Kokubo and T. Nakamura (2009). "Biomimetic apatite deposition on polymeric microspheres treated with a calcium silicate solution." J Biomed Mater Res B Appl Biomater **91**(1): 239-247.

Leonor, I. B., E. T. Baran, M. Kawashita, R. L. Reis, T. Kokubo and T. Nakamura

(2008). "Growth of a bonelike apatite on chitosan microparticles after a calcium silicate treatment." Acta Biomater **4**(5): 1349-1359.

Leonor, I. B., A. Ito, K. Onuma, N. Kanzaki and R. L. Reis (2003). "In vitro bioactivity of starch thermoplastic/hydroxyapatite composite biomaterials: an in situ study using atomic force microscopy." Biomaterials **24**(4): 579-585.

Leonor, I. B. and R. L. Reis (2003). "An innovative auto-catalytic deposition route to produce calcium-phosphate coatings on polymeric biomaterials." J Mater Sci Mater Med **14**(5): 435-441.

Leung, S. Y., M. Browne and A. M. New (2008). "Smooth surface micro finite element modelling of a cancellous bone analogue material." Proc Inst Mech Eng H **222**(1): 145-149.

Li, H. and J. Chang (2013). "Bioactive silicate materials stimulate angiogenesis in fibroblast and endothelial cell co-culture system through paracrine effect." Acta Biomater **9**(6): 6981-6991.

Li, J., P. Habibovic, H. Yuan, M. van den Doel, C. E. Wilson, J. R. de Wijn, C. A. van Blitterswijk and K. de Groot (2007). "Biological performance in goats of a porous titanium alloy-biphasic calcium phosphate composite." Biomaterials **28**(29): 4209-4218.

Li, S., Z. Zheng, Q. Liu, J. R. de Wijn and K. de Groot (1998). "Collagen/apatite coating on 3-dimensional carbon/carbon composite." J Biomed Mater Res **40**(4): 520-529.

Li, X., J. Shi, Y. Zhu, W. Shen, H. Li, J. Liang and J. Gao (2007). "A template route to the preparation of mesoporous amorphous calcium silicate with high in vitro bone-forming bioactivity." J Biomed Mater Res B Appl Biomater **83**(2): 431-439.

Li, Z., L. Yubao, Z. Yi, W. Lan and J. A. Jansen (2009). "In vitro and in vivo evaluation on the bioactivity of ZnO containing nano-hydroxyapatite/chitosan cement." J Biomed Mater Res A **93**(1): 269-279.

Lin, K., J. Chang and R. Cheng (2007). "In vitro hydroxyapatite forming ability and dissolution of tobermorite nanofibers." Acta Biomater **3**(2): 271-276.

Lin, Q., Y. Li, X. Lan, C. Lu, Y. Chen and Z. Xu (2009). "The apatite formation ability of CaF2 doping tricalcium silicates in simulated body fluid." Biomed Mater **4**(4): 045005.

Lin, Y., T. Wang, L. Wu, W. Jing, X. Chen, Z. Li, L. Liu, W. Tang, X. Zheng and W. Tian (2007). "Ectopic and in situ bone formation of adipose tissue-derived stromal cells in biphasic calcium phosphate nanocomposite." J Biomed Mater Res A **81**(4): 900-910.

Linde, F., P. Norgaard, I. Hvid, A. Odgaard and K. Soballe (1991). "Mechanical properties of trabecular bone. Dependency on strain rate." J Biomech **24**(9): 803-809.

Linthurst, J. (2008). In vivo osteoinductivity characterization of demineralized bone matrix and DBM pastes and putties. Virginia Beach, VA, LifeNet Health.

Liu, D. M. (1998). "Preparation and characterization of porous hydroxyapatite bioceramic via a slip-casting route." Ceram. Int. **24**: 441-446.

Liu, G., L. Zhao, L. Cui, W. Liu and Y. Cao (2007). "Tissue-engineered bone formation using human bone marrow stromal cells and novel beta-tricalcium phosphate." Biomed Mater **2**(2): 78-86.

Liu, H., H. Li, W. Cheng, Y. Yang, M. Zhu and C. Zhou (2006). "Novel injectable calcium phosphate/chitosan composites for bone substitute materials." Acta Biomater **2**(5): 557-565.

Liu, X., R. K. Fu, R. W. Poon, P. Chen, P. K. Chu and C. Ding (2004). "Biomimetic growth of apatite on hydrogen-implanted silicon." Biomaterials **25**(25): 5575-5581.

Lopes, P., M. Corbellini, B. L. Ferreira, N. Almeida, M. Fredel, M. H. Fernandes and R. Correia (2009). "New PMMA-co-EHA glass-filled composites for biomedical applications: Mechanical properties and bioactivity." Acta Biomater **5**(1): 356-362.

Lu, H. H., S. F. El-Amin, K. D. Scott and C. T. Laurencin (2003). "Three-dimensional, bioactive, biodegradable, polymer-bioactive glass composite scaffolds with improved mechanical properties support collagen synthesis and mineralization of human osteoblast-like cells in vitro." J Biomed Mater Res A **64**(3): 465-474.

Lu, H. H., A. Tang, S. C. Oh, J. P. Spalazzi and K. Dionisio (2005). "Compositional effects on the formation of a calcium phosphate layer and the response of osteoblast-like cells on polymer-bioactive glass composites." Biomaterials **26**(32): 6323-6334.

Lu, J., M. C. Blary, S. Vavasseur, M. Descamps, K. Anselme and P. Hardouin (2004). "Relationship between bioceramics sintering and micro-particles-induced cellular damages." J Mater Sci Mater Med **15**(4): 361-365.

Lu, W., W. Duan, Y. Guo and C. Ning (2010). "Mechanical Properties and in Vitro Bioactivity of Ca5(PO4)2SiO4 Bioceramic." J Biomater Appl.

Maeda, H., V. Maquet, T. Kasuga, Q. Z. Chen, J. A. Roether and A. R. Boccaccini (2007). "Vaterite deposition on biodegradable polymer foam scaffolds for inducing bone-like hydroxycarbonate apatite coatings." J Mater Sci Mater Med **18**(12): 2269-2273.

Marcolongo, M., P. Ducheyne and W. C. LaCourse (1997). "Surface reaction layer formation in vitro on a bioactive glass fiber/polymeric composite." J Biomed Mater Res **37**(3): 440-448.

Mariappan, C. R., D. M. Yunos, A. R. Boccaccini and B. Roling (2009). "Bioactivity of electro-thermally poled bioactive silicate glass." Acta Biomater **5**(4): 1274-1283.

Marsell, R. and T. A. Einhorn (2011). "The biology of fracture healing." Injury **42**(6): 551-555.

Martini, F. (1998). Fundamentals of Anatomy and Phsyriology, Prentice Hall.

Mason, D. J., R. A. Hillam and T. M. Skerry (1996). "Constitutive in vivo mRNA expression by osteocytes of beta-actin, osteocalcin, connexin-43, IGF-I, c-fos and c-jun, but not TNF-alpha nor tartrate-resistant acid phosphatase." J Bone Miner Res **11**(3): 350-357.

Matsuoka, H., H. Akiyama, Y. Okada, H. Ito, C. Shigeno, J. Konishi, T. Kokubo and T. Nakamura (1999). "In vitro analysis of the stimulation of bone formation by highly bioactive apatite- and wollastonite-containing glass-ceramic: released calcium ions promote osteogenic differentiation in osteoblastic ROS17/2.8 cells." J Biomed Mater Res **47**(2): 176-188.

Mauney, J. R., S. Sjostorm, J. Blumberg, R. Horan, J. P. O'Leary, G. Vunjak-Novakovic, V. Volloch and D. L. Kaplan (2004). "Mechanical stimulation promotes osteogenic differentiation of human bone marrow stromal cells on 3-D partially demineralized bone scaffolds in vitro." Calcif Tissue Int **74**(5): 458-468.

McCalden, R. W., J. A. McGeough and C. M. Court-Brown (1997). "Age-related changes in the compressive strength of cancellous bone. The relative

importance of changes in density and trabecular architecture." J Bone Joint Surg Am **79**(3): 421-427.

McFarland, C. D., C. H. Thomas, C. DeFilippis, J. G. Steele and K. E. Healy (2000). "Protein adsorption and cell attachment to patterned surfaces." J Biomed Mater Res **49**(2): 200-210.

McGarry, J. G., J. Klein-Nulend and P. J. Prendergast (2005). "The effect of cytoskeletal disruption on pulsatile fluid flow-induced nitric oxide and prostaglandin E2 release in osteocytes and osteoblasts." Biochem Biophys Res Commun **330**(1): 341-348.

McGarry, J. G. and P. J. Prendergast (2004). "A three-dimensional finite element model of an adherent eukaryotic cell." Eur Cell Mater **7**: 27-33; discussion 33-24.

McKeown-Longo, P. and T. Panetti (1996). "Structure and Function of Vitronectin." Trends Glycosci.Glycotechnol **8**: 327-340.

McKibbin, B. (1978). "The biology of fracture healing in long bones." J Bone Joint Surg Br **60-B**(2): 150-162.

Meille, S. and E. J. Garboczi (2001). "Linear elastic properties of 2D and 3D models of porous materials made from elongated objects." Modelling and Simulation in Materials Science and Engineering **9**(5): 371.

Miake, Y., T. Yanagisawa, Y. Yajima, H. Noma, N. Yasui and T. Nonami (1995). "High-resolution and analytical electron microscopic studies of new crystals induced by a bioactive ceramic (diopside)." J Dent Res **74**(11): 1756-1763.

Miyata, N., K. Fuke, Q. Chen, M. Kawashita, T. Kokubo and T. Nakamura (2002). "Apatite-forming ability and mechanical properties of PTMO-modified CaO-SiO2 hybrids prepared by sol-gel processing: effect of CaO and PTMO contents." Biomaterials **23**(14): 3033-3040.

Miyaza, T., H. M. Kim, T. Kokubo, C. Ohtsuki, H. Kato and T. Nakamura (2002). "Mechanism of bonelike apatite formation on bioactive tantalum metal in a simulated body fluid." Biomaterials **23**(3): 827-832.

Miyazaki, M., H. Tsumura, J. C. Wang and A. Alanay (2009). "An update on bone substitutes for spinal fusion." Eur Spine J **18**(6): 783-799.

Miyazaki, T., M. Imamura, E. Ishida, M. Ashizuka and C. Ohtsuki (2009). "Apatite formation abilities and mechanical properties of hydroxyethylmethacrylate-based organic-inorganic hybrids incorporated with sulfonic groups and calcium ions." J Mater Sci Mater Med **20**(1): 157-161.

Miyazaki, T., C. Ohtsuki, M. Kyomoto, M. Tanihara, A. Mori and K. Kuramoto (2003). "Bioactive PMMA bone cement prepared by modification with methacryloxypropyltrimethoxysilane and calcium chloride." J Biomed Mater Res A **67**(4): 1417-1423.

Mladenovic, Z., A. Johansson, B. Willman, K. Shahabi, E. Bjorn and M. Ransjo (2014). "Soluble silica inhibits osteoclast formation and bone resorption in vitro." Acta Biomater **10**(1): 406-418.

Mohamed, A. M. (2008). "An overview of bone cells and their regulating factors of differentiation." Malays J Med Sci **15**(1): 4-12.

Monroe, E. A., W. Votava, D. B. Bass and J. McMullen (1971). "New calcium phosphate ceramic material for bone and tooth implants." J Dent Res **50**(4): 860-861.

Morejon-Alonso, L., R. G. Carrodeguas and J. A. Garcia-Menocal (2008). "Transformations in CDHA/OCP/beta-TCP scaffold during ageing in simulated body fluid at 36.5 degrees C." J Biomed Mater Res B Appl

Biomater **84**(2): 386-393.
Mori, A., C. Ohtsuki, T. Miyazaki, A. Sugino, M. Tanihara, K. Kuramoto and A. Osaka (2005). "Synthesis of bioactive PMMA bone cement via modification with methacryloxypropyltri-methoxysilane and calcium acetate." J Mater Sci Mater Med **16**(8): 713-718.
Mullender, M., A. J. El Haj, Y. Yang, M. A. van Duin, E. H. Burger and J. Klein-Nulend (2004). "Mechanotransduction of bone cells in vitro: mechanobiology of bone tissue." Med Biol Eng Comput **42**(1): 14-21.
Na, K., S. W. Kim, B. K. Sun, D. G. Woo, H. N. Yang, H. M. Chung and K. H. Park (2007). "Osteogenic differentiation of rabbit mesenchymal stem cells in thermo-reversible hydrogel constructs containing hydroxyapatite and bone morphogenic protein-2 (BMP-2)." Biomaterials **28**(16): 2631-2637.
Nagatomi, J., B. P. Arulanandam, D. W. Metzger, A. Meunier and R. Bizios (2003). "Cyclic pressure affects osteoblast functions pertinent to osteogenesis." Ann Biomed Eng **31**(8): 917-923.
Ni, S. and J. Chang (2009). "In vitro degradation, bioactivity, and cytocompatibility of calcium silicate, dimagnesium silicate, and tricalcium phosphate bioceramics." J Biomater Appl **24**(2): 139-158.
Ni, S., J. Chang and L. Chou (2006). "A novel bioactive porous CaSiO3 scaffold for bone tissue engineering." J Biomed Mater Res A **76**(1): 196-205.
Ni, S., J. Chang and L. Chou (2008). "In vitro studies of novel CaO-SiO2-MgO system composite bioceramics." J Mater Sci Mater Med **19**(1): 359-367.
Ni, S., K. Lin, J. Chang and L. Chou (2008). "Beta-CaSiO3/beta-Ca3(PO4)2 composite materials for hard tissue repair: in vitro studies." J Biomed Mater Res A **85**(1): 72-82.
Ning, C. Q. and Y. Zhou (2002). "In vitro bioactivity of a biocomposite fabricated from HA and Ti powders by powder metallurgy method." Biomaterials **23**(14): 2909-2915.
Nunamaken, D. (1998). "Experimental models of fracture repair. ." Clin Orthop Relat Res **355**: S56-S65.
O'Donnell, M. D., S. J. Watts, R. G. Hill and R. V. Law (2009). "The effect of phosphate content on the bioactivity of soda-lime-phosphosilicate glasses." J Mater Sci Mater Med **20**(8): 1611-1618.
Oh, S. H., S. Y. Choi, Y. K. Lee, K. N. Kim and S. H. Choi (2003). "Effects of lithium fluoride and maleic acid on the bioactivity of calcium aluminate cement: Formation of hydroxyapatite in simulated body fluid." J Biomed Mater Res A **67**(1): 104-111.
Ohgushi, H. and M. Okumura (1990). "Osteogenic capacity of rat and human marrow cells in porous ceramics. Experiments in athymic (nude) mice." Acta Orthop Scand **61**(5): 431-434.
Ohgushi, H., M. Okumura, S. Tamai, E. C. Shors and A. I. Caplan (1990). "Marrow cell induced osteogenesis in porous hydroxyapatite and tricalcium phosphate: a comparative histomorphometric study of ectopic bone formation." J Biomed Mater Res **24**(12): 1563-1570.
Oki, A., B. Parveen, S. Hossain, S. Adeniji and H. Donahue (2004). "Preparation and in vitro bioactivity of zinc containing sol-gel-derived bioglass materials." J Biomed Mater Res A **69**(2): 216-221.
Okubo, Y., K. Bessho, K. Fujimura, Y. Konishi, K. Kusumoto, Y. Ogawa and T. Iizuka (2000). "Osteoinduction by recombinant human bone morphogenetic protein-2 at intramuscular, intermuscular, subcutaneous and intrafatty sites."

Int J Oral Maxillofac Surg **29**(1): 62-66.

Okumura, M., H. Ohgushi and S. Tamai (1991). "Bonding osteogenesis in coralline hydroxyapatite combined with bone marrow cells." Biomaterials **12**(4): 411-416.

Oliveira, A. L., P. B. Malafaya and R. L. Reis (2003). "Sodium silicate gel as a precursor for the in vitro nucleation and growth of a bone-like apatite coating in compact and porous polymeric structures." Biomaterials **24**(15): 2575-2584.

Oliveira, J. M., S. S. Silva, P. B. Malafaya, M. T. Rodrigues, N. Kotobuki, M. Hirose, M. E. Gomes, J. F. Mano, H. Ohgushi and R. L. Reis (2009). "Macroporous hydroxyapatite scaffolds for bone tissue engineering applications: physicochemical characterization and assessment of rat bone marrow stromal cell viability." J Biomed Mater Res A **91**(1): 175-186.

Oliveira, S. M., D. Q. Mijares, G. Turner, I. F. Amaral, M. A. Barbosa and C. C. Teixeira (2009). "Engineering endochondral bone: in vivo studies." Tissue Eng Part A **15**(3): 635-643.

Organisation, I. S. (2006). Adaptation of standard NF EN ISO 10993 Biological Evaluation of Medical Devices Part 2 : Animal welfare requirements. Part 6 (2007): Tests for local effects after implantation. **10993**.

Orii, Y., H. Masumoto, Y. Honda, T. Anada, T. Goto, K. Sasaki and O. Suzuki (2010). "Enhancement of octacalcium phosphate deposition on a titanium surface activated by electron cyclotron resonance plasma oxidation." J Biomed Mater Res B Appl Biomater **93**(2): 476-483.

Ouyang, J., G. T. Yang, W. Z. Wu, Q. A. Zhu and S. Z. Zhong (1997). "Biomechanical characteristics of human trabecular bone." Clin Biomech (Bristol, Avon) **12**(7-8): 522-524.

Ozawa, S. and S. Kasugai (1996). "Evaluation of implant materials (hydroxyapatite, glass-ceramics, titanium) in rat bone marrow stromal cell culture." Biomaterials **17**(1): 23-29.

Park, J. B. and J. D. Bronzino (2003). Biomaterials.

Patel, N. (2003). "Comparison of Sintering and Mechanical Properties of Hydroxyapatite and Silicon-Substituted Hydroxyapatite." Key Engineering Materials **Bioceramics 15 (Volumes 240 - 242)**: 919-922.

Patel, N., S. M. Best, W. Bonfield, I. R. Gibson, K. A. Hing, E. Damien and P. A. Revell (2002). "A Comparative Study on the *in vivo* Behaviour of Hydroxyapatite and Silicon Substituted Hydroxyapatite Granules." Journal of Materials Science: Materials and Medicine **13**: 1199-1206.

Patel, N., R. A. Brooks, M. T. Clarke, P. M. Lee, N. Rushton, I. R. Gibson, S. M. Best and W. Bonfield (2005). "In vivo assessment of hydroxyapatite and silicate-substituted hydroxyapatite granules using an ovine defect model." J Mater Sci Mater Med **16**(5): 429-440.

Pattanayak, D. K., S. Yamaguchi, T. Matsushita and T. Kokubo (2011). "Nanostructured positively charged bioactive TiO(2) layer formed on Ti metal by NaOH, acid and heat treatments." J Mater Sci Mater Med **22**(8): 1803-1812.

Pavalko, F. M., N. X. Chen, C. H. Turner, D. B. Burr, S. Atkinson, Y. F. Hsieh, J. Qiu and R. L. Duncan (1998). "Fluid shear-induced mechanical signaling in MC3T3-E1 osteoblasts requires cytoskeleton-integrin interactions." Am J Physiol **275**(6 Pt 1): C1591-1601.

Peltola, T., M. Jokinen, H. Rahiala, E. Levanen, J. B. Rosenholm, I. Kangasniemi

and A. Yli-Urpo (1999). "Calcium phosphate formation on porous sol-gel-derived SiO2 and CaO-P2O5-SiO2 substrates in vitro." J Biomed Mater Res **44**(1): 12-21.

Peltola, T., M. Jokinen, S. Veittola, H. Rahiala and A. Yli-Urpo (2001). "Influence of sol and stage of spinnability on in vitro bioactivity and dissolution of sol-gel-derived SiO2 fibers." Biomaterials **22**(6): 589-598.

Pereira MM, C. A., Hench LL (1994). "Calcium phosphate formation on sol-gel derived bioactive glasses in vitro." Biomedical Mater Res **18**: 693-698.

Phillips, A. T., P. Pankaj, C. R. Howie, A. S. Usmani and A. H. Simpson (2006). "3D non-linear analysis of the acetabular construct following impaction grafting." Comput Methods Biomech Biomed Engin **9**(3): 125-133.

Piecuch, J. F. (1982). "Extraskeletal implantation of a porous hydroxyapatite ceramic." J Dent Res **61**(12): 1458-1460.

Pirhonen, E., H. Niiranen, T. Niemela, M. Brink and P. Tormala (2006). "Manufacturing, mechanical characterization, and in vitro performance of bioactive glass 13-93 fibers." J Biomed Mater Res B Appl Biomater **77**(2): 227-233.

Pollick, S., E. C. Shors, R. E. Holmes and R. A. Kraut (1995). "Bone formation and implant degradation of coralline porous ceramics placed in bone and ectopic sites." J Oral Maxillofac Surg **53**(8): 915-922; discussion 922-913.

Porter, A. E., S. M. Best and W. Bonfield (2004). "Ultrastructural comparison of hydroxyapatite and silicon-substituted hydroxyapatite for biomedical applications." J Biomed Mater Res A **68**(1): 133-141.

Porter, A. E., C. M. Botelho, M. A. Lopes, J. D. Santos, S. M. Best and W. Bonfield (2004). "Ultrastructural comparison of dissolution and apatite precipitation on hydroxyapatite and silicon-substituted hydroxyapatite in vitro and in vivo." J Biomed Mater Res A **69**(4): 670-679.

Porter, A. E., N. Patel, J. N. Skepper, S. M. Best and W. Bonfield (2003). "Comparison of in vivo dissolution processes in hydroxyapatite and silicon-substituted hydroxyapatite bioceramics." Biomaterials **24**(25): 4609-4620.

Porter, A. E., N. Patel, J. N. Skepper, S. M. Best and W. Bonfield (2004). "Effect of sintered silicate-substituted hydroxyapatite on remodelling processes at the bone-implant interface." Biomaterials **25**(16): 3303-3314.

Puleo, D. A. and A. Nanci (1999). "Understanding and controlling the bone-implant interface." Biomaterials **20**(23-24): 2311-2321.

Rammelt, S., M. Neumann, U. Hanisch, A. Reinstorf, W. Pompe, H. Zwipp and A. Biewener (2005). "Osteocalcin enhances bone remodeling around hydroxyapatite/collagen composites." J Biomed Mater Res A **73**(3): 284-294.

Ranly, D. M., C. H. Lohmann, D. Andreacchio, B. D. Boyan and Z. Schwartz (2007). "Platelet-rich plasma inhibits demineralized bone matrix-induced bone formation in nude mice." J Bone Joint Surg Am **89**(1): 139-147.

Ranly, D. M., J. McMillan, T. Keller, C. H. Lohmann, T. Meunch, D. L. Cochran, Z. Schwartz and B. D. Boyan (2005). "Platelet-derived growth factor inhibits demineralized bone matrix-induced intramuscular cartilage and bone formation. A study of immunocompromised mice." J Bone Joint Surg Am **87**(9): 2052-2064.

Rashid, N. (2008). "Nano-scale manipulation of silicate-substituted apatite chemistry impacts surface charge, hydrophilicity, protein adsorption and cell attachment." Int. J. Nano and Biomaterials **1**(3).

Ravaglioli, A. (1992). Bioceramics, Chapman and Hall.

Reffitt, D. M., N. Ogston, R. Jugdaohsingh, H. F. Cheung, B. A. Evans, R. P. Thompson, J. J. Powell and G. N. Hampson (2003). "Orthosilicic acid stimulates collagen type 1 synthesis and osteoblastic differentiation in human osteoblast-like cells in vitro." Bone **32**(2): 127-135.

Rennert, R. C., M. Sorkin, R. K. Garg and G. C. Gurtner (2012). "Stem cell recruitment after injury: lessons for regenerative medicine." Regen Med **7**(6): 833-850.

Rhee, S. H., J. Y. Choi and H. M. Kim (2002). "Preparation of a bioactive and degradable poly(epsilon -caprolactone)/silica hybrid through a sol-gel method." Biomaterials **23**(24): 4915-4921.

Rho, J. Y., R. B. Ashman and C. H. Turner (1993). "Young's modulus of trabecular and cortical bone material: ultrasonic and microtensile measurements." J Biomech **26**(2): 111-119.

Rho, J. Y., M. C. Hobatho and R. B. Ashman (1995). "Relations of mechanical properties to density and CT numbers in human bone." Med Eng Phys **17**(5): 347-355.

Ripamonti, U. (1991). "The morphogenesis of bone in replicas of porous hydroxyapatite obtained from conversion of calcium carbonate exoskeletons of coral." J Bone Joint Surg Am **73**(5): 692-703.

Ripamonti, U. (1996). "Osteoinduction in porous hydroxyapatite implanted in heterotopic sites of different animal models." Biomaterials **17**(1): 31-35.

Ripamonti, U., S. S. Ma, B. van den Heever and A. H. Reddi (1992). "Osteogenin, a bone morphogenetic protein, adsorbed on porous hydroxyapatite substrata, induces rapid bone differentiation in calvarial defects of adult primates." Plast Reconstr Surg **90**(3): 382-393.

Roach, H. I. (1994). "Why does bone matrix contain non-collagenous proteins? The possible roles of osteocalcin, osteonectin, osteopontin and bone sialoprotein in bone mineralisation and resorption." Cell Biol Int **18**(6): 617-628.

Roelofsen, J., J. Klein-Nulend and E. H. Burger (1995). "Mechanical stimulation by intermittent hydrostatic compression promotes bone-specific gene expression in vitro." J Biomech **28**(12): 1493-1503.

Rohl, L., E. Larsen, F. Linde, A. Odgaard and J. Jorgensen (1991). "Tensile and compressive properties of cancellous bone." J Biomech **24**(12): 1143-1149.

Rouahi, M., E. Champion, O. Gallet, A. Jada and K. Anselme (2006). "Physico-chemical characteristics and protein adsorption potential of hydroxyapatite particles: influence on in vitro biocompatibility of ceramics after sintering." Colloids Surf B Biointerfaces **47**(1): 10-19.

Rouahi, M., O. Gallet, E. Champion, J. Dentzer, P. Hardouin and K. Anselme (2006). "Influence of hydroxyapatite microstructure on human bone cell response." J Biomed Mater Res A **78**(2): 222-235.

Rubin, P. A., J. K. Popham, J. R. Bilyk and J. W. Shore (1994). "Comparison of fibrovascular ingrowth into hydroxyapatite and porous polyethylene orbital implants." Ophthal Plast Reconstr Surg **10**(2): 96-103.

Saint-Jean, S. J., C. L. Camire, P. Nevsten, S. Hansen and M. P. Ginebra (2005). "Study of the reactivity and in vitro bioactivity of Sr-substituted alpha-TCP cements." J Mater Sci Mater Med **16**(11): 993-1001.

Salinas, A. J., J. M. Merino, F. Babonneau, F. J. Gil and M. Vallet-Regi (2007). "Microstructure and macroscopic properties of bioactive CaO-SiO2-PDMS hybrids." J Biomed Mater Res B Appl Biomater **81**(1): 274-282.

Samizadeh, S., M. Coathup, J. Amogbokpa, S. Fang, K. Hing, T. Buckland and G.

Blunn (2007). Osseoinduction by calcium phosphate substitutes is a function of chemical composition and structure. Orthop Res Soc 53rd annual meeting San Diego, USA

San Miguel, B., R. Kriauciunas, S. Tosatti, M. Ehrbar, C. Ghayor, M. Textor and F. E. Weber (2009). "Enhanced osteoblastic activity and bone regeneration using surface-modified porous bioactive glass scaffolds." J Biomed Mater Res A **94**(4): 1023-1033.

Sanchez-Salcedo, S., F. Balas, I. Izquierdo-Barba and M. Vallet-Regi (2009). "In vitro structural changes in porous HA/beta-TCP scaffolds in simulated body fluid." Acta Biomater **5**(7): 2738-2751.

Schaeren, S., C. Jaquiery, F. Wolf, A. Papadimitropoulos, A. Barbero, E. Schultz-Thater, M. Heberer and I. Martin (2010). "Effect of bone sialoprotein coating of ceramic and synthetic polymer materials on in vitro osteogenic cell differentiation and in vivo bone formation." J Biomed Mater Res A **92**(4): 1461-1467.

Schmitz, J. P. and J. O. Hollinger (1986). "The critical size defect as an experimental model for craniomandibulofacial nonunions." Clin Orthop Relat Res(205): 299-308.

Schwarz, K. (1973). "A bound form of silicon in glycosaminoglycans and polyuronides." Proc Natl Acad Sci U S A **70**(5): 1608-1612.

Seol, Y. J., K. H. Kim, Y. M. Kang, I. A. Kim and S. H. Rhee (2009). "Bioactivity, pre-osteoblastic cell responses, and osteoconductivity evaluations of the electrospun non-woven SiO2-CaO gel fabrics." J Biomed Mater Res B Appl Biomater **90**(2): 679-687.

Sepulveda, P., J. R. Jones and L. L. Hench (2002). "In vitro dissolution of melt-derived 45S5 and sol-gel derived 58S bioactive glasses." J Biomed Mater Res **61**(2): 301-311.

Shen, Y., J. Zhu, H. Zhang and F. Zhao (2006). "In vitro osteogenetic activity of pearl." Biomaterials **27**(2): 281-287.

Shi, X., Y. Wang, L. Ren, N. Zhao, Y. Gong and D. A. Wang (2009). "Novel mesoporous silica-based antibiotic releasing scaffold for bone repair." Acta Biomater **5**(5): 1697-1707.

Shirkhanzadeh, M. and M. Azadegan (1998). "Formation of carbonate apatite on calcium phosphate coatings containing silver ions." J Mater Sci Mater Med **9**(7): 385-391.

Sikavitsas, V. I., G. N. Bancroft, H. L. Holtorf, J. A. Jansen and A. G. Mikos (2003). "Mineralized matrix deposition by marrow stromal osteoblasts in 3D perfusion culture increases with increasing fluid shear forces." Proc Natl Acad Sci U S A **100**(25): 14683-14688.

Sikavitsas, V. I., G. N. Bancroft, J. J. Lemoine, M. A. Liebschner, M. Dauner and A. G. Mikos (2005). "Flow perfusion enhances the calcified matrix deposition of marrow stromal cells in biodegradable nonwoven fiber mesh scaffolds." Ann Biomed Eng **33**(1): 63-70.

Sikavitsas, V. I., J. S. Temenoff and A. G. Mikos (2001). "Biomaterials and bone mechanotransduction." Biomaterials **22**(19): 2581-2593.

Simmons, D. (1976). The Biochemistry and Physiology of Bone, pp. 445. New York, Academic Press.

Siriphannon, P., Y. Kameshima, A. Yasumori, K. Okada and S. Hayashi (2000). "Influence of preparation conditions on the microstructure and bioactivity of alpha-CaSiO(3) ceramics: formation of hydroxyapatite in simulated body

fluid." J Biomed Mater Res **52**(1): 30-39.
Sorkin, A. M., K. C. Dee and M. L. Knothe Tate (2004). ""Culture shock" from the bone cell's perspective: emulating physiological conditions for mechanobiological investigations." Am J Physiol Cell Physiol **287**(6): C1527-1536.
Staller, G. S., D. W. Richardson, D. M. Nunamaker and M. Provost (1995). "Contact area and static pressure profile at the plate-bone interface in the nonluted and luted bone plate." Vet Surg **24**(4): 299-307.
Standring, S. (2008). Grays Anatomy.
Stegen, S., N. van Gastel and G. Carmeliet (2015). "Bringing new life to damaged bone: The importance of angiogenesis in bone repair and regeneration." Bone **70**: 19-27.
Sterck, J. G., J. Klein-Nulend, P. Lips and E. H. Burger (1998). "Response of normal and osteoporotic human bone cells to mechanical stress in vitro." Am J Physiol **274**(6 Pt 1): E1113-1120.
Stevenson, S., S. E. Emery and V. M. Goldberg (1996). "Factors affecting bone graft incorporation." Clin Orthop Relat Res(324): 66-74.
Suchanek, W., M. Yashima, M. Kakihana and M. Yoshimura (1996). "Processing and mechanical properties of hydroxyapatite reinforced with hydroxyapatite whiskers." Biomaterials **17**(17): 1715-1723.
Sugino, A., T. Miyazaki, G. Kawachi, K. Kikuta and C. Ohtsuki (2008a). "Relationship between apatite-forming ability and mechanical properties of bioactive PMMA-based bone cement modified with calcium salts and alkoxysilane." J Mater Sci Mater Med **19**(3): 1399-1405.
Sugino, A., T. Miyazaki and C. Ohtsuki (2008b). "Apatite-forming ability of polyglutamic acid hydrogels in a body-simulating environment." J Mater Sci Mater Med **19**(6): 2269-2274.
Synthes DBX Demineralized Bone Matrix Brochure. Synthes. Paoli, PA, USA.
Taddei, F., A. Pancanti and M. Viceconti (2004). "An improved method for the automatic mapping of computed tomography numbers onto finite element models." Med Eng Phys **26**(1): 61-69.
Tadic, D. and M. Epple (2004). "A thorough physicochemical characterisation of 14 calcium phosphate-based bone substitution materials in comparison to natural bone." Biomaterials **25**(6): 987-994.
Takadama, H., H. M. Kim, T. Kokubo and T. Nakamura (2001). "TEM-EDX study of mechanism of bonelike apatite formation on bioactive titanium metal in simulated body fluid." J Biomed Mater Res **57**(3): 441-448.
Takikawa, S., T. W. Bauer, H. Kambic and D. Togawa (2003). "Comparative evaluation of the osteoinductivity of two formulations of human demineralized bone matrix." J Biomed Mater Res A **65**(1): 37-42.
Tampieri, A., M. Sandri, E. Landi, D. Pressato, S. Francioli, R. Quarto and I. Martin (2008). "Design of graded biomimetic osteochondral composite scaffolds." Biomaterials **29**(26): 3539-3546.
Tanaka, S. M., H. B. Sun, R. K. Roeder, D. B. Burr, C. H. Turner and H. Yokota (2005). "Osteoblast responses one hour after load-induced fluid flow in a three-dimensional porous matrix." Calcif Tissue Int **76**(4): 261-271.
Thain, M. and M. Hickman (1994). Dictionary of Biology, Penguin Reference.
Tilley, S., B. J. Bolland, K. Partridge, A. M. New, J. M. Latham, D. G. Dunlop and R. O. Oreffo (2006). "Taking tissue-engineering principles into theater: augmentation of impacted allograft with human bone marrow stromal cells."

Regen Med **1**(5): 685-692.

Towler, M. R., D. Boyd, C. Freeman, I. M. Brook and P. Farthing (2009). "Comparison of in vitro and in vivo bioactivity of SrO-CaO-ZnO-SiO2 glass grafts." J Biomater Appl **23**(6): 561-572.

Tseng, Y. H., C. Y. Mou and J. C. Chan (2006). "Solid-state NMR study of the transformation of octacalcium phosphate to hydroxyapatite: a mechanistic model for central dark line formation." J Am Chem Soc **128**(21): 6909-6918.

Twomey, P. J. and M. H. Kroll (2008). "How to use linear regression and correlation in quantitative method comparison studies." Int J Clin Pract **62**(4): 529-538.

Uemura, T., A. Nemoto, Y.-K. Liu, H. Kojima, Dong, T. Yabe, T. Yoshikawa, H. Ohgushi, T. Ushida and T. Tateishi (2001). "Osteopontin involvement in bone remodeling and its effects on in vivo osteogenic potential of bone marrow-derived osteoblasts/porous hydroxyapatite constructs." Materials Science and Engineering: C **17**(1-2): 33-36.

Urist, M. R. (1965). "Bone: formation by autoinduction." Science **150**: 893-899.

Urist, M. R. and B. S. Strates (1971). "Bone morphogenetic protein." J Dent Res **50**(6): 1392-1406.

Vaidya, R., R. Weir, A. Sethi, S. Meisterling, W. Hakeos and C. D. Wybo (2007). "Interbody fusion with allograft and rhBMP-2 leads to consistent fusion but early subsidence." J Bone Joint Surg Br **89**(3): 342-345.

Vakiparta, M., A. P. Forsback, L. V. Lassila, M. Jokinen, A. U. Yli-Urpo and P. K. Vallittu (2005). "Biomimetic mineralization of partially bioresorbable glass fiber reinforced composite." J Mater Sci Mater Med **16**(9): 873-879.

Vallet-Regi, M., I. Izquierdo-Barba and A. J. Salinas (1999). "Influence of P2O5 on crystallinity of apatite formed in vitro on surface of bioactive glasses." J Biomed Mater Res **46**(4): 560-565.

van Gaalen, S. (2009). "Goat Bone Tissue Engineering: Comparing an intramuscular with a posterolateral lumbar spine location." Tissue Eng **In press**.

Vani, R., E. K. Girija, K. Elayaraja, S. Prakash Parthiban, R. Kesavamoorthy and S. Narayana Kalkura (2009). "Hydrothermal synthesis of porous triphasic hydroxyapatite/(alpha and beta) tricalcium phosphate." J Mater Sci Mater Med **20 Suppl 1**: S43-48.

Veiga, S. S., M. Elias, W. Gremski, M. A. Porcionatto, R. da Silva, H. B. Nader and R. R. Brentani (1997). "Post-translational modifications of alpha5beta1 integrin by glycosaminoglycan chains. The alpha5beta1 integrin is a facultative proteoglycan." J Biol Chem **272**(19): 12529-12535.

Wang, J., H. Ma, X. Jin, J. Hu, X. Liu, L. Ni and P. X. Ma (2011). "The effect of scaffold architecture on odontogenic differentiation of human dental pulp stem cells." Biomaterials **32**(31): 7822-7830.

Wang, J., L. Qu, X. Meng, J. Gao, H. Li and G. Wen (2008). "Preparation and biological properties of PLLA/beta-TCP composites reinforced by chitosan fibers." Biomed Mater **3**(2): 025004.

Wang, X. J., H. Huang, F. Yang, L. G. Xia, W. J. Zhang, X. Q. Jiang and F. Q. Zhang (2011). "Ectopic study of tissue-engineered bone complex with enamel matrix proteins, bone marrow stromal cells in porous calcium phosphate cement scaffolds, in nude mice." Cell Prolif **44**(3): 274-282.

Wang, Y., T. Uemura, J. Dong, H. Kojima, J. Tanaka and T. Tateishi (2003). "Application of perfusion culture system improves in vitro and in vivo osteogenesis of bone marrow-derived osteoblastic cells in porous ceramic materials." Tissue Eng **9**(6): 1205-1214.

Weng, J., Q. Liu, J. G. Wolke, X. Zhang and K. de Groot (1997). "Formation and characteristics of the apatite layer on plasma-sprayed hydroxyapatite coatings in simulated body fluid." Biomaterials **18**(15): 1027-1035.

Weng, J., M. Wang and J. Chen (2002). "Plasma-sprayed calcium phosphate particles with high bioactivity and their use in bioactive scaffolds." Biomaterials **23**(13): 2623-2629.

Westbroek, I., N. E. Ajubi, M. J. Alblas, C. M. Semeins, J. Klein-Nulend, E. H. Burger and P. J. Nijweide (2000). "Differential stimulation of prostaglandin G/H synthase-2 in osteocytes and other osteogenic cells by pulsating fluid flow." Biochem Biophys Res Commun **268**(2): 414-419.

Will, J., A. Hoppe, F. A. Muller, C. T. Raya, J. M. Fernandez and P. Greil (2010). "Bioactivation of biomorphous silicon carbide bone implants." Acta Biomater **6**(12): 4488-4494.

Winter, G. D. (1970). "Heterotopic bone formation in a synthetic sponge." Proc R Soc Med **63**(11 Part 1): 1111-1115.

Winter, M., Griss, P. (1981). "Comparative histocompatability testing of seven calcium phoshpate ceramics." Biomaterials **2**: 159-161.

Wong, A. S., A. M. New, G. Isaacs and M. Taylor (2005). "Effect of bone material properties on the initial stability of a cementless hip stem: a finite element study." Proc Inst Mech Eng H **219**(4): 265-275.

Wong, D. A., A. Kumar, S. Jatana, G. Ghiselli and K. Wong (2008). "Neurologic impairment from ectopic bone in the lumbar canal: a potential complication of off-label PLIF/TLIF use of bone morphogenetic protein-2 (BMP-2)." Spine J **8**(6): 1011-1018.

Wren, A., D. Boyd and M. R. Towler (2008). "The processing, mechanical properties and bioactivity of strontium based glass polyalkenoate cements." J Mater Sci Mater Med **19**(4): 1737-1743.

Wu, Z. Y., R. G. Hill, S. Yue, D. Nightingale, P. D. Lee and J. R. Jones (2011). "Melt-derived bioactive glass scaffolds produced by a gel-cast foaming technique." Acta Biomater **7**(4): 1807-1816.

Xynos, I. D., A. J. Edgar, L. D. Buttery, L. L. Hench and J. M. Polak (2001). "Gene-expression profiling of human osteoblasts following treatment with the ionic products of Bioglass 45S5 dissolution." J Biomed Mater Res **55**(2): 151-157.

Yang, Z., H. Yuan, W. Tong, P. Zou, W. Chen and X. Zhang (1996). "Osteogenesis in extraskeletally implanted porous calcium phosphate ceramics: variability among different kinds of animals." Biomaterials **17**(22): 2131-2137.

Yang, Z. J., H. Yuan, P. Zou, W. Tong, S. Qu and X. D. Zhang (1997). "Osteogenic responses to extraskeletally implanted synthetic porous calcium phosphate ceramics: an early stage histomorphological study in dogs." J Mater Sci Mater Med **8**(11): 697-701.

Yaszemski, M. J., R. G. Payne, W. C. Hayes, R. Langer and A. G. Mikos (1996). "Evolution of bone transplantation: molecular, cellular and tissue strategies to engineer human bone." Biomaterials **17**(2): 175-185.

Yonggang, Y., J. G. Wolke, L. Yubao and J. A. Jansen (2007). "In vitro evaluation of different heat-treated radio frequency magnetron sputtered calcium phosphate coatings." Clin Oral Implants Res **18**(3): 345-353.

Yoon, B. H., H. E. Kim and H. W. Kim (2008). "Bioactive microspheres produced from gelatin-siloxane hybrids for bone regeneration." J Mater Sci Mater Med **19**(6): 2287-2292.

Yoshida, A., T. Miyazaki, M. Ashizuka and E. Ishida (2006). "Bioactivity and

mechanical properties of cellulose/carbonate hydroxyapatite composites prepared in situ through mechanochemical reaction." J Biomater Appl **21**(2): 179-194.

Young, M. F. (2003). "Bone matrix proteins: their function, regulation, and relationship to osteoporosis." Osteoporos Int **14 Suppl 3**: S35-42.

Yu, S., Z. Yu, G. Wang, J. Han, X. Ma and M. S. Dargusch (2011). "Biocompatibility and osteoconduction of active porous calcium-phosphate films on a novel Ti-3Zr-2Sn-3Mo-25Nb biomedical alloy." Colloids Surf B Biointerfaces **85**(2): 103-115.

Yuan, H., J. D. De Bruijn, Y. Li, J. Feng, Z. Yang, K. De Groot and X. Zhang (2001a). "Bone formation induced by calcium phosphate ceramics in soft tissue of dogs: a comparative study between porous alpha-TCP and beta-TCP." J Mater Sci Mater Med **12**(1): 7-13.

Yuan, H., J. D. de Bruijn, X. Zhang, C. A. van Blitterswijk and K. de Groot (2001b). "Bone induction by porous glass ceramic made from Bioglass (45S5)." J Biomed Mater Res **58**(3): 270-276.

Yuan, H., H. Fernandes, P. Habibovic, J. de Boer, A. M. Barradas, A. de Ruiter, W. R. Walsh, C. A. van Blitterswijk and J. D. de Bruijn (2010). "Osteoinductive ceramics as a synthetic alternative to autologous bone grafting." Proc Natl Acad Sci U S A **107**(31): 13614-13619.

Yuan, H., K. Kurashina, J. D. de Bruijn, Y. Li, K. de Groot and X. Zhang (1999). "A preliminary study on osteoinduction of two kinds of calcium phosphate ceramics." Biomaterials **20**(19): 1799-1806.

Yuan, H., Y. Li, J. D. de Bruijn, K. de Groot and X. Zhang (2000). "Tissue responses of calcium phosphate cement: a study in dogs." Biomaterials **21**(12): 1283-1290.

Yuan, H., C. A. van Blitterswijk, K. de Groot and J. D. de Bruijn (2006a). "A comparison of bone formation in biphasic calcium phosphate (BCP) and hydroxyapatite (HA) implanted in muscle and bone of dogs at different time periods." J Biomed Mater Res A **78**(1): 139-147.

Yuan, H., C. A. van Blitterswijk, K. de Groot and J. D. de Bruijn (2006b). "Cross-species comparison of ectopic bone formation in biphasic calcium phosphate (BCP) and hydroxyapatite (HA) scaffolds." Tissue Eng **12**(6): 1607-1615.

Yuan, H., Z. Yang, J. D. De Bruij, K. De Groot and X. Zhang (2001). "Material-dependent bone induction by calcium phosphate ceramics: a 2.5-year study in dog." Biomaterials **22**(19): 2617-2623.

Yuan, H., Z. Yang, Y. Li, X. Zhang, J. D. De Bruijn and K. De Groot (1998). "Osteoinduction by calcium phosphate biomaterials." J Mater Sci Mater Med **9**(12): 723-726.

Yuan, H., P. Zou, Z. Yang, X. Zhang, J. D. De Bruijn and K. De Groot (1998). "Bone morphogenetic protein and ceramic-induced osteogenesis." J Mater Sci Mater Med **9**(12): 717-721.

Zander, T., A. Rohlmann, C. Klockner and G. Bergmann (2002). "Effect of bone graft characteristics on the mechanical behavior of the lumbar spine." J Biomech **35**(4): 491-497.

Zhang, H., X. J. Ye and J. S. Li (2009). "Preparation and biocompatibility evaluation of apatite/wollastonite-derived porous bioactive glass ceramic scaffolds." Biomed Mater **4**(4): 045007.

Zhang, J., D. Barbieri, H. Ten Hoopen, J. D. de Bruijn, C. A. van Blitterswijk and H. Yuan (2014). "Microporous calcium phosphate ceramics driving osteogenesis

through surface architecture." J Biomed Mater Res A.

Zhang, J., X. Luo, D. Barbieri, A. M. Barradas, J. D. de Bruijn, C. A. van Blitterswijk and H. Yuan (2014). "The size of surface microstructures as an osteogenic factor in calcium phosphate ceramics." Acta Biomater **10**(7): 3254-3263.

Zhang, M., R. M. Powers, Jr. and L. Wolfinbarger, Jr. (1997a). "Effect(s) of the demineralization process on the osteoinductivity of demineralized bone matrix." J Periodontol **68**(11): 1085-1092.

Zhang, M., R. M. Powers, Jr. and L. Wolfinbarger, Jr. (1997b). "A quantitative assessment of osteoinductivity of human demineralized bone matrix." J Periodontol **68**(11): 1076-1084.

Zhang, Q., J. Chen, J. Feng, Y. Cao, C. Deng and X. Zhang (2003). "Dissolution and mineralization behaviors of HA coatings." Biomaterials **24**(26): 4741-4748.

Zhang, Q., Y. Leng, X. Lu, R. Xin, X. Yang and J. Chen (2009). "Bioactive films on metallic surfaces for osteoconduction." J Biomed Mater Res A **88**(2): 481-490.

Zhang, S., T. Mao and F. Chen (2011). "Influence of platelet-rich plasma on ectopic bone formation of bone marrow stromal cells in porous coral." Int J Oral Maxillofac Surg **40**(9): 961-965.

Zhang, Y. and M. Zhang (2002). "Three-dimensional macroporous calcium phosphate bioceramics with nested chitosan sponges for load-bearing bone implants." J Biomed Mater Res **61**(1): 1-8.

Zhao, W., J. Chang, J. Wang, W. Zhai and Z. Wang (2007). "In vitro bioactivity of novel tricalcium silicate ceramics." J Mater Sci Mater Med **18**(5): 917-923.

Zhao, W., J. Chang and W. Zhai (2008). "Self-setting properties and in vitro bioactivity of Ca3SiO5/CaSO4.1/2H2O composite cement." J Biomed Mater Res A **85**(2): 336-344.

Zhao, W., J. Wang, W. Zhai, Z. Wang and J. Chang (2005). "The self-setting properties and in vitro bioactivity of tricalcium silicate." Biomaterials **26**(31): 6113-6121.